



**DEVELOPMENT OF A GROUNDWATER FLOW MODEL FOR  
WATER RESOURCES MANAGEMENT AT THE DEVELOPMENT  
AREA WEST OF THE ROSETTA BRANCH,  
EGYPT**

**Dissertation**

to obtain the academic degree

Doctor of Natural Sciences (Dr. rer. nat.)

submitted to the faculty of Natural Sciences III  
of the Martin Luther University, Halle-Wittenberg

BY

**RAAFAT S. WASSEF**

Born on: 28.10.1967

in Cairo, Egypt

Referee:

1. Prof. Dr. Peter Wycisk
  2. Prof. Dr. Mario Schirmer
- Halle (Saale),

*But they that wait upon the LORD shall renew their strength:  
they shall mount up with wings as eagles:  
they shall run, and not be weary; and they shall walk, and not faint.*

*(Isaiah 40:31)*

---

## Acknowledgements

Let us foremost give thanks unto the Beneficent and Merciful God, our loving heavenly Father, for He has shielded, rescued, kept, supported, and brought us unto this hour.

I would like to express my deep gratitude to Prof. Dr. Peter Wycisk not only for his supervision, guidance and for providing me important data and literature, but also for his keen interest in my topic and for his continuous support and encouragement throughout the duration of this study.

I express my sincere thanks to Dr. habil. Wolfgang Gossel for educating me a lot of modeling knowledge, for his guidance, rich discussions and suggestions and for his valuable comments on the manuscript.

I express my appreciation to the Institute of Geosciences, Martin Luther University, Halle-Wittenberg for providing me many facilities to study and research and for financing the language review of the final text of my thesis.

I am very grateful to Prof. Dr. Eng. Ahmed Khater, Prof. Dr. Eng. Nahed El-Araby and Eng. Nahed Khalil for their support and discussions in the early stages of this research.

My heartiest gratitude for the wonderful contribution of the working group of hydrogeology and environmental geology: Dr. Ahmed Sefelnasr, Dipl. Geol. Ronny Lähne, Tobias Hubert, Reiner Stollberg, MSc. Jay Thakur, Christian Wolfig, Cand. Dipl. Geol. Julius Fritzsch, Michael Wagner and Ms. Daniela Rothe.

I would like also to thank gratefully the KAAD for granting me the scholarship and generously financing my study. I am also very much thankful to Mr. Hans Landsberg for being a strong intermediate “referent” between the KAAD and me.

Finally, I would like to express my genuine thanks to my family and my friends for the moral support. They stood behind me encouraging, to bring this work in its final form.

---

## Abstract

The issue of population growth is one of the most important national problems confronting the Egyptian government. The current population of Egypt is approximately 83 million with an annual increase of about 1.8 million children. If the population continues to increase at the current rates, it is expected to reach 118 million by the year 2030 and 161 million by the year 2050. On the other hand, the agricultural area is about 4% of the total area of Egypt and the per capita agricultural land is only about 2.8 carats (490 m<sup>2</sup>). Not only is there a need to decrease the rate of population increase, but there is also parallel need to increase the agricultural area and fight the desertification phenomena in Egypt. The limited availability of renewable fresh water in the groundwater aquifers in Egypt is a significant sign of the need for scientific research that studies the management of water resources. The regional area of interest in this study locates in the West of the Rosetta branch between longitudes 29° 30' and 31° 15' E and latitudes 30° 00' and 31° 30' N. It occupies an area of about 15 000 km<sup>2</sup> bounded by the Mediterranean Sea from the north and the Rosetta branch from the East. The surface of this area is characterised by a network of surface water main canals such as the Rosetta branch, the El-Rayah El-Behery, the El-Mahmoudia canal, the El-Rayah El-Nasery, and the El-Noubarya canal, which together with the surplus water from irrigation are considered the main rechargers of the groundwater aquifer systems. The subsurface of the study area is differentiated into aquifers, aquitards and aquicludes. Up to 1000 m below sea level, the study area consists of three explicit aquifer systems that were created in three different epochs. The Moghra aquifer was created in the Miocene Epoch and consists of coarse sand and gravel with intercalation of sandstone and clay. The Wadi El-Natron basin was created in the Pliocene Epoch and it is made up of alternating sand and clay with limestone at the top. Lastly, the Delta aquifer was created in the Pleistocene Epoch and consists of graded sand and gravel intercalated by clay lenses, with a large part of it is covered with a thin, semi-pervious, silty clay layer. The extraction of groundwater grows rapidly along with the expansion of the irrigational-, industrial-, and urbanized activities in the desert especially in many locations along both sides of the Cairo-Alexandria Highway where groundwater is heavily exploited. Much research has been done on the groundwater resources in the area west of the Nile Delta and has focused either on the regional groundwater hydrodynamics or on the local-scale case studies. This study is an attempt to develop a three-dimensional transient groundwater flow model for an efficient, integrated, and sustainable management plan for groundwater resources in order to evaluate the groundwater potentiality and test the alternative management scenarios for the groundwater extraction schemes in the next 50

---

years. A GIS-based model has been developed for the study area to provide analytical tools and visualization capabilities for pre and post-processing information involved in groundwater modeling. The GIS database consists of the interpolated geological and hydrogeological data in a digital elevation model of eight main layers constituting the study area up to depth of 1000 m (bmsl). The developed model was calibrated against historical groundwater heads observed since the year 1990 when development based on groundwater began to become noticeable in the study area.

## Table of Contents

Acknowledgements.....	I
Abstract.....	II
Table of Contents.....	IV
List of Figures.....	VII
List of Tables.....	XII
List of Abbreviations.....	XIII
1 Introduction.....	1
1.1 Background and motivation.....	1
1.2 Purpose and scope.....	2
1.3 Previous work.....	3
1.4 Structure of the thesis.....	7
2 Geographical Setting.....	9
2.1 Outlines and Location.....	9
2.2 Geomorphological Features.....	11
2.2.1 The alluvial plains.....	13
2.2.1.1 <i>The young alluvial plains</i> .....	13
2.2.1.2 <i>The old alluvial plains</i> .....	13
2.2.2 The structural plains.....	13
2.2.2.1 <i>The depressions</i> .....	13
2.2.2.2 <i>The folded ridges and structural plateaus</i> .....	14
2.2.3 The tablelands.....	14
2.2.4 The shifting sand.....	14
2.3 Climate and coastal processes.....	15
3 Geological Setting.....	17
3.1 Stratigraphy.....	17
3.1.1 Tertiary deposits.....	17
3.1.1.1 <i>Paleocene-Eocene deposits</i> .....	17
3.1.1.2 <i>Eocene deposits</i> .....	17
3.1.1.3 <i>Eocene-Oligocene deposits</i> .....	20
3.1.1.4 <i>Oligocene deposits</i> .....	20
3.1.1.5 <i>Miocene deposits</i> .....	20
3.1.1.6 <i>Miocene-Pliocene deposits</i> .....	20
3.1.1.7 <i>Pliocene deposits</i> .....	21
3.1.2 Quaternary deposits.....	21
3.1.2.1 <i>Undifferentiated Quaternary deposits</i> .....	21
3.1.2.2 <i>Gravel</i> .....	22
3.1.2.3 <i>Calcarenite bars</i> .....	22
3.1.2.4 <i>Protonile deposits</i> .....	22
3.1.2.5 <i>Prenile deposits</i> .....	22
3.1.2.6 <i>Neonile deposits</i> .....	22
3.1.2.7 <i>Stabilized dunes</i> .....	22
3.1.2.8 <i>Sabkha deposits</i> .....	22

	3.1.2.9 <i>Wadi deposits</i> .....	22
	3.1.2.10 <i>Sand dunes</i> .....	23
	3.1.2.11 <i>Nile silt</i> .....	23
	3.2 Major structural framework .....	23
4	Hydrogeological Setting .....	25
	4.1 Aquifer systems in Egypt .....	25
	4.2 The aquifer systems in the area of study .....	27
	4.2.1 Nile Delta aquifer .....	27
	4.2.2 Clay cap aquitard .....	29
	4.2.3 Wadi El-Natrun aquifer .....	30
	4.2.4 Moghra aquifer .....	30
	4.3 Groundwater levels and depths .....	31
	4.4 Recharge .....	32
	4.5 Discharge .....	32
	4.6 Environmental situation .....	34
	4.7 Groundwater residence time .....	34
	4.8 Aquifer parameters .....	35
	4.9 The surface water system .....	36
5	Methodology .....	41
	5.1 Introduction .....	41
	5.2 Basic equations .....	41
	5.3 Conceptualization .....	46
	5.4 Discretization .....	47
	5.5 Data processing .....	48
	5.6 Boundary conditions .....	50
	5.7 Initial conditions .....	52
	5.8 Calibration .....	53
	5.9 Validation of a model .....	55
6	Regional Model .....	56
	6.1 Introduction .....	56
	6.2 Data acquirement .....	56
	6.3 Model design .....	57
	6.3.1 GIS-Database .....	57
	6.3.2 Creation of digital maps .....	58
	6.3.3 Interpolation and layers generation .....	59
	6.3.4 Boundary conditions .....	62
	6.3.5 Initial conditions .....	63
	6.3.6 Recharge and discharge .....	63
	6.3.7 Numerical model development .....	64
	6.3.8 Discretization .....	65
	6.4 Integration of GIS - data in a groundwater model .....	68
	6.5 Calibrating the numerical model .....	68
	6.6 Regional model results .....	72
	6.6.1 Hydraulic heads .....	72
	6.6.2 Drawdown .....	72
	6.6.3 Depth to groundwater .....	80
	6.6.4 Groundwater balance .....	83
	6.6.5 The differences between the two scenarios .....	86

---

6.6.6	Effect of the extraction rates on seawater intrusion.....	88
7	Local Model.....	93
7.1	Historical introduction.....	93
7.2	Location and climate.....	93
7.3	Geomorphological background.....	95
7.4	Geological background.....	96
7.5	Hydrogeological background.....	103
7.6	Model input and structure.....	104
7.7	Model output.....	105
7.7.1	Scenario 1.....	105
7.7.2	Scenario 2.....	109
7.7.3	The conjunctive use between surface water and groundwater.....	111
7.7.4	Scenario 3.....	112
7.7.5	Scenario 4.....	114
7.8	Sustainability and feasible scenario.....	116
7.9	Up-coning effect.....	117
8	Summary and Conclusions.....	120
	Bibliography.....	126
	Appendices.....	140



**List of Figures**

Fig. 2.1: Location of the study area in Egypt (source: NASA 2005, 2006) ..... 9

Fig. 2.2: Outlines of the study area with main features and names ..... 10

Fig. 2.3: Topography of the study area. Sources: NASA 2006 & EGSMA 1950; 1990.... 11

Fig. 2.4: Geomorphology of the study area. (Compiled after RIGWA 1993 & Ibrahim 2005)..... 12

Fig. 2.5: Distribution of rainfall in the study area. (Compiled after RIGW 1992)..... 16

Fig. 3.1: Schematic geological map of the study area. Digitized from maps of CONOCO (1987)..... 18

Fig. 3.2: Lithostratigraphic cross sections along the study area as shown in the overview map. Digitized from maps of RIGW (1992 & 2006)..... 19

Fig. 3.3: General structural framework of the study area, adapted from Said (1990). ..... 24

Fig. 4.1: The aquifer systems in Egypt. Modified after RIGW (2004)..... 25

Fig. 4.2: The base levels of the quaternary aquifer. Digitized after RIGW (1992) ..... 28

Fig. 4.3: The contour lines of groundwater salinity. Digitized after RIGW (1992)..... 28

Fig. 4.4: The differences between surface water and groundwater heads. Digitized after RIGW (1980)..... 29

Fig. 4.5: Distribution of wells in the study area in year 1990 on the left and in year 2006 on the right (MWRI 1990 & 2006)..... 33

Fig. 4.6: Development of the extraction rate in the study area from 1985 to 2006 (Source: Dawoud et al. 2005 and RIGW 2006) ..... 33

Fig. 4.7: Overview of the hydraulic conductivities in the study area. .... 35

Fig. 4.8: Water levels in the Rosetta branch throughout the year. (Compiled after MWRI 1992)..... 38

Fig. 4.9: Water levels in the Edfina barrage throughout the year. (Compiled after MWRI 2007)..... 38

Fig. 4.10: Water levels in the Rayah Behery Canal throughout the year. (Compiled after MWRI 2006)..... 39

Fig. 4.11: Water levels in the Rayah Nasery Canal throughout the year. (Compiled after MWRI 1992)..... 39

Fig. 4.12: Water levels in the El-Noubaria Canal throughout the year. (Compiled after MWRI 1992)..... 40

---

Fig. 4.13: Discharge fluctuation in the canals throughout the year. (Compiled after MWRI 1992).....	40
Fig. 5.1: The effect of time increment on the simulation of the groundwater hydraulic head's decay. A solid line represents the analytical solutions and the points represent the numerical solutions (modified after Townley and Wilson 1980).....	47
Fig. 5.2: A variogram components clarify the experimental curve and the model curve. Compiled from Surfer ® 8 User's Guide (2002).....	49
Fig. 5.3: Regional flow systems representing the physical and hydraulic boundaries. Compiled after Anderson and Woessner (1992). ....	51
Fig. 5.4: Flowchart showing the major steps of calibrating a model and using it to make predictions. Adapted from Hill and Tiedeman (2007).....	54
Fig. 6.1: A spherical variogram for the bottom of the first layer.....	61
Fig. 6.2: Digital Elevation Model in relief shape for the ground surface and lower surface of the Miocene layer. ....	61
Fig. 6.3: Flowchart showing logical movement of data used to investigate the numerical model. ....	66
Fig. 6.4: Schematic map describing the structure of the layers and slices. ....	67
Fig. 6.5: Result of model calibration under transient conditions and spatial distribution of field observations in the upper aquifer. ....	69
Fig. 6.6: Histogram representing the frequency range of the residuals.....	70
Fig. 6.7: Scatter diagram showing simulated heads versus measured heads.....	71
Fig. 6.8: Hydrograph of history matching a comparison between observed and simulated heads with time. ....	71
Fig. 6.9: Distribution of the simulated hydraulic heads at the study area in the year 2010. ....	73
Fig. 6.10: Decline in the hydraulic heads in the stressed areas from 1990 to 2010.....	74
Fig. 6.11: Distribution of the simulated hydraulic heads in the study area in the year 2035 according to the extraction rates of Scenario 1.....	76
Fig. 6.12: Distribution of the simulated hydraulic heads in the study area in the year 2060 according to the extraction rates of Scenario 1.....	76
Fig. 6.13: Distribution of the simulated hydraulic heads in the study area in the year 2035 according to the extraction rates of Scenario 2.....	77
Fig. 6.14: Distribution of the simulated hydraulic heads in the study area in the year 2060 according to the extraction rates of Scenario 2.....	77
Fig. 6.15: Drawdown in the stressed areas in the year 2035 according to the extraction rates of Scenario 1 .....	78

Fig. 6.16: Drawdown in the stressed areas in the year 2060 according to the extraction rates of Scenario 1 .....	78
Fig. 6.17: Drawdown in the stressed areas in the year 2035 according to the extraction rates of Scenario 2 .....	79
Fig. 6.18: Drawdown in the stressed areas in the year 2060 according to the extraction rates of Scenario 2 .....	79
Fig. 6.19: Depth to groundwater in the year 2035 according to the extraction rates of Scenario 1 .....	81
Fig. 6.20: Depth to groundwater in the year 2060 according to the extraction rates of Scenario 1 .....	81
Fig. 6.21: Depth to groundwater in the year 2035 according to the extraction rates of Scenario 2 .....	82
Fig. 6.22: Depth to groundwater in the year 2060 according to the extraction rates of Scenario 2 .....	82
Fig. 6.23: Groundwater balance for Scenario 1 in the study area from 1990 to 2060.....	84
Fig. 6.24: Groundwater balance for Scenario 2 in the study area from 1990 to 2060.....	84
Fig. 6.25: Cumulative decrease in groundwater storage of the study area for Scenario 1 during the period from 1990 to 2060.....	85
Fig. 6.26: Cumulative decrease in groundwater storage of the study area for Scenario 2 during the period from 1990 to 2060.....	85
Fig. 6.27: Difference between the average drawdown according to the extraction rates of Scenario 1 and 2 in the year 2060.....	87
Fig. 6.28: Comparison between the cumulative decrease in groundwater storage of the study area for Scenario 1 and 2 for the period 1990 to 2060.....	87
Fig. 6.29: Salinity distribution of groundwater in the year 1990. Interpolated after RIGW (1992).....	89
Fig. 6.30: Scale dependence of dispersivity. (After Beims, 1983).....	89
Fig. 6.31: Difference in salinity due to sea-water intrusion between 1990 and 2060 according to Scenario 1. ....	90
Fig. 6.32: Difference in salinity due to seawater intrusion between 1990 and 2060 according to Scenario 2. ....	91
Fig. 6.33: Difference in salinity between Scenario 1 and Scenario 2 in the year 2060.....	92
Fig. 7.1: Mean values of the relative humidity throughout the year (Atlas, 1996).....	94
Fig. 7.2: Mean values of the temperatures throughout the year (Atlas, 1996). ....	94
Fig. 7.3: Vertical cross sections show the ground levels of the Wadi El-Natron depression. ....	95

---

Fig. 7.4: Location map of the Wadi El-Natrun depression showing the main features and topography. The topography is obtained from both the contour map 1:100,000 (EGSMA 1950) and DEM of the SRTM-03 (USGS 2004; NASA 2005). .....	96
Fig. 7.5: Wadi El-Natrun testing well. Compiled from Shata and El-Fayoumi (1967)....	102
Fig. 7.6: Location map of the Wadi El-Natrun showing the distribution of pumping wells. ....	104
Fig. 7.7: Distribution of the simulated hydraulic heads at the Wadi El-Natrun in the year 2010. ....	106
Fig. 7.8: Simulated decline in Wadi El-Natrun by 2010. ....	106
Fig. 7.9: Depth to groundwater in Wadi El-Natrun in the year 2010 .....	107
Fig. 7.10: Distribution of the simulated hydraulic heads at the Wadi El-Natrun in the year 2060 according to the extraction rates of Scenario 1 .....	107
Fig. 7.11: Simulated decline in Wadi El-Natrun by 2060 for Scenario 1.....	108
Fig. 7.12: Depth to groundwater in Wadi El-Natrun in year 2060 according to the extraction rates of Scenario 1.....	108
Fig. 7.13: Distribution of the simulated hydraulic heads at the Wadi El-Natrun in year 2060 according to the extraction rates of Scenario 2.....	109
Fig. 7.14: Simulated decline in Wadi El-Natrun by 2060 for Scenario 2.....	110
Fig. 7.15: Depth to groundwater in Wadi El-Natrun in the year 2060 according to the extraction rates of Scenario 2.....	110
Fig. 7.16: Proposed canal to Wadi El-Natrun for the conjunctive use between groundwater and surface water. ....	111
Fig. 7.17: Distribution of the simulated hydraulic heads at the Wadi El-Natrun in the year 2060 according to the extraction rates of Scenario 3.....	112
Fig. 7.18: Simulated decline in Wadi El-Natrun by 2060 for Scenario 3.....	113
Fig. 7.19: Depth to groundwater in Wadi El-Natrun in the year 2060 according to the extraction rates of Scenario 3.....	113
Fig. 7.20: Distribution of the simulated hydraulic heads at the Wadi El-Natrun in the year 2060 according to the extraction rates of Scenario 4.....	114
Fig. 7.21: Simulated decline in Wadi El-Natrun by 2060 for Scenario 4.....	115
Fig. 7.22: Depth to groundwater in Wadi El-Natrun in the year 2060 according to the extraction rates of Scenario 4.....	115
Fig. 7.23: Sketch showing the saltwater up-coning beneath a pumping well.....	118
Fig. 7.24: Rough estimation for the increase in groundwater salinity in the Wadi El-Natrun area in the year 2060 due to the up-coning effect in the Miocene aquifer according to Scenario 4. ....	119

---

Appendix 1: A Gaussian variogram for the bottom of the second layer.....	140
Appendix 2: A Gaussian variogram for the bottom of the third layer.....	140
Appendix 3: A Gaussian variogram for the bottom of the fourth layer.....	141
Appendix 4: A Gaussian variogram for the bottom of the fifth layer.....	141
Appendix 5: A Gaussian variogram for the bottom of the sixth layer.....	142
Appendix 6: A Gaussian variogram for the bottom of the seventh layer.....	142
Appendix 7: A Spherical variogram for the bottom of the eighth layer.....	143
Appendix 8: Groundwater balance for Scenario 3 at the study area for the period from 1990 to 2060.....	144
Appendix 9: Cumulative decrease in groundwater storage of the study area for Scenario 3 at the period from 1990 to 2060.....	144
Appendix 10: Groundwater balance for Scenario 4 at the study area for the period from 1990 to 2060.....	145
Appendix 11: Cumulative decrease in groundwater storage of the study area for Scenario 4 at the period from 1990 to 2060.....	145
Appendix 12: Simulated decline in Wadi El-Natrun by 2035 for Scenario 1.....	146
Appendix 13: Simulated decline in Wadi El-Natrun by 2035 for Scenario 2.....	146
Appendix 14: Simulated decline in Wadi El-Natrun by 2035 for Scenario 3.....	147
Appendix 15: Simulated decline in Wadi El-Natrun by 2035 for Scenario 4.....	147

## List of Tables

Table 2-1: Summary of the average meteorological data in the study area.....	16
Table 6-1: The different extraction scenarios (Million m <sup>3</sup> /a) for the different stressed areas. .....	64
Table 6-2: Statistics for the calibration process at the study area.....	70
Table 6.3: The average changes in hydraulic heads, drawdown and depth to groundwater for the development areas .....	75

---

## List of Abbreviations

amsl	above mean sea level
bgl	below ground level
bmsl	below mean sea level
CEDARE	Centre for Environment & Development for the Arab Region and Europe
CONOCO	Continental Oil and Transportation Company, USA
DEM	Digital Elevation Model
EGSMA	Egyptian Geological Survey and Mining Authority
ESRI	Environmental Systems Research Institute
FAO	Food and agriculture organization
FEM	Finite Element Method
FDM	Finite Difference Method
GIS	Geographic Information System
GPS	Global Positioning System
MALR	Ministry of Agriculture and Land Reclamation, Egypt
MWRI	Ministry of Water Resources and Irrigation, Egypt
NASA	National Aeronautics and Space Administration
REGWA	General Company for Research and Ground Water, Cairo
RIGW	Research Institute for Ground Water, Egypt
SRTM	Shuttle Radar Topography Mission
TDS	Total Dissolved Solids
TIFF	Tagged Image File Format
TIN	Triangular Irregular Network
UN	United Nations
UNDP	United Nations Development Program
UNESCO	United Nations Educational, Scientific and Cultural Organization
USGS	United States Geological Survey
UTM	Universal Transverse Mercator
WGS84	World Geodetic System 1984

# 1 Introduction

## 1.1 Background and motivation

Groundwater is the main source for fresh water in the desert areas that rely on it especially to achieve the country's strategic objectives to expand agricultural areas outside of the narrow Nile Valley, which represents only 4% of Egypt's area in order to overcome the problem of overpopulation. The western Nile Delta region covers the area between Cairo and Alexandria, west of the Rosetta branch, and extends westward to the desert area up to the eastern edge of the Qattara Depression. Due to its location, accessibility, and investment facilities provided by the government, this area is characterized by a rapid development based on surface and groundwater in the fields of agriculture, industry, and recreation investments.

The study area is approximately 15000 km<sup>2</sup> and includes three aquifers from the Pleistocene (Delta), Pliocene (Wadi El-Natrun) and Miocene (Moghra) periods. The groundwater of these aquifers is partially rechargeable, mainly by the leakage from the Nile River and its canals and from the infiltration and downward leakage of excess irrigation water. The study area includes development areas that depend mainly on groundwater such as Kafr Dawood, Birigat, Khatatba, South Khatatba, South Highway, North Highway, Dina, Sadat City and Wadi El-Natrun. In the year 1990, the number of wells in the study area were about 1650 wells that were extracting about 460 million m<sup>3</sup>/a. Nowadays the number of wells in the study area are more than 6500 wells that extract about 1700 million m<sup>3</sup>/a, representing an increase of approximately 270%. This increase in the extraction rates has led to a continuous decline in groundwater levels, which means that the discharge rates are more than the recharge rates.

It is necessary to draw regional views for the environmental impact in the future in order to avoid a severe decline in the groundwater levels due to the unmanaged extraction rates. Additionally, this will help to avoid degradation of groundwater quality due to either sea water intrusion or the up-coning effect from the low quality water in the underlying layers of the aquifers and protect the economic feasibility of the current investments in the study area. These views will be presented in this thesis by establishing an integrated 3D groundwater numerical model for the study area depending on a GIS-database including



the geological layers, the hydrogeological parameters, and the stress factors that affect the aquifer systems such as pumping wells, which will be represented in the numerical model individually (each well will be identified by its position and by its extraction rate). The numerical model will be used further “locally” to study the suitable scenario of water resources management for a development area within the study area.

The management goal in this thesis can be defined as the orderly utilization of aquifer reserves (of a system with some pre-existing development) with expected benefits and predicted impacts over a specific time-frame.

## 1.2 Purpose and scope

In the scope of sustainable groundwater management for the aquifer system of the study area in the western Nile Delta, the focus of this work was divided into two main tasks. The first task concerns fundamental analyses, which has the objective of understanding the physical processes of the aquifer systems. The second task is problem oriented and concerns the management decisions to be made. Related to the two main tasks are the following specific objectives:

- Establishing a GIS-database using the available data for the aquifer system. It comprises the geological and hydrogeological information from previous studies and the data of the drilled wells in the study area.
- The GIS-Database is developed to create a conceptual framework, which is considered the main step in developing a numerical groundwater flow model simulating the real hydrogeologic system. The conceptual framework includes the different assumptions which lead to the estimation or quantification of the different components of the aquifer system, including hydraulic conductivities, storativities, etc.
- Construction of a 3D numerical regional groundwater flow model for the study area to simulate the real system by using the GIS-database.
- Calibration of the groundwater flow model with the predefined criteria using numerical simulation techniques.
- Studying the effects of the current extraction rates and the full extraction rates in the development areas on the decline of groundwater levels during the next 50 years by using the calibrated 3D numerical flow model.
- Establishing a 3D transport model from the 3D flow model and studying the effects of the current extraction rates and the full extraction rates in the development areas on sea-water intrusion in the next 50 years.
- Integrating a local model for the Wadi El-Natrun area by refining the mesh (grid cells) of the calibrated regional model of the study area to involve the local details and study

the feasible scenario for the conjunctive use between groundwater and surface water in the Wadi El-Natrun depression so that it may be developed it without overtaking the permissible decline in groundwater levels in the year 2060.

- The calibrated model can be further used to determine the impact of any future planned extraction rates on the aquifer behavior.

### 1.3 Previous work

The western Nile Delta desert is a part of the great desert that stretches from the Atlantic Ocean and across the north of Africa through the Arabic Peninsula. Many researchers have investigated the geomorphology, geology, hydrogeology and hydrochemistry of the study area. Brief notes on the historical development of the most well known research works are arranged chronologically as follows:

**Pavlov (1962)** explained that the depression of Wadi El-Natrun acts as a large drain collecting groundwater from all sides with high velocity toward the lakes in the depression where the evaporation rates reaches about 16 mm/day.

**Saad (1962)** indicated that the groundwater flow direction in the western area of the Rosetta branch is from the Northeast to the Southwest, feeding in the East from the Rosetta branch and its distributaries and in the North from the Nubaria Canal.

**Said (1962)** concluded, from the drilled wells in Wadi El-Natrun, that the thickness of the Pleistocene and Pliocene deposits together is about 335 m and noticed that there are lateral changes in the lithofacies in the area between Qattara Depression and Wadi El-Natrun, where the Marmarica limestone is laterally changed into sandy limestone facies.

**Shata (1962)** pointed out that in Wadi El-Natrun, both the Pliocene and Miocene deposits have a thickness of about 200 m. The Pliocene deposits differentiated into two parts; the upper part is dominated by calcareous grit and quartz sand, and the lower part is dominated by green, sandy clay. The Miocene deposits are dominated by coarse and fine-grained sand and the base is gravelly.

**El-Fayoumy (1964)** differentiated the groundwater aquifers that cover the area between Wadi El-Natrun and Nile Delta into three parts. The first part on the top consists of sandy deposits with a thickness of about 10 m; the second part is from the Pleistocene Epoch and is made up of sandy and gravelly deposits with a thickness of about 100 m; and the third part is further classified into three parts. The first is a Pliocene succession developed into loose sand, sandstone, and clay with about 70 m thickness, the second consists also of

Pliocene deposits developed into loose sand of shallow marine with about 50 m thickness, and the third is built by the Miocene sandy beds of about 200 m thickness.

**Hall and Dracup (1970)** proposed some factors for optimal management of a groundwater basin such as the safe yield, the annual volume of natural recharge, the volume of reserves, the long-term storage capacity, the transmission system, the water quality and the energy required for normal and/or modified pumping lift that is necessary for water level fluctuation.

**Shata et al. (1970)** concluded that the area between the Nile Delta and Wadi El Natrun is a part of the old deltaic plains, and the Pleistocene aquifer in this area is made up of deltaic sediments with a thickness of about 300 m near the Nile Delta, and it vanishes in the eastern part of Wadi El-Natrun.

**Idris (1970)** pointed out three sources of recharge in the Wadi El Natrun aquifer system: The first is infiltration from the Nile Delta groundwater aquifer, the second is seepage from irrigation water, and the third is infiltration from the western side of Wadi El-Natrun where the groundwater levels are higher than in it.

**El Etr and El Baz (1979)** concluded with help of satellite images that Wadi El-Natrun is developed by water erosion in Pluvial periods and modified by later (sub-recent) arid deflation.

**Diab et al. (1980)** concluded, using the available surface and subsurface geological data in the area along Cairo-Alexandria Highway to the axis south of Wadi El-Natrun, that the Pliocene deposits are made up of quartzitic sands and clay with a thickness up to 165 m, and the Quaternary deposits made up of deltaic and fluviomarine deposits with undifferentiated thickness.

**Swailam et al. (1980)** recognized by using Tritium analysis that the groundwater aquifer system in Wadi El-Natrun is recharged from the Nile Delta with a traveling time of about 25 year from the southern, southeastern and northeastern directions.

**Mustafa (1982)** studied the location of the interface between seawater and fresh water in the Nile Delta Quaternary aquifer using an analytical one-dimensional steady state model.

**Abdel Baki (1983)** established a groundwater contour map for the Pleistocene aquifer system and clarified that the flow direction west of the Nile Delta is from east to west direction and the average transmissivity of the aquifer is  $58.2 \times 10^{-3} \text{ m}^2/\text{sec}$ .

**Farid (1984)** discussed the different plans for development of groundwater in the Nile Delta region and its impact on sea water intrusion, using a dynamic management program linked to a one-layer finite element simulation program under steady state and transient conditions and presented the position and shape of interface between sea water and fresh water.

**Abu-Zied (1991)** concluded that the groundwater aquifer in Nile Delta is recharged by deep percolation from canals and drainage systems and the capacity of the aquifer is about 300 km<sup>3</sup>, with an average salinity in Cairo of about 500 ppm increasing to 5000 ppm near the Mediterranean coastal zone due to the effect of salt water intrusion from the sea.

**Matsukawa et al. (1992)** studied the optimal conjunctive use management policies where surface and ground water resources can be described in a simulation model linked with a non-linear large scale programming algorithm for optimization and concluded that the model minimizes the total operational cost of groundwater pumping by choosing the suitable areas for digging extraction wells.

**Research Institute of Groundwater, RIGW/IWACO (1992)** studied the possibilities of developing the groundwater in the Nile Delta aquifer system and recommended three main strategies. The first is a long-term strategy by pumping against current drainage surplus year round; the second is a seasonal strategy by pumping against annual current drainage surplus during six months of the year; and the third is an inter-annual strategy by pumping with a maximum possible capacity for at least five successive years. The pumped water in each strategy was recommended for use in conjunction with surface water in irrigation.

**Fekry (1993)** concluded that the lowering in groundwater heads south and east of Wadi EI-Natron will be from 10 m to 15 m in the coming 50 years due to the rapid increase in the reclamation projects.

**Mostafa (1993)** studied the geological and hydrogeological aspect of the Moghra aquifer system and estimated that the recharge of the aquifer is about  $84 \times 10^6$  m<sup>3</sup>/year from the Nile Delta in the East and from EI- Tahrir province in the Northeast.

**Gomma (1995)** studied the hydrochemical aspects of the Pleistocene and Pliocene aquifers west of the Nile Delta, and classified the Pleistocene aquifer into three water types (sodium-bicarbonate, sodium-chloride and sodium-sulphate) and the Pliocene aquifer into two water types (sodium-bicarbonate and sodium chloride).

**Hassaneen et al. (1997)** indicated, by using geoelectrical survey at the study area between km 114 and km 116 of Cairo-Alexandria desert road, that there are three fault systems forming a small structural basin where the lacustrine deposits are accumulated to a depth of about 100 m and below it the Pliocene aquifer.

**Ahmed (1999)** estimated from using the isotopes in groundwater at the area of Wadi EI-Natrun and Sadat City that the groundwater in the Pliocene aquifer may be mixed with waters of deeper aquifers.

**Ibrahim (2000)** reported that groundwater levels in the year 1999 at the area south of El-Khatatba Road in Wadi EI-Farigh, ranged from -2.00 m (amsl) to -4.00 m (amsl) and the cone of depression reached to -7.00 m (amsl) since 1996.

**Youssef (2000)** noticed that the geoelectrical succession up to a depth of 250 m in Wadi EI-Farigh is made up of four geoelectrical layers. The first, from the Miocene Epoch, is dry and consists of sand and gravel with clay intercalations, and its thickness ranges from about 30 m to 104 m. The second is a water bearing layer of the Miocene aquifer, consisting of coarse sand and clay with a thickness that ranges from about 14 m to 167 m. The third is made up mainly of basalt from the Oligocene Epoch with an average thickness of about 28 m. The fourth layer is to some extent a water bearing layer from the Oligocene Epoch that consists of sand and ferruginous sandstone with clay intercalations.

**El Sheikh (2000)** studied the flow direction of the groundwater at the area and concluded that the groundwater flow direction is from east to west toward Wadi EI-Natrun through the old alluvial plain and from the EI-Nasr canal in the north to the south.

**Mohamed (2002)** produced a land use map for the study area in the western Delta at two dates in 1987 and 1998 and detected the changes in the irrigated areas between the two dates using remote sensing techniques, and evaluated the impact of these changes on the groundwater.

**Dawoud et al. (2005)** presented a GIS based model for the aquifer system at a study area west of the Nile Delta using the numerical program package TRIWACO for simulation. He pointed out that the improvement of the irrigation system would decrease the annual aquifer potentiality by approximately 91% due to the decrease in the infiltration rates.

**Soliman et al. (2005)** compared the analysis of two satellite images in 1987 and in 1998 using remote sensing and geographic information system technology for studying the land reclamation expansion in the west Nile Delta region and observed a high rate of increasing

cultivated areas reach to 310% east of Wadi El-Farigh. He recommended evaluating the impact of this increasing rate on the aquifer system in the present and future with a numerical groundwater flow model.

**Gaame (2005)** evaluated the design of wells west of Nile Delta region with an emphasis on the Wadi El-Natron and Wadi El-Farigh areas, and concluded that the quality of groundwater had deteriorated in these areas due to over-pumping, poor well design and the return groundwater flow phenomenon.

**Ibrahim (2005)** established management criteria and decision supporting maps for the sustainable development of groundwater resources in the study area in Wadi El-Farigh using remote sensing and geographic information system techniques for two satellite images in 1993 and 2002. He concluded that the groundwater level decline in the Miocene aquifer is around 1m/year, and recommended that the aquifer system in the area should be subjected to a proper mathematical model.

#### 1.4 Structure of the thesis

This thesis is composed of eight chapters as follows:

**Chapter One** is a general introduction. It introduces a general background on the problem, an overview of the well-known previous works, the objectives, and the ideas behind this research.

**Chapter Two** sets the scene within the study area by describing the outlines, location, and important regional physical setting controlling the area of interest in terms of the geomorphological features and climate.

**Chapter Three** produces the geological settings of the study area, discusses the lithological as well as the stratigraphic units composing the study area, and presents the major structural framework.

**Chapter Four** describes the hydrogeology of the study area. The purpose is to characterize the structure and the properties of the system, to provide a hydrogeologic framework, and to develop a conceptual model. It delineates the extension, boundaries, subunits, and basins of the study area and presents the aquifer systems in Egypt, the environmental situation, sources of groundwater in the aquifer, recharge and discharge, a discussion of the hydraulic parameters, and the surface water systems in the study area.

**Chapter Five** highlights and debates the concept and proposed computation methodology of groundwater flow modeling.

**Chapter Six** investigates the procedure of creating a GIS-database and the development of a coherent, reliable conceptual model for the study area. The boundary conditions, initial conditions, as well as the calibration of the regional groundwater flow model of the study area are characterized and delineated. In addition, the results of the regional groundwater flow modeling in terms of the decline of the hydraulic head, depth to groundwater and the effect of the extraction rates schemes on seawater intrusion are introduced, examined, and interpreted in this chapter.

**Chapter Seven** scopes the Wadi El-Natrun at the regional flow model within the study area. The groundwater management options are investigated and discussed in terms of studying the impact of applying different groundwater extraction schemes on the aquifer behavior in addition to studying the effects of using the conjunctive use between surface water (through a proposed canal) and groundwater in irrigation at Wadi El-Natrun.

**Chapter Eight** integrates the information from the preceding chapters into a final discussion and presents conclusions regarding the main problems addressed in the thesis.

# 2 Geographical Setting

## 2.1 Outlines and Location

The study area lies in the western area of the Rosetta branch, in the area between Cairo and Alexandria and covers an area of about 15 000 km<sup>2</sup>. It extends from latitude 30° N to 31° 30' N and from longitude 29° 30' E to 31° 15' E (Fig. 2.1), with an average east-west extension of about 120 km and an average north-south extension of about 125 km.

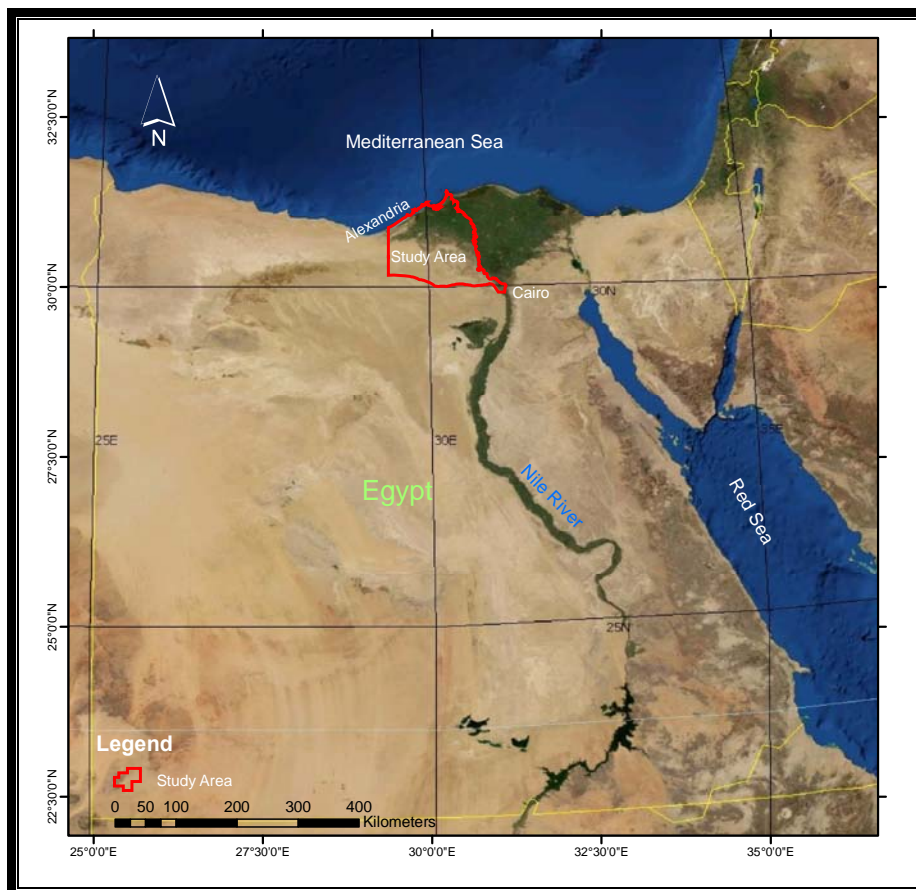


Fig. 2.1: Location of the study area in Egypt (source: NASA 2005, 2006)

The northern boundary of the area is the Mediterranean Sea, Edku Lake, and Maryout Lake. The study area includes a net of irrigational canals within its eastern and northern portion. The main canal is the Rosetta branch of the Nile River at the eastern boundary. Two parallel canals (Rayah Behery and Rayah Nasery) that have two intakes from the Rosetta branch near Cairo. The El-Noubaria canal begins at the end of Rayah Nasery canal



and its outlet lies in Maryout Lake. Elkhandak canal starts as an extension of Rayah Behery canal and ends at El-Mahmoudiya canal. Both the El-Nasr and the Bustan canals are fed by surface water from the El-Noubaria canal through pumping stations. About 31% of the study area is traditionally cultivated, 26% is barren desert, 13% was planned to be irrigated by surface water, about 14% was planned to be irrigated by groundwater and about 3% is irrigated by the conjunctive use of surface and ground water. The remainder of the study area, about 13%, is non-irrigated areas. The areas which were assumed to be irrigated by groundwater lie around the Desert Highway between Cairo and Alexandria, such as Kafr Dawod, Tahadi, Brigat, South Tahrir, Khatatba, South Khatatba, South and North Highway, Dina farm with its extension, Wadi El-Farigh and Wadi El-Natrun (Fig. 2.2). The climatic features of the study area also led to favorable conditions for agricultural development and attracted many investors to cultivate the land.

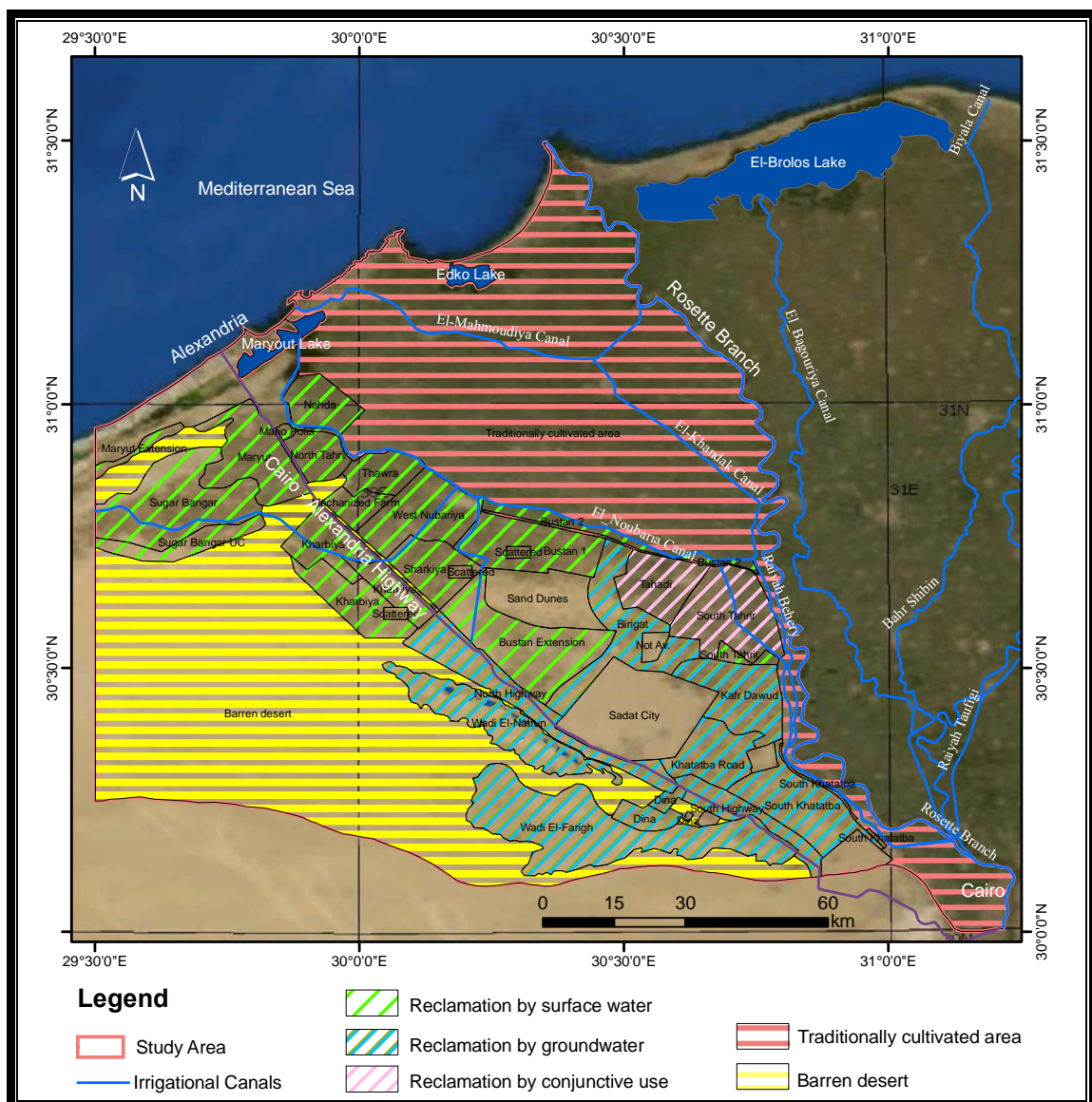


Fig. 2.2: Outlines of the study area with main features and names

### 2.2 Geomorphological Features

There is a wide variation in the landscape and the elevations of the study area where it is bounded from the South by a series of highlands up to 200 m above sea level, consisting of folded ridges and structural plateaus. On the other hand, it includes two main features, Wadi El-Farigh southeast of the study area with about 600 km<sup>2</sup> and the Wadi El-Natron depression in the middle of the study area of about 273 km<sup>2</sup>. One of the conspicuous features in the Wadi El Natrun depression are the natural water lakes located at about 23.00 m below sea level (Fig. 2.3).

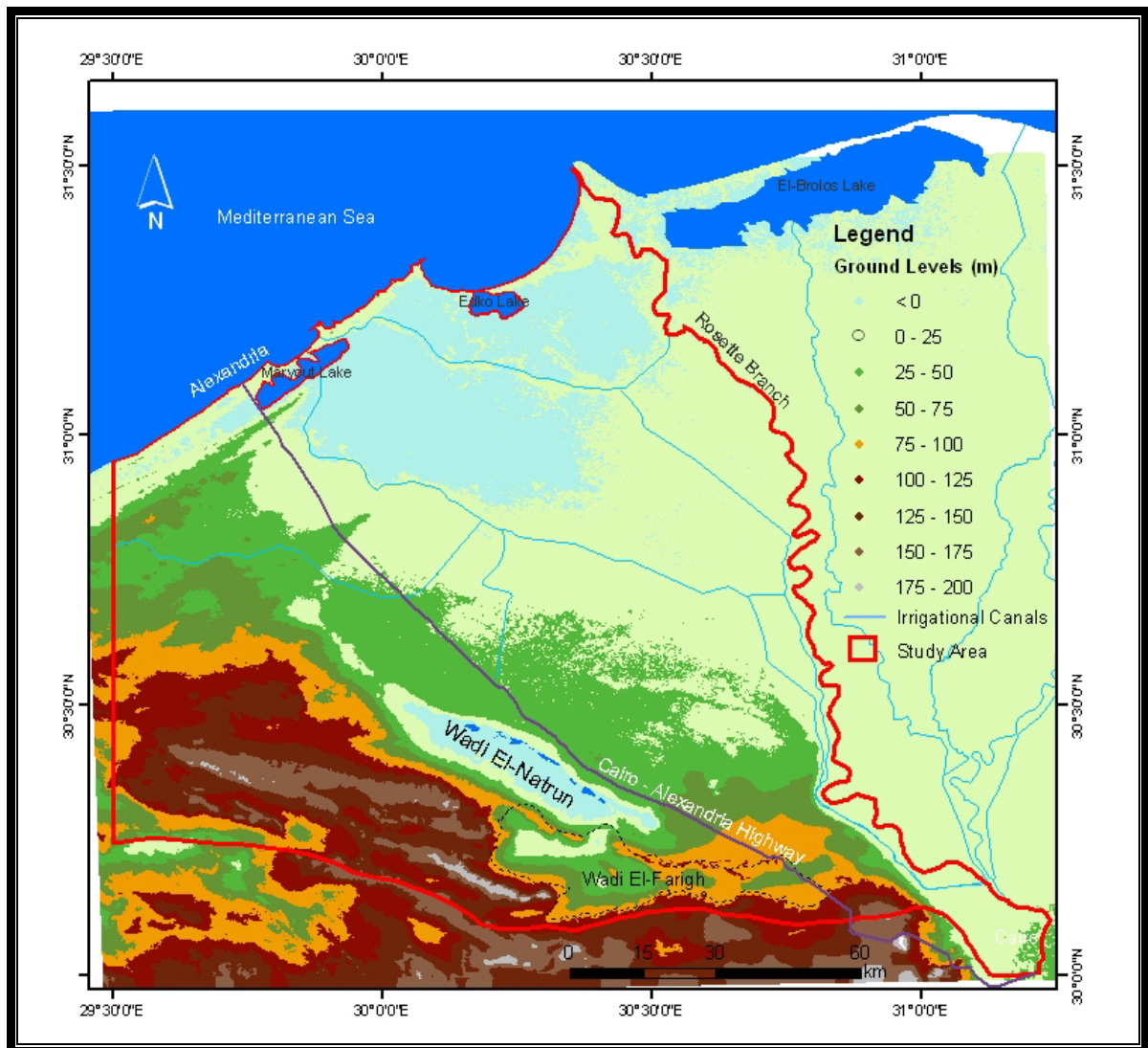


Fig. 2.3: Topography of the study area. Sources: NASA 2006 & EGSMA 1950; 1990.

According to Shata (1962), Shata et al. (1970), Attia (1975), Omara and Sanad (1975), Abdel Baki (1983) and Shieded (1989), the area can be divided into four geomorphological units (Fig. 2.4):

- The alluvial plains
- The structural plains
- The tablelands
- The shifting sand

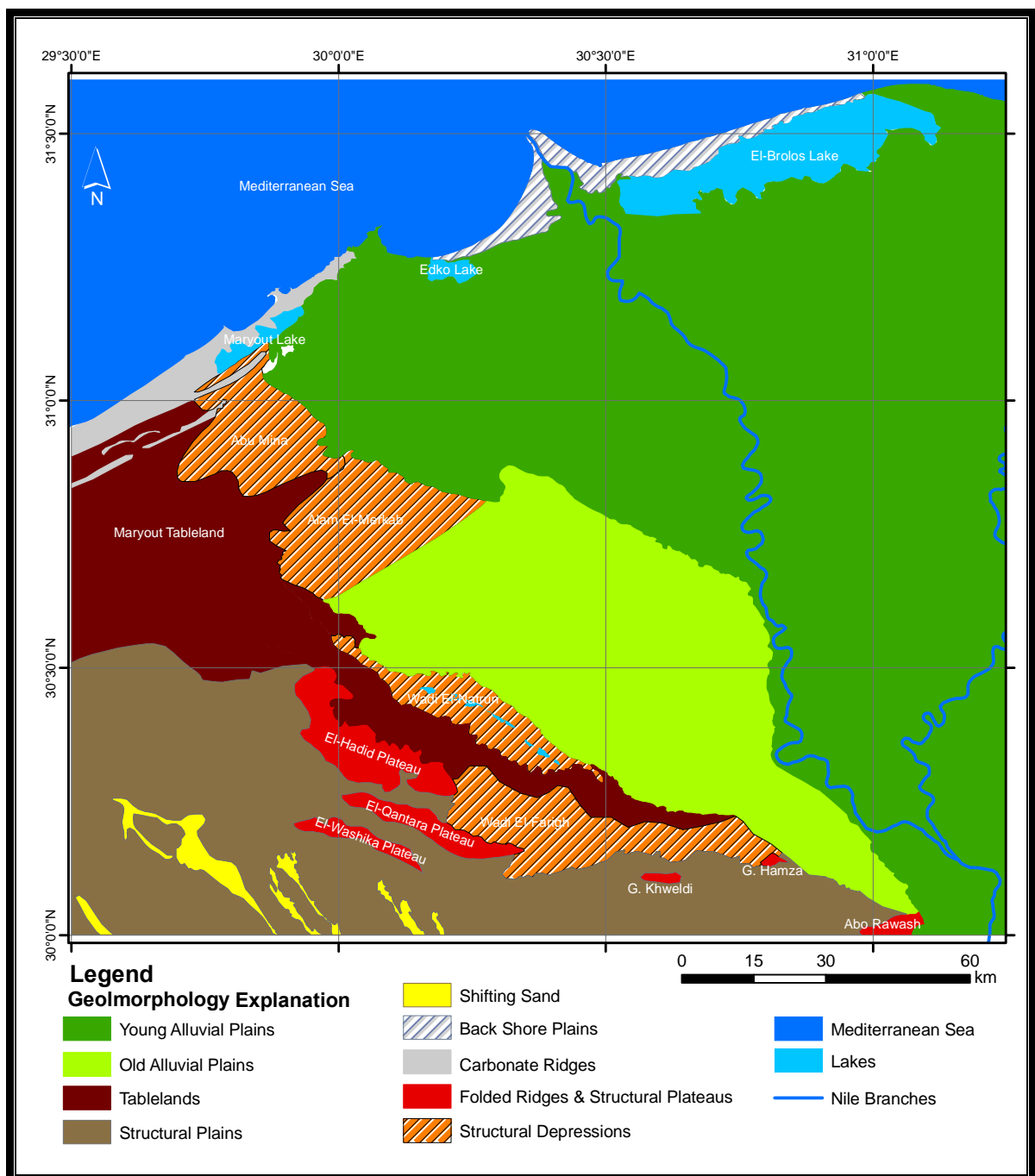


Fig. 2.4: Geomorphology of the study area. (Compiled after RIGWA 1993 & Ibrahim 2005)

### **2.2.1 The alluvial plains**

The alluvial plains extend between the Rosetta branch and the eastern borders of Wadi El-Natroun and are mainly differentiated into young and old alluvial plains as explained by the following two points.

#### **2.2.1.1 *The young alluvial plains***

The young alluvial plains are covered mostly by the cultivated lands in the Delta and consisting of recent silt and loam deposited by floods of Nile River. The young alluvial plains extend from the Rosetta branch toward the El-Raiyah El-Behery at the West and from the El-Noubaria Canal toward the Mediterranean Sea in the North. The surface is nearly flat with an elevation of about 21 m (amsl) at the Southeast and gradually decreases towards the North and Northwest with an average gradient of about 10 cm/km.

#### **2.2.1.2 *The old alluvial plains***

The old alluvial plains are bounded by the young alluvial plains in the East and North and by the depression of Wadi El-Natroun in the West. The old alluvial plains consist of dark brown gravels and coarse sand. The elevation varies from 20 m (amsl) near the El-Raiyah El-Behery to 40 m (amsl) near the depression of Wadi El-Natroun.

### **2.2.2 The structural plains**

The structural plains are limited from the East and Northeast by the old alluvial plains. The landscape of these plains consists of depressions, a number of alternating folded ridges, and structural plateaus as explained by the following two points.

#### **2.2.2.1 *The depressions***

The main depressions are Wadi El-Natroun and Wadi El-Farigh. Wadi El-Natroun is oriented in a NW-SE direction between the latitudes 30° 17' and 30° 33' N and between longitude 30° 02' and 30° 30' E. Its length is about 55 km, and it is narrow at both ends (about 1.9 km) and wider in the middle (about 9 km). The lowest level in Wadi El-Natroun lies 23 m below sea level and its main characteristics are a series of about 20 small disconnected lakes. About half of the lakes are relatively larger in size and have permanent water reservoirs in all or some of their parts, while the other lakes become dry during the summer months. The largest lakes are Lake Al-Gaar on the northwest side of the depression and Lake Umm Risha in the Southeast direction. The level of the water in these lakes fluctuates seasonally, becoming higher in winter and lower in summer.

Water enters the Wadi El-Natroun by two means: as springs in some of the lakes, like the one found in Lake Hamara and as very small streams on the sloping edges of the lakes.

The main geological feature is the Wadi El-Natrun anticline, which trends in a northwest direction for about 35 km, from Ras El-Solymania in the North to the Deir Macarious in the South. A large part of this depression is underlain by soft deposits dominated by gypseous sandy clays and sands that belong to the Middle Pliocene Age.

The Wadi El-Farigh depression lies south of Wadi El-Natrun having a length of about 80 km and an average width of about 7 km. This depression is regionally oriented in the E-W direction and its ground elevation goes down to 4 m below mean sea level at the northeastern part. The main escarpments bounding the depression on the northern and southern sides (monoclinical edges) have an average elevation of about 100 m (amsl) and are underlain by hard sandy conglomeratic and flinty limestone (Pliocene).

#### **2.2.2.2 *The folded ridges and structural plateaus***

The height of folded ridges and structural plateaus range from about 25 m to about 200 m (amsl) as follows: Gebel Khashab synclinal ridge (25 m amsl), Abu Roash folded ridge (200 m amsl), El-Khweldi - Gebel Hamza synclinal plateau (110 m amsl to 193 m amsl), El-Washika plateau (190 m amsl), El-Hadid plateau and El-Quantara plateau (180 m amsl). Most of the ridges are covered with a gravelly layer derived from sedimentary and igneous rocks dominating the eastern highlands. The surface of most plateaus is underlain by ferruginous sandstone (Miocene), and conglomeratic limestone (Early Pliocene).

#### **2.2.3 The tablelands**

The tableland is described as an area of highlands usually consisting of relatively flat rural terrain. In the study area the tablelands are differentiated into Maryut tableland at the Northwest of the study area and its extension south of Wadi El-Natrun, the marginal tableland.

#### **2.2.4 The shifting sand**

A series of elongated sand dunes south of the study area are named El-Heneishat; it is controlled by the northwest wind direction.

### 2.3 Climate and coastal processes

The main feature of the Egyptian climate is the almost uniform aridity. The climate is characterized by a long, dry summer and a short temperate winter with a maximum temperature of about 36°C and a minimum temperature of about 6°C.

The rainfall period ranges from October to March (Saleh, 1980) with a mean annual rainfall that increases from 25 mm/a in the Southeast of the study area to about 200 mm/a in the Northwest of it as shown in Figure 2.5.

The relative humidity ranges from 62 % to 75 % in the evening and from 32 % to 54 % at noon. The average wind speed ranges from 4.8 km/h at Wadi El-Natron to 15.7 km/h at Alexandria with a prevailing wind direction toward the Northwest in the summer and toward the West to Southwest in the winter. Owing to the large expanse of the desert, Egypt is exposed in the spring to hot dry sand-winds called “Khamasin” with a wind speed reaching more than 100 km/h in the desert.

The Nile Delta coast is influenced every year by an average of 17 major storms, called “nawat”. The wind speeds during these storms are more than 50 km/h for at least one hour. In general, the storm season extends from September to July and those with high intensity occur from November to March.

The area is characterized by a high rate of evapotranspiration. The average actual evapotranspiration intensity in the study area decreases from about 9 mm/day in the south to about 4.4 mm/day in the north and from summer to winter.

The average meteorological data were provided by the Egyptian Meteorological Authority from six metrological stations in Giza, Shibin El-Kom, El-Tahrir, Wadi El-Natron, Damanhour and Alexandria. The climatic elements of the study area are summarized in Table 2.1.

The Nile Delta coast is affected by a wave regimen that varies with the seasons (Fanos 1996). In spring the average wave height is 0.4 m with a predominant NW wave direction. In winter the average wave height is 0.5 m with a predominant NNW wave direction. The maximum-recorded wave height was 4.45 m during the winter months, while the significant wave height was 1.04 m. The peak and significant wave periods are 12.3 and 6.2 s, respectively (El Banna 2007). The tide along the coast is semi-diurnal with a range in the order of 25 to 30 cm (Fanos 1992).

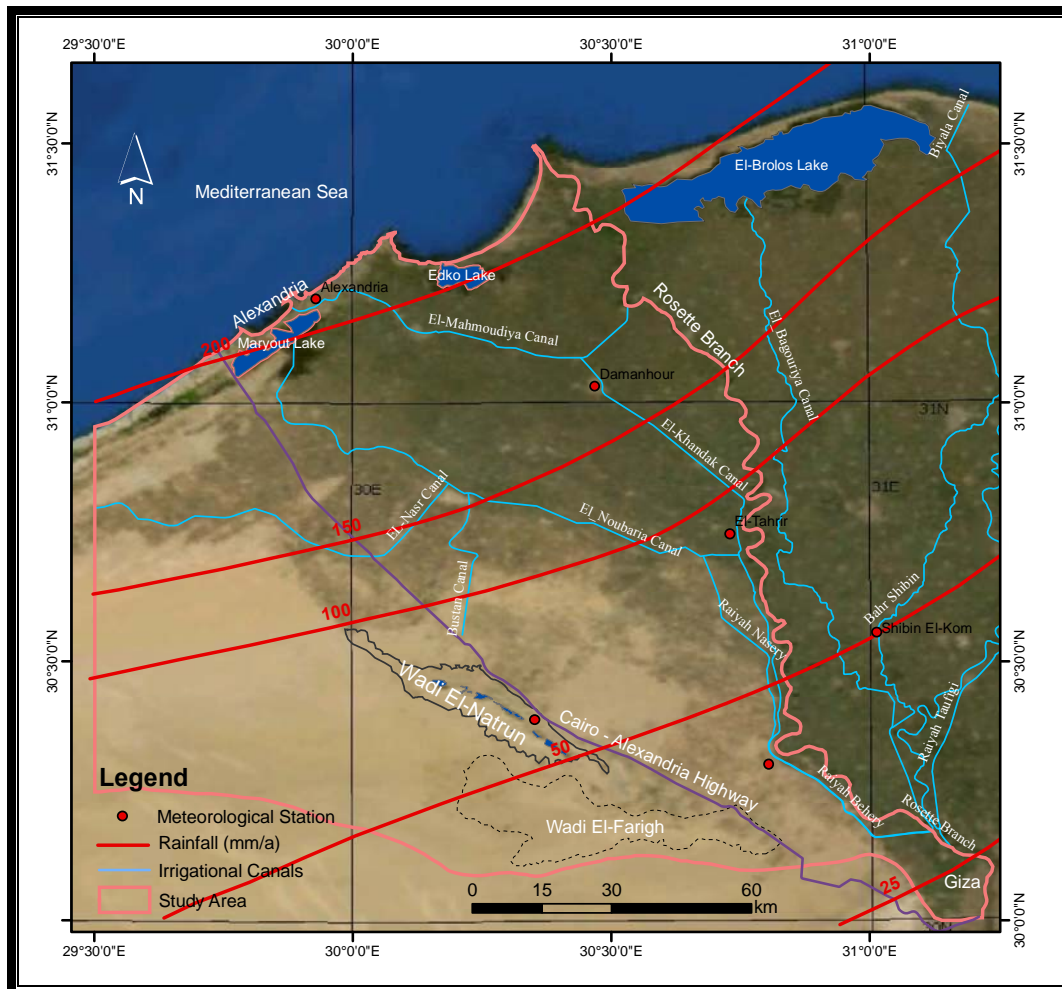


Fig. 2.5: Distribution of rainfall in the study area. (Compiled after RIGW 1992)

Table 2-1: Summary of average meteorological data in the study area.

Station	Temperature (°C)		Relative Humidity	Evapotranspiration	Rainfall
	Max.	Min.	(%)	(mm/day)	(mm/a)
Giza	35	7.6	59.7	8.8	41.8
Wadi El-Natrun	35.7	8	53.7	9.6	55.1
Shibin El-Kom	34.4	6.6	57.5	8.6	48.2
El-Tahrir	35	6	69.2	6.6	92.6
Damanhour	32.8	7.8	61.5	4.4	163.2
Alexandria	33	9.2	63.4	5	201.7



# 3 Geological Setting

The region in the west to the Rosetta branch was the subject of many geological studies of varying scales. These studies presented modern knowledge about the geology of western Delta. Among the relevant studies in the area, the following are of particular interest: Shata (1955), La Moreaux (1962), Said (1962), Shata (1962), Shata et al. (1970), Attia (1975), Omara and Sanad (1975), Abdel Baki (1983) and Shieded (1989).

## 3.1 Stratigraphy

The geological map published by CONOCO in 1987 (Fig. 3.1) and the lithostratigraphic cross sections published by RIGW in 1992 and 2006 (Fig. 3.2), describe the different lithostratigraphic units forming the body of the study area and aquifer systems. These units are covered with extensive exposures of sedimentary rocks ranging from the early Miocene to the Holocene ages and are hereafter presented from the oldest to the youngest layers.

### 3.1.1 Tertiary deposits

Regarding the deep wells and the geophysical survey at the study area the Tertiary deposits were studied and differentiated into five stages.

#### 3.1.1.1 *Paleocene-Eocene deposits*

The first subsurface deposit, located in the Southeast of the study area in a depth of about 600 m, is called the Esna formation. It consists of a Paleocene to lower Eocene sandstone and clay, intercalated with thick bands of marl with increasing carbonates. The average thickness of this formation is about 300 m (Cherif et al. 2006). The second deposit, which overlays the Esna formation is named Apollonia formation. It is made up of a limestone unit that is occasionally dolomitic or chalky with an average thickness of 450 m (Said 1962 & Said 1990).

#### 3.1.1.2 *Eocene deposits*

The Eocene deposits appear on the ground surface outside the Southeast corner of the study area. The formation is named the Maadi formation, and it consists of shallow marine shale with intercalations of limestone and minor sandstone with an average thickness of about 70 m (Said 1962).



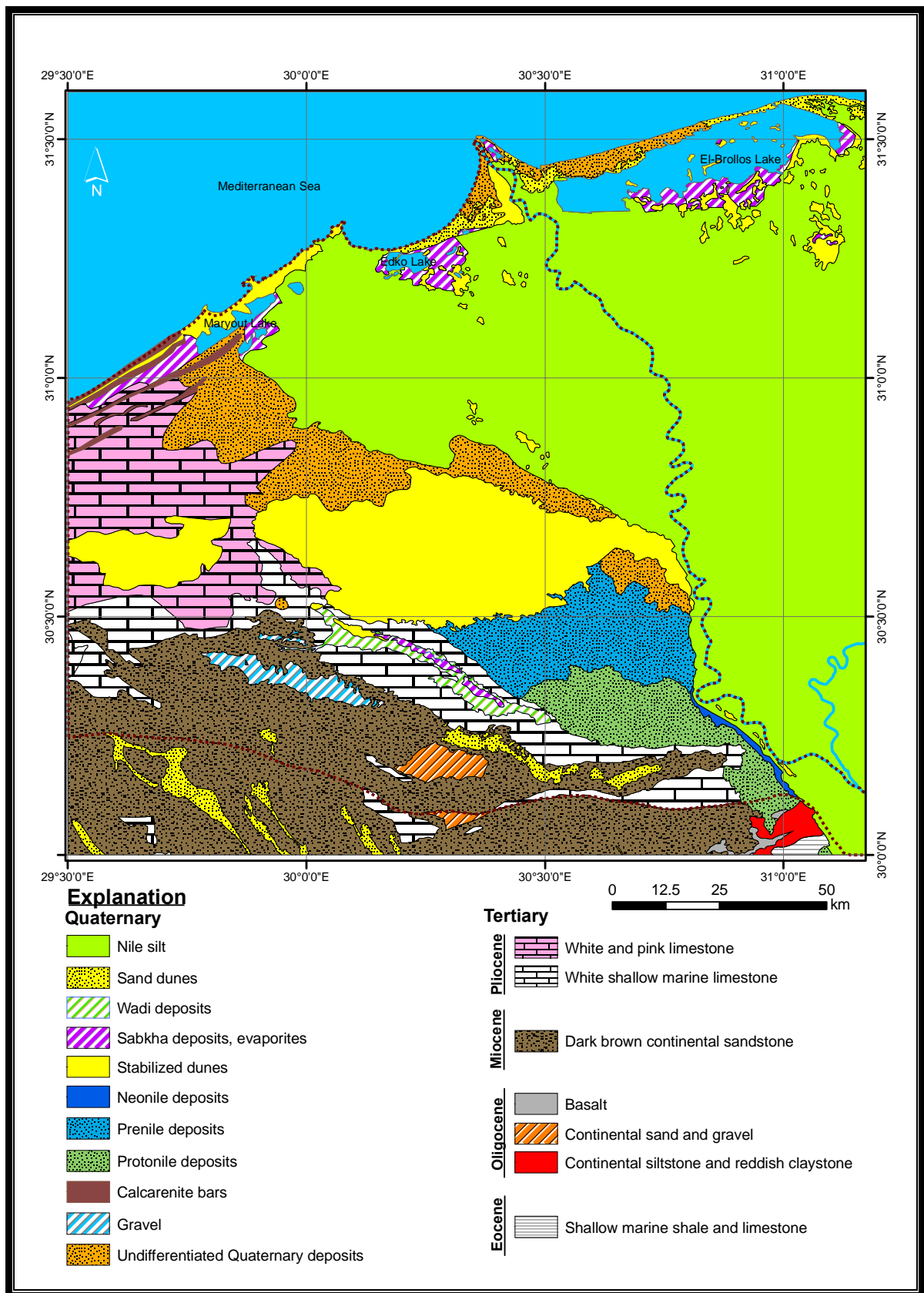
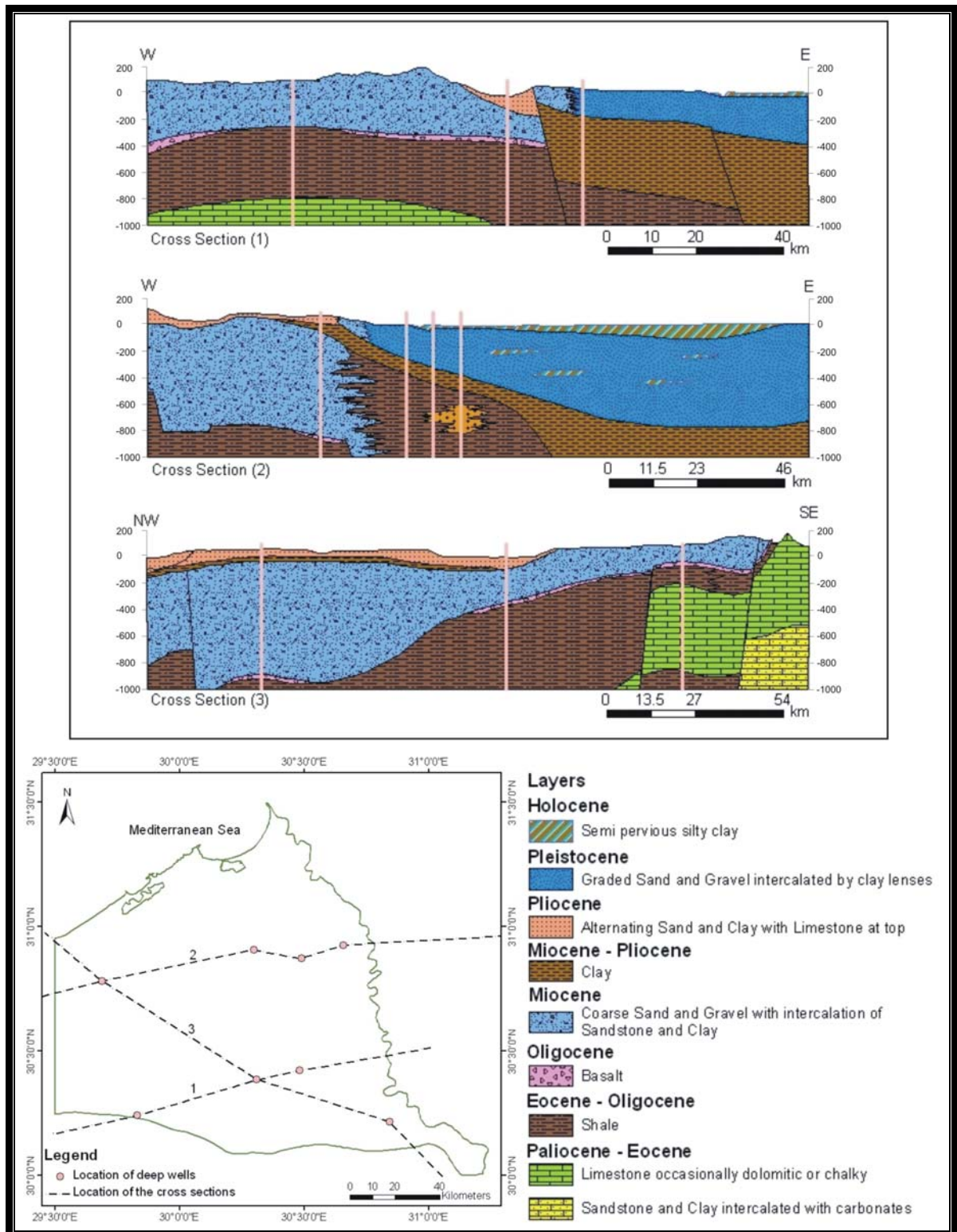


Fig. 3.1: Schematic geological map of the study area. Digitized from maps of CONOCO (1987).



**Fig. 3.2:** Lithostratigraphic cross sections along the study area as shown in the overview map. Modified after RIGW (1992 & 2006).

### 3.1.1.3 *Eocene-Oligocene deposits*

A subsurface unit of upper Eocene-Oligocene marine shale named the Dabaa formation is made up of light grey to greenish shale with subordinate thin beds of limestone, and rests on the Apollonia formation (Limestone unit from the Paleocene - Eocene) with minor disconformities and a sharp contact, with an average thickness of 400 m (Said 1990).

### 3.1.1.4 *Oligocene deposits*

The Oligocene deposits can be differentiated into three main lithostratigraphical units in the study area (Hermina et al. 1989).

- The first unit appears on the surface at the South of the study area where the Oligocene deposits developed into vividly colored sands and gravel in what is called the “Gebel Ahmer” formation with an average thickness of 50 m.
- The second unit, located in the Southeast of the study area, is called the Gebel Qatrani formation. It appears on the surface and consists of burrowed siltstone and reddish claystone with minor carbonate lenses and carbonaceous shale. The average thickness of this unit is about 250 m.
- The third unit is basalt from the Oligocene. It appears on the surface at the Southeast of the study area and in the subsurface between the Moghra formation and the Dabaa formation separating the Miocene and Oligocene-Eocene deposits at different locations in the South and Southwest of the study area, with an average thickness of about 30 m.

### 3.1.1.5 *Miocene deposits*

The Miocene deposits appear on the ground surface at the South of the study area forming the Moghra formation. It is made up mainly of variegated sandstone with fossil wood and vertebrate remains in its lower part followed upwards by marly sandstone, yellow marl with gypsum veins, and conglomeratic nodular limestone, with frequent shale intercalations that increase to the West. The average thickness of the formation is about 203 m (Said 1962) and becomes thinner towards the west, where it reaches a thickness of about 57 m. The Miocene deposits forming the Gabal Khashab formation in the Wadi El-Natrun, which is made up of vividly colored unfossiliferous sand and gravel.

### 3.1.1.6 *Miocene-Pliocene deposits*

This formation is named the Mikheimin. It is built up of gray to yellowish gray, moderately hard to hard conglomeratic sandstone and conglomerate. It underlies unconformably the Gar El-Meluk formation and overlies the Gabal Khashab formation. The average thickness of this formation in Wadi El-Natrun is about 30 m.

### 3.1.1.7 *Pliocene deposits*

The Pliocene deposits can be differentiated into three lithostratigraphical units that appear on the surface.

- The first unit, the Hagif formation, appears at the eastern side of Jabal Al Hagif in the Northwestern desert. It has a thickness that varies from 30 to 40 m and begins at the base with loose quartzitic, medium grained, well-sorted and cross-bedded sandstone with claystone streaks. The sand is topped by a fossiliferous limestone sequence, which is hard and massive at the base. The middle part of the succession consists of gray sticky and massive claystone followed by grayish-white, fine-grained argillaceous sandstone. The upper part of the succession is made up of a white, massive, moderately hard, fossiliferous limestone bed, followed by a 7 m thick bed of a crystalline gypsum sequence displaying a glassy luster (Omara and Sanad 1975).
- The second unit, named the Hamzi formation appears at 35 km northwest of Cairo. It has an average thickness of 35 m consisting of white shallow marine limestone having the appearance of statuary marble. Its base is always marked by a conglomerate bed consisting mostly of limestone fragments (Sandford and Arkell 1939).
- The third unit, the Gar El-Meluk formation, forms most of the rocky hills protruding the floor of the Wadi El-Natron Depression. It consists mainly of thick, gray, laminated to massive claystone intercalated with fine, well-sorted sandstone. Few yellowish-white limestone bands are recorded in the upper part of the succession. In the North, the rock unit tends to become gypsiferous, i.e. it changes to a lagoonal facies (Cherif et al. 2006). The average thickness of the formation is about 90 m.

### 3.1.2 **Quaternary deposits**

The Nile Delta aquifer comprises the Quaternary alluvial deposits, which consist of Pleistocene sands and gravels with some intercalations of clay lenses. The average thickness of the aquifer is 500 m and decreases gradually towards the west.

The aquifer is semi-confined in the Delta and Nubaria area, where it is overlain by a Holocene layer of sandy clay and silt and loamy deposits. The Quaternary deposits that appear on the surface of the study area (Fig. 3.1) were studied and classified as follows:

#### 3.1.2.1 *Undifferentiated Quaternary deposits*

Some areas at the northern and eastern border of the Nile silt deposits are made up of alluvial fans, Wadi deposits, sand, gravel and recent coastal deposits.

### 3.1.2.2 *Gravel*

The gravel deposits are located at an area southeast of the Wadi El-Natron (Hermina et al. 1989).

### 3.1.2.3 *Calcarenite bars*

The Oolitic detrital limestone builds a number of elongated bars parallel to the coast named the Alexandria formation from the Pleistocene age. Lagoonal marl and gypsum separate the calcarenitic bars. The carbonate granules were formed under water and transported inland by the retreat of the sea and by the action of the wind. They represent fossil off-shore bars (Hermina et al. 1989).

### 3.1.2.4 *Protonile deposits*

The Protonile deposits were built by two rivers, the Prenile and the Neonile. These deposits consist mainly of the gravel-sized quartzite of the Idfu formation and the conglomerates of the Arment formation of the early Quaternary (Hermina et al. 1989).

### 3.1.2.5 *Prenile deposits*

The deposits of the Prenile are made up of massive cross-bedded fluvial sands interbedded with dune sand (Hermina et al. 1989).

### 3.1.2.6 *Neonile deposits*

The Neonile deposits take place at the western edge of the Rosetta branch in the Southeast region of the study area. These deposits made up of silt, fine sand and gravel, constituting low terraces skirting the cultivated land of the Nile Delta (Hermina et al. 1989).

### 3.1.2.7 *Stabilized dunes*

These dunes take place at the middle and at the northern coastal strip boarder of the study area (Cherif et al. 2006).

### 3.1.2.8 *Sabkha deposits*

These deposits are located in the Wadi El-Natron and in the northern lakes. They consists mainly of silts and clay mixed with evaporites and mostly covered by water that constitutes salt marshes (Cherif et al. 2006).

### 3.1.2.9 *Wadi deposits*

These deposits take place mainly in the Wadi El-Natron. It is made up of alluvial gravel, sand and silt (Cherif et al. 2006).

#### 3.1.2.10 *Sand dunes*

These dunes take place at south of the study area and also in the northern coastal strip, where there are some vegetated coastal dunes. These deposits are, in part, sediments of braided streams (Said in Hermina et al. 1989) and the average thickness is about 15 m.

#### 3.1.2.11 *Nile silt*

The Nile silt deposits is located mainly in the Delta and extends in the west direction up to the El-Nubaria canal. They consists of silt, clay and sand along the alluvial of the Nile and the average thickness is about 25 m.

### 3.2 Major structural framework

The northern part of the desert west of the Nile forms generally an almost featureless plain except for the small folded and faulted area in the Abu Roash complex at the north of the Giza pyramids. The northern part of this desert offers few prominent topographical or geological features that would reflect its intricate geological history. Most of the surface is covered with gentle-dipping Neogene strata of reasonable lithological uniformity. There are a few lines of major faults, and the few folds noted are minor rolls with gentle dips and large amplitude (Hantar 1990). The most conspicuous fold-elements are Wadi El-Farigh and Wadi El-Natron anticlinal structures.

Many tectonic events affected the north of this desert. The tectonic elements include features that continued to be active from the late Paleozoic, new Mesozoic features, and features that were inverted in late Mesozoic or early Cenozoic times (Sestini 1984). During the Jurassic Period, which was accompanied by major plate movements including the separation of the Apulian microplate, many of the emergent lands of north Egypt became submerged by the newly formed Neotethys. The end of the Jurassic Period witnessed a major orogenic movement, which resulted in the emergence of the land.

The trends of the basement fractures have influenced the sites and orientation of basins and other structures, which can be seen in the basement megastructures that lie along the stable-unstable shelf contact at the southern boundary of the study area as a northeast-southwest trend and as an east-west trend. The northeast-southwest trend, named Kattaniya High, is centred about 50 km from Cairo with 25 to 30 km wide, and forms a horst block bounded by faults in the north. The east-west trend, named Sharib-Sheiba High, does not show on the surface but is indicated from the aeromagnetic measurements. It extends from about longitude 28° to 30° E.

The northwestern desert structure is dominated by many faults with different displacements that can be identified from seismic and well data (Fig. 3.3). The majority are steep normal faults and most have a long history of growth. The biggest displacements faults are limited to the Kattaniya horst (northeast-southwest) with a magnitude between 1500 to 3000 m (Hantar 1990). The depression of Wadi El-Natron is characterized by a number of normal faults that have separated it from the surroundings. The trend of the majority of these faults is NW-SE (Ibrahim 2005).

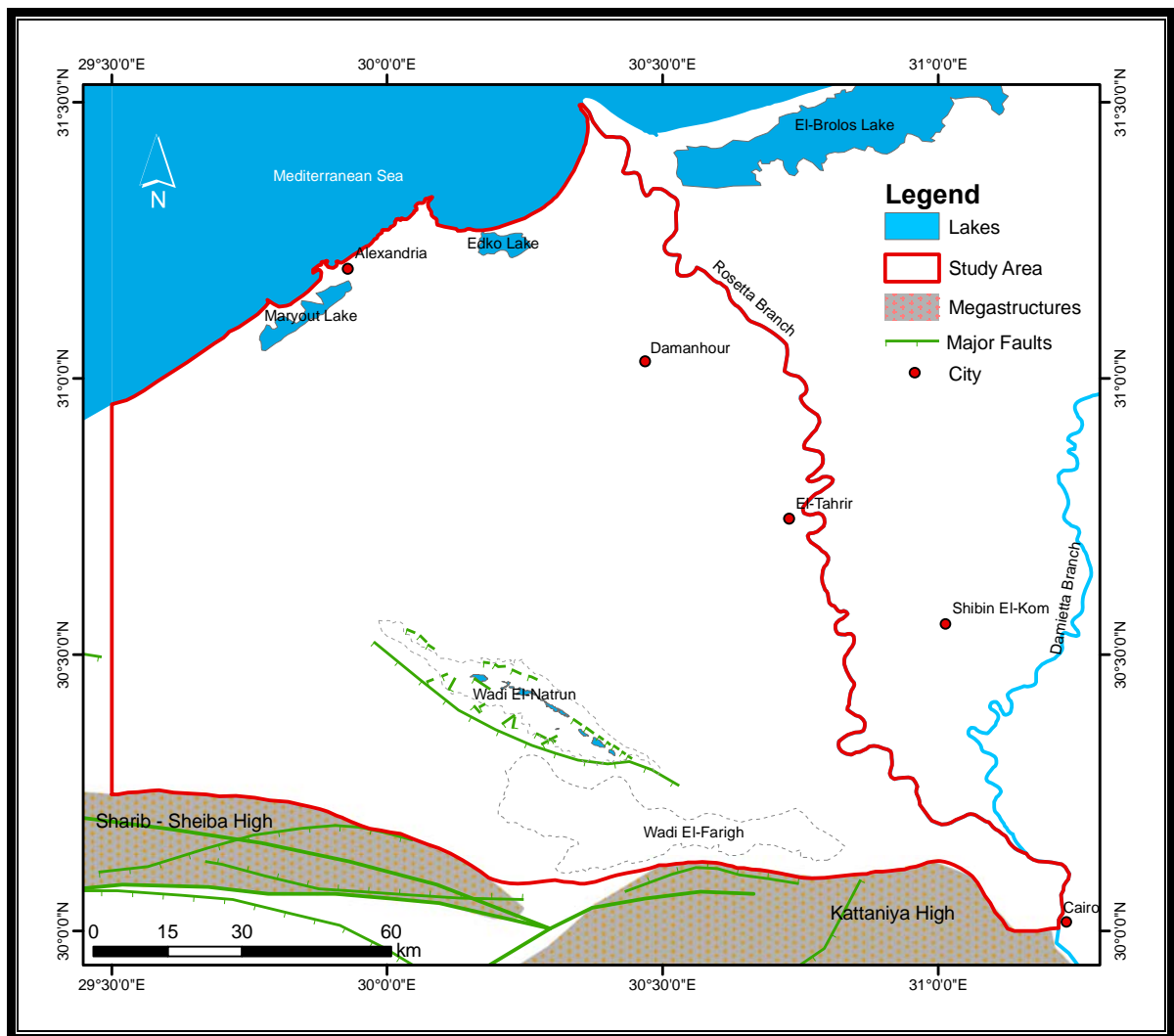


Fig. 3.3: General structural framework of the study area, adapted from Said (1990).

# 4 Hydrogeological Setting

## 4.1 Aquifer systems in Egypt

The hydrogeological framework of Egypt can be differentiated into five main aquifer systems (Figure 4.1): the Nile aquifer, the Moghra aquifer, the Nubian aquifer, the Carbonate aquifer and the Coastal aquifer (RIGW 1988, 1993; Allam et al. 2002). Each aquifer has its unique properties that differ from the other aquifers' general characteristics such as hydraulic conductivity, transmissivity, storage, recharge, etc. The Nile and Moghra aquifers partially share the area of study.

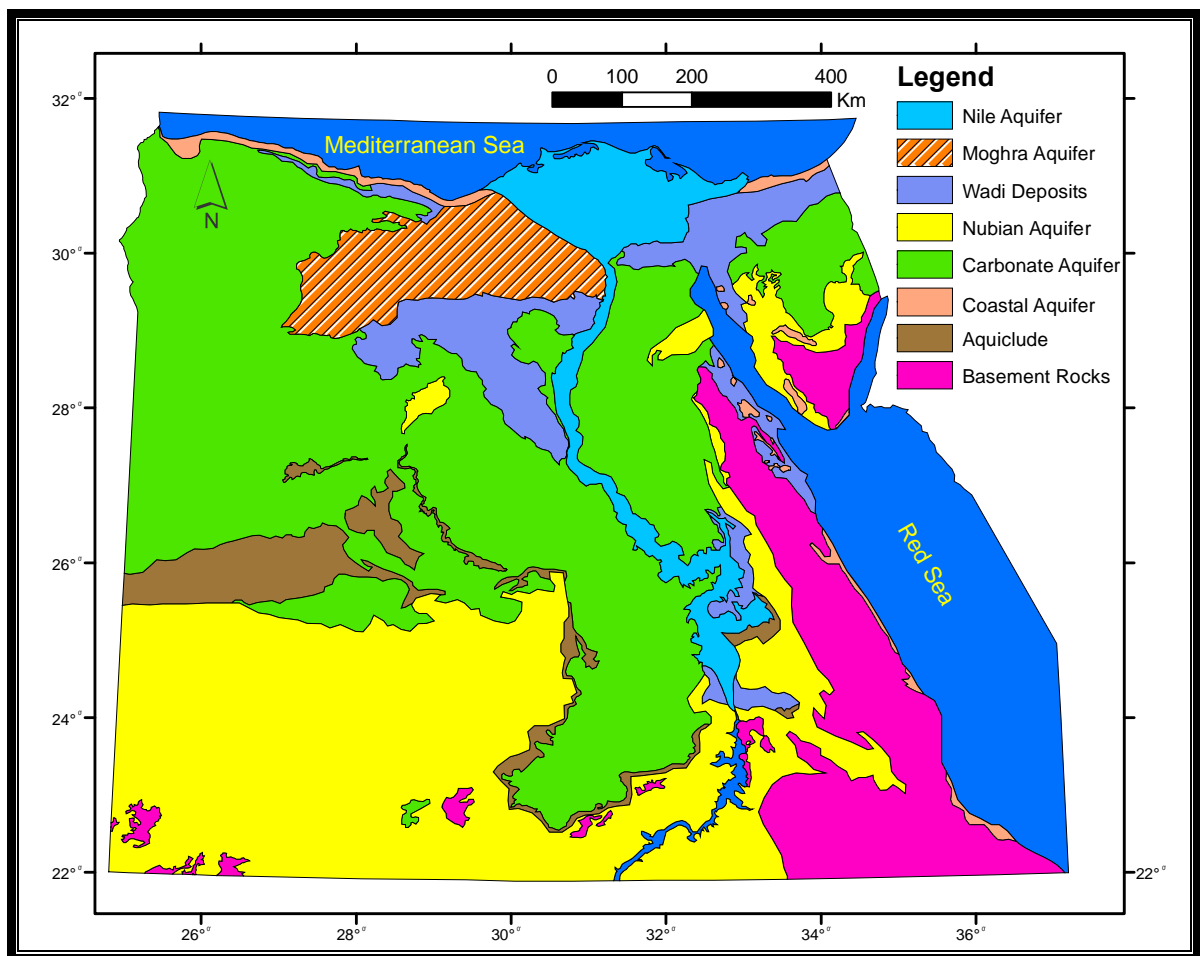


Fig. 4.1: The aquifer systems in Egypt. Modified after RIGW (2004)



- The Nile Aquifer exists in both the Nile flood plain and the Nile Delta. It is assigned to the Quaternary and Late Tertiary and consists of a thick layer of graded sand and gravel covered by a clay to silty clay layer. The aquifer thickness varies from 300 m south of Egypt to only a few meters in Cairo where it begins to increase gradually until it reaches more than 1000 m in the North along the Mediterranean coast line. The transmissivity of the aquifer is about  $0.116 \text{ m}^2/\text{s}$ . The aquifer is recharged from the Nile, seepage from irrigation and drainage canals, and from deep percolation (Attia 1985).
- The Moghra aquifer system is assigned to the Lower Miocene. It covers the western edge of the Delta up to the Qattara Depression. The aquifer thickness varies from about 60 m to about 900 m. The aquifer transmissivity varies from  $5.8 \times 10^{-3}$  to  $5.8 \times 10^{-2} \text{ m}^2/\text{s}$ . Groundwater quality varies from good to high saline. The aquifer is recharged by deep percolation in the East from the Nile alluvium (Diab et al. 1995).
- The coastal aquifer systems are assigned to the Quaternary and late Tertiary periods. They are found in the littoral zones along the Mediterranean and the Red Sea coasts. In the western Mediterranean littoral zone, the water-bearing formation consists of oolitic limestone and calcareous sandstone with a thickness of about 40 m. Groundwater is generally under phreatic conditions in the form of thin lenses of fresh water floating over saline water. The groundwater is brackish in general and recharged mainly by rainfall (Allam et al. 2002).
- The fissured carbonate aquifer system is assigned to the Eocene and to the Upper Cretaceous periods. It dominates basically in the North and middle parts of the western desert, covering a surface area of about 50% of Egypt. The rocks consist of limestone, dolomite, chalk and marl. Locally, they may include phosphate and shale intercalations. The thickness of the carbonate aquifer system varies from 200 m to about 900 m. Recharge of the aquifer is mainly achieved through upward leakage from the underlying sandstone, groundwater flow from adjacent formations, and infiltration from the surface. The groundwater salinity ranges from 1000 to 8000 ppm (Attia 1998; RIGW 1993).
- The Nubian sandstone aquifer system is assigned to the Paleozoic-Mesozoic sediments (Wycisk 1993, 1994; Klitzsch and Wycisk 1999). It covers a large area in the western desert, and parts of the eastern desert and Sinai. The depth to groundwater is either shallow, where the water bearing formation (horizon) is exposed as in the Siwa oasis, or deep (up to 1,500 m) as in east Uweinat and Kharga, where the aquifer is (semi) confined. The aquifer transmissivity is

generally medium to low, varying from  $1.16 \times 10^{-2}$  to  $4.63 \times 10^{-2}$  m<sup>2</sup>/s. The aquifer contains a huge amount of non-renewable groundwater dating back to the humid periods (5,000 to 10,000 years and > 25,000 years). The groundwater quality is generally good (<500 ppm) in the major parts, except near the coastal regions and Sinai (Sefelnasr 2007).

## 4.2 The aquifer systems in the area of study

### 4.2.1 Nile Delta aquifer

A large groundwater basin with an area of approximately 12000 km<sup>2</sup> is located under the Delta of the Nile, bound in the North by the Mediterranean Sea and by the Suez Canal in the East. The aquifer is found along the entire Nile Delta alluvial plain. It consists of Pleistocene graded sand and gravel, changing to fine and clayey facies in the north. The majority of the aquifer system is overlain by a clay cap which is considered to be a semi-confining layer with a thickness that ranges between 10 m in the south up to 30 m in the north, and vanishes at the eastern and western desert fringes (This is described in the next point). The Nile delta aquifer is underlain by Pliocene marine clay that acts as a sealing bed for the aquifer. The thickness of the Pleistocene layer reaches its high value within the study area near the Mediterranean (about 800 m) and decreases steeply toward the south direction up to half of the study area, where it then decreases gradually until it nearly vanishes near Cairo. The aquifer extends in the east-west direction in a concave shape, with its highest values at the middle of the Delta and its lowest values in the West where it vanishes at the desert fringes (Fig 4.2). The aquifer is recharged by the water from the two branches of the Nile River, Damietta and the Rosetta, as well as by percolated rain water and seepage water from canals. The total volume of groundwater of the delta aquifer exceeds 400 km<sup>3</sup>. It is used for irrigation, water supply, and industrial needs. The total groundwater withdrawal for irrigation, municipal and industrial usage is approximately 2.4 km<sup>3</sup>/year (El-Fishawi 1993). Because of its connection to the Mediterranean Sea, the aquifer is influenced by saline water intrusion that penetrates into the aquifer up to a distance of about 130 km (Kashef 1983). The groundwater salinity of the aquifer ranges from less than 1000 ppm in the south and increases until it reaches more than 35000 ppm in the north (Fig 4.3). The results of the chemical analysis of groundwater in the aquifer clarifies that the quality in the southern part of the delta is affected by the surface water from canals and from irrigation. However, the northern part of the Delta is affected by sea water (RIGW/IWACO 1998). The groundwater salinity increases also with depth, where the density of fresh water with salinity less than 1000 ppm takes a convex lens in shape, with the largest thickness (about 300 m) in the southern third of the Delta and then decreasing in all directions (RIGW 1980).

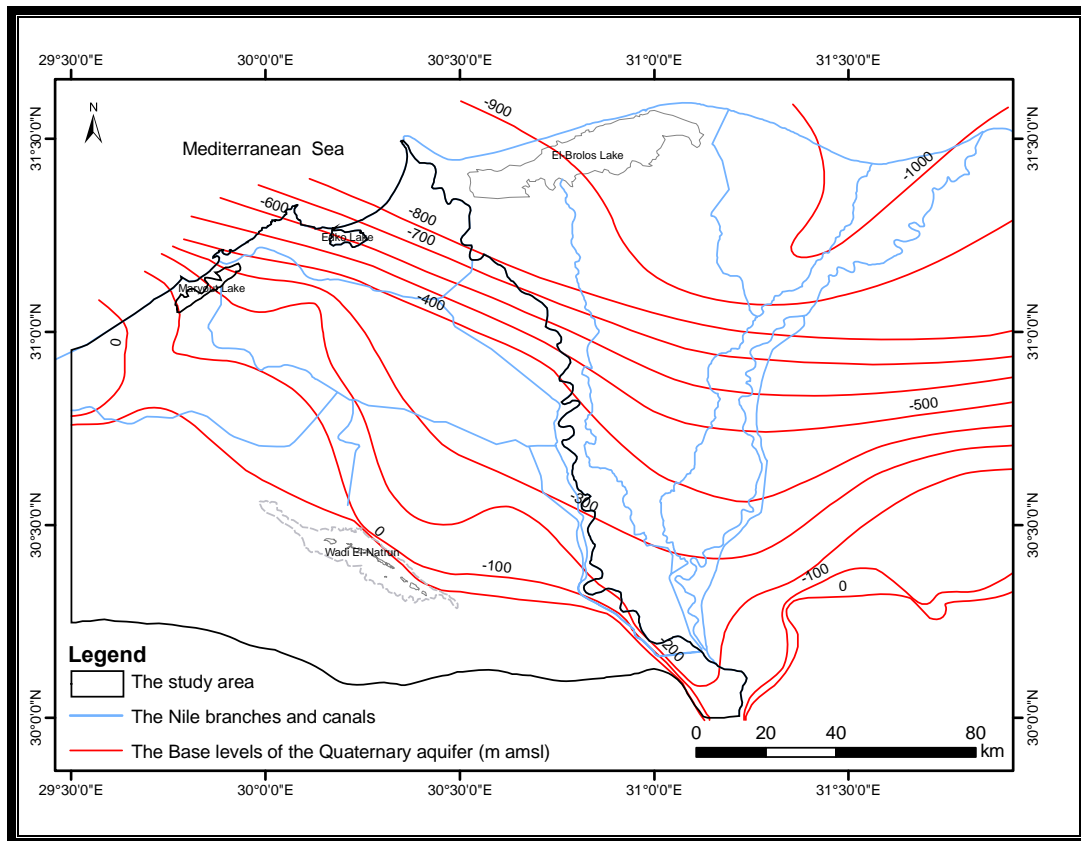


Fig. 4.2: The base levels of the quaternary aquifer. Digitized after RIGW (1992)

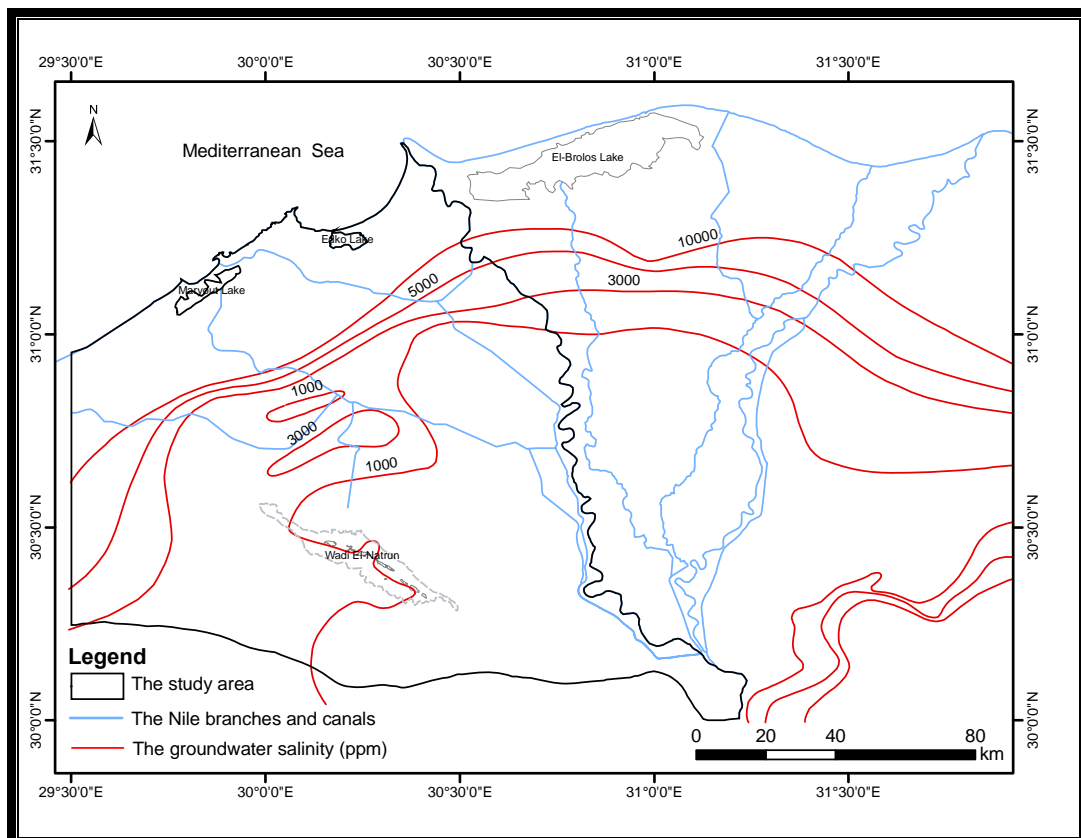
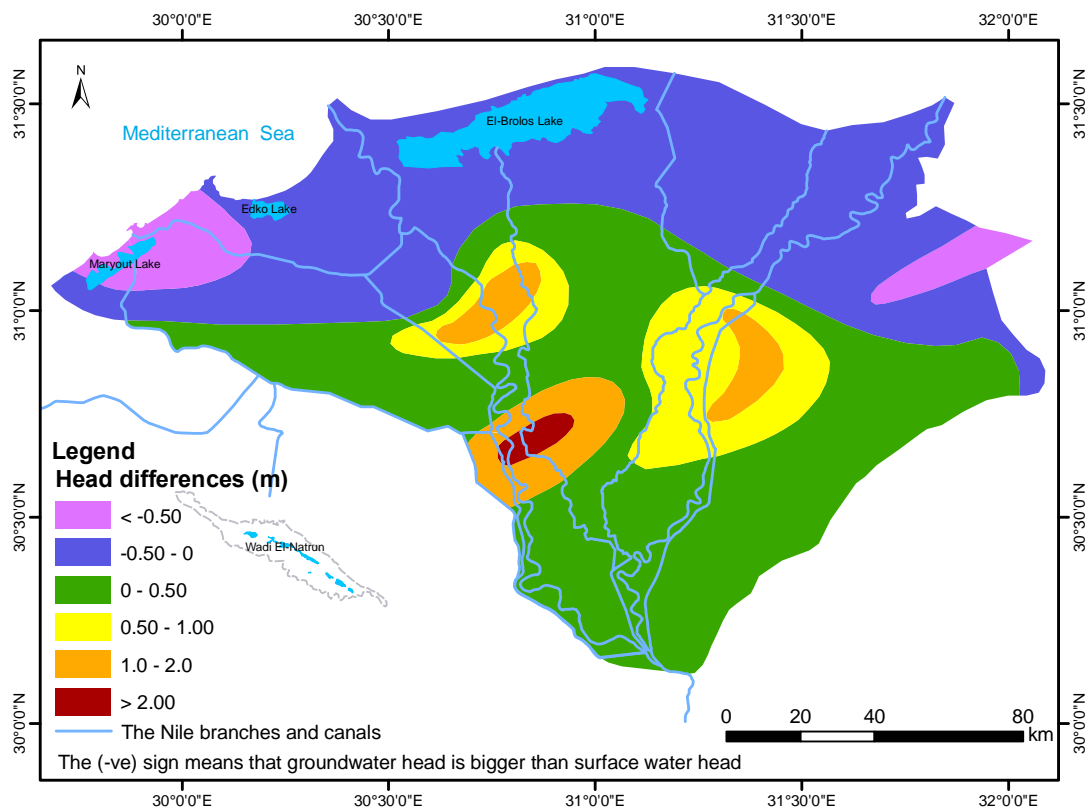


Fig. 4.3: The contour lines of groundwater salinity. Digitized after RIGW (1992)

### 4.2.2 Clay cap aquitard

The Nile Delta aquifer, covered by a layer described as a clay cap aquitard, was formed from the Nile alluvium deposits during the Holocene Epoch. It is composed of two main deposits. The upper deposits are clay and silt with a thickness less than 20 m in the South and up to 70 m in the North, and the lower deposits are clayey sand with a thickness that does not exceed 10 m. These deposits cover the Nile Delta with a non-uniform thickness increasing in the North and vanishing in the East and West fringes of the Delta. The main importance of this layer is that it contains the surface water body in the Nile Delta and thus can be described as a “reservoir” for water losses from irrigation and for the infiltration from the condensed irrigation net in the Nile Delta. The direction of the water exchange between the surface water in the clay cap and the groundwater in the Nile Delta aquifer depends on the water table in the clay cap and the piezometric head in the Nile Delta aquifer. The general direction is downward if the water table is higher than the piezometric head and vice versa. The hydraulic contact between the surface water in canals and the hydraulic heads of groundwater in the Nile Delta aquifer depends mainly on the thickness of the clay layer and/or clayey sand layer below the canal bed. Fig 4.4 shows a contour map for the differences between surface water in the canals and groundwater in the aquifer.



**Fig. 4.4:** The differences between surface water and groundwater heads. Digitized after RIGW (1980)

### 4.2.3 Wadi El-Natron aquifer

The Wadi El-Natron aquifer covers the depression of Wadi El-Natron in the western desert that could be observed from the Cairo-Alexandria Desert Highway in the middle between Cairo and Alexandria. Its name was assigned to this depression because it was one of the local resources of Natrun ( $\text{Na}_2\text{CO}_3 \cdot 10\text{H}_2\text{O}$ ) and Salt ( $\text{NaCl}$ ) (Sadek et al 2005). It was named also the salt field. The ancient Egyptians called it Ain Horus, which means the eye of the God Horus because it appears to be shaped like an eye. This aquifer consists of an alternation of sand and clay layers that were formed during the middle and upper Pliocene by brackish water deposits, composed of limestone, clay, sand, and gypsum beds (Wadi El-Natron formation). The aquifer is underlain by the Moghra aquifer but separated from it by a clay layer that was formed during the early Pliocene period when this area subsided, forming a semi morphotectonic basin filled with sea water forming a gulf region where pyretic clay was deposited on the Miocene layer (Shata et al., 1970). The piezometric isolines show radial flow towards the Wadi El-Natron depression and the groundwater is discharged through a great number of seepage zones into small lakes, ponds, and sabkhas (Dawoud et al 2005). The depth to water table ranges from 15 to 40 m. According to Saad (1962) the average fresh water bearing thickness in the Wadi El-Natron aquifer is about 30 m. However according to REGWA (1993) the fresh water thickness ranges from 15 to 25 m.

### 4.2.4 Moghra aquifer

The Moghra aquifer covers the majority of Wadi El-Farigh and extends westward towards the Qattara Depression. It was formed during the lower Miocene and consists of fluvial and fluvio-marine coarse sand and gravel with clay intercalations increasing in northward direction toward the Mediterranean Sea (RIGW 2006). The aquifer in general is phreatic but confined in the eastward direction at the contact with the Delta aquifer and with the Wadi El-Natron aquifer where Pliocene clay overlays the Miocene aquifer. On the other hand, Oligocene basaltic sheets underlay the Moghra aquifer creating a confining bed with thickness ranging from 20 to 30 m. The saturated thickness of the aquifer ranges from 100 m in the South direction up to 900 m in the North direction (RIGW 1992). The groundwater level varies from 10 m below mean sea level at the border with the Nile Delta aquifer to about 60 m below mean sea level near the Qattara Depression in the west (Hefny and Shata 2006). The flow of groundwater in the aquifer goes from east to west through Wadi El-Farigh toward the Qattara Depression (Dawoud et al 2005). The Moghra aquifer is recharged mainly through lateral seepage from the Pleistocene aquifer at its eastern border. According to El-Ghazawi and Attwa (1994), the faults in the area are responsible for elevating the Oligocene basaltic sheet and led to a hydraulic connection between the Miocene aquifer and the underlying Oligocene clay layer that is characterized by relatively

high water salinity because of the dissolving salts of the Oligocene fluviomarine deposits during the circulation of the water. This hydraulic contact may lead to the increase of the salinity in the Miocene aquifer with every increase in the groundwater extraction from the Miocene aquifer (Abdel Baky 1983).

### 4.3 Groundwater levels and depths

The groundwater piezometric head in the study area (Fig 4.6) ranges from 16 m (amsl) in Cairo to 1 m (amsl) near the coast. The piezometric level decreases from south to north with a gradient of about 11 cm/km. In the Wadi El Natrun area the piezometric head is about -20 m (amsl) due to the topographic depression in this area. In the area of West El-Noubaria, between the El-Noubaria Canal and the El-Nasr Canal, there is a groundwater high with a piezometric head up to 20 m (amsl) and the gradient ranges between 70 cm/km in the North and 150 cm/km in the South. It has gradually formed since 1960 due to the high infiltration rate from the surplus of the traditional flood irrigation water of the old reclamation projects based on surface water and the non-effective drainage system that was unsuitable for the soil type in this area. The groundwater levels are usually oscillate up and down as a result of the level of water in the Nile River and its branches, the method and frequency of irrigation, and the extraction rate. Due to the extensive groundwater extraction southeast of the study area in Wadi El Farigh where many recent private reclamation projects have developed, a local depression cone started to appear and led to a continuous deterioration of groundwater in this area (RIGW 2006).

The depth to the groundwater can be differentiated into four parts in the study area from north to south as follows:

- The first part locates in between the Mediterranean Sea and the El-Noubaria Canal, where the depth to groundwater is less than 3 m.
- The second part starts at the El-Noubaria Canal and extends to the border of the Wadi El Natrun Depression, where the depth to groundwater increases gradually from 3 m to about 40 m.
- The third part is the Wadi El Natrun Depression where the depth to groundwater decreases from about 40 m to the ground surface at the lakes of Wadi El Natrun.
- The fourth part is south of the Wadi El Natrun Depression where the depth to groundwater increases, due to the high topography in this areas, from 40 m up to about 150 m at the Southeast and up to about 190 m at the Southwest (RIGW 1992).

#### 4.4 Recharge

Recharge of groundwater takes place in the area of study by the infiltration and downward leakage of excess irrigation water, leakage from canals, infiltration of rainfall and inter-aquifer flow of groundwater. The recharge by rainfall takes place mainly during the winter months. The average rainfall ranges from 25 mm/a in the southeast to about 200 mm/a in the northwest. The Nile Delta aquifer system in the flood plain is recharged by seepage from surface water, especially from irrigation canals and by downward percolation of subsurface drainage water in the traditionally cultivated lowlands. In the central and southern parts of the flood plain, the leakage towards the aquifer ranges between 90 and 290 mm/a depending on soil type, irrigation and drainage practices. In the desert areas, relatively high leakage rates are observed for the basins. For instance it is about 360-550 mm/a for sprinkler irrigation and about 40-180 mm/a for drip and central pivot irrigation. In areas with traditional irrigation practices (the old reclamation projects), large amounts of irrigation water percolate into the subsoil and cause a considerable recharge of the aquifer. The groundwater table subsequently rises causing water logging and drainage problems (Dawoud et al. 2005).

#### 4.5 Discharge

The discharge of groundwater takes place either naturally through the outflow into the drainage system, evapotranspiration and inter-aquifer flow of groundwater or artificially through the direct extraction by wells which is the main discharge component from the aquifer. The average rate of evapotranspiration in the study area is about 1900 mm/a (REGWA 1993) and the average rate of evaporation from the lakes of Wadi El-Natrun is about 6000 mm/a (Dawoud 2005).

According to the observation of RIGW, the data of MWRI, and the geological distribution of the aquifers in the study area, the annual extraction for both drinking water and irrigation in 1985 was about 353 million cubic meters from the Pleistocene aquifer, 1 million cubic meter from the Pliocene aquifer, and 106 million cubic meters from the Miocene aquifer with a total extraction of about 460 million cubic meters from approximately 1650 wells. Due to the increase of reclamation in the region west to the Nile Delta at the end of the 90s, the annual extraction of groundwater increased dramatically by the year 2006 to be about 1040 million cubic meters from the Pleistocene aquifer, 15.4 million cubic meters from the Pliocene aquifer and 599.6 million cubic meters from the Miocene aquifer. In total, the extraction rose to about 1655 million cubic meters from 6500 wells. Fig 4.5 shows the increase in the number of wells between the years 1990 and 2006 and Fig 4.6 shows the development of the extraction from year 1985 to 2006 in the study area.

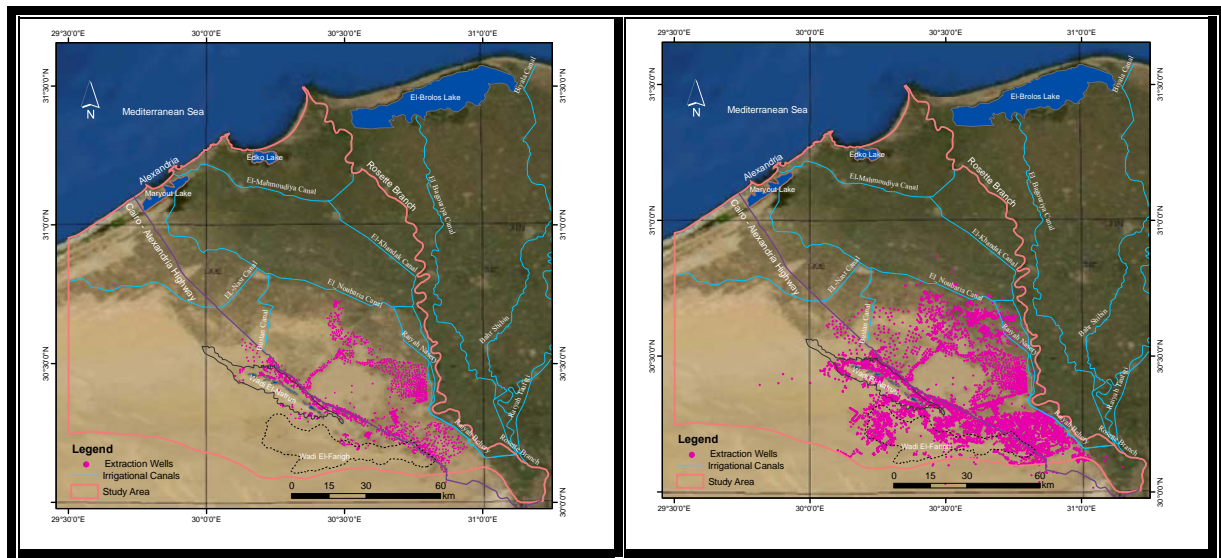


Fig. 4.5: Distribution of wells in the study area in year 1990 on the left and in year 2006 on the right (MWRI 1990 & 2006)

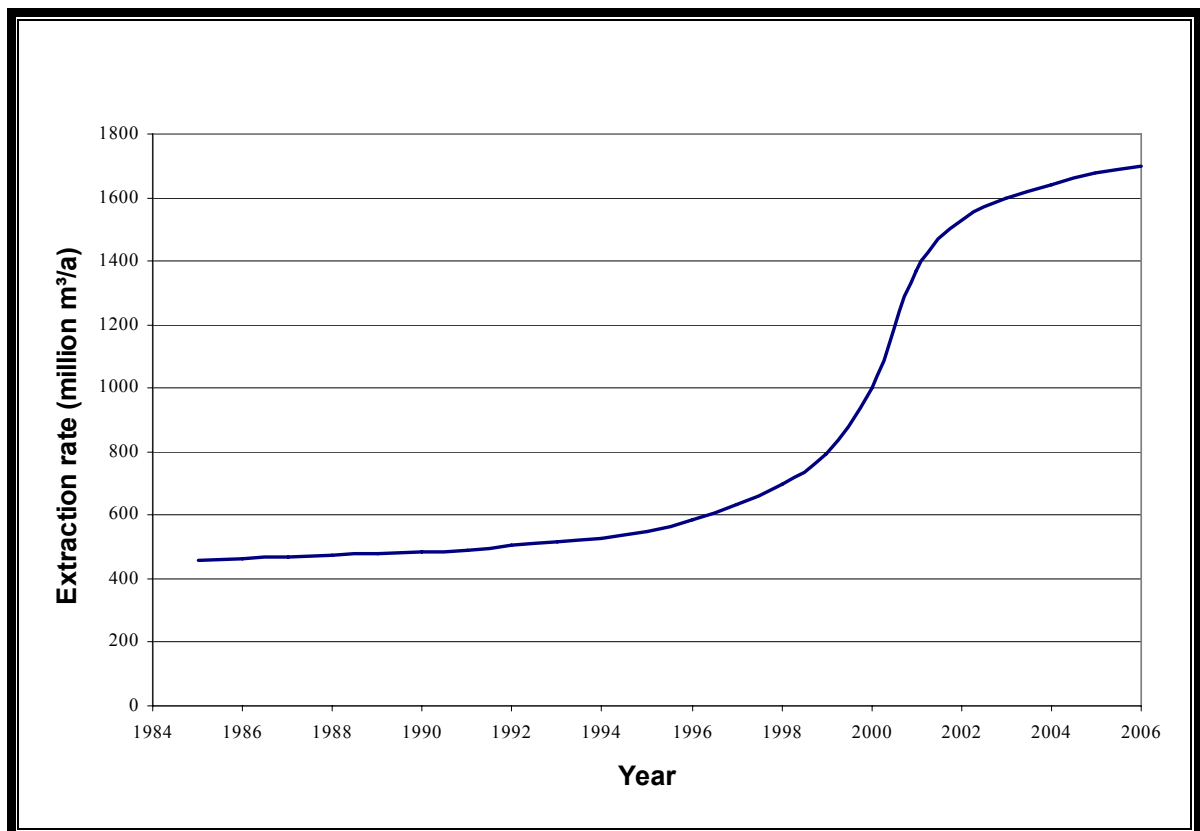


Fig. 4.6: Development of the extraction rate in the study area from 1985 to 2006 (Source: Dawoud et al. 2005 and RIGW 2006)



#### 4.6 Environmental situation

The time span required for groundwater replenishment in the study area is generally lengthy when compared to the normal time frame of human activities and water resources planning that affects the environmental situation as follows:

- The groundwater withdrawal builds cones of depression around the wells, which in turn lower the groundwater level and increase the depth to groundwater. With successive increases of the depth to groundwater, water pumping becomes uneconomic.
- Continuous lowering of groundwater levels directly affects the hydraulic gradient as well as the transmissivity.
- Through the groundwater high velocities, steepness of the hydraulic gradient, and inverse gradients, the groundwater quality suffers noticeable changes due to the occurrence of saltwater upconing.
- Groundwater velocity increases because of the steepness of the hydraulic gradient.
- In cases of groundwater overexploitation, the salt concentration in groundwater increases, and by using it in irrigation, the soil becomes saltified in addition to the degradation of the organic matter.

Under the conditions of low rate groundwater replenishment of the study area, the utilization of this resource through groundwater exploitation must be governed by principles of rationality, wisdom, and sustainable development in order to avoid the mining of the aquifer storage reserves rather than an uneconomic lifting of the groundwater.

#### 4.7 Groundwater residence time

By assuming that aquifer properties and recharge rates are constant and the existence of steady-state flow conditions, Focazio et al. (1998) have defined the residence time as the ratio of the volume of aquifer void space to the volumetric rate of water moved through the aquifer. In other words, the groundwater residence time in the aquifer is directly proportional to the porosity and the aquifer thickness and inversely proportional to the rate of water moved through the aquifer. According to the Isotopic content of water samples, the average residence time in the El-Khatatba area and the Kafr Dawud area ranges from 10 to 410 years. However, the average residence time in the northwestern area of the Nile Delta is relatively low (about 40 years) because the aquifer in this area is influenced by intensive surface water irrigation projects in this area (Awad et al. 1992).

#### 4.8 Aquifer parameters

The hydraulic parameters of the aquifers in the study area are collected from diverse literature and from the analysis made for different pumping and recovery tests in the study area. The aquifer parameters vary from layer to layer within the transition between aquifers and aquitards. Furthermore, they vary slightly within the same layer, especially within local considerations. A general overview of the hydraulic parameters of the study area can be briefly introduced in cross sections up to -900 m amsl as shown in Figure 4.7.

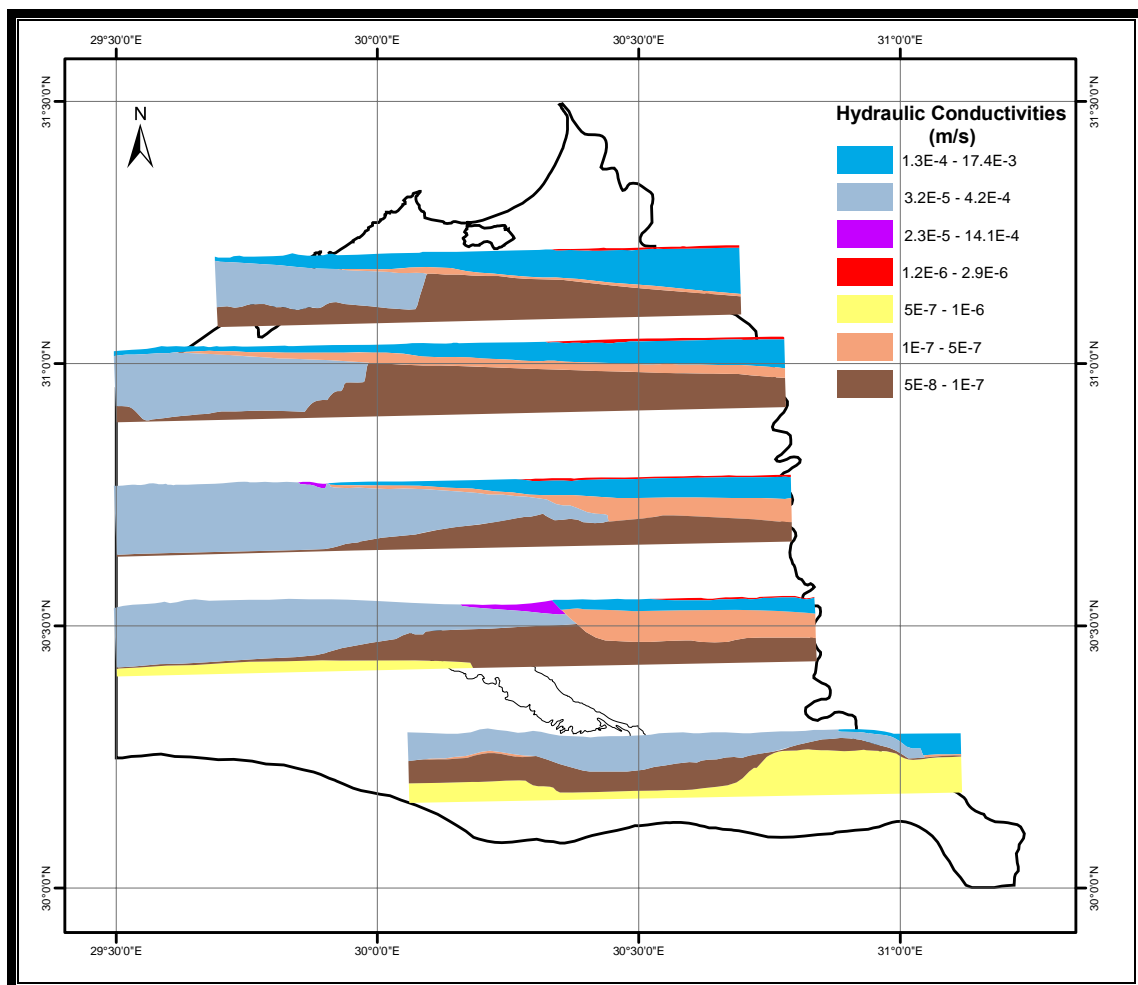


**Fig. 4.7:** Overview of the hydraulic conductivities in the study area.

- Nile Delta aquifer parameters

According to many authors who have studied the hydraulic parameters of the Nile Delta aquifer such as Pavlov (1962), Saad (1962), Shata (1970), Bahr (1975), El-Shazly et al. (1975), Farid (1980), Shahien (1985), Zaghoul (1985), Laeven (1991), Ahmed (1999) and Ibrahim (2000), the hydraulic conductivity ranges from  $1.3 \times 10^{-4}$  m/s to  $1.7 \times 10^{-3}$  m/s and the transmissivity of the aquifer is considerably high and has a wide variety of values that range from  $2.9 \times 10^{-2}$  m<sup>2</sup>/s to  $8.6 \times 10^{-2}$  m<sup>2</sup>/s. This makes the aquifer a good conductor of water from recharge to discharge locations. According to

RIGW (1992) the storage coefficient ranges from  $1 \times 10^{-3}$  to  $1 \times 10^{-4}$  and the porosity ranges from 25% to 40%. The average storage capacity of the system is about 500 km<sup>3</sup>. The specific yield ranges from 0.15 to 0.2 (Shahien 1985, Zaghloul 1985). The high productivity of the aquifer and the shallow depth to groundwater allow for artificial extraction at high rates (100-300 m<sup>3</sup>/hour) with relatively shallow wells (50-150 m).

- Moghra aquifer parameters

An analysis of approximately 58 pumping tests was conducted at different locations in the Moghra aquifer system. REGWA (1993) analyzed the results of 18 pumping tests along the Cairo-Alexandria Desert Highway and recorded that the hydraulic conductivity ranges from  $2.2 \times 10^{-5}$  m/s to  $6.4 \times 10^{-4}$  m/s. Ibrahim (2005) analyzed the results of about 40 pumping and recovery tests in different places in Wadi El Farigh in the Moghra aquifer system and indicated that the hydraulic conductivity ranges from  $3.2 \times 10^{-5}$  m/s to  $4.2 \times 10^{-4}$  m/s and the transmissivity ranges from  $3 \times 10^{-3}$  to  $5.3 \times 10^{-2}$  m<sup>2</sup>/s. The average storage coefficient is  $1.2 \times 10^{-4}$  (Mostafa 1993).

- Wadi El Natrun aquifer parameters

According to the analysis of pumping tests of 41 production wells at different locations in the Wadi El-Natrun, it has been indicated that the hydraulic conductivity ranges from  $2.3 \times 10^{-5}$  to  $1.4 \times 10^{-3}$  m/s (REGWA 1993) and the storage coefficient ranges from  $1.35 \times 10^{-3}$  to  $7.5 \times 10^{-3}$  (Saad 1964).

The accuracy of these parameters depends on the locality and number of aquifer tests carried out. For instance, the number of pumping tests for the Moghra Aquifer is 1.5 times higher than for the Wadi El Natrun aquifer. Meanwhile, the area of the Moghra aquifer is more than twice the area of the Wadi El-Natrun aquifer.

#### 4.9 The surface water system

The surface water system in the study area consists of a network of irrigation and drainage canals that are considered the main source of groundwater recharge. The main irrigation canals in the study area (Fig. 2.1) are the Rosetta branch of the Nile River, the Rayah Behery Canal, the Rayah Nasery Canal, the El-Noubaria Canal, the Elkhandak Canal, the El-Mahmoudiya Canal, the El-Nasr Canal and the Bustan Canal. In addition to the irrigation system, a drainage system was established. The main drains are the Ity El-Barod drain which starts from Ity El-Barod city and ends in the Idku Lake; the Abu Qir drain

which flows into the Mediterranean Sea in Abu Qir city; and the Hosh Essa drain, which is connected with the El-Umum drain and flows into the Maryout Lake (Sayed 2006).

The large canals in the study area are taken as external and internal boundary conditions taking into consideration the water levels and the discharges as observed by the MWRI in different years as follows:

- The Rosetta branch is the eastern boundary of the study area. Its water level is controlled by the Rosetta barrage in El-Qanatir-El-khairiya, which is about 16 km north of Cairo. The average water level in the upstream is about 16.39 m (amsl) and 13.08 m (amsl) in the downstream with an average flow of about 164 m<sup>3</sup>/s. The end of the Rosetta branch is controlled by the Edfina barrage where the upstream is about 2.35 m (amsl) and 0.17 m (amsl) in the downstream before the outlet in the Mediterranean Sea.
- Rayah Behery is a canal parallel to the Rosetta branch with an intake from the Rosetta branch and outlet in the El-Mahmoudia canal with an average water level in the upstream of about 16.34 m (amsl) and 15.66 m (amsl) in the downstream, and an average flow of about 252 m<sup>3</sup>/s.
- Rayah Nasery is a canal parallel to the Rayah Behery canal and it gets its water from the Rosetta branch and ends in the El\_Noubaria canal. The average water level in the upstream is about 16.34 m (amsl) and in the downstream is about 15.32 m (amsl) with an average flow of about 74 m<sup>3</sup>/s.
- The El\_Noubaria Canal starts from the end of the Rayah Nasery canal with an intake from the Rayah Behery canal. The average water level in the upstream is about 9.38 m (amsl) and in the downstream is about 9.12 m (amsl) with an average flow of approximately 116 m<sup>3</sup>/s.

Figures 4.8 - 4.12 show the water levels in the up streams and down streams through the year in the Rosetta branch, Edfina barrage, Rayah Behery canal, Rayah Nasery canal and El-Noubaria canal respectively and figure 4.13 shows the discharge fluctuation in these canals.

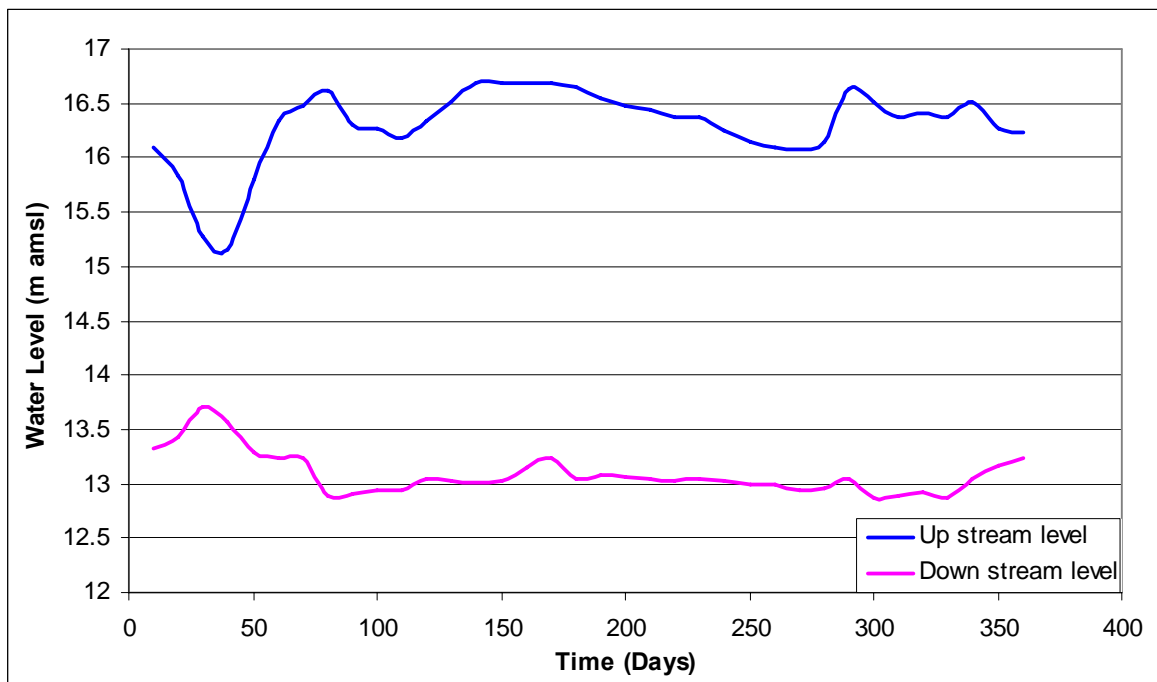


Fig. 4.8: Water levels in the Rosetta branch throughout the year. (Compiled after MWRI 1992)

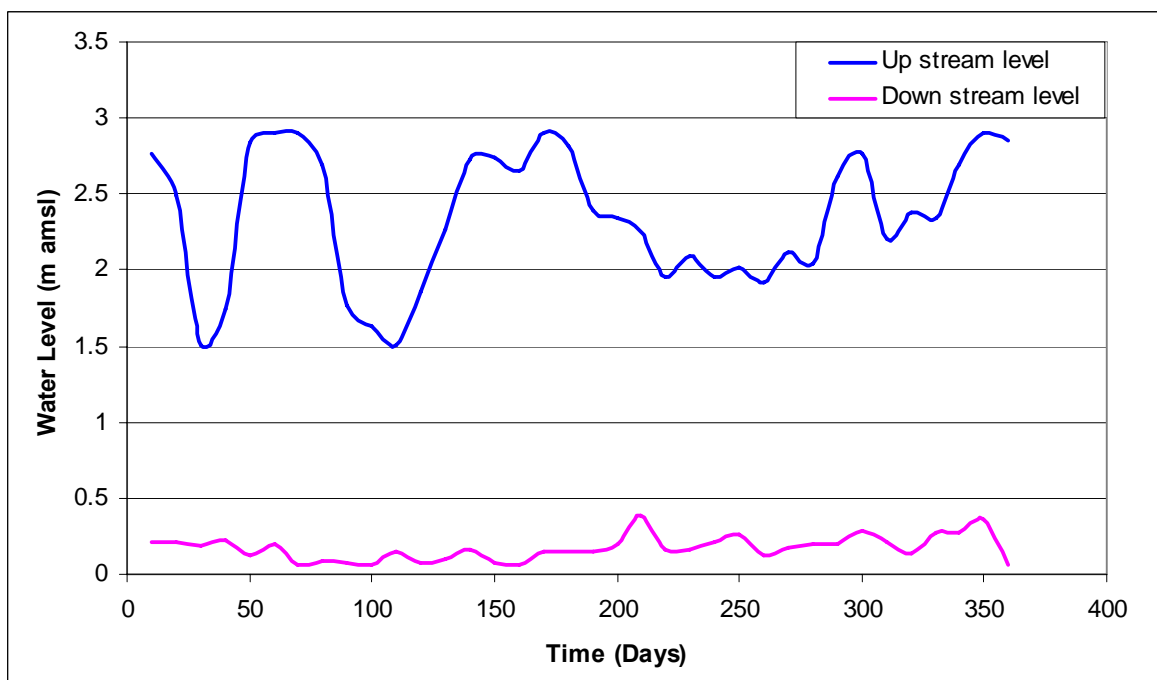


Fig. 4.9: Water levels in the Edfina barrage throughout the year. (Compiled after MWRI 2007)

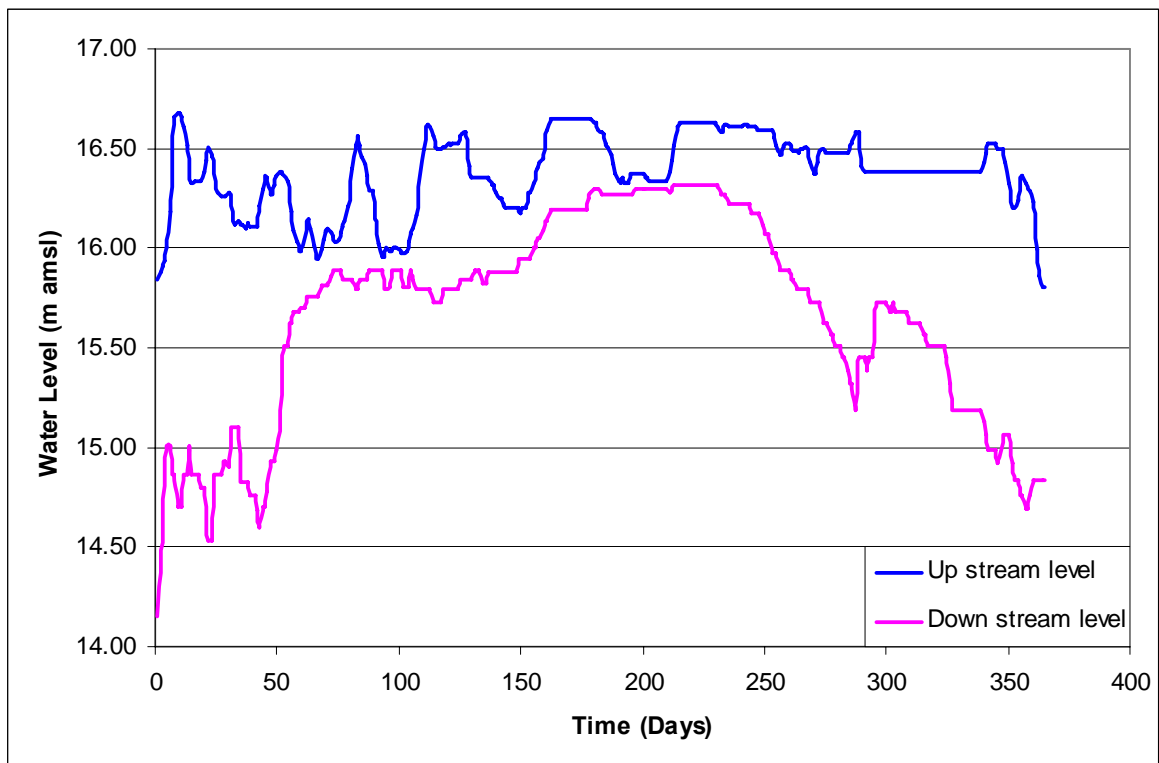


Fig. 4.10: Water levels in the Rayah Behery Canal throughout the year. (Compiled after MWRI 2006)

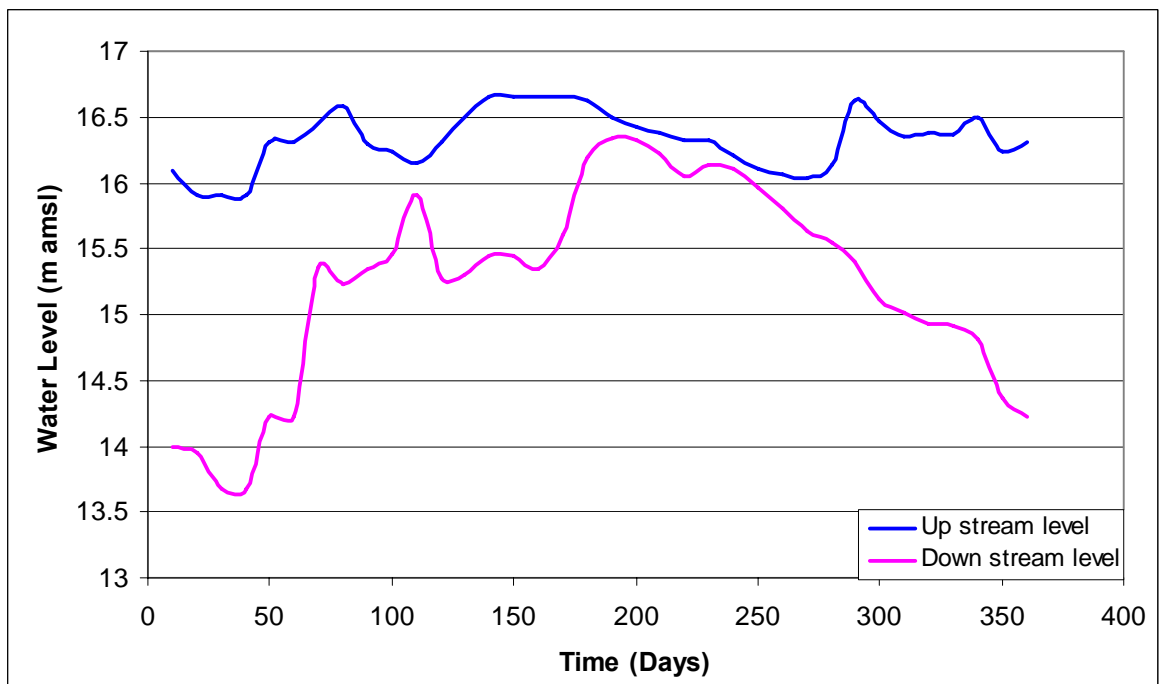


Fig. 4.11: Water levels in the Rayah Nasery Canal throughout the year. (Compiled after MWRI 1992)

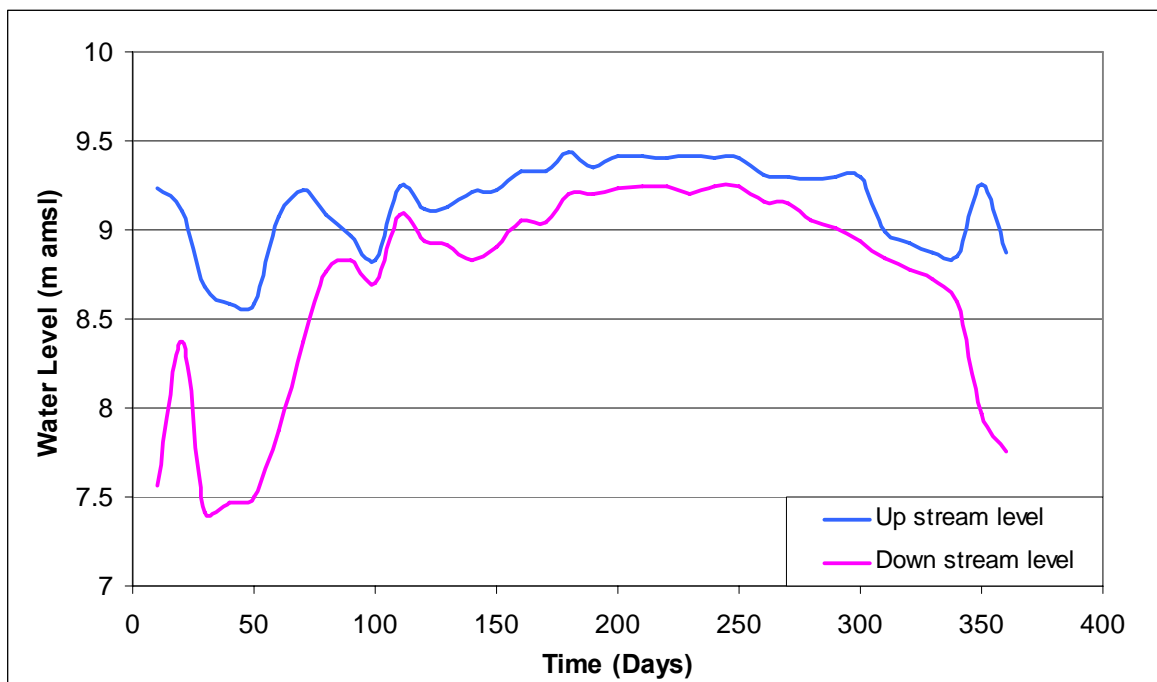


Fig. 4.12: Water levels in the El-Noubaria Canal throughout the year. (Compiled after MWRI 1992)

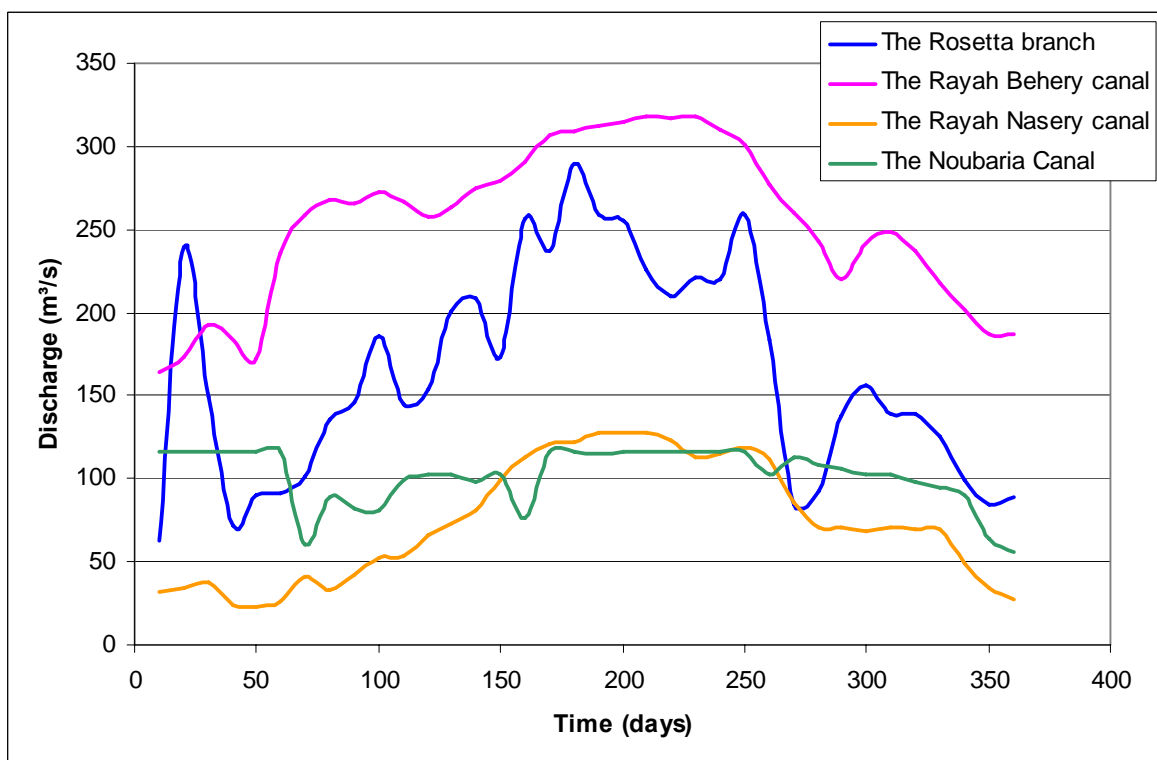


Fig. 4.13: Discharge fluctuation in the canals throughout the year. (Compiled after MWRI 1992)

# 5 Methodology

## 5.1 Introduction

Groundwater models are tools designed to represent a simplified version of reality in order to test various management schemes and to predict the effects of certain action (Wang and Anderson 1995). The study of groundwater systems involves both water quantity and water quality considerations, which have led to the development of many types of groundwater models. These models include flow models, which are used to study the movement of water and other fluids through saturated or unsaturated porous media or fractured rock; transport models, which are used to study the transport of water-soluble constituents and transformation of contaminants by chemical, biological, and physical processes; and coupled models, which are used to study the movement and the state of balance between two liquids with different density.

The flow of groundwater can be described by differential equations derived from basic principles of physics. Their solutions are either analytical when the medium is homogeneous and isotropic or using numerical techniques, which are favoured after the wide availability of digital computers. There are two types of numerical modelling techniques: finite-difference models and finite-element models. In each type a system of nodal points is superimposed over the problem domain including a set of boundary and initial conditions, site-specific parameter values, and hydraulic stresses (Anderson and Woessner, 1992). Many computer programs have been written to solve the governing equations of the model under its boundary conditions such as MODFLOW (McDonald and Harbaugh 1988), TRIWACO (Royal Haskoning 1992), FEFLOW (Diersch 1998), and others. The reliability of predictions using a groundwater model depends on how the model will approximate the field situation by making simplifying assumptions.

## 5.2 Basic equations

The continuity equation and Darcy's law are the principles considered as the basic level upon which subsequent equations are based. Many studies present these basic principals of



groundwater flow through porous media such as Freeze and Witherspoon (1967), Bear (1972), Freeze and Cherry (1979), Langguth and Voigt (1980), Verruijt (1982), Dagan (1989), Fetter (1994), Domenico and Schwartz (1998) and Lee (1999).

In the modelling of unsaturated-saturated flow processes several alternatives exist for numerically solving the governing balance equations with their nonlinear constitutive relationships. The Darcy equation of fluid motion and the continuity equation form the physical basis as follows:

The ideal fundamental balance equation is (continuity equation):

$$\sum I - \sum O = \sum A \quad [\text{Eq 5.1}]$$

where:

$I$  is the Input

$O$  is the Output

$A$  is the Accumulation

The groundwater flow in response to the head gradients in “x” direction ( $\frac{\partial h}{\partial x}$ ) in accordance with Darcy’s law is as follows:

$$v_x = -K_x \frac{\partial h}{\partial x} \quad [\text{Eq 5.2}]$$

where:

$v_x$  is the component of the rate of flow (flux) in the “x” direction ( $\text{LT}^{-1}$ )

$K_x$  is the component of the hydraulic conductivity in the “x” direction ( $\text{LT}^{-1}$ )

The law of conservation of mass for transient flow in a saturated porous medium requires that the net rate of fluid mass flow into any elemental control volume is equal to the time rate of change of fluid mass storage within the element, which gives the equation of continuity in the form

$$-\frac{\partial}{\partial x}(\rho v_x) - \frac{\partial}{\partial y}(\rho v_y) - \frac{\partial}{\partial z}(\rho v_z) = \frac{\partial(\rho n)}{\partial t} \quad [\text{Eq 5.3}]$$

where:

$\rho$  is the fluid density ( $\text{ML}^{-3}$ )

$n$  is the total porosity (Dimensionless)

By expanding the right-hand side of equation (5.3) the equation takes the form

$$-\frac{\partial}{\partial x}(\rho v_x) - \frac{\partial}{\partial y}(\rho v_y) - \frac{\partial}{\partial z}(\rho v_z) = n \frac{\partial(\rho)}{\partial t} + \rho \frac{\partial(n)}{\partial t} \quad [\text{Eq 5.4}]$$

The first term in the right-hand side is controlled by the compressibility of the fluid ( $\beta$ ) and the second term by the compressibility of the aquifer ( $\alpha$ ). In order that the change in ( $\rho$ ) and the change in ( $n$ ) are both produced by a change in the hydraulic head ( $h$ ), and that the volume of water produced by the two mechanisms for a unit decline in head is the specific

storage ( $S_s$ ) given by the form  $S_s = \rho g (n\beta + \alpha)$  and the mass rate of water produced is  $\rho S_s \partial h / \partial t$  (Freeze and Cherry 1979), thus equation (5.4) can be rewritten as follows:

$$-\frac{\partial}{\partial x}(\rho v_x) - \frac{\partial}{\partial y}(\rho v_y) - \frac{\partial}{\partial z}(\rho v_z) = \rho S_s \frac{\partial h}{\partial t} \quad [\text{Eq 5.5}]$$

Substituting Darcy's law into the flow balance equation (5.5) to get the equation of continuity in its different cases:

1. Heterogeneous, anisotropic aquifer with 3-dimensional transient flow

$$\frac{\partial}{\partial x} \left( K_x \frac{\partial h}{\partial x} \right) + \frac{\partial}{\partial y} \left( K_y \frac{\partial h}{\partial y} \right) + \frac{\partial}{\partial z} \left( K_z \frac{\partial h}{\partial z} \right) = S_s \frac{\partial h}{\partial t} \quad [\text{Eq 5.6}]$$

Equation (5.3) can be simplified by integration over the saturated part of the aquifer's thickness to the equation for two-dimensional horizontal flow in porous media (Pelka 1988).

2. Heterogeneous, anisotropic unconfined aquifer with 2-dimensional horizontal flow (including source/sink term for recharge/leakage):

- a) Non horizontal base (Saturated thickness =  $b$ )

$$\frac{\partial}{\partial x} \left( K_x b \frac{\partial h}{\partial x} \right) + \frac{\partial}{\partial y} \left( K_y b \frac{\partial h}{\partial y} \right) + q_s(x, y, t) = S \frac{\partial h}{\partial t} \quad [\text{Eq 5.7}]$$

where:

- $b$  is the saturated thickness (L)
- $S$  is the storage coefficient =  $S_s b + n_o$  (Dimensionless)
- $n_o$  is the effective porosity (Dimensionless)

- b) Dupuit assumption: Horizontal base at  $Z = 0$  and gradient equal to slope of water table ( $h = b$ )

$$\frac{\partial}{\partial x} \left( T_x \frac{\partial h}{\partial x} \right) + \frac{\partial}{\partial y} \left( T_y \frac{\partial h}{\partial y} \right) + q_s(x, y, t) = S \frac{\partial h}{\partial t} \quad [\text{Eq 5.8}]$$

where:

- $T_x$  is the  $h$ -dependent tensor of transmissivity (Pseudotransmissivity) ( $L^2 T^{-1}$ )
- $T_x = K_x(x, y) \cdot h(x, y, t)$  &  $T_y = K_y(x, y) \cdot h(x, y, t)$

3. Homogeneous, anisotropic, Dupuit assumption:

$$K_x \frac{\partial}{\partial x} \left( h \frac{\partial h}{\partial x} \right) + K_y \frac{\partial}{\partial y} \left( h \frac{\partial h}{\partial y} \right) + q_s(x, y, t) = S \frac{\partial h}{\partial t} \quad [\text{Eq 5.9}]$$

4. Homogeneous, isotropic, Dupuit assumption (The Boussinesq equation):

$$\frac{\partial}{\partial x} \left( h \frac{\partial h}{\partial x} \right) + \frac{\partial}{\partial y} \left( h \frac{\partial h}{\partial y} \right) + \frac{q_s(x, y, t)}{K} = \frac{S}{K} \frac{\partial h}{\partial t} \quad [\text{Eq 5.10}]$$

5. Linearized form of Boussinesq equation, h is approximately constant (i.e. small gradients):

$$\frac{\partial^2(h^2)}{\partial x^2} + \frac{\partial^2(h^2)}{\partial y^2} + 2 \frac{q_s(x, y, t)}{K} = \frac{S}{T} \frac{\partial(h^2)}{\partial t} \quad [\text{Eq 5.11}]$$

in which  $\left( h \frac{\partial h}{\partial x} \cong \frac{1}{2} \frac{\partial h^2}{\partial x} \right)$ ,  $\left( \frac{\partial h}{\partial t} \cong \frac{1}{2h} \frac{\partial(h^2)}{\partial t} \right)$  and  $(T = Kh)$

6. Linearized form of Boussinesq equation, h is approximately constant (i.e. small gradients) and large saturated thickness:

$$\frac{\partial^2 h}{\partial x^2} + \frac{\partial^2 h}{\partial y^2} + \frac{q_s(x, y, t)}{T} = \frac{S}{T} \frac{\partial h}{\partial t} \quad [\text{Eq 5.12}]$$

in which  $\left( \frac{\partial^2(h^2)}{\partial x^2} \cong 2h \frac{\partial^2 h}{\partial x^2} \right)$

7. Transient unsaturated flow

In the case of partially saturated flow, the equation of continuity must reveal the time rate of change of the moisture content as well as the time rate of change of storage, i.e. the  $(\rho n)$  term in equation (5.3) should become  $(\rho n \theta')$  where  $\theta'$  is the degree of saturation and  $n \theta' = \theta$  the moisture content, and consequently the equation (5.4) becomes:

$$-\frac{\partial}{\partial x}(\rho v_x) - \frac{\partial}{\partial y}(\rho v_y) - \frac{\partial}{\partial z}(\rho v_z) = n \theta' \frac{\partial \rho}{\partial t} + \rho \theta' \frac{\partial n}{\partial t} + n \rho \frac{\partial \theta'}{\partial t} \quad [\text{Eq 5.13}]$$

For unsaturated flow, the first two terms in the right-hand side of equation (5.13) are much smaller than the third term. By discarding these two terms, cancelling the  $\rho$ 's from both sides, substituting Darcy's law and by recognizing that  $n \partial \theta' = \partial \theta$  leads to:

$$\frac{\partial}{\partial x} \left( K(\psi) \frac{\partial h}{\partial x} \right) + \frac{\partial}{\partial y} \left( K(\psi) \frac{\partial h}{\partial y} \right) + \frac{\partial}{\partial z} \left( K(\psi) \frac{\partial h}{\partial z} \right) = \frac{\partial \theta}{\partial t} \quad [\text{Eq 5.14}]$$

where:

$\psi$  is the pressure head =  $h - z$

$K(\psi)$  is the hydraulic conductivity for unsaturated soil

It is usual to put equation (5.14) into a form where the independent variable is either  $\theta$  or  $\psi$ . For the latter case it is necessary to multiply the top and bottom of the right-hand side by  $\partial\psi$ , where  $\partial\theta/\partial\psi=C(\psi)$  is the specific moisture capacity. The last substitutions lead to the  $\psi$ -based equation of transient flow through an unsaturated porous medium (Richards equation).

$$\frac{\partial}{\partial x}\left(K(\psi)\frac{\partial\psi}{\partial x}\right)+\frac{\partial}{\partial y}\left(K(\psi)\frac{\partial\psi}{\partial y}\right)+\frac{\partial}{\partial z}\left(K(\psi)\left(\frac{\partial\psi}{\partial z}+1\right)\right)=C(\psi)\frac{\partial\psi}{\partial t} \quad [\text{Eq 5.15}]$$

The solution of  $\psi(x,y,z,t)$  describes the pressure head field at any point of a flow field at any time, and it can be easily converted into a hydraulic head solution  $h(x,y,z,t)$  through the relation  $h = \psi + z$  (Freeze and Cherry 1979).

In the application of the finite element method to the transient flow equation, the spatial problem domain is subdivided into elements that are defined by nodes along their edges. However, in the transient flow case, the nodal values of head  $h_L(t)$  are a function of time. The Galerkin method “as a technique to solve partial differential equations” is applied to the transient flow equation to get a system of differential equations containing the first order time derivatives  $\partial h_L/\partial t$ .

For finding approximate solutions of the above partial differential equations, a numerical technique is required. In solving partial differential equations, the primary challenge is to create an equation that approximates the equation to be studied, but is numerically stable, meaning that errors in the input data and intermediate calculations do not accumulate and cause the resulting output to be meaningless. There are many ways to do that, for instance by using the Finite Element Method (FEM) or the Finite Difference Method (FDM), all with advantages and disadvantages. The differences between FEM and FDM can be summarized as follows:

- The finite difference method is an approximation in the differential equation, while the finite element method is an approximation in the solution of the differential equation.
- The FEM has the ability to handle complex geometries (and boundaries) with relative ease, while FDM in its basic form is restricted and can handle only rectangular shapes and simple alterations. The handling of geometries in FEM is theoretically straightforward.
- The finite differences method is easier to implement where it simplifies the geometries into rectangles.
- There are several ways one could consider the FDM a special case of the FEM approach. The basic functions might be chosen as either piecewise constant functions or Dirac delta functions. In both approaches, the approximations are defined on the entire domain, but need not be continuous. Alternatively, the function might be defined

on a discrete domain, with the result that the continuous differential operator no longer makes sense: however, this approach is not the FEM but the FDM.

- There are reasons to consider the mathematical foundation of the finite element approximation more sound: for instance, the quality of the approximation between grid points is poor in FDM.

### 5.3 Conceptualization

A conceptual groundwater model is a basic graphical representation of a groundwater flow system that can be easily adjusted. The elements of a conceptual model include defining the extents and characteristics of the aquifer system as well as developing an understanding of groundwater flow directions, sources, and sinks. Conceptualization takes into consideration the overall objective of the model, the schedule and resources for reaching the objective, and the available geological, hydrogeological, and hydrological data (Anderson and Woessner 1992). The geological and hydrogeological conceptual models are based primarily on a synthesis of data and information including the geological properties of the study area, dividing it into a number of layers, when the presentation is in three dimensions, each has a lithology, and structure. The geological data can be obtained from geological maps, well logs and borings, geophysics and cross sections. The hydrologic data include the following:

- Defining the boundaries of the model, both external and internal, such as the surface water in canals and no flow boundaries due to the watershed effect (groundwater divides) or due to the very low permeable contact between different geological units.
- Specifying the hydrostratigraphic units which Seaber (1982; 1986; 1988) defined as bodies of rock distinguished by porosity and permeability. Specifying the hydrostratigraphic units is important to identify the number of layers within the study area and accordingly the hydraulic conductivity and storativity along each layer.
- Identifying the inflow budget, for instance, from precipitation, seepage from surface water, or surplus from irrigation water and the outflow budget either from evapotranspiration or from direct extraction.
- Defining the flow system such as groundwater levels at the initial condition that describes the directions of groundwater flow as well as the hydraulic gradient. In addition, defining the relation between the beds levels of canals and the groundwater levels and the hydraulic relation between each other.

In addition to the geological and hydrological data, it is essential to identify the mathematical functions that describe the development of the activities along the study area such as the recharge and the discharge with time.

### 5.4 Discretization

Discretization in mathematics concerns the process of transferring continuous models and equations into discrete counterparts. This process is usually carried out as a step toward making them suitable for numerical evaluation and implementation on digital computers. The discretization of the model domain is a main task because of its direct effect on the result of the numerical model. The finer the discretization, the more detailed and precise is the simulated groundwater flow. Despite the rapid development of processors and improved computational time, the time needed for computing power remains of regional groundwater model is still a constraint for the discretization (Jagelke et al. 2005). The grid of the model should be finer if there are wide variations in the properties of the aquifer. In the irrigation areas that depend mainly on groundwater through a condensed net of pumping wells, the distribution of these wells in the area of study play a major role on the grid size, especially in the finite element models where the pumping wells are assigned to the nodes of the grid. Nevertheless, in finite difference models the pumping wells are assigned to the cell itself. The mesh size is affected, to a wide extent, by the modeling objectives itself.

A groundwater model can be represented in one of two conditions, either as steady state flow modeling or as transient flow modeling. In the case of steady state flows there is no change in the storage value because the outflow is equal to the inflow and time is irrelevant. Alternatively, transient flow modeling simulates the stresses on the aquifer through time. Consequently, this time is divided into time steps, either manually by the user to reflect any temporal stresses on the aquifer such as discharge and recharge, or automatically controlled by the balances of head changes along each time step.

While it is beneficial to use a mesh with small nodal spacing, it is also favorable to apply small time increments for obtaining minor changes of aquifer behavior with time at a higher accuracy without losing the stability of the model (Fig. 5.1).

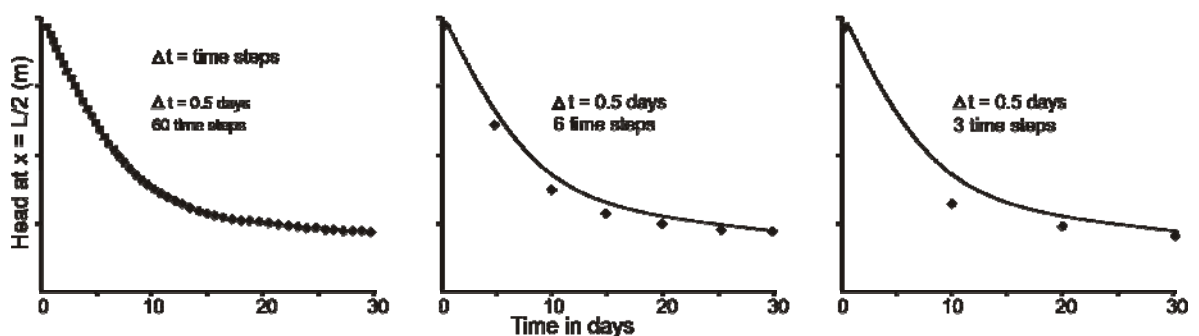


**Fig. 5.1:** The effect of time increment on the simulation of the groundwater hydraulic head's decay. A solid line represents the analytical solutions and the points represent the numerical solutions (modified after Townley and Wilson 1980).

## 5.5 Data processing

In order to construct a conceptual hydrogeological model representing a groundwater flow system, it is required to compile all available data (geologic, hydrogeologic, etc.) that cover the modeled area such as:

- geological data from geological maps
- profiles and cross sections
- digital elevation model (DEM)
- contour maps, for example for ground surface as well as groundwater levels
- topographic maps
- isopach maps for the different layers in the study area
- groundwater and surface water levels
- coordinates of pumping wells and their extraction rates
- hydraulic properties of the aquifers from pumping tests
- saturated thickness of the aquifer
- sources of recharge and their rates
- climate data
- boundary conditions of the modeled area

In some cases, the measurements of the aquifer parameters are not enough to represent the whole area of interest, and the data are found as scattered measurements in the study area. However, in order to develop a reliable groundwater flow model that can represent the aquifer behavior, it is required to define the aquifer parameters in each node or cell of the domain. Therefore there is a need to use the tools of statistics as well as geostatistics to estimate the unknown parameters based on the known parameters. Geostatistical methods are more feasible in hydrogeological applications for parameters estimation, as well as their ability to quantify spatial uncertainties by applying the process of interpolation. The geostatistical methods are explained by many authors in the literature including Isaaks and Srivastava (1989), Yarus (1994), Armstrong (1998), Chiles and Delfiner (1999), Schafmeister (1999), Houlding (2000), Webster (2007) and Pilz (2009).

One of the representative geostatistical methods concerning geological and hydrogeological information is the kriging method which is identified as an optimal interpolation technique based on statistical analysis of the observed values surrounding data points, weighted according to spatial covariance values (Bohling 2005). Kriging is similar in some ways to the inverse distance weighting (IDW) interpolation. Comparing the two techniques provides insight into the benefits of kriging. With IDW each grid node is estimated using sample points which fall within a circular radius. The degree of influence that each of these points has on the calculated value is based upon the weighted

distance of each of the sample points from the estimated grid node. The disadvantage of the IDW interpolation technique is that it treats all sample points that fall within the search radius in the same way, where in the kriging method, every possible distance weighting function is calculated. This is done by generating an experimental variogram of the data set and choosing a mathematical model which best approximates the shape of the variogram. The model provides a smooth, continuous function for determining appropriate weights for increasingly distant data points (Fig. 5.2).

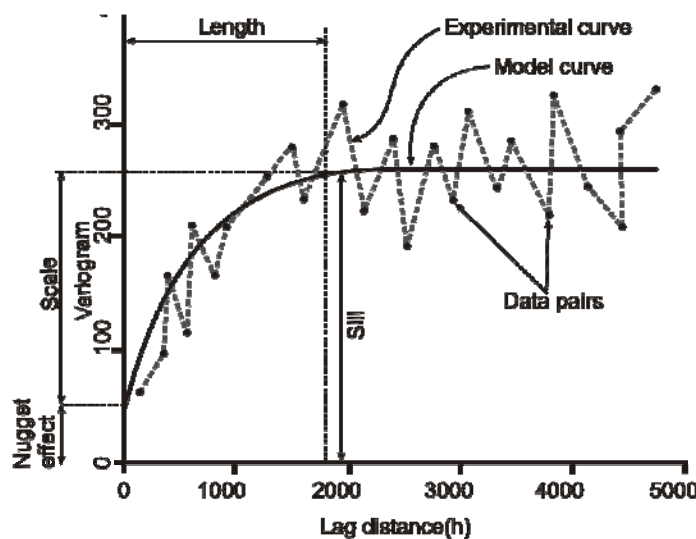


Fig. 5.2: A variogram components clarify the experimental curve and the model curve. Compiled from Surfer ® 8 User’s Guide (2002).

The variogram can be explained in equation (5.16) as a function describing the degree of spatial dependence of a spatial random field or stochastic process  $Z(x_i)$ .

$$2\gamma(h, x) = E\left([Z(x_i + h) - Z(x_i)]^2\right) \quad [\text{Eq 5.16}]$$

where  $\gamma(h, x)$  is called semivariogram, both  $Z(x_i)$  and  $Z(x_i + h)$  are the random variables separated by distance “h”.

The variogram is said to be isotropic if it depends only on the modulus of “h” and anisotropic if it depends on both the distance “h” and the direction.

For a sample consisting of “N” data location, there are “N<sub>h</sub>” experimental pairs ( $x_i, x_{i+h}$ ), the sample variogram is defined as:

$$\gamma(h) = \frac{1}{2N(h)} \sum_{i=1}^{N(h)} [Z(x_i + h) - Z(x_i)]^2 \quad [\text{Eq 5.17}]$$

After obtaining the experimental variogram  $\gamma(h)$ , there is a requirement to identify the type of variogram model (e.g. linear, spherical, exponential, gaussian, logarithmic, etc.) and the parameters of the variogram model components, such as the nugget effect, sill



(scale) and range (length). The modelling of  $\gamma(h)$  is an iterative process that involves changing the values of the variogram model components until finding the best fit of the variogram model related to the experimental variogram.

## 5.6 Boundary conditions

The boundary conditions of any groundwater flow model are the mathematical statements specifying the dependent variable (head) or the derivative of the dependant variable (flux) at the boundaries of the dependant domain, either inside the model area or at its edges. When groundwater systems are heavily stressed, the physical features that bound the system can change in response to the stress (Thomas 2001). The most common types of boundary conditions are those that represent surface water in streams in groundwater flow models. The type of interaction between the surface water in streams and groundwater defines the boundary condition type. Streams can either gain water from the groundwater system when the water table in the stream is lower than the groundwater table, or lose water to the groundwater system when the water table in the stream is higher than the groundwater table. The last case differentiates into two types; either the connection between surface water and groundwater is in a continuous saturated zone between the bed of the stream and groundwater table, or it can be in a disconnected unsaturated zone. There are many ways to represent a stream in a numerical model, and each way treats the interaction of the stream with the groundwater system. A stream may be represented as a specified head boundary (Dirichlet condition, first-kind), a specified-flow (flux) boundary (Neumann condition, second-kind), or head-dependent flux or leaky boundary (Cauchy condition, third-kind). Furthermore, the stresses affecting the aquifer system by pumping or injection wells are considered as well boundaries (fourth-kind). A special case of the second kind of boundary conditions is the streamlines in the groundwater flow system, which form a certain hydraulic and physical boundary known as “groundwater divide” or “no flow boundary” (Fig 5.3). The mathematical explanation of different types of boundary conditions is as follows:

- **Dirichlet condition**

The first kind of boundary condition is known as a specified head. It is defined mathematically as a type of boundary condition (Dirichlet condition). When imposed on an ordinary or a partial differential equation, it specifies the values of the head on the boundary of the domain. The mathematical description of the head in such case, according to Delleur (1999) is:

$$h(x, y, z, t) = \text{Specified value} \quad [\text{Eq 5.18}]$$

where “ $h(x, y, z, t)$ ” is the hydraulic head (L) at certain location and time on the domain.

• **Neuman condition**

The second kind of boundary condition is known as a specified flow boundary. In mathematics, it is defined as a type of boundary condition (Neumann condition). When imposed on an ordinary or a partial differential equation it specifies the flux that the derivative of a solution takes on the boundary of the domain. The mathematical equation was expressed by Franke et al. (1987) as:

$$\frac{dh(x,y,z,t)}{dn} = \text{Specified flux} \quad [\text{Eq 5.19}]$$

where “*h*” is the head (L) and “*n*” is a directional coordinate normal to the boundary (L). In the case of no flow boundary, the derivatives of the head are set to zero. This condition takes place, for instance, between two adjacent geological layers; the first layer is a highly permeable geological unit and the second is a much lower permeable geological unit, in case of water divides, in case of existing faults, or in case of a stable interface between saltwater and fresh water in coastal aquifers (Zhang 2001).

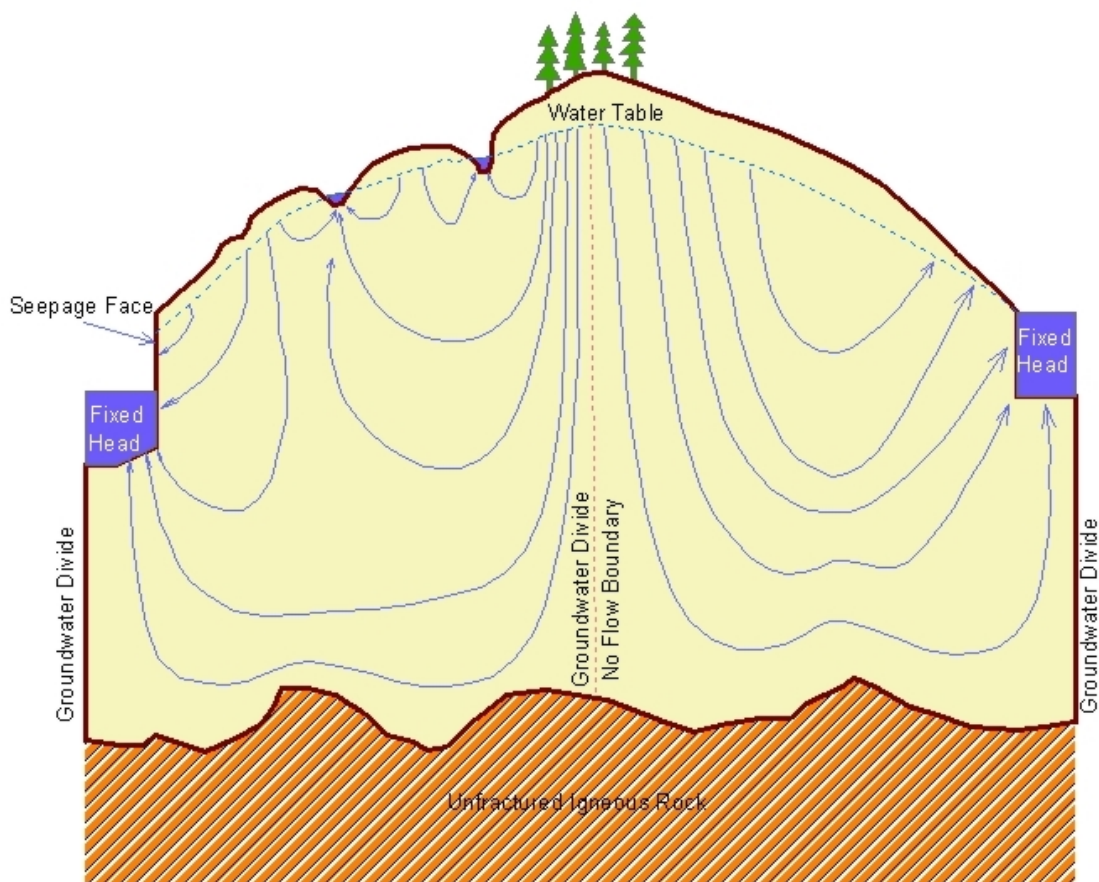


**Fig. 5.3:** Regional flow systems representing the physical and hydraulic boundaries. Compiled after Anderson and Woessner (1992).

• **Cauchy condition**

The third kind of boundary condition is known as a head dependent flow boundary. It is defined mathematically as a type of boundary condition (Cauchy condition). When imposed on an ordinary or a partial differential equation, it specifies both the values head and the related flux on the boundary of the domain. In other words this type of boundary condition is a connection between both Dirichlet and Neumann condition, because it relates boundary head to boundary flow (Anderson and Woessner 1992). The mathematical expression of this boundary type is:

$$\frac{dh}{dn} + ch = \text{Value-dependent flux} \quad [\text{Eq 5.20}]$$

where “*h*” is the head (L) , “*n*” is a directional coordinate normal to the boundary (L) and “*c*” is a constant.

The Cauchy boundary condition can be applied to express leakage from surface water canals into groundwater, where the flux is directly proportional to the hydraulic conductivity of the boundary and inversely proportional to the difference between surface water table and groundwater level.

• **Extraction/Injection condition**

The fourth kind of boundary condition is the stress that affects the groundwater system either as extraction or as injection at a singular point source. The change in the hydraulic head due to extraction or injection wells is a function of the aquifer parameters and the discharge/recharge rates in an elapsed time.

It is not possible for both groundwater head and vertical inflow to be specified at the same location. If a vertical inflow is applied at a nodal point or cell, the groundwater head distribution can be determined whenever the transmissivity and boundary conditions are known. However, if the groundwater head is specified, the recharge or the discharge can be determined whenever the transmissivity and boundary conditions are known (Rushton 2003).

**5.7 Initial conditions**

Defining a time-variant problem in mathematical terms requires specifying the initial conditions as accurately as possible. The initial condition can be defined as the head distribution within the model area at a certain time, usually denoted as  $t = 0$ . Consequently, the selection of appropriate initial conditions that represent the historical response of the aquifer, and also provide appropriate flow conditions at the start of the simulation, is a crucial aspect to consider. There are two available alternatives to specify initial conditions for numerical solutions: either the simulation is started from specified groundwater heads

or the simulation starts with specified flows (although when specified flows are imposed, groundwater heads must be defined at some locations to achieve a stable solution). In general, the distribution of the measured heads can serve as the initial conditions. The need of the initial heads distribution to solve steady-state flow problems acts as a physical requirement (Spitz et al. 1996), where a good estimation of the initial condition accelerates the convergence in numerical calculations, especially for unsaturated-flow problems. However, unlike the steady state flow, the initial conditions for transient flow are numerical requirements, where the results of a simulation are heavily dependent upon the initial conditions. Usually the initial conditions for transient flow problem are taken from the results of solving the same problem in the case of steady-state flow.

## 5.8 Calibration

In order to use a groundwater model for future predictions, proof must be developed to show its ability for reasonable simulations of the historic past. Calibration is the process of adjusting the model parameters until a good fit with historical measurements is achieved (ASCE 1996). During calibration, many parameters such as system geometry, properties, initial conditions, boundary conditions, and stresses should be adjusted within the range of the observed or measured data until the model becomes accurate enough to represent the simulated system (Hill and Tiedeman 2007). The basic steps of model calibration are shown in Figure 5.4. Model calibration should be performed for both steady-state conditions and transient conditions. Calibration for steady state condition alone is not adequate because it does not take into consideration the storage properties of the aquifer and the behavior of the aquifer with the time, whereas the groundwater flow is time dependent by its nature. Model calibration can be achieved either by using manual trial-and-error adjustments or automatic parameter estimation.

Trial-and-error calibration was the first technique applied in groundwater modeling. Although it depends heavily on the user's experience, it is always recommended to perform this type of calibration, at least partially. The modeler develops a better feeling for the model and the assumptions on which its design is based by changing parameter values and analyzing the corresponding effects. During manual calibration boundary conditions, parameter values, and stresses have the ability to be adjusted for each consecutive model run until the results of the simulation match the measured data. Trial-and-error calibration means adjusting the input values and running the model tens of times to reach the target. The worst-case scenario involves a complete redesign of the model. The main disadvantage of this method is that it is time consuming, which leads to an attempt to develop it by estimating the parameter values using a mathematical model of system processes and a set of relevant observations in what is called the inverse method for

calibration. The inverse modeling methods have been classified into direct and indirect method (Neuman, 1973; Yeh, 1986; Sun, 1994). In direct inverse modeling, the available observations are interpolated and/or extrapolated everywhere in the model domain. Using these observations, the differential equations describing the simulated processes are used to calculate the model parameters directly. This method has been shown to be unstable if there are some measurements errors (Yeh, 1986). In addition, the indirect method uses both available observation data and optimization techniques to estimate model input values.

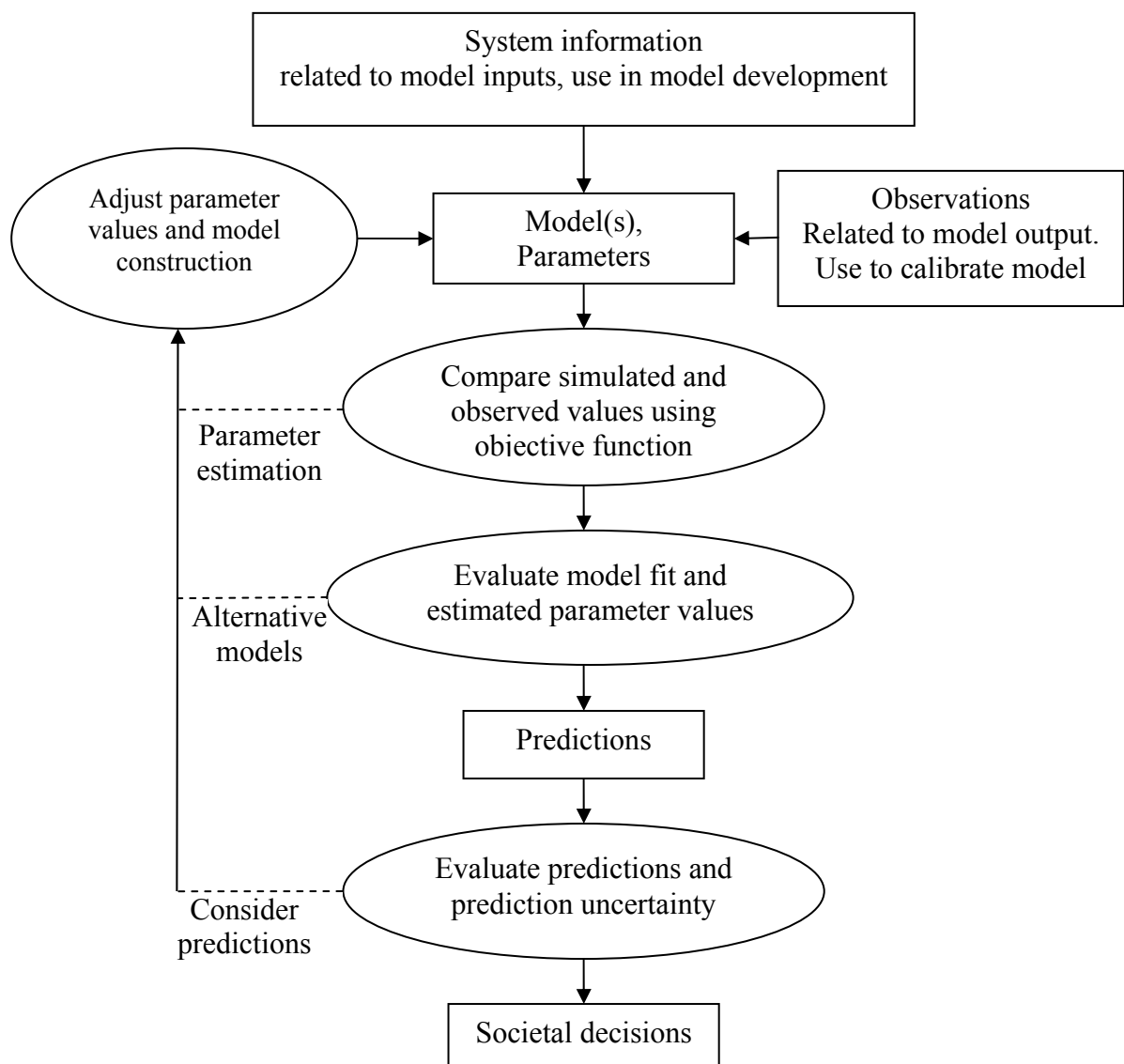


**Fig. 5.4:** Flowchart showing the major steps of calibrating a model and using it to make predictions. Adapted from Hill and Tiedeman (2007).

The first phase of calibration ends when there is a good visual match between the calculated and measured targets (for instance the hydraulic heads). The next phase consists of quantification of the model error with various statistical parameters, such as standard deviation, and distribution of model residuals, i.e., differences between calculated and measured values. Once this error is minimized through a lengthy process of calibration, and satisfies a preset criterion, the model is ready for predictive use (Kresic 2006).

### **5.9 Validation of a model**

Validation of safety assessment models is defined as the processes of building scientific confidence in the used methods to perform such assessments (Neuman 1992). Retchey and Rumbaugh (1997) have defined validation as the processes, which compare the calibrated model with another set of field observations representing a different set of boundary conditions or stresses. Sometimes validation of numerical models of natural systems is not easy because natural systems are never closed and because model results are never unique. The process of model validation cannot ensure model prediction; rather, it provides a safeguard against inadequately tested models. Groundwater validation is one of the most challenging issues facing modelers. The more complex the groundwater model is, the wider the gap between model predictions and the confidence in predictions. There is no specific procedure that can be adapted to determine the validity of groundwater models, except the iterative loop between the different processes of constructing, calibrating and validating the model (Hassan 2003).

# 6 Regional Model

## 6.1 Introduction

The main objective of this study is to develop a groundwater flow model for the area west to the Rosetta branch in order to study the suitable scenario for groundwater extraction rates and its effects on the hydraulic heads during the next 50 years with a focus on the Wadi El-Natrun depression. The formulation of a conceptual model for this area required a thorough hydrogeological evaluation of the various rock types, which are schematized into aquifers, aquitards, and aquicludes (Nonner, 2006). Preparation of the model data includes defining the top and the bottom of each layer in the model, coefficients of permeability, storage coefficients, boundary conditions, initial conditions, recharge and discharge. The defined data was stored in a geographic information system, “GIS-database”. For the numeric simulation of the aquifer system within the study area, the computer code “FEFLOW” has been selected as a numerical program package for the three-dimensional simulation of groundwater flow under steady state and transient conditions on the basis of a finite element technique. The computational method in the computer code needs a specific mesh that consists of cells with the shape of triangles. The mesh can be refined into sub areas, where there are dense activities based on groundwater such as pumping wells. The finite element computer code is capable of constructing an optimal mesh with nodes in each well’s position. The model obtained the data through linking it with the GIS-database. To determine the parameters within all the cells of the grid, a statistical interpolation method is required. Before using the flow model to calculate the suitable scenarios for the study area, a calibration process should be repeated by comparing the simulated heads with the measured heads until a satisfactory match between computed and observed values is obtained.

## 6.2 Data acquirement

There are different sources of the collected data that have been used to construct the database for the study area. The main sources are as follows:

- Topographic maps from the Egyptian Geological Survey and Mining Authority (EGSMA 1950, 1951, 1990).
- Geological maps (CONOCO 1987).

- Hydrogeological maps and cross sections from the Research Institute for Ground Water, Egypt (RIGW 1988, 1992, 1993).
- Available data regarding extraction rates from the Research Institute for Ground Water, Egypt (RIGW 2006).
- Observed data of surface water in canals from the Ministry of Water Resources and Irrigation, Egypt (MWRI 1992, 2006, 2007).
- Available data regarding an agricultural project from the General Company for Research and Ground Water, Egypt (REGWA 1993).
- Digital elevation models from the National Aeronautics and Space Administration (NASA 2005)
- Many national as well as international technical and academic reports and literature (All are mentioned in the bibliography).

### 6.3 Model design

#### 6.3.1 GIS-Database

The data in the study area were obtained in different forms including topographic maps, geological and hydrogeological maps, geological cross sections, well logs, drilling data, and existing digital data from satellite images. In order to construct the groundwater flow model, a GIS-database was built using ArcGIS (ESRI ® ArcMap™ 9.2, 2007), (ESRI ® ArcMap™ 9.3, 2008). In addition to efficient data integration, GIS provides means to handle large and complex data sets. The ESRI geodatabase has been described by Zeiler (1999) as an object-oriented model introduced with the ArcGIS software. For groundwater modeling purposes, GIS was adopted not only to prepare the spatial data for 3D groundwater models, but also to provide a basic platform to input and extract information from maps in different scales and projections and make the required transformation between coordinate systems, such as from the World Geodetic system (WGS 1984) coordinate system to the Universal Transversal Mercator (UTM) coordinate system. The modification of the spatial references of the input data is easier via a GIS-database and considered as time saving especially when conflicts or problems during the simulation phase of the 3D groundwater model exist. For different applications of the flow model, a GIS was used to analyze the results by comparing them with each other or by overlaying them with other thematic maps. Evaluation of available data, either spatially or temporally, requires a well-organized database and efficient tools for accessing and displaying the data with the relevant background information. The GIS-database in this study is made up of the digital elevation model of the ground surface, the spatial distribution of each geological layer, the hydrogeological parameters, the initial groundwater heads, the boundary conditions, the recharge, the discharge, and all well locations and their extraction rates (Wassef et al. 2008, Wassef et al. 2010). The link between the GIS-database and the



groundwater flow model was achieved by saving all the data in the same format (ESRI shape-files) and same coordinate system (UTM Zone 36N). All data in the GIS-database were represented as point data features with appropriate attributes within the domain. The GIS-database provides the ability of information query and search during and after the simulation phase.

### 6.3.2 Creation of digital maps

The first step in generating a GIS-database is the scanning and georeferencing of all analog maps, sheets, and cross sections to convert them to digital bitmaps (raster data). These bitmaps are composed of pixels independent of the dimensions of the drawings that the raster represents where the georeferencing process translates the bitmaps into the real dimensions. Georeferencing should be performed carefully because it is the link between the analog features and the digital features and the spatial distribution of the data sets depending upon it. An inaccurate translation results in misplacement, which leads to the same geographic features, as represented on different maps, not aligning with and overlaying each other. Most of the bitmaps of the study area have a geographic coordinate system. They were spatially georeferenced into an international coordinate system “World Geodetic System 1984 (WGS-84)” (DMA TR8350.2, 1997; Galati 2006). The geological cross sections were georeferenced by setting the horizontal axis according to the calculation of the real coordinates of the projection of the profile in the plan and the vertical axis according to the elevations given in the cross section multiplied by an exaggeration factor. The tools of ArcMap 9.2 were used for the process of georeferencing.

The second step involves converting the raster data by the tools of digitizing into a digital vector format consisting of polygons, lines or points. This digitizing process includes attributing the vector data, which is an important process in the construction of any geographic information system. For example, any point will have attributes for its coordinates and any polygon could get attributes for its area and any other appropriate variables.

The third step after the digitizing process (for either geologic or hydrogeologic maps according to the geographic coordinate system) was converting a copy of the vector data into a projected coordinate system, the Universal Transversal Mercator (UTM), using the tools of ArcToolbox to convert the units from arc degrees, arc minutes, and arc seconds into meters to be suitable for the modeling code.

An example for the encoding and translation procedure was the production of the geological map of the study area illustrated in figure (3.1), which was digitized and acquired from the CONOCO maps (CONOCO 1987).

### 6.3.3 Interpolation and layers generation

Generating layers based on the geological framework is a major step in constructing a 3D groundwater model. Because of the difficulties obtaining exhaustive values of data at every point in the domain and due to the scattered distribution of the data for the establishment of a 3D groundwater flow model, there is a need for statistical management of the available data. The chosen method for geological interpolation is the kriging method. It predicts the unknown values from the observed data at known locations by using variograms to analyze the spatial variation and surface roughness (Barnes 1991). The process of interpolation using the kriging method is done by applying an appropriate variogram model (Exponential, Gaussian, Linear, Logarithmic, Power, Quadratic and Spherical) on each data set. The spatial data for a data factor (elevations) were exported from ArcGIS in a form of (X, Y, Z) where “X” and “Y” are the UTM coordinates and “Z” is the required value to interpolate. These data were imported to an interpolation software program (Surfer 8.0, Golden Software 2002). The appropriate variogram model was chosen depending on the best matching model curves for the experimental variogram. The resulting grids were designed to have a resolution of 100 m spacing covering the whole modeled area for both “x” and “y” directions from the UTM coordinates (161300, 3320000) to (331300, 3488000), and forming 1,701 rows and 1,681 columns and 2,859,381 data points for each interpolated surface.

The study area was divided into eight main layers arranged stratigraphically from the top as follows: Holocene layer (Delta cap), Pleistocene aquifer, Pliocene aquifer, Miocene-Pliocene Clay layer, Miocene aquifer, Oligocene Basalt layer, Eocene-Oligocene Shale layer, and Paleocene-Eocene layer (Fig. 3.2). Each layer in the modeled area has at first some scattered elevation data derived from the constructed cross sections, isopach maps and the data from boreholes. To produce the elevation data in a uniformly distributed form, the kriging interpolation method with its related variograms was used where the appropriate variogram model (Fig. 6.1) was applied on the available data to establish the unknown spatial data in the modelled area. The interpolation process was repeated for each slice in the geological system (nine slices for eight layers) and the accuracy of the interpolation results is directly proportional to the density of the input data. The interpolation results were linked with the groundwater flow model via the tools of ArcGIS, which converted the format of the interpolation results into shape-file format. To adjust the

hydraulic conductivity between slices, where the interpolation technique of the hydraulic conductivities between cells in the modeling code “Feflow” are based on the arithmetic mean, each interior main layer was divided into three layers having the same hydraulic conductivity and both the upper and the lower parts are very thin compared to the thickness of the main layer. However, the top and the bottom layers (exterior layers) were divided only into two parts. The thin part takes place at the side of the flow exchange. The slice of the ground surface was created (Fig. 6.2) from both available contour maps (1:100,000) and the Digital Elevation Model (DEM) from the Shuttle Radar Topography Mission (SRTM) (USGS 2004; NASA 2005) with a resolution of about 90x90 m and an accuracy of about  $\pm 9$  m. After finishing the interpolation process and the construction of the layers, slice elevations as shown in Figure 6.2 were imported by the modeling software, which has the ability to discover any crossing between slices that prevent the model program from running.

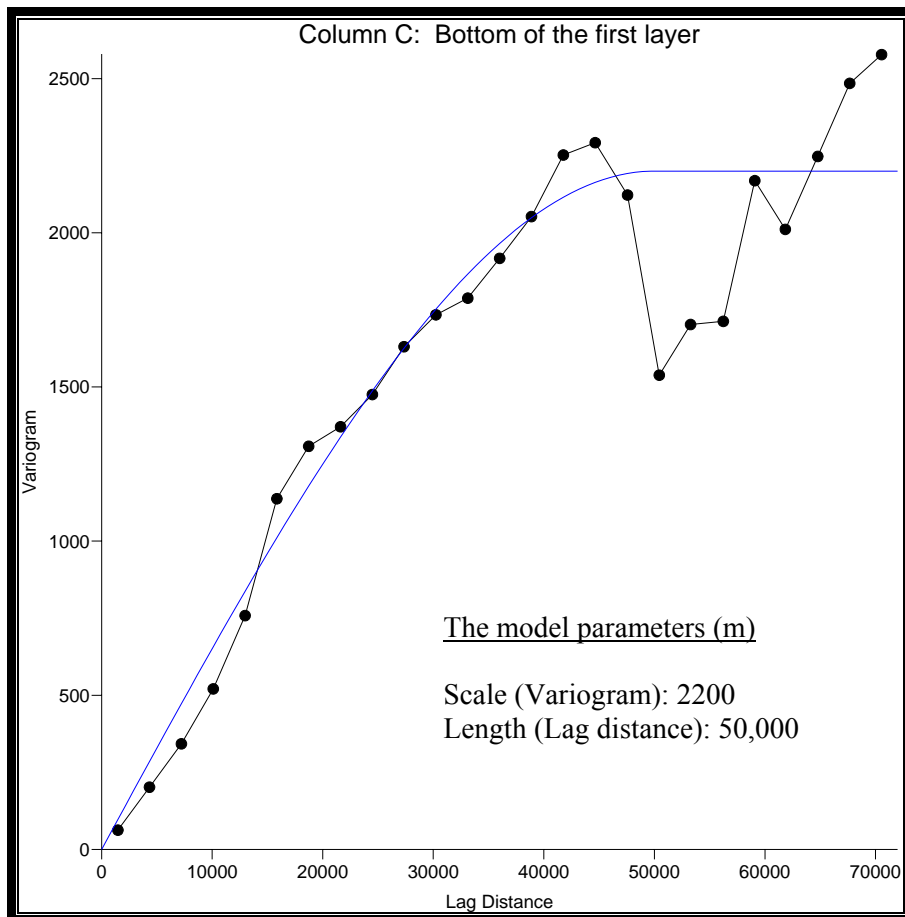


Fig. 6.1: A spherical variogram for the bottom of the first layer.

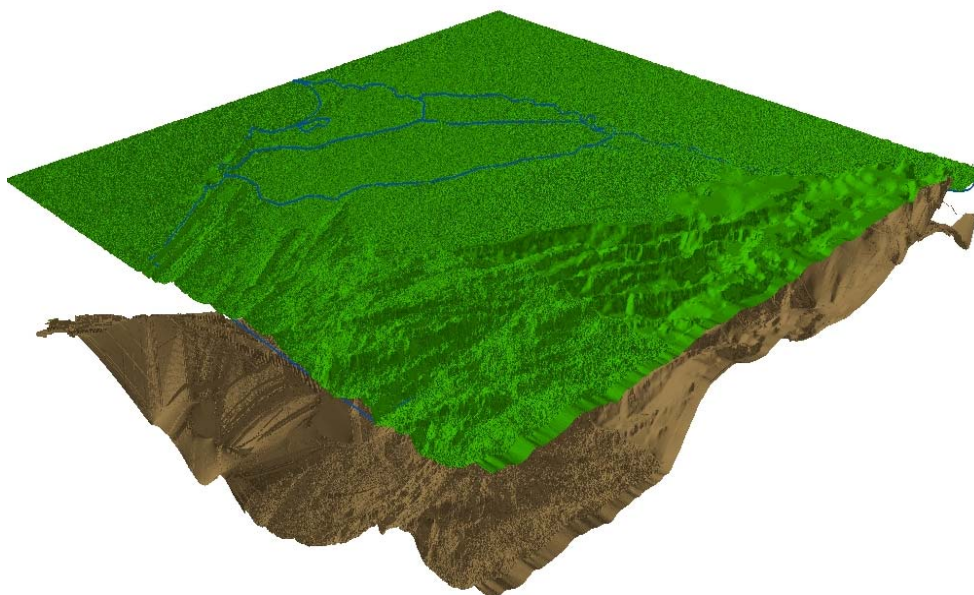


Fig. 6.2: Digital Elevation Model in relief shape for the ground surface and lower surface of the Miocene layer.

### 6.3.4 Boundary conditions

Four kinds of boundary conditions in the study area are distributed in the outer boundary and inside the domain as follows:

- **Dirichlet boundary condition ( First kind)**

The fixed head boundary condition is represented in this model for the Rosetta branch, the Noubaria Canal, and for the surface water body at the northern lakes and the Mediterranean Sea, where the surface water level is about 0 m (amsl).

- **Neuman boundary condition ( Second kind)**

The fixed flux boundary condition is applied to the west and south boundary as a “water divides boundary” where the borders of the study area are perpendicular to the groundwater contours. In addition, in the south boundary at its east direction there is an existing fault as mentioned in Section 3.2. and Fig. 3.3.

- **Cauchy boundary condition (Third kind)**

This boundary was set to the surface water in canals along the domain such as the Rayah Behery and the Rayah Nasery, in which the flux across the boundary is dependent on the magnitude of the difference in head across the boundary, with the head along the boundary being input to the model and the head asides of the boundary being calculated by the model.

- **Wells boundary condition ( Fourth kind)**

This type of boundary condition is presented by the discharge of the pumping wells in the study area. Each well should have a power function representing the values of the extraction rates during the time period of simulation. All wells in the study area (more than 6500 wells) were classified into 137 groups according to their time dependant functions.

### 6.3.5 Initial conditions

The initial conditions for transient models define the state of the system at the beginning of the simulation. When the simulation begins, the state changes from the initially specified state to become consistent with the simulated initial processes and properties and ongoing stresses (Hill and Tiedeman 2007). If changes in the conditions at the system during the simulation are rapid, the ongoing stresses will dominate the solution and as a result, the comparison between observed and simulated values becomes meaningful after a relatively short time. However, if the changes in the conditions are slow, it is required to begin the transient simulation with the initial conditions that were produced by the steady state simulation. The inconsistencies of initial conditions can endure for long period simulation in groundwater systems that change with slow rate and can affect the model fit. The initial conditions in this study were the observed groundwater levels derived from the groundwater contour map of RIGW (1990) in addition to the available individual records of the groundwater levels around the year 1990 (Fig. 6.7).

### 6.3.6 Recharge and discharge

The recharge in the study area is represented mainly by the seepage from the surface water of the Nile River and its branches and distributaries, from the infiltration and downward leakage of excess irrigation water, and from the infiltration of rainfall. According to Sections 4.4 and 4.5, the effective recharge rates were estimated as follows: the higher recharge rates in the study area (from 100 to 300 mm/a) were set in the central portions beside the El-Noubaria Canal where there is a groundwater rise and water logging problem. In the desert areas that use modern irrigation methods (drip and central pivot irrigation), the effective recharge rates were set from 0 to about 50 mm/a. The effective flux from both the recharge and the evapotranspiration was represented in the GIS as constant value points in the domain and it was applied to the top layer of the finite element grid of the model.

The main discharge component in the study area is the extraction rates by wells. As shown in Table (6.1), there are two extraction schemes for the next 50 years. The first scenario is the actual groundwater exploitation at the stressed region as given from the official records of groundwater extraction for irrigation, industrial, and domestic water supply, with an annual extraction rate of about 1066 million m<sup>3</sup>. The second scenario is based on the actual circumstances in addition to the extraction rate for the case of irrigation 100% of the stressed areas with total annual extraction rate of about 2529 million m<sup>3</sup> (Table 6.1).

**Table 6.1:** Extraction scenarios (million m<sup>3</sup>/a) for stressed areas.

ID	Region	Area (km <sup>2</sup> )	Scenario 1 (Mio m <sup>3</sup> /a)	Scenario 2 (Mio m <sup>3</sup> /a)
1	Kafr Dawood	219.22	164.28	260.98
2	Birigat	262.10	80.02	312.02
3	Khatatba	157.59	73.11	187.61
4	South Khatatba	229.92	273.72	273.72
5	South Highway	155.00	166.02	184.52
6	North Highway	254.88	125.43	303.43
7	Dina	71.49	34.00	80.00
8	Wadi El-Natrun	273.09	60.82	310.82
9	Sadat City	83.99	40.98	99.98
	<b>Total</b>	<b>1707.28</b>	<b>1018.39</b>	<b>2013.09</b>

### 6.3.7 Numerical model development

A conceptual groundwater flow model is a framework where the data of the subsurface can be considered. To describe the aquifer systems in a model, data should be collected from the available sources as illustrated in Figure 6.3 and several hypotheses have to be considered regarding the available data. In this study, the groundwater flow model code (Feflow) was used to construct a three dimensional numerical model for the simulation of groundwater flow under the steady state and the transient conditions by using the Galerkin-based finite-element technique. All the required physical and hydrogeological data for developing a numerical model were imported through the link with the GIS-database.

The model was set up as a multi-layered system by linking the available cross sections with the data from boreholes and isopach-maps in an interpolation program. Considering that the lithologic description for the study area differs from one location to another, it is differentiated into eight main hydrostratigraphic units depending on the geology and the hydraulic parameters as follows:

- The top unit represents the semi-pervious silty clay (Holocene).
- The second unit represents graded sand and gravel intercalated by clay lenses (Pleistocene aquifer).
- The third unit represents alternating sand and clay with occasional limestone at the top (Pliocene aquifer).
- The fourth unit represents a clay layer (Miocene - Pliocene).

- The fifth unit represents the Miocene aquifer, which consists of coarse sand and gravel with intercalation of sandstone and clay.
- The sixth unit represents a basalt layer (Oligocene).
- The seventh unit represents shale with occasional gravelly sandstone intercalations (Eocene - Oligocene).
- The last unit represents a limestone layer, occasionally dolomitic or chalky (Paliocene - Eocene).

A node-related boundary condition was used in the model to accommodate Dirichlet boundary conditions (first kind); Neumann, (second kind); Cauchy, (third kind); and the wells boundary conditions (fourth kind). The pumping wells of the study area and their extraction rates were located in the transient flow model and were described by power functions to clarify their behavior over time. Groundwater recharge and the evapotranspiration were modeled within the domain of the study area as “in-/outflow on top”, in which the modeling code has the ability to represent it either as a constant or as a time dependent value. All parameters (hydraulic conductivities, storativity, porosity, etc.) were handled on an element level, i.e. they can differ from element to element. To ensure maximum quality for the distribution of data in the conceptual model, the node elevations and conductivities of the grid were interpolated using universal kriging for the discussed reasons in Section 5.5.

### 6.3.8 Discretization

To construct the three dimensional groundwater flow model, the study area was discretized stratigraphically into eight main layers. To rectify hydraulic conductivities each layer was further discretized into three layers, except for the first and the last layers, which were discretized into two layers. This discretization in the vertical direction led the model to consist of 22 layers with 23 slices (Fig. 6.4). Each layer was discretized into 53,329 triangular prismatic elements with 27,061 nodes in each slice. The total number of elements in the model is 1,173,238 with a total of 622,403 nodes. The finite element mesh was generated manually by applying different sub-regions in the study area according to the distribution of surface water canals and modeling interests and the mesh refinement of the model took place where there are irrigational activities based on extraction wells. The distances between nodes in each slice ranged between less than 100 m to 1000 m in the refined area and from 500 m up to 2800 m in the remainder of the area. Time discretization was applied using the automated time stepping schemes based on the Gresho-Lee-Sani (GLS) predictor-corrector time integrator for second order (Adams-Bashforth/trapezoidal rule) controlled with a maximum time step limited by five days to ensure the stability of the results.



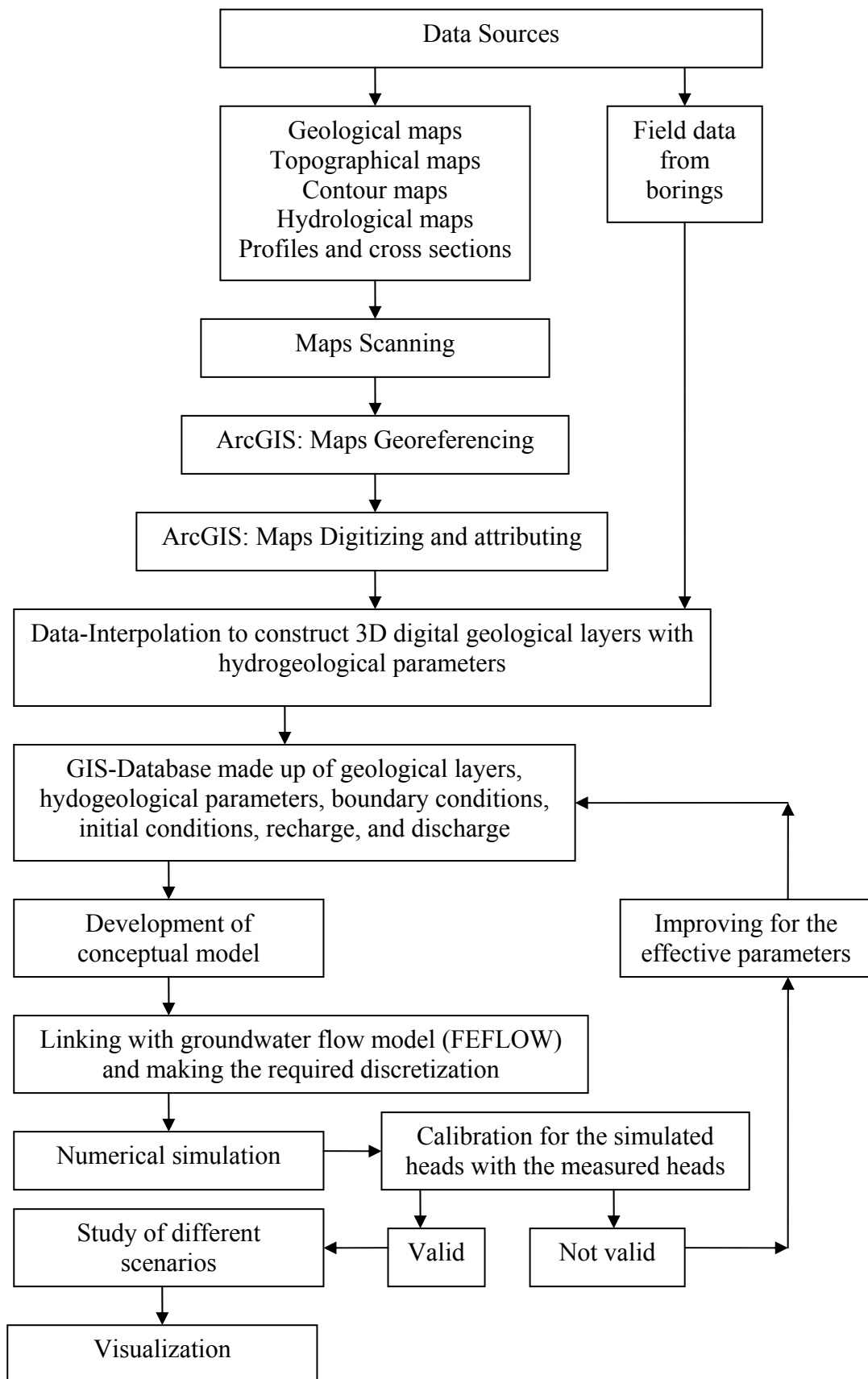


Fig. 6.3: Flowchart showing logical movement of data used to investigate the numerical model.

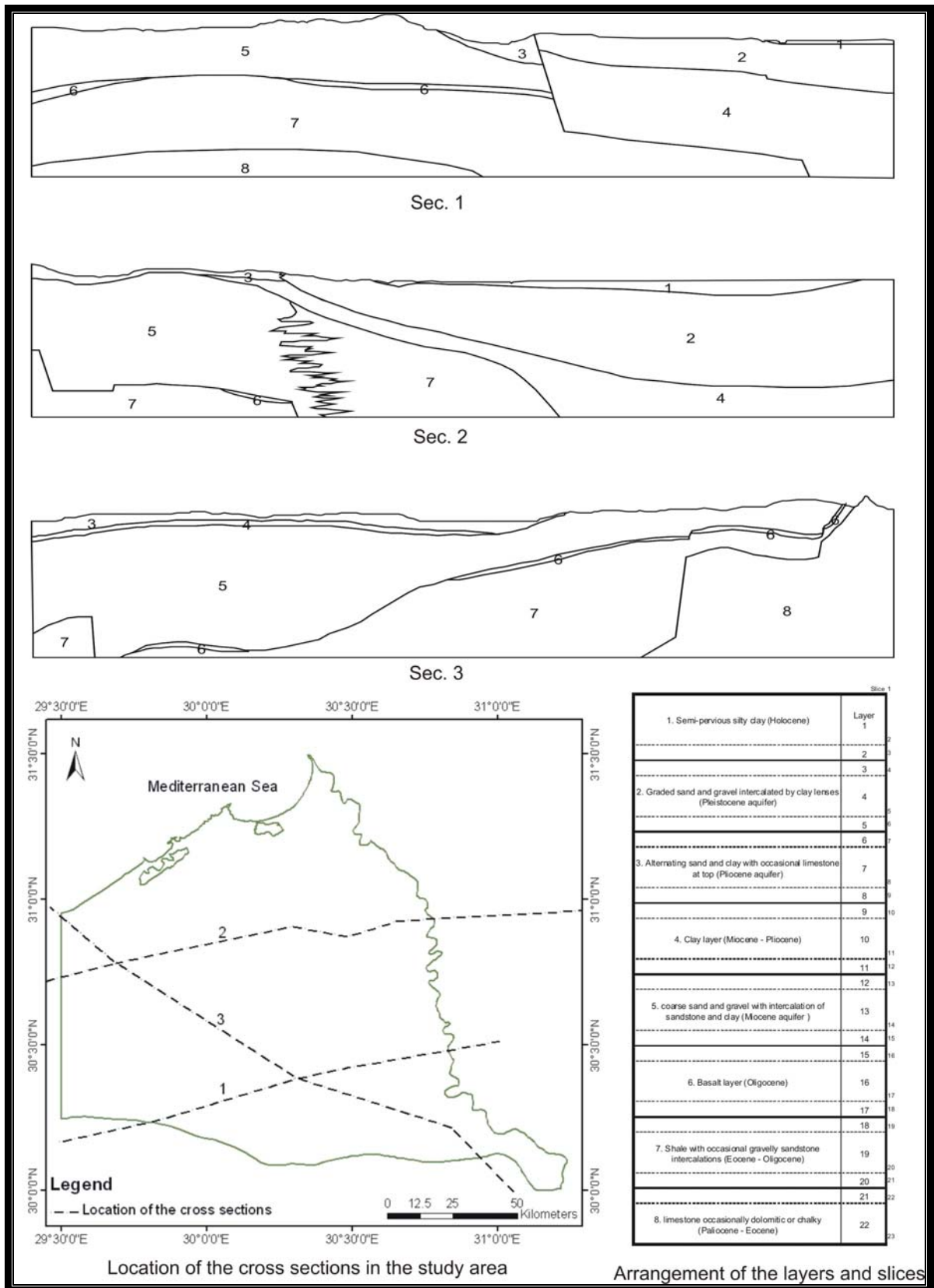


Fig. 6.4: Schematic map describing the structure of the layers and slices.

## 6.4 Integration of GIS - data in a groundwater model

There are various possibilities for integrating GIS data into a groundwater model. The first is transferring data from the GIS to a groundwater model, where the groundwater model and GIS are separate and computer routines in the model are used to make the data in the GIS available to be read by the model and to convert the model outputs into GIS format. The second is via embedding modelling capabilities within a GIS, which involves a database without data conversions. The first possibility is used in this study to transfer the GIS data to the computer code (FEFLOW). This approach involves a stronger linkage through a database and a user interface to facilitate the data exchanges. It makes modeling operations easier, more efficient, and removes database redundancy (Johnson, 2009).

## 6.5 Calibrating the numerical model

The objective of the calibration was to ascertain the validity of the hydraulic conductivity distribution in the numerical model as provided by the hydrogeological testing. There is a need for the calibration process because there are unknown, unmeasured, or unrepresented conditions and uncertainty in the measured input data. The calibration process was chosen for the period 1990-2006 (from the beginning of the increase in the development rate in this area) where the extraction rates, the recharge from excess irrigation water, the irrigational areas based on groundwater, and the observed groundwater heads are recorded and available. The calibration procedure for the model was tried initially to base on the inverse modeling technique “Automated parameter estimation” but there were not enough different types of complete observation data for these techniques to be successful. The other calibration option was to use the trial-and-error method, which required a great effort. Under both the steady state and transient flow conditions, and via a series of groundwater flow simulations, the numerical model was calibrated by the method of trial-and-error, where typical parameters should be varied within measured or estimated ranges and parameter distributions should be limited to geologically feasible hypotheses until a satisfactory match between simulated and observed hydraulic heads is achieved. For the areas where there are no available observation data, the calibration was assigned on the hydraulic gradient and the flow direction. Evaluating goodness-of-fit takes place both visually by comparing contour maps of simulated heads with measured hydraulic heads (Fig. 6.5) and quantitatively by comparing the observed data of the heads with the simulated heads using the “Pearson-correlation-coefficient” indicator. The statistical analysis of the residuals in 336 points between simulated and observed water levels data clarified that the difference between simulated and observed heads ranges from -1.73 to 1.8 m with a range of 3.53 m and a standard deviation of 0.41 m.

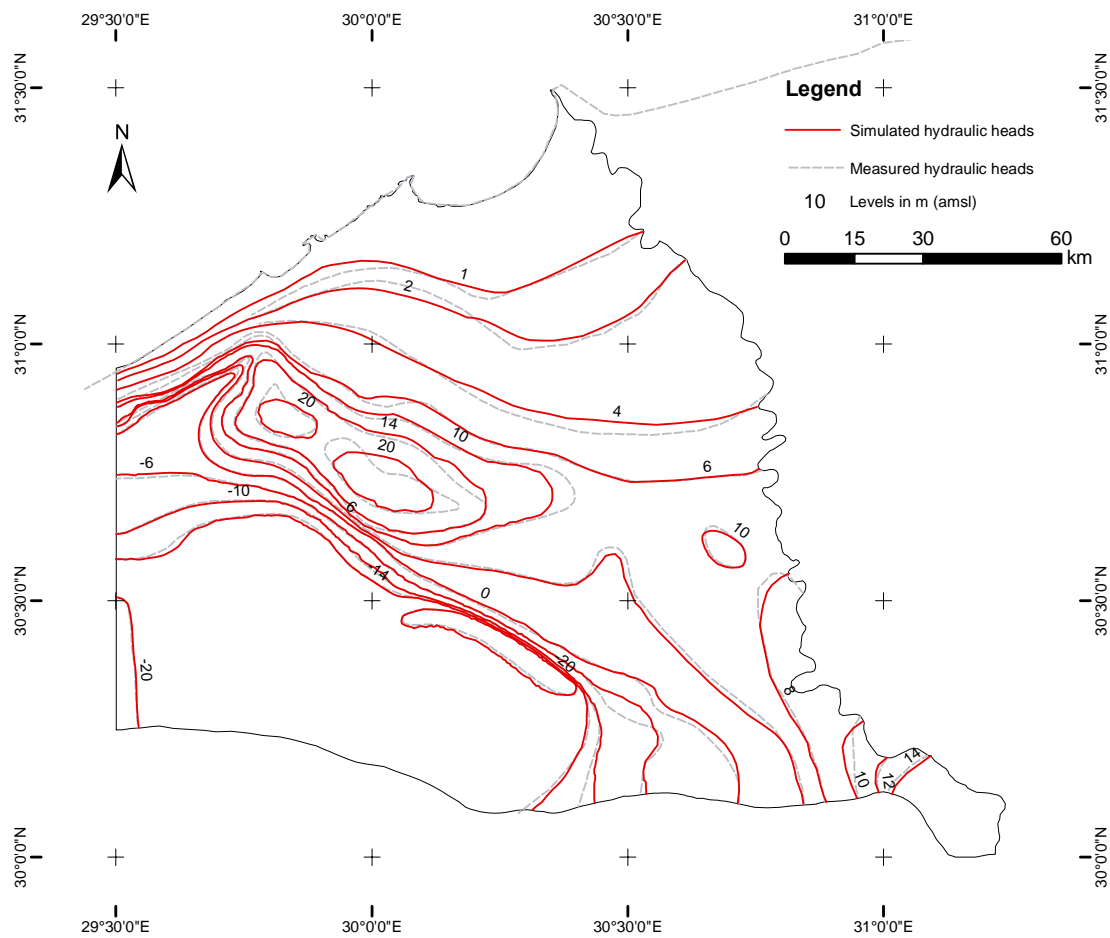


**Fig. 6.5:** Result of model calibration under transient conditions and spatial distribution of field observations in the upper aquifer.

The mean of residuals between observed and simulated heads is positive (Table 6.2), which also appears in the histogram of the residuals (Fig. 6.6) where it is skewed towards the observed heads indicating that the observed heads in general are slightly higher than the simulated heads. The distribution of the observed heads versus the calculated heads is depicted in Figure 6.7 comparing with the 1:1 line. The correlation-coefficient “ $r_{xy}$ ” between observed and simulated heads was calculated according to the equation (6.1) and equal 0.98. The hydrographs of wells were used where long-term water-level data were available (Figure 6.8).

$$r_{xy} = \frac{\sum (x_i - \bar{x})(y_i - \bar{y})}{(n - 1)s_x s_y} \quad [\text{Eq 6.1}]$$

Where “ $x_i$ ” is the observed head, “ $y_i$ ” is the simulated head, “ $\bar{x}$ ” is the mean of the observed heads, “ $\bar{y}$ ” is the mean of the simulated heads, “ $n$ ” is the number of points, “ $s_x$ ”

is the standard deviation of the observed heads, and “ $s_y$ ” is the standard deviation of the simulated heads.

**Table 6-2:** Statistics for the calibration process at the study area.

Statistics	Values
Number of observations	336
Range of residuals (m)	3.53
Minimum residual (m)	-1.73
Maximum residual (m)	1.8
Mean of residuals (m)	0.034
Standard deviation of residuals (m)	0.41
Pearson correlation coefficient ( $r_{xy}$ )	0.98

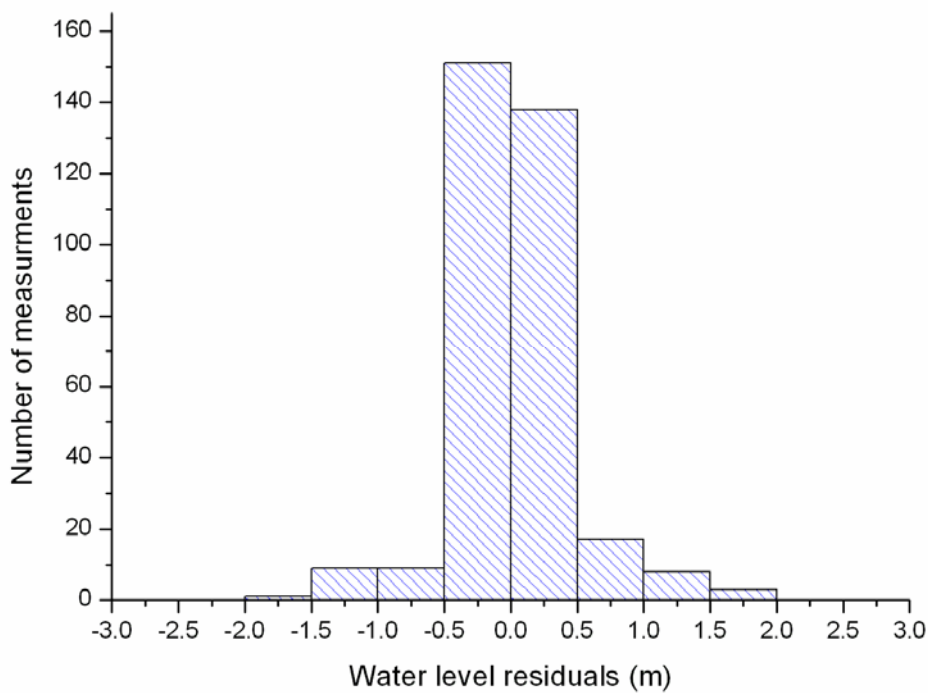


**Fig. 6.6:** Histogram representing the frequency range of the residuals.

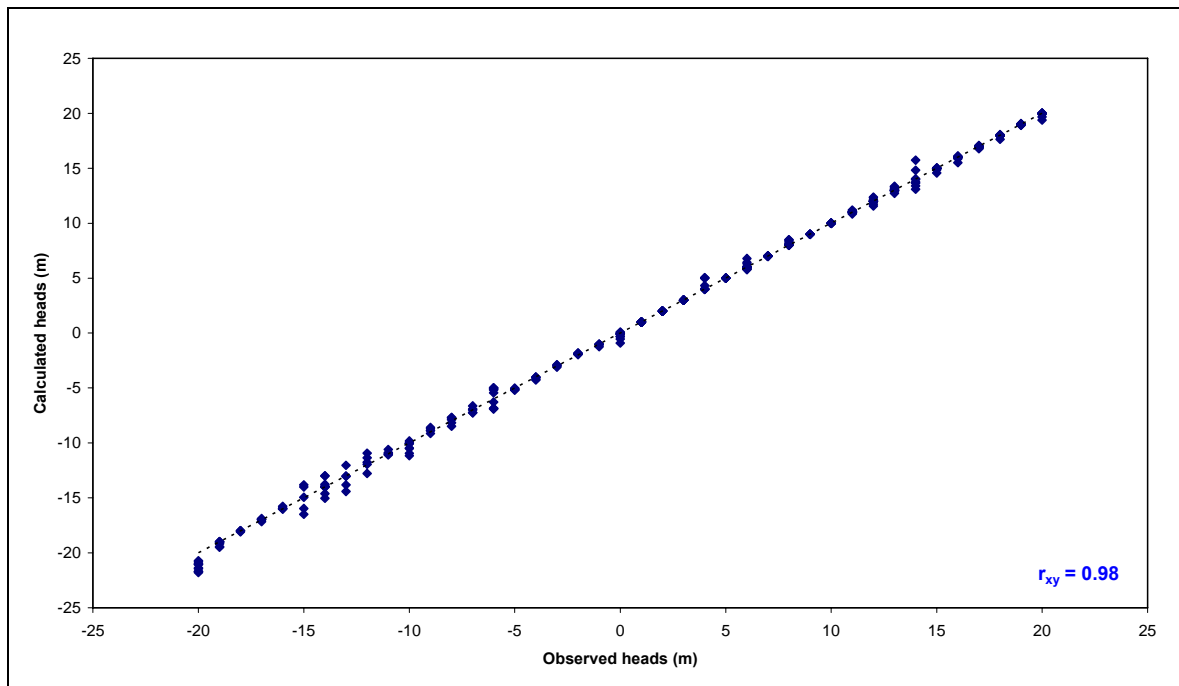


Fig. 6.7: Scatter diagram showing simulated heads versus measured heads.

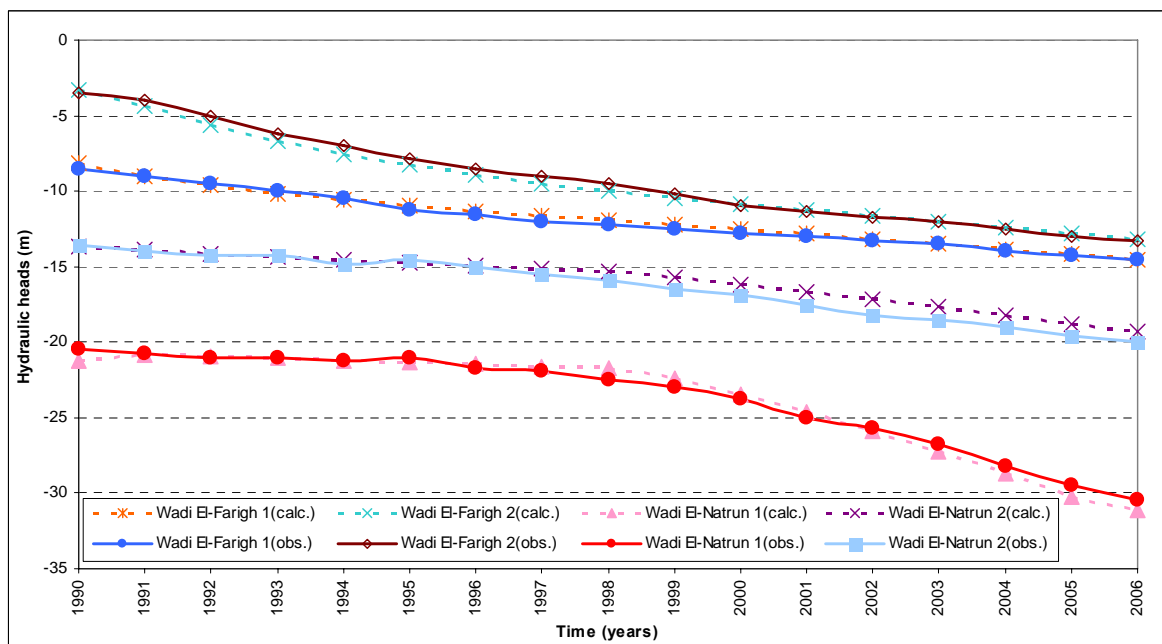


Fig. 6.8: Hydrograph of history matching a comparison between observed and simulated heads with time.

## 6.6 Regional model results

The calibrated regional model was used initially to predict the changes in the flow regime that resulted in the Miocene aquifer system from stresses based on the extraction rates up to year 2060. During the analysis procedure of the simulation results to evaluate the response of the aquifer systems to the stresses, certain emphasis is given to the changes in the hydraulic heads, drawdown, depth to groundwater, and the groundwater balance. The current hydraulic head distribution and drawdown (state 2010) are depicted respectively in Figure 6.9 and Figure 6.10.

### 6.6.1 Hydraulic heads

The direction of groundwater flow within the regional model area is kept in general by the original trend of the initial head presented by RIGW (1990) as shown in Figure 6.5. However, the values and local trends of these contours have some changes within the Pleistocene aquifer but the major changes can be stated for the Pliocene and the Miocene aquifers as in the Wadi El-Natrun and the Wadi El-Farigh depressions and in the development areas such as Sadat city and North Highway, where the contour lines had lower values than in the initial heads. Table 6.3 gives a representation of the average hydraulic heads, drawdown, and depth to groundwater in the stressed areas.

The major changes in the pattern of the groundwater contour lines for Scenario 1 and Scenario 2 for the years 2035 and 2060 according to the extraction values in Table 6.1 are shown in Figure 6.11 through Figure 6.14. In case of Scenario 1, the contours started to change slightly, especially in the depressions of Wadi El-Natrun, and Wadi Farigh compared to the results of Scenario 2 with full capacity extraction rates at the stressed areas.

### 6.6.2 Drawdown

The drawdown at the study area during the period from 1990 to 2060 for the studied scenarios can be differentiated into areas, where the drawdown ranges from less than 5 m to more than 60 m. At the regions that depend mainly on surface water such as the Delta and its vicinities, the drawdown was found to be less than 5 m. In the regions that depend mainly on groundwater (the stressed areas), the drawdown started to become obvious after the year 1990 due to the expansion in investment projects and the rapid development in different fields such as irrigation, industry, and recreation. The decline of the groundwater levels by time in the stressed areas had a continuous drop. Consequently, the amount of the stored groundwater in the aquifer started to decrease, leaving a noticeable decline in the potentiometric levels. The model simulations helped in following up and defining this decline in the hydraulic heads within the areas of interest (Table 6.3).

By analyzing the obtained results of the numerical model for the first scenario from the year 1990 to 2060, it was indicated that the major cones of depression are located south of the desert margin (outside the Delta) based on the Moghra aquifer in the study area, with average drawdown ranges from about 17 m in the year 2010 to 22 m in the year 2035 increasing gradually to about 30 m in the year 2060 (Fig. 6.15 and Fig. 6.16). However, the decline in the groundwater levels appears significantly in the second scenario where steep hydraulic gradients and wide, deep cones of depression were created with an average drawdown in year the 2035 ranging from less than 5 m up to about 55 m and increasing up to about 73 m in year the 2060 (Fig. 6.17 and Fig. 6.18). Comparing the situation in Scenario 2 with the situation in Scenario 1, it is noticeable that the area of more than 25 m drawdown showed an increase from about 1900 km<sup>2</sup> in the first scenario to be about 7000 km<sup>2</sup> in the second scenario. The average rate of increase in drawdown in scenario 1 is about 0.4 m/a. However, the average rate of increase in drawdown in Scenario 2 is about 1 m/a. The allowable drawdown was considered by RIGW and REGWA (1992) as 25 m for the 50 years from 1990 to 2040, which equals to 0.5 m/a. Thus both of the North Highway area, Wadi El-Natron, Sadat city and Dina farm are considered critical areas affected by the high differences in groundwater levels between 1990 to 2060.

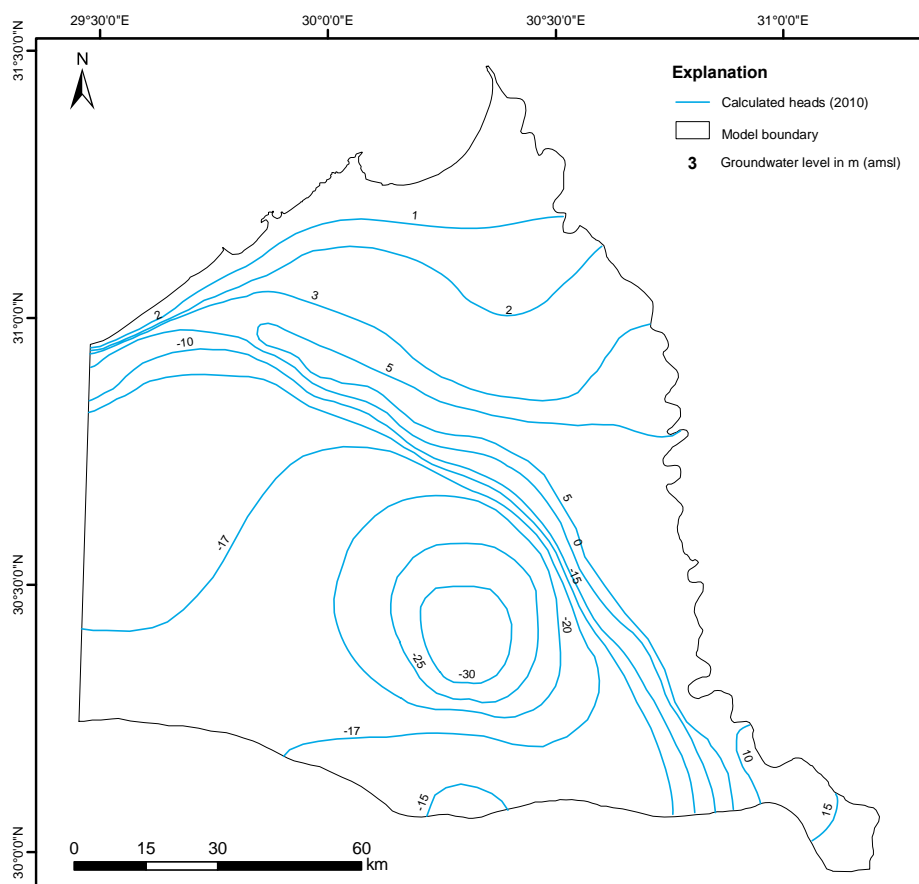


Fig. 6.9: Distribution of the simulated hydraulic heads at the study area in the year 2010.



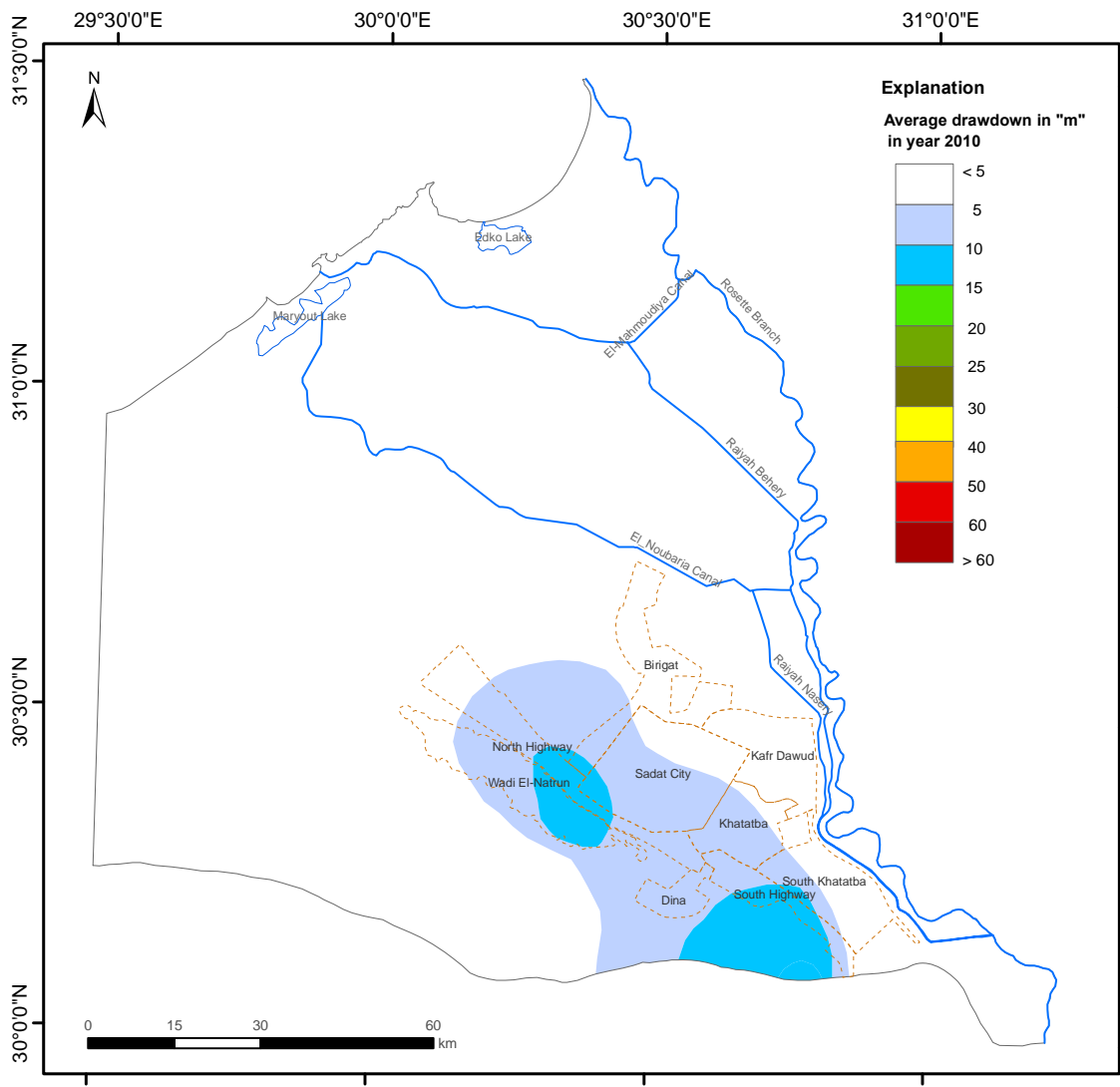
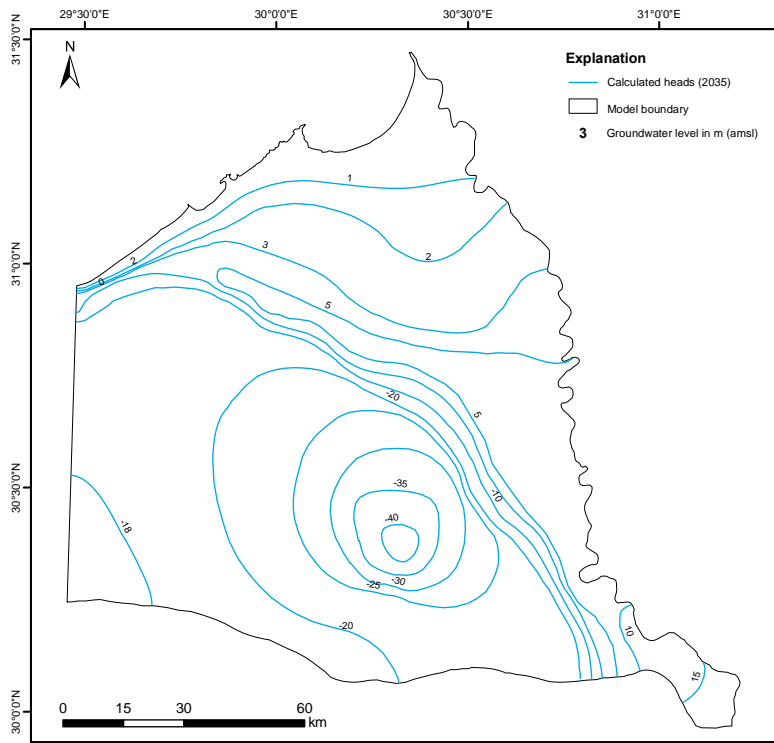


Fig. 6.10: Decline in the hydraulic heads in the stressed areas from 1990 to 2010.

**Table 6.3:** Average changes in hydraulic heads, drawdown and depth to groundwater for the development areas

Location	Scenario	Hydraulic head (m amsl)			Drawdown (m)			Depth to groundwater (m bgl)		
		2010	2035	2060	2010	2035	2060	2010	2035	2060
Kafir Dawood	1	2.16	0.90	-0.39	1.12	2.38	3.67	14.95	16.21	17.50
	2	2.16	0.30	-1.56	1.12	2.98	4.84	14.95	16.81	18.67
Birigat	1	-14.50	-17.00	-18.80	1.70	4.20	6.00	39.82	42.32	44.12
	2	-14.50	-25.80	-32.90	1.70	13.00	20.10	39.82	51.12	58.22
Khatatba	1	-14.70	-21.70	-26.70	6.30	13.30	18.30	74.88	81.88	86.88
	2	-14.70	-25.70	-36.50	6.30	17.30	28.10	74.88	85.88	96.68
South Khatatba	1	-0.30	-2.70	-4.70	2.22	4.62	6.62	70.60	73.00	75.00
	2	-0.30	-3.40	-6.90	2.22	5.32	8.82	70.60	73.70	77.20
Dina	1	-16.50	-23.30	-28.40	7.90	14.70	19.80	97.80	104.64	109.70
	2	-16.50	-28.00	-39.20	7.90	19.40	30.60	97.80	109.34	120.60
South Highway	1	-12.80	-20.30	-25.60	9.30	16.80	22.10	112.78	120.28	125.58
	2	-12.80	-23.70	-34.50	9.30	20.20	31.00	112.78	123.68	134.48
North Highway	1	-26.00	-31.80	-35.40	7.60	13.40	17.00	64.80	70.60	74.20
	2	-26.00	-60.90	-73.00	7.60	42.50	54.60	64.80	99.70	111.80
Wadi El-Natrun	1	-28.20	-33.80	-37.30	8.20	13.80	17.30	15.65	21.25	24.75
	2	-28.20	-65.70	-78.10	8.20	45.70	58.10	15.65	53.15	65.55
Sadat City	1	-21.40	-28.00	-32.40	6.30	12.90	17.30	48.76	55.36	59.76
	2	-21.40	-40.10	-52.40	6.30	25.00	37.30	48.76	67.46	79.76
The allowable drawdown should not exceed 0.5 m/a (RIGW and REGWA 1992)										



**Fig. 6.11:** Distribution of the simulated hydraulic heads in the study area in the year 2035 according to the extraction rates of Scenario 1.

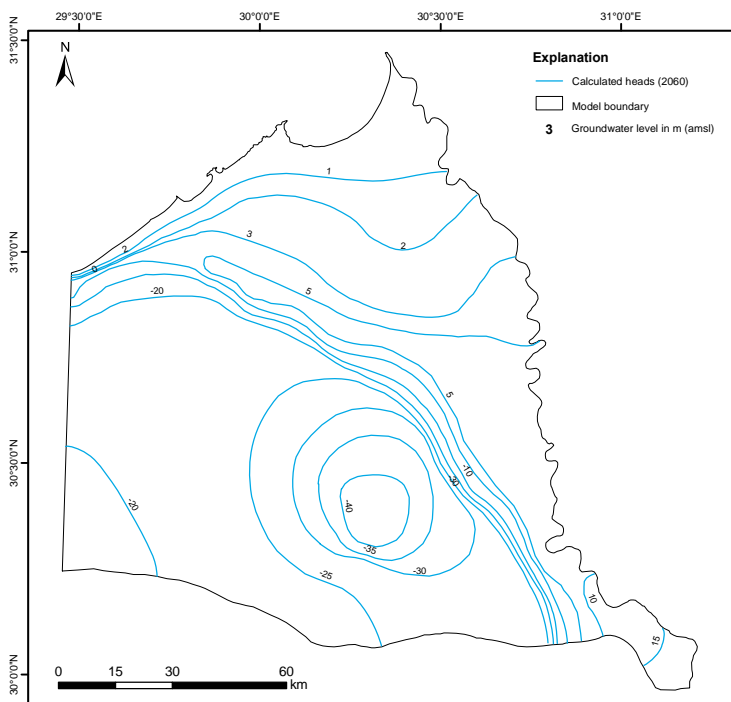


**Fig. 6.12:** Distribution of the simulated hydraulic heads in the study area in the year 2060 according to the extraction rates of Scenario 1.

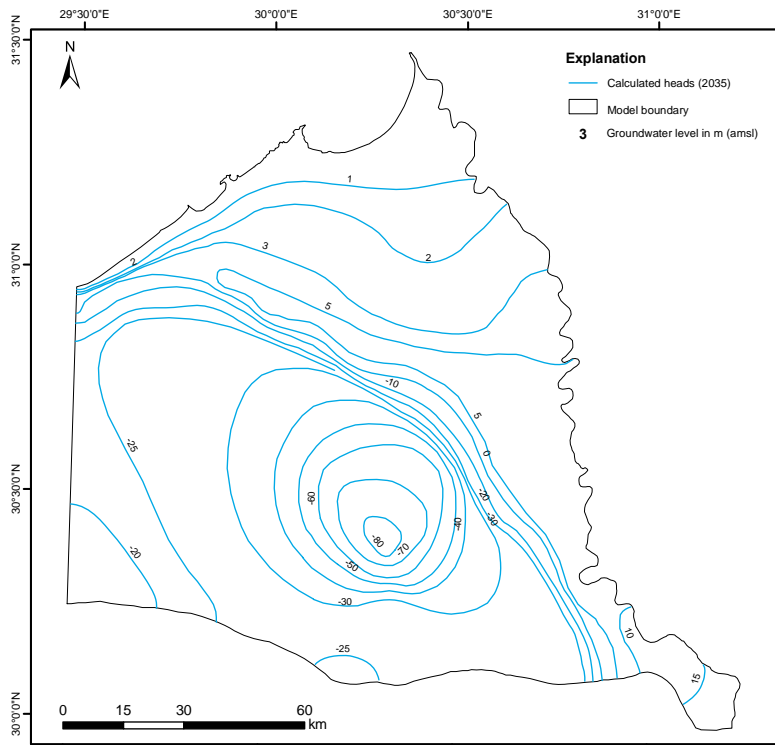


**Fig. 6.13:** Distribution of the simulated hydraulic heads in the study area in the year 2035 according to the extraction rates of Scenario 2.

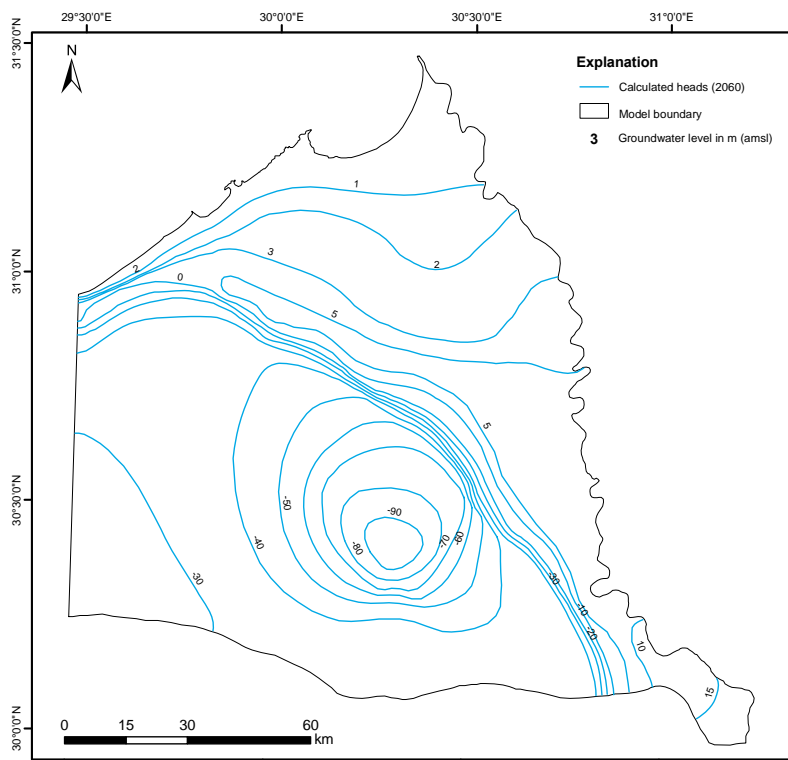


**Fig. 6.14:** Distribution of the simulated hydraulic heads in the study area in the year 2060 according to the extraction rates of Scenario 2.

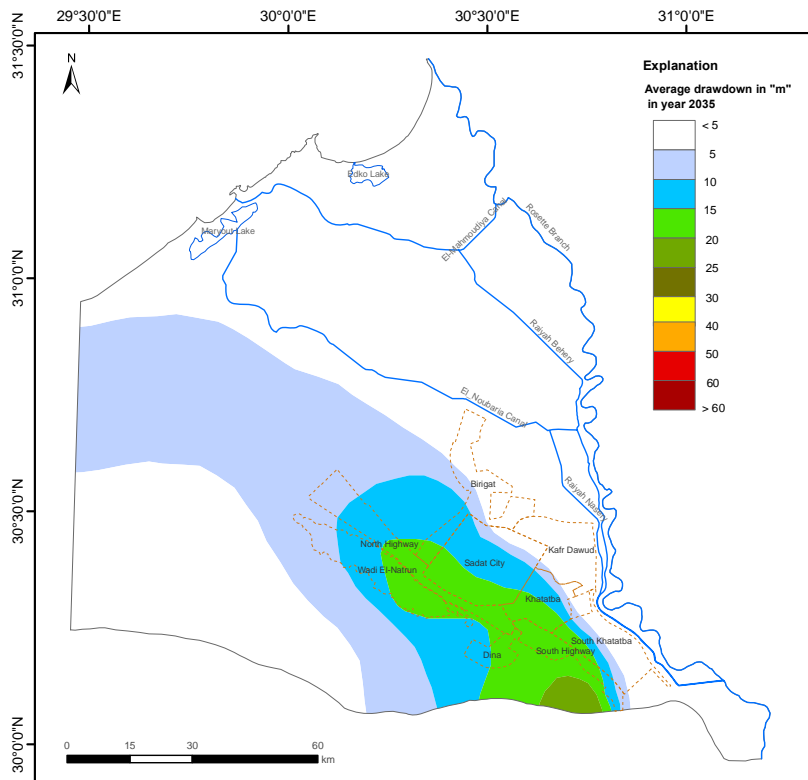


Fig. 6.15: Drawdown in the stressed areas in the year 2035 according to the extraction rates of Scenario 1

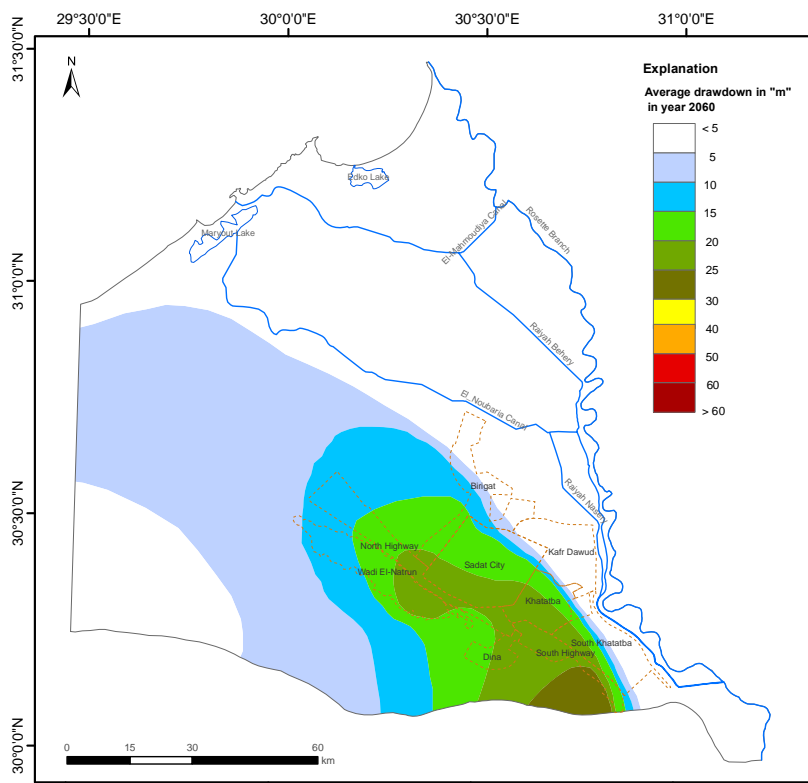


Fig. 6.16: Drawdown in the stressed areas in the year 2060 according to the extraction rates of Scenario 1

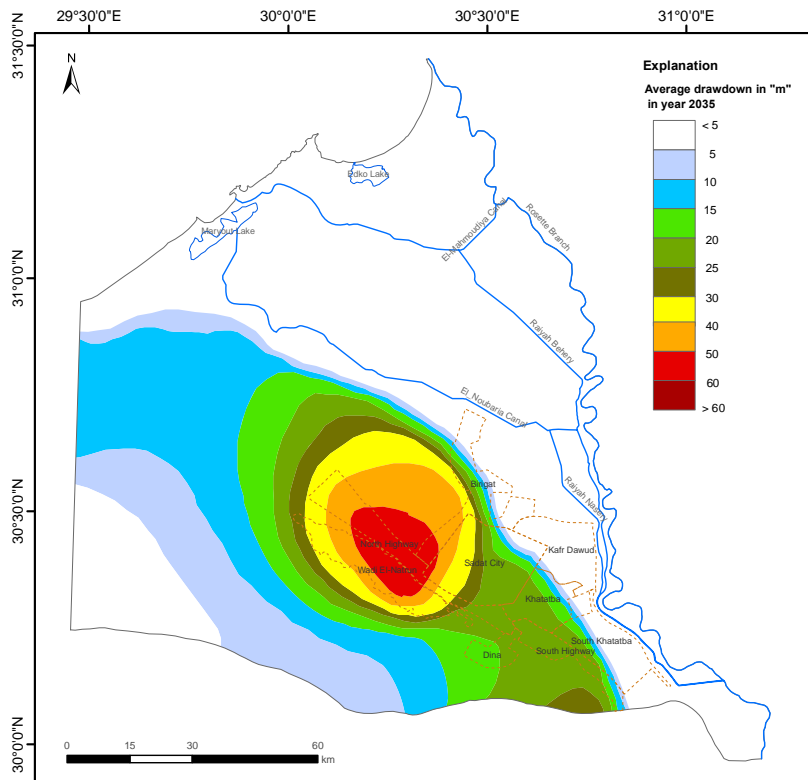


Fig. 6.17: Drawdown in the stressed areas in the year 2035 according to the extraction rates of Scenario 2

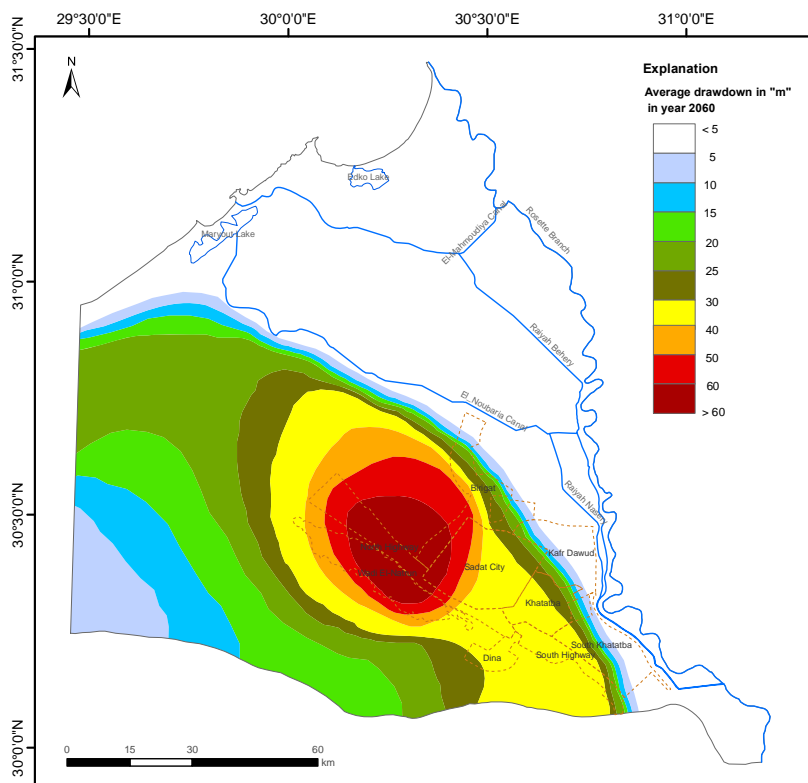


Fig. 6.18: Drawdown in the stressed areas in the year 2060 according to the extraction rates of Scenario 2

### 6.6.3 Depth to groundwater

In the area between the east side of the El-Noubaria Canal and the Mediterranean Sea and in some areas between the Rosetta branch and the Rayah Nasery Canal, the initial depth to the groundwater level is less than 3 m. The depth to groundwater decreases northward and to the northeast direction. Conversely, the depth to groundwater increases gradually toward the desert westward of both the Nubaria Canal and the Rayah Nasery Canal to reach about 78 m in Scenario 1 and 125 m in Scenario 2 at the fringes of the Wadi El-Natrun depression especially at the North Highway.

The average calculated depth to groundwater in Wadi El-Natrun within scenario 1 ranges from about 4 m to 35 m, whereas in scenario 2 it ranges from about 15 m up to 61 m. However in the Wadi El-Farigh, the depth to groundwater ranges from about 35 m in the east to 125 m in the west in scenario 1 and from about 50 m to 150 m in scenario 5. Due to the topography in the southwest of the study area (Fig. 2.3), the average depth to groundwater level in the year 1990 ranged from about 65 m to 196 m and in the year 2060, the depth is expected to range from about 80 m to 205 m in Scenario 1 and from 100 m to 226 m in Scenario 2. At the areas where the depth to ground water is more than 100 m, it will be difficult to engage in development based on the groundwater, where the economic vision will play a big role. The extraction rates are still feasible for most of the areas at the fringes of the Delta and the Noubaria Canal, where the economic lifting depths are not exceeded. The depth to groundwater south of Sadat City will reach about 92 m by 2035 and 105 m by 2060 if the full capacity extraction rate is applied. Therefore, it is concluded that the extraction rates of Scenario 2 for both the North Highway and Sadat City could be feasible, but only for short time and not for long-term sustainable development. At the area of South Highway, the current average depth to groundwater exceeded 100 m. The same impact will appear in the area of Dina by the year 2035.

Figures 6.19, 6.20, 6.21 and 6.22 show the depth to the groundwater in the year 2035 and 2060 for Scenario 1 and Scenario 2.

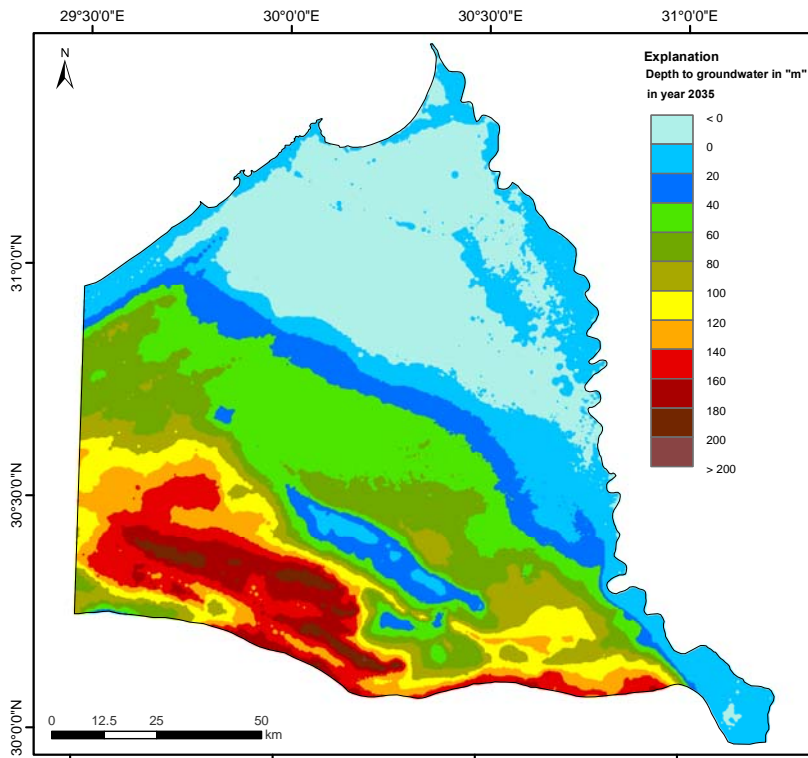


Fig. 6.19: Depth to groundwater in the year 2035 according to the extraction rates of Scenario 1

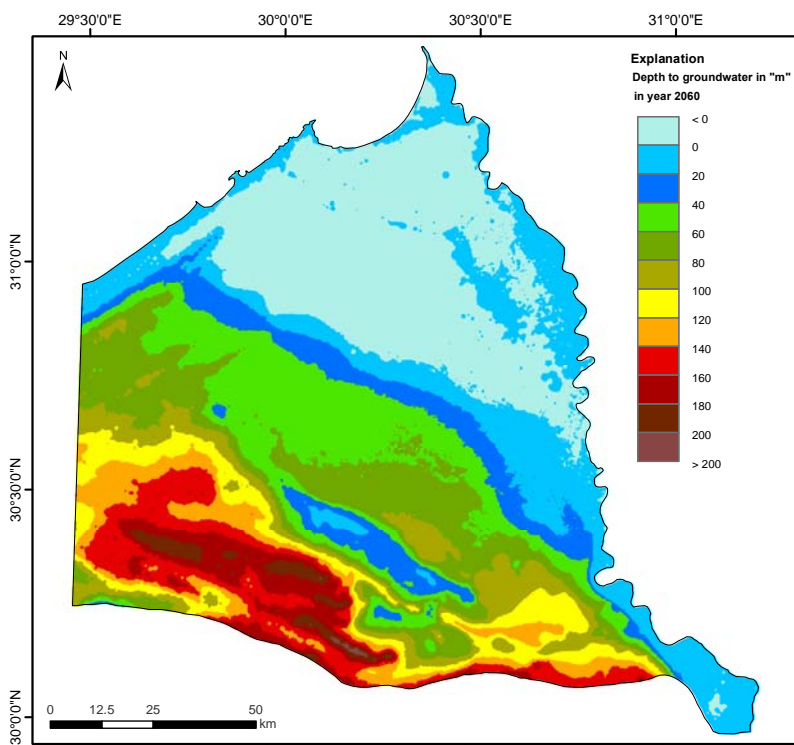


Fig. 6.20: Depth to groundwater in the year 2060 according to the extraction rates of Scenario 1



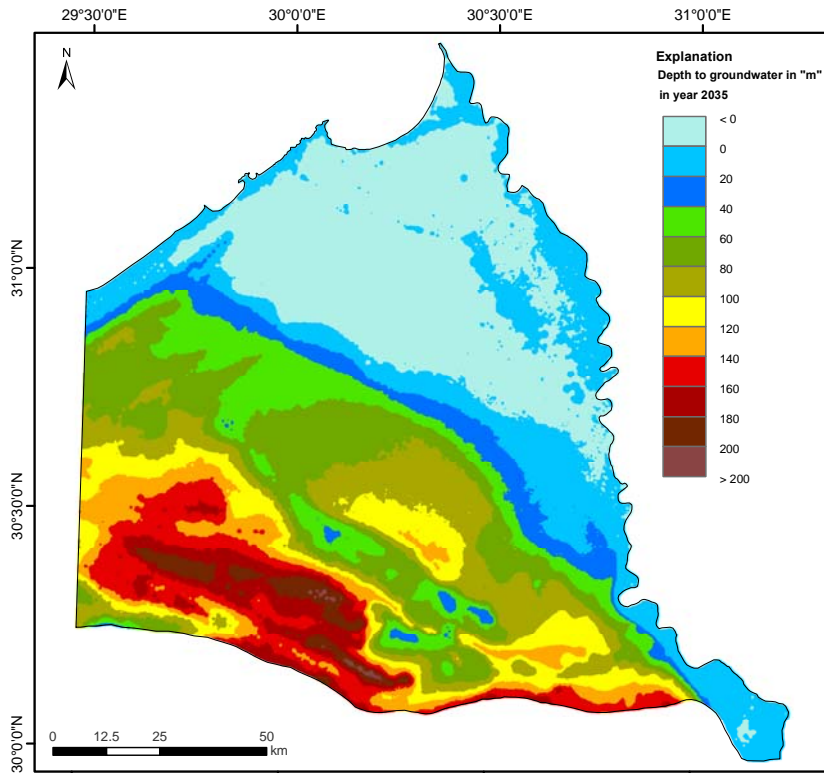


Fig. 6.21: Depth to groundwater in the year 2035 according to the extraction rates of Scenario 2

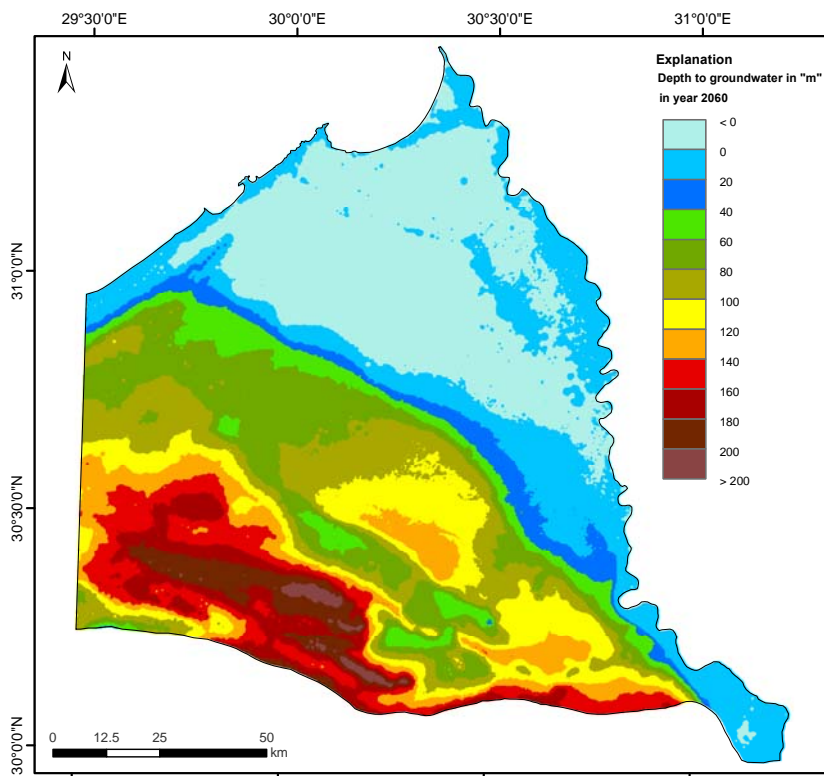


Fig. 6.22: Depth to groundwater in the year 2060 according to the extraction rates of Scenario 2

#### 6.6.4 Groundwater balance

To evaluate the groundwater resources in the study area, the calibrated model has been used to calculate the groundwater balance and the cumulative change in storage. The balance between the flux in and out of the study area tends toward the side of the flux out, with a value of about 350 million m<sup>3</sup>/a. On the other hand, the annual effective aerial recharge from different sources such as rainwater, surplus of irrigation water and the seepage from the surface water canals, ranges between 500 to 700 million m<sup>3</sup>/a.

The groundwater balance for the study area in the period from 1990 to 2060 was calculated under the stress of both the actual extraction rates (Scenario 1) and the full extraction rates (Scenario 2) for the prediction period to obtain a clear view for the behavior of the aquifer system concerning the different extraction rates. The groundwater balance was expressed as a change in the storage, which equals the sum of the in- and outflow of the system. Figure 6.23 and Figure 6.24 represent the flow components of the study area for Scenario 1 and 2, respectively, while Figure 6.25 and Figure 6.26 show the total cumulative decrease in groundwater potentiality as a response of applying the discharge rates of Scenario 1 and 2, respectively.

It can be concluded that the annual change in storage is affected mainly by changes in the extraction rates in each scenario, except for the very beginning of the simulation, where the extraction rates were relatively small and the change of storage was affected to some extent by the component of the effective aerial recharge. For example, in Scenario 1 (Fig. 6.23) the extraction rate increases gently to reach about 0.65 km<sup>3</sup>/a by 1995 and due to the continuous increase in the rate of extraction, it reached about 1.06 km<sup>3</sup>/a by 2000. Meanwhile the annual change in storage reaches about -1.30 km<sup>3</sup> after 15 years from the beginning of the simulation. The negative sign of the change of storage indicates that every additional extraction rate is considered as a groundwater mining.

It can also be concluded that during the period from 1990 to 2006, the total artificial discharge by pumping increased from 0.46 km<sup>3</sup>/a to 1.66 km<sup>3</sup>/a (with an increase of about 260%). Regarding Scenario 1, the actual extraction rates are considered constant up to the end of the simulation as shown in Figure 6.23. It is evident from the cumulative change in storage in Scenario 1 (Fig. 6.25) that the groundwater volume decreased by about 17 km<sup>3</sup> by the year 2010, and if the present extraction rates are kept constant until the year 2060 the predicted decrease of groundwater volume will be about 84 km<sup>3</sup>. However, by applying the full extraction rate in Scenario 2, the groundwater volume will decrease by about 156 km<sup>3</sup> (Fig. 6.26).

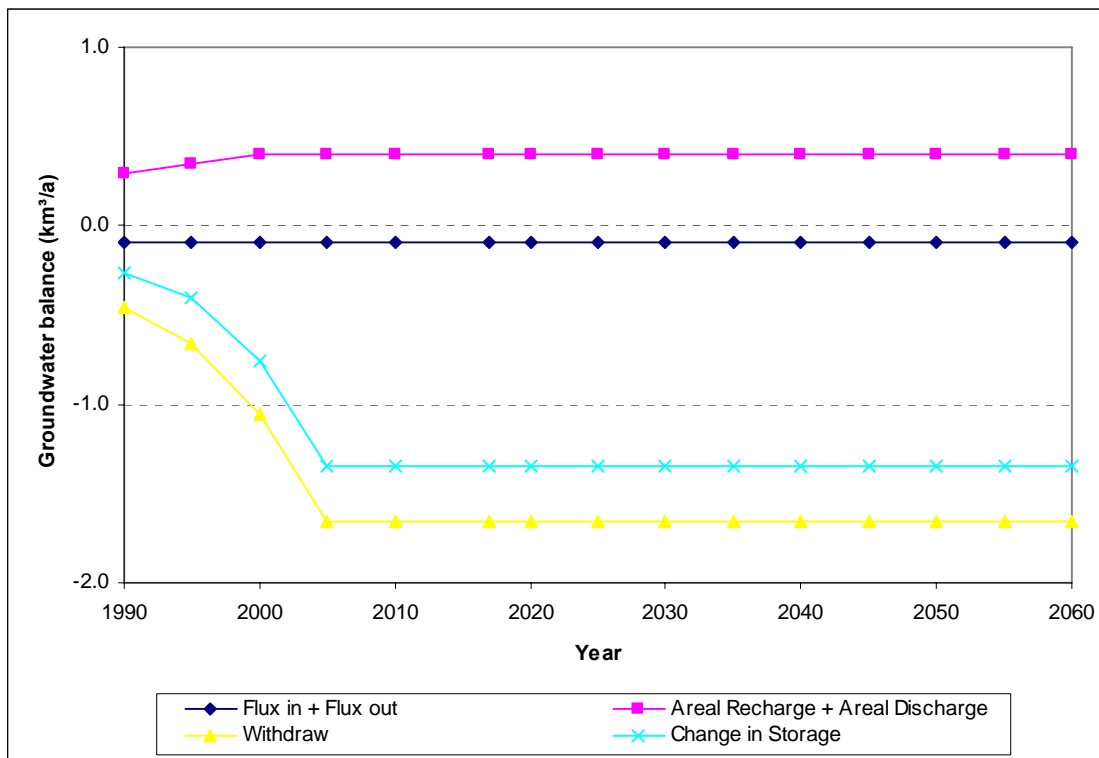


Fig. 6.23: Groundwater balance for Scenario 1 in the study area from 1990 to 2060.

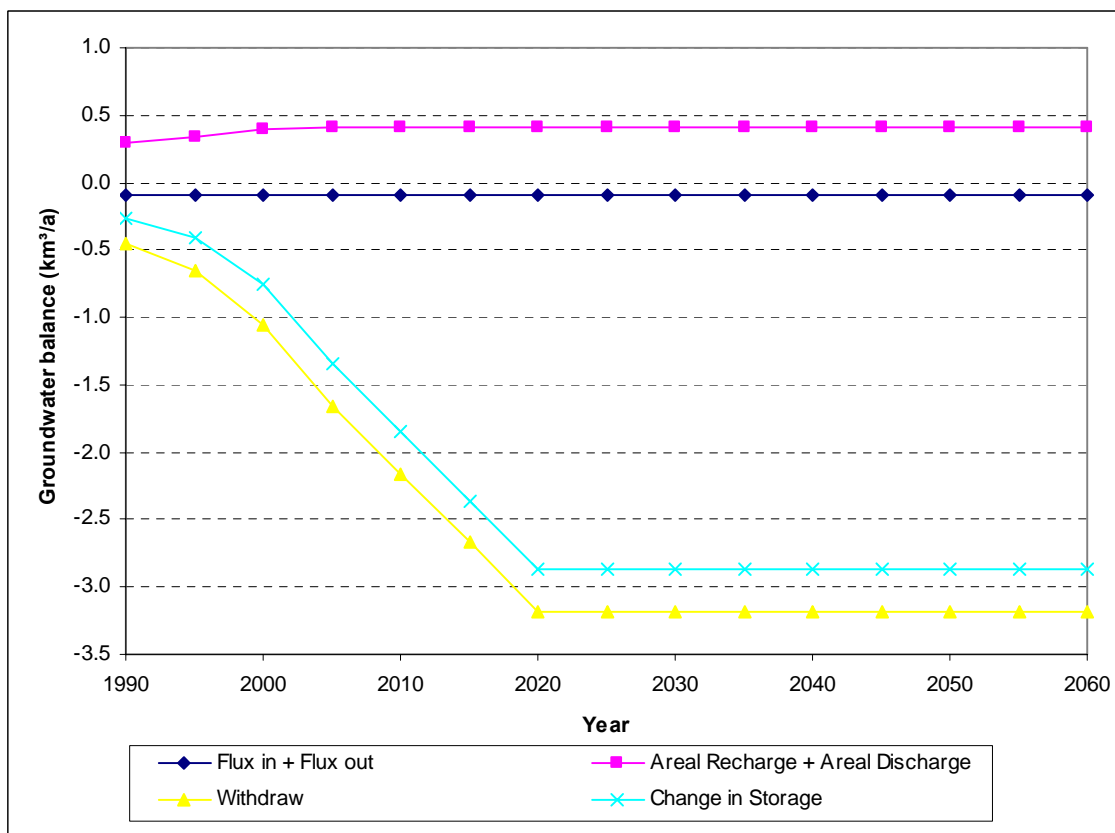


Fig. 6.24: Groundwater balance for Scenario 2 in the study area from 1990 to 2060.

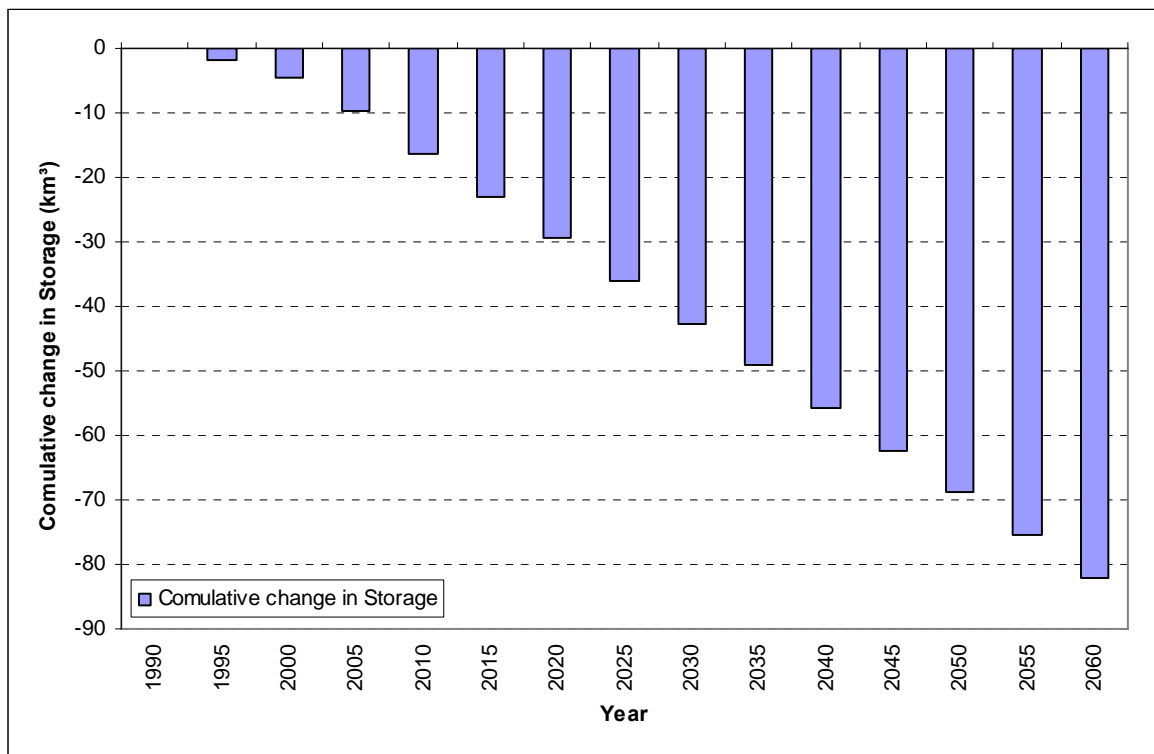


Fig. 6.25: Cumulative decrease in groundwater storage of the study area for Scenario 1 during the period from 1990 to 2060.

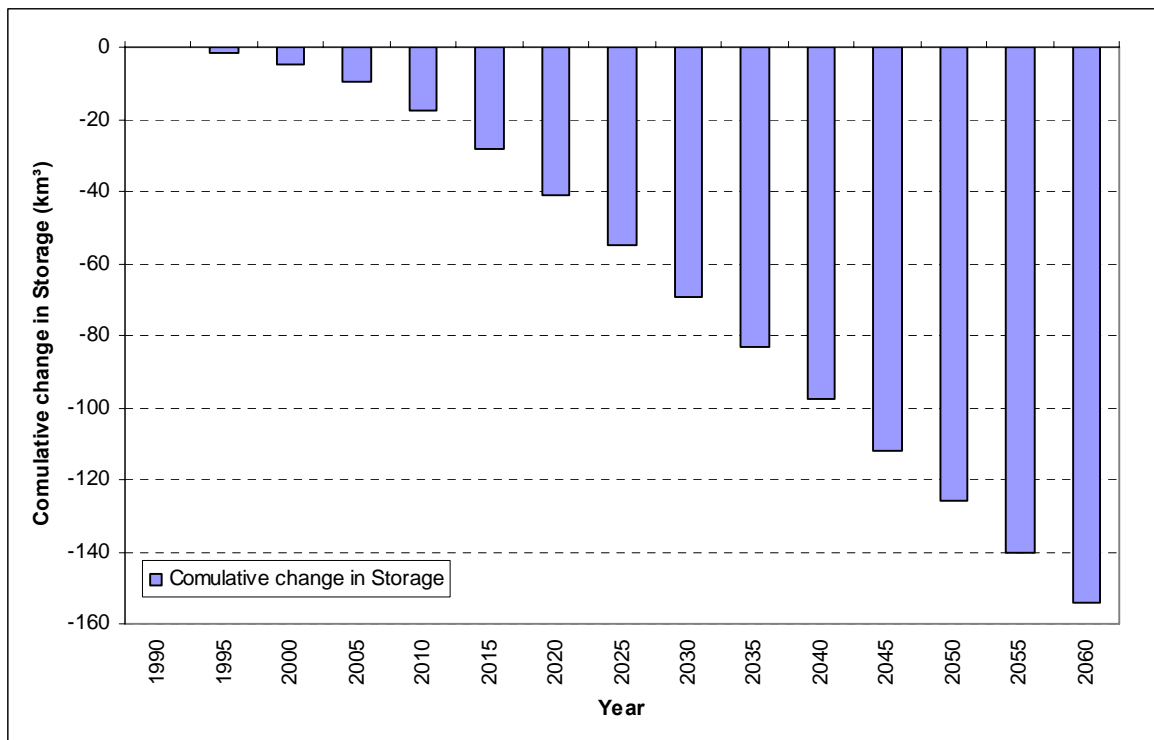


Fig. 6.26: Cumulative decrease in groundwater storage of the study area for Scenario 2 during the period from 1990 to 2060.

### 6.6.5 The differences between the two scenarios

According to the results of the decline in groundwater levels in the Miocene aquifer of the study area, it can be noticed that the decline in groundwater levels in the Miocene aquifer in Scenario 2 is much greater than the decline in groundwater levels in Scenario 1. The difference in drawdown between the two scenarios in the year 2060 has a wide range, from 0 to 60 m (Fig. 6.27). About 43.5% of the area has a difference of less than 5 m at the northern part of the area that is covered with a net of surface water canals and does not primarily depend on groundwater for irrigation. About 16.5% of the study area has a difference from 20 to 60 m which indicates that the intensive extraction rates in the stressed areas and the lack of replenishment in Scenario 2 are much higher compared with Scenario 1. About 40% of the study area has a difference in drawdown ranges from 5 m to 20 m, especially in the South and Southwest region of the study area, although there are no intensive extraction rates in this area. This can be explained by the privation from surface water canal nets in this area that act as a natural source of recharge. The South and Southwest regions of the study area are not only affected by the extraction rates in the stressed area but also affected by the topography, where biggest depths to groundwater in the Southwest is ranging from 120 m to more than 200 m. The rate of increase in the decline of groundwater levels is about 0.4 m/a and 1 m/a in Scenario 1 and 2 respectively with a difference of about 0.6 m/a. There is a difference in the cumulative decrease in groundwater storage by the year 2060 of about 72 km<sup>3</sup> between Scenario 2 and scenario 1 (Fig. 6.28), i.e. the reduction in the groundwater volume from 1990 to 2060 in Scenario 2 will be about 86% more than Scenario 1. Regarding the permissible drawdown “0.5 m/a” (RIGW and REGWA 1992), Scenario 1 is still considered within the allowable limit, which could not be achieved by Scenario 2.

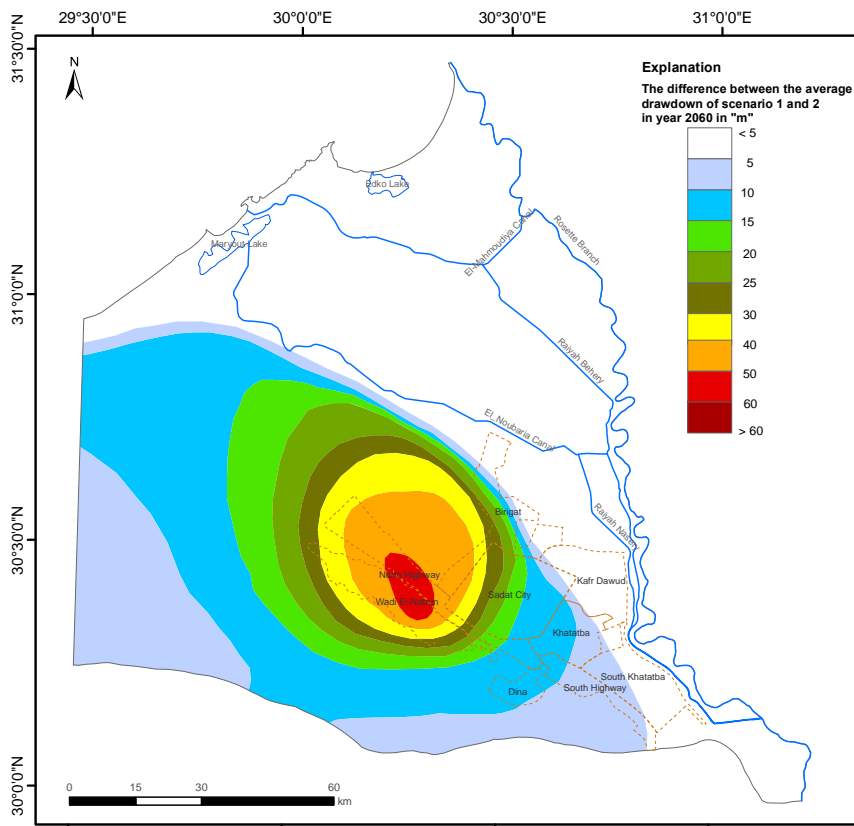


Fig. 6.27: Difference between the average drawdown according to the extraction rates of Scenario 1 and 2 in the year 2060

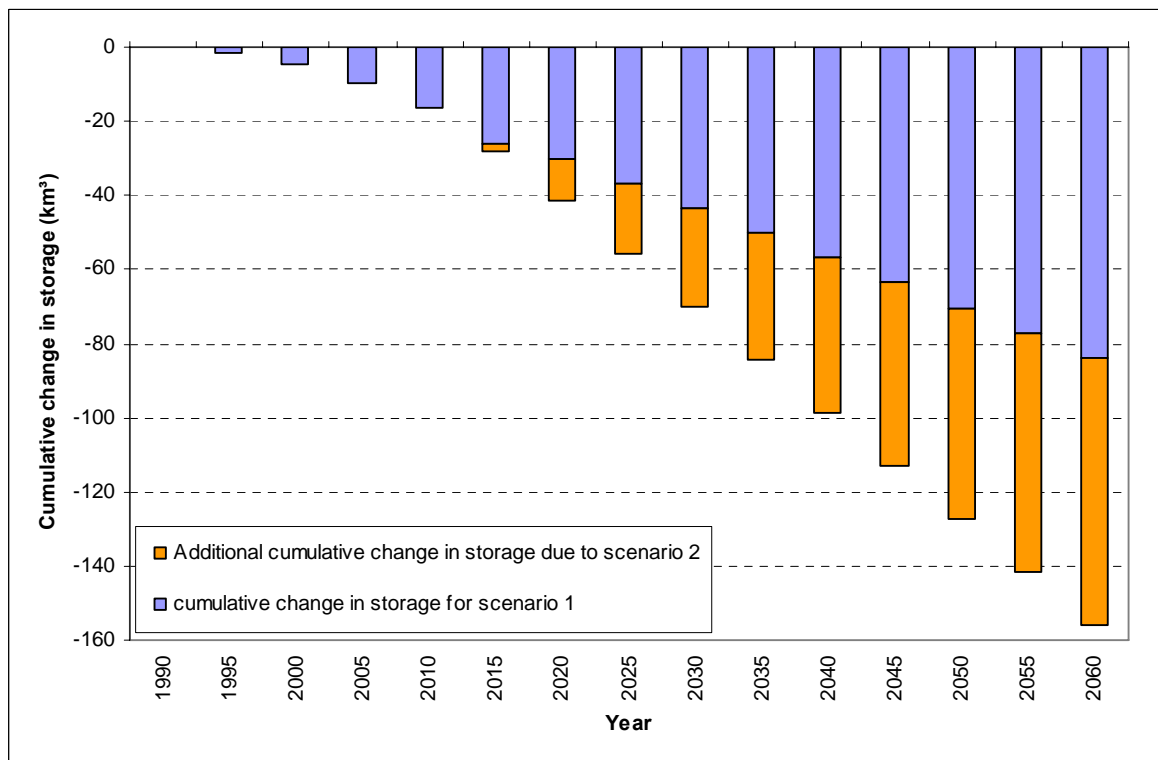


Fig. 6.28: Comparison between the cumulative decrease in groundwater storage of the study area for Scenario 1 and 2 for the period 1990 to 2060.

### 6.6.6 Effect of the extraction rates on seawater intrusion

Extracting groundwater from aquifers near the coast has to always be under control to prevent seawater from penetrating the aquifer. The controlling parameter in this case is the density difference between fresh water (density  $\rho_f = 1 \text{ g/cm}^3$ ) and seawater (density  $\rho_s = 1.025 \text{ g/cm}^3$ ), which allows fresh water to float on seawater. According to the Ghyben-Herzberg principal (Herzberg 1901) on the static condition between seawater and fresh water in an aquifer: for every meter of fresh water above sea level ( $h$ ), there is a depth to seawater ( $d$ ) equal to 40m (bsl) as shown in Equation (6.1).

$$d = \frac{\rho_f}{\rho_s - \rho_f} h = 40h \quad [\text{Eq 6.1}]$$

In practice, due to the water movement, the hydrogeological conditions are more complex. To explore the effect of the extraction rates on seawater intrusion in the study area, a density-driven model derived from the regional flow model with nonlinear coupled simulation for a “density ratio” ( $\rho_s - \rho_f / \rho_f$ ) = 0.025 was used. The initial condition, boundary condition, and the dispersivity were set up as follows:

- **Initial condition**

The salinity distribution in the year 1990 was considered as the transport initial condition. In this year, and according to the FAO classification of saline water (Rhoades et al. 1992), about 48% of the study area at the southeast part had a slightly saline water (less than 1500 mg/l), about 29% of the study area had a moderately saline water (from 1500 to 7000 mg/l) and about 9% of the study area had a high saline water (from 7000 to 15000 mg/l). The rest of the area, about 14% in the northwest direction, had a very highly saline water (more than 15000 mg/l) as shown in Figure (6.29).

- **Boundary condition**

The North side of the study area is bounded by the Mediterranean Sea at a length of about 120 km. The mass transport boundary condition was set up as a constant concentration of about 40000 mg/l on the north border (Dirichlet condition).

- **Dispersivity**

According to Beim (1983), the longitudinal dispersivity depends on the dispersion length “length scale of the phenomenon” (Fig. 6.30), which is about 120 km in the study area. However the transversal dispersivity is about 10% of the longitudinal dispersivity (Kinzelbach 1992 and Lege et al. 1996).

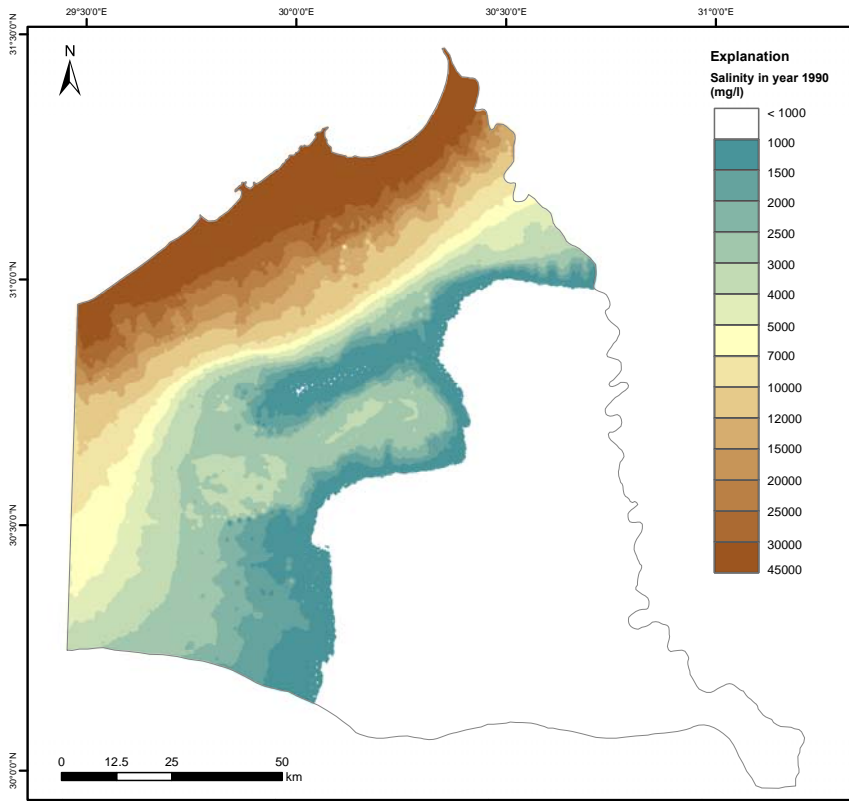


Fig. 6.29: Salinity distribution of groundwater in the year 1990. Interpolated after RIGW (1992)

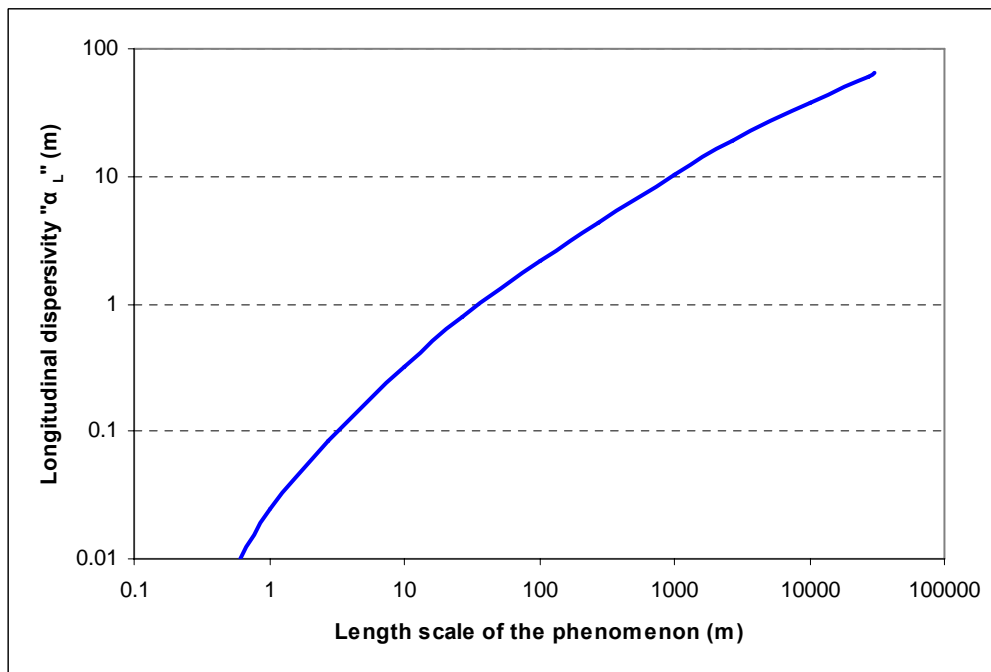
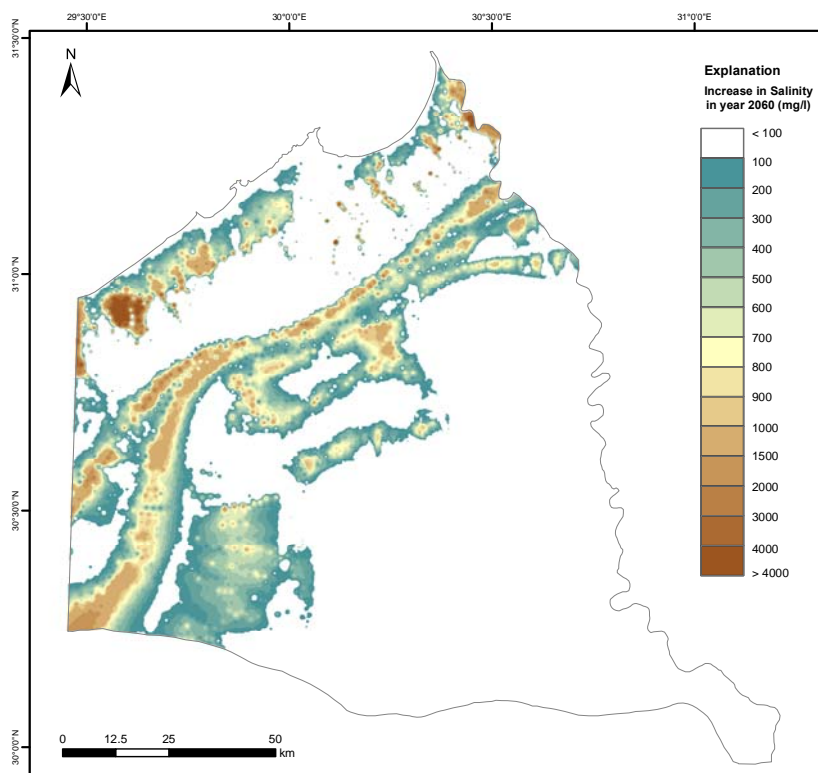


Fig. 6.30: Scale dependence of dispersivity. (After Beims, 1983)



**Model output**

The current and the full extraction rates in the development areas, according to Scenario 1 and 2 respectively, were applied to the density-driven 3D model in order to study their effects on seawater intrusion. The changes, which were obtained after applying the two scenarios in a simulation period through the year 2060, were noticed only in the northern half of the study area (Fig. 6.31 and Fig. 6.32), where the differences range from less than 100 mg/l up to 4000 mg/l. The rate of increase in salinity concentration ranges from 1% to 10% of its initial distribution in the year 1990.



**Fig. 6.31:** Difference in salinity due to sea-water intrusion between 1990 and 2060 according to Scenario 1.

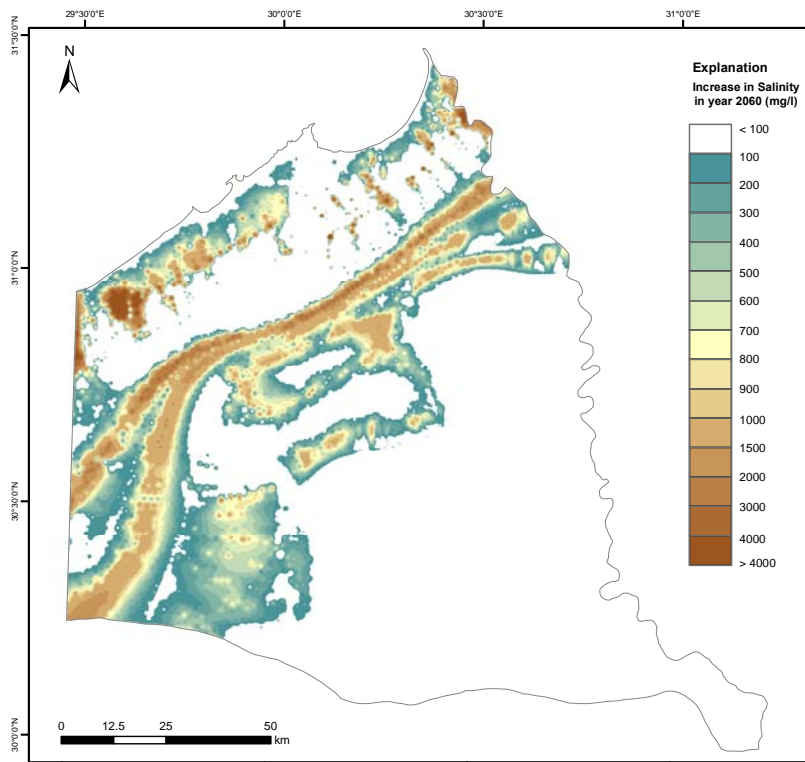


**Fig. 6.32:** Difference in salinity due to seawater intrusion between 1990 and 2060 according to Scenario 2.

**Discussion of the results**

The average difference in salinity between Scenario 1 and Scenario 2 is about 300 mg/l in the northern part and less than 100 mg/l in the southern part (Fig.6.33).

The behavior of the resulting extraction rates’ effect on the seawater intrusion during the following 50 years can be explained by the following processes:

- The groundwater levels in the adjacent area of the coast are still higher than sea level, and the groundwater flow direction is toward the sea up to the end of the simulation.
- The limited drawdown along the coast.
- The development area location is about 110 km far from the Mediterranean Sea.
- The infiltration from irrigation and the seepage from surface water canals, which locate in between the extraction areas and the Mediterranean Sea.
- The hydraulic conductivity of the aquifer beneath the coast is relatively low due to the clay intercalations with the aquifer system in the northern part.

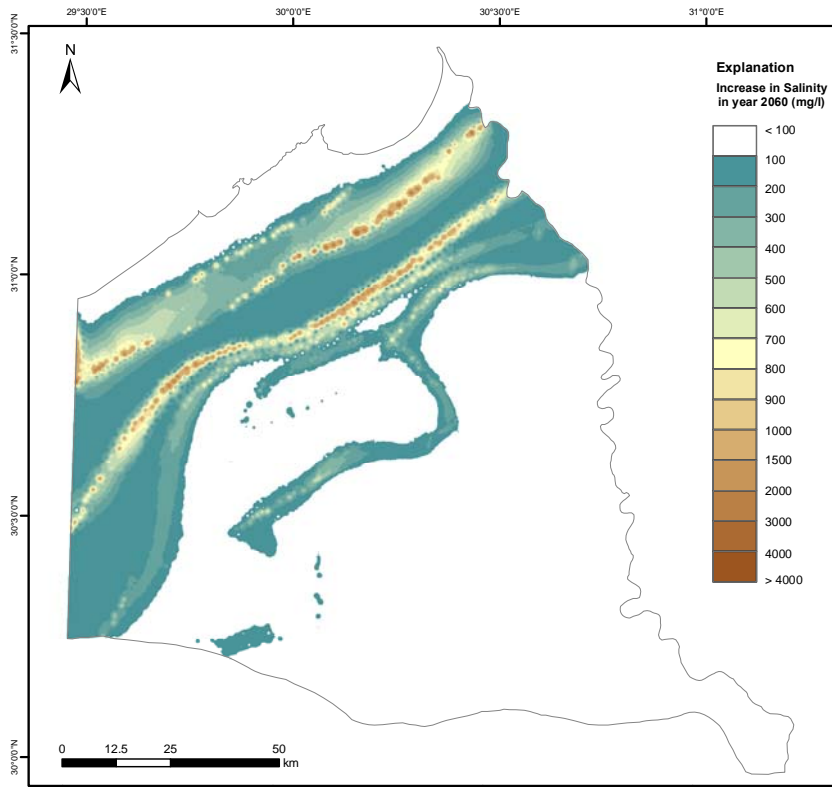


Fig. 6.33: Difference in salinity between Scenario 1 and Scenario 2 in the year 2060.

# 7 Local Model

## 7.1 Historical introduction

The Wadi El-Natrun is a name consisting of two parts. The first part means “valley,” and the second part refers to the Latin name for sodium, natrium. This name was derived from the different lakes in this valley that are rich in natrun salt. The salt occurs in solutions in the lakes, forming a crust around the lakes’ edges and in deposits on their bottom. These natural deposits were used for the production of caustic soda, soap and low grade glass (Sadek et al. 2005). The Wadi El-Natrun is also known as one of the most sacred regions in Christianity where the Holy Family stopped during their flight to Egypt. In the fourth century A.D., Saint Macarius the Great retired to the desert in the Wadi El-Natrun, and in the seventh century A.D., this region attracted thousands of people from around the world to join the hundreds of monasteries of the Wadi El-Natrun Desert. The desolate region became a sanctuary for the desert fathers and for monastic communities. Many anchorites, hermits and monks lived in the desert and the hills around the region, which led to know this place in Coptic language at that time as “Shee-Hyt” that means the balance of the hearts and in the Greek language as “Scetes” that means ascetics. Nowadays only four monasteries exist in Wadi El-Natrun (the Monastery of Saint Macarius the Great, the Paromeos Monastery, the Monastery of Saint Pishoy, and the Syrian Monastery). The region of Wadi El-Natrun consists of five main lakes (El-Hamra, El-Gaar, El-Bida, Moubarak and Abo Ghazala). The economy of Wadi El-Natrun is based on agriculture, production of handicrafts, and some tourism. The value of exporting fruits from the area of Wadi El-Natrun to the EU countries ranges between \$300 million and \$500 million annually.

## 7.2 Location and climate

The Wadi El-Natrun is an elongated depression oriented in a NW-SE direction and located approximately 90 km northwest of Cairo between the latitudes  $30^{\circ} 17'$  and  $30^{\circ} 33'$  N and between the longitude  $30^{\circ} 02'$  and  $30^{\circ} 30'$  E. The Wadi El-Natrun depression extends in a NW-SE direction for more than 50 km and its average width is about 9 km.

The climate of Wadi El-Natrun lies between the arid and semi arid zones. The average annual rainfall is about 55 mm, mostly in November and December. The mean temperature

varies from 12.5° C to 26.5° C (Fig. 7.1). The mean relative humidity ranges from 60% to 70% (Fig. 7.2) and wind velocities range from 11 km/h to 20 km/h (Youssef et al. 2009).

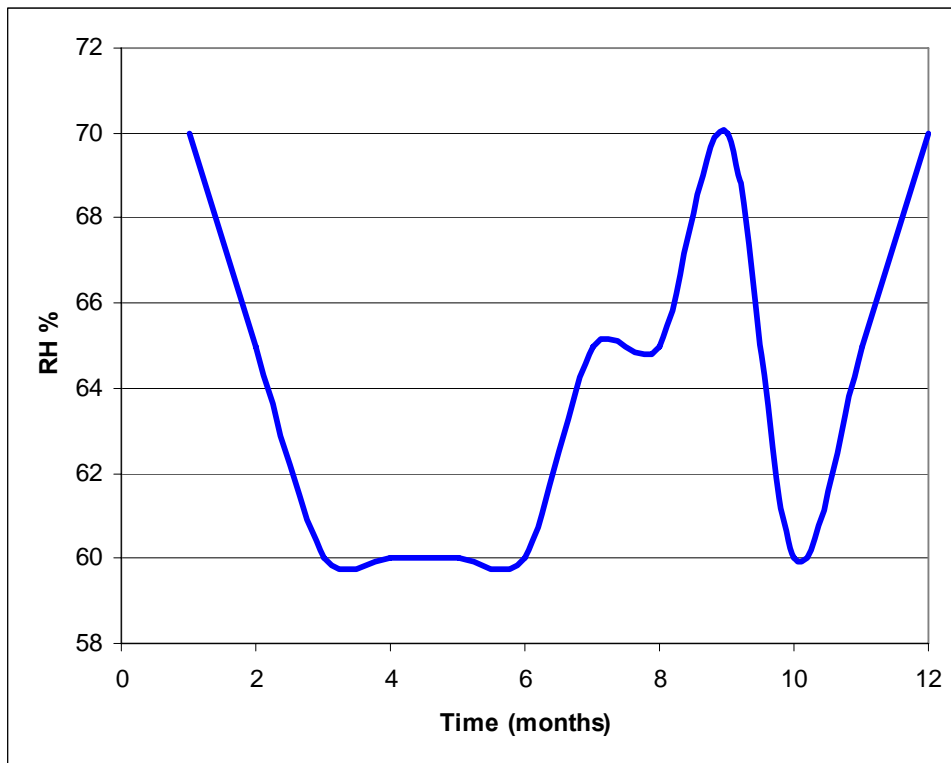


Fig. 7.1: Mean values of the relative humidity throughout the year (Atlas, 1996).

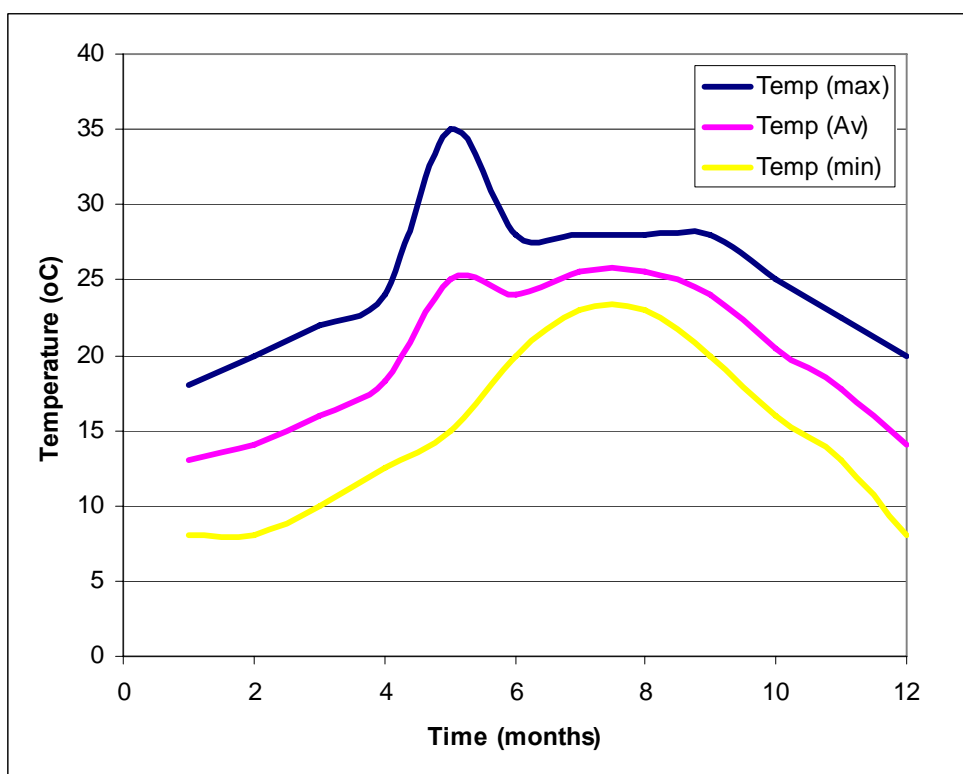


Fig. 7.2: Mean values of the temperatures throughout the year (Atlas, 1996).

### 7.3 Geomorphological background

The topography of the region western Nile Delta in general and the Wadi El-Natron in particular, was a subject of different studies e.g., Shata and El Fayoumi (1967), El-Etr and El-Baz (1979), and Sadek et. al (2005). The depression of the Wadi El-Natron extends from Ras El-Solymania in the Northwest to Deir Macarius in the Southeast encompassing an area of about 273 km<sup>2</sup> surrounded by the contour line of mean sea level. The axis passes through most of the lakes of the depression. The area of the lakes in Wadi El-Natron depression is about 12 km<sup>2</sup>. Before the construction of the high dam, the water in the lakes once came from the Rosetta branch during the summer flood period. At present, the amount of water in the lakes seems to originate from surface water in the Rayah Behery and in the Nubaria Canal (GPC 1987).

The main topographical feature of Wadi El-Natron is the scarp (Fig. 7.3), which bounds and overlooks this depression on its sides with an incline that ranges from 19 m/km to 27 m/km. The lowest point of this depression is about 23 m below sea level, and the bed of the depression is generally 50 m below the level of the northern plain and from 100 to 200 m below the level of the southern boundaries (Fig. 7.4). The majority area of this depression is underlain by soft deposits dominated by gypseous sandy clays and sands from the Middle Pliocene age.

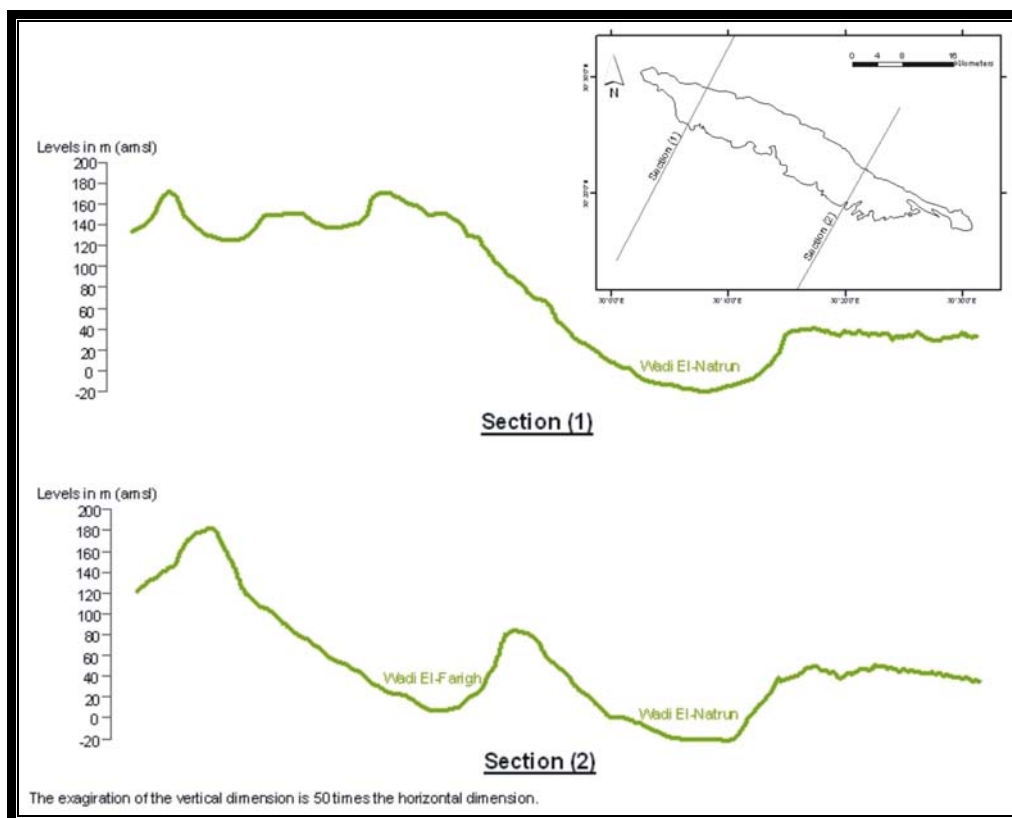
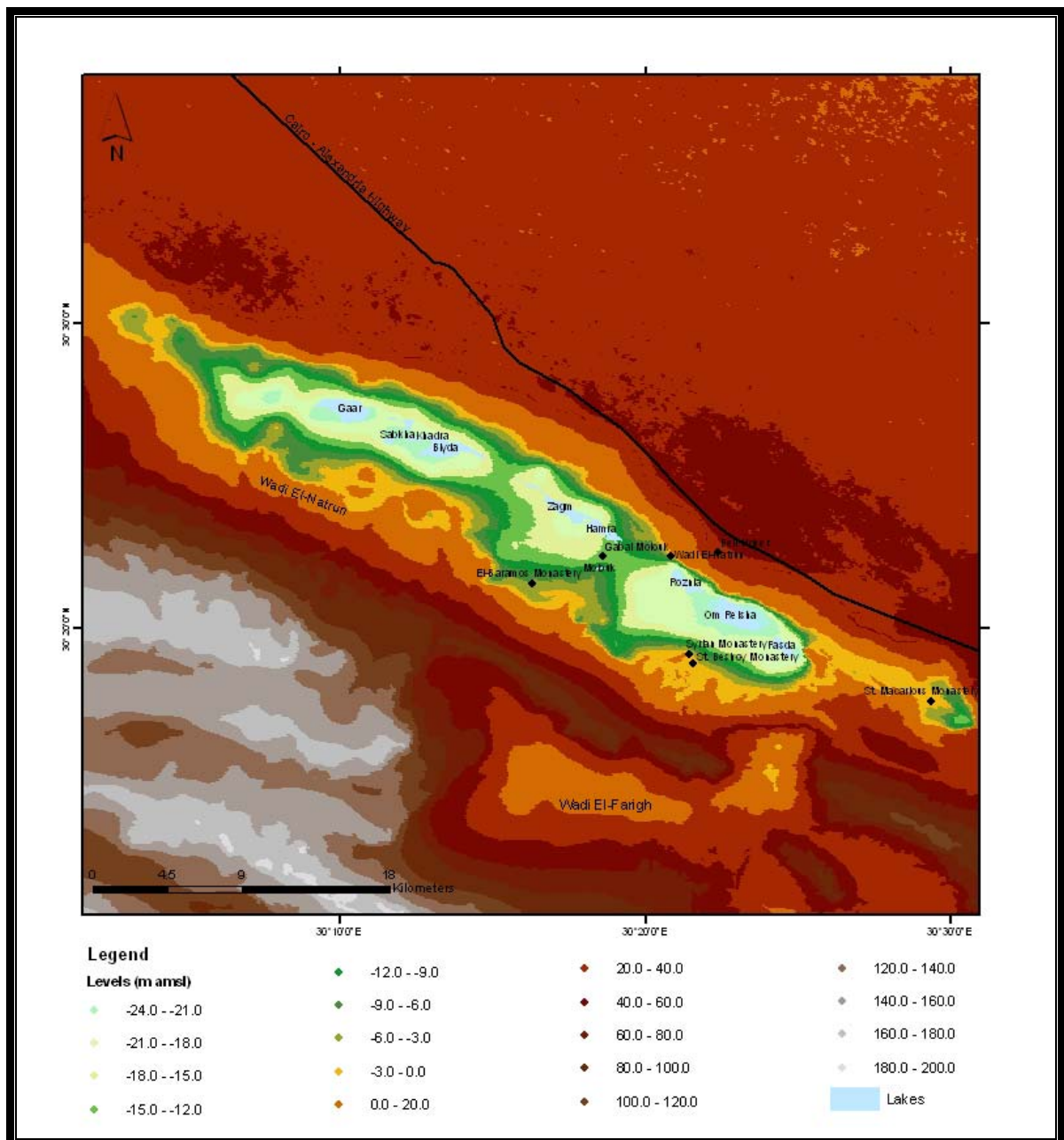


Fig. 7.3: Vertical cross sections show the ground levels of the Wadi El-Natron depression.



**Fig. 7.4:** Location map of the Wadi El-Natron depression showing the main features and topography. The topography is obtained from both the contour map 1:100,000 (EGSMA 1950) and DEM of the SRTM-03 (USGS 2004; NASA 2005).

### 7.4 Geological background

Many authors have studied the geology of Wadi El-Natron including La Moreaux (1962), Shata and El Fayoumi (1967), Abdallah (1970), Marzouk (1970), Abu Khadrah (1973), Philip et al. (1973, 1975), Abu Zeid (1984), Sadek et al. (2005) and EGSMA (2006).

The lithostratigraphic column from the Wadi El-Natrun testing well (30° 23' 27" N and 30° 18' 31" E) published by Shata and El-Fayoumi (1967) (Fig. 7.5), described the different lithostratigraphic units forming the body of this area and aquifer systems which are covered with extensive exposures of sedimentary rocks ranging from Triassic to Pliocene and are hereafter presented from the oldest to the youngest layers.

#### (a) Jurassic

The subsurface Jurassic deposits of the Wadi EI- Natrun area are differentiated into the following rock stratigraphic units, arranged from the base to the top:

##### - Wadi EI-Natrun Formation

The Wadi EI-Natrun Formation consists of shale, and limestone strings grade into argillaceous limestone of the Triassic or an early Jurassic age (Norton 1967). It is located in the interval from 3780 to 4000 m in the testing well. This formation rests unconformably over the basement, in which the contact is usually sharp and clear. The Wadi EI-Natrun Formation is always overlain by the Khatatba Formation.

##### - Khatatba Formation

The Khatatba Formation consists of alternating fine grained limestone and sandy shale with carbonaceous material coal from the Middle Jurassic age (Norton 1967). It is located in the interval from 3190 to 3780 m in the testing well. The clastic section of the Khatatba Formation has a few limestone interbeds and is made up of sandstone and shale. The sandstone is fine to medium-grained and brown in color. The shale is grey to brownish grey. The limestone interbeds become thicker and more frequent near the upper part of the section. Thin coal seams are present at different levels of the section. The formation rests conformably over the Wadi EI-Natrun Formation and it underlies conformably the Masajid Formation. The contact with the Masajid is sharp and is marked by the change of facies from the dominantly clastic section of the Khatatba to the more calcareous section of the Masajid (Sadek et al. 2005).

##### - Masajid Formation

The Masajid Formation was proposed by Al Far (1966). It is typically a massive limestone sequence from the middle to late Jurassic period. The carbonate sequence is cherty in some places. Pyrite and carbonaceous matter occur locally. The Masajid Formation is clearly marked in most of the area. It overlies conformably the clastic Khatatba Formation and underlies unconformably the clastic Lower Cretaceous sequence. The Masajid Formation is thickest in the Wadi EI-Natrun area (Hantar 1990). It is located in the interval from 2650 to 3190 m in the Wadi EI-Natrun testing well.



**(b) Cretaceous**

The Cretaceous in the area of Wadi EI-Natron is divided into a lower unit made up primarily of clastics belonging to the Lower Cretaceous and an upper unit made up mainly of carbonates and belonging to the Upper Cretaceous (Sadek et al. 2005). These units are arranged from the base to the top as follows:

**-Betty Formation**

The Betty Formation underlies conformably the Alam EI-Bueib formation and unconformably overlies the Masajid formation. The Betty formation is mainly composed of loose sand with thin lenses of shale (Norton 1967). The boundaries between the formation and both the underlying and overlying rock units are mainly detected by lithologic characteristics and wireline logs contrast. The underlying Masajid Formation is mainly represented by limestone, while the overlying Alam EI-Bueib Formation is mainly sandstone. The upper boundary of the Betty Formation is set at the top of the last thick shale beds, just underlying the sandstone rich sequence. The Betty Formation has been assigned by many authors to the early Cretaceous age (Sadek et al. 2005). The maximum recorded thickness of the Betty Formation reaches about 550 m.

**- Alam EI-Bueib Formation**

The Alam EI-Bueib Formation underlies the well-marked Alamein dolomite member. It is a sandstone unit with frequent shale and occasional limestone beds (Tawadros 2001). It is located in the interval from 2000 to 2100 m. The deposition environment is shallow marine with more continental influence toward the South.

**- Alamein Dolomite Formation**

This is a widely spread unit known all over North Africa and Arabia. It is composed of light brown hard crystalline dolomite with vuggy porosity (Tawadros 2001). A few thin shale interbeds are present. The unit contrasts with the clastics of the Alam EI-Bueib that underlies it. It is located in the interval from 1800 to 2000 m. The Alamein Dolomite grades laterally into shales along a narrow belt that runs to the North and parallel to latitude 30° N between longitude 31° and 27° E in the Matruh area. The unit seems to have been deposited in a shallow marine, low to moderate energy environment (Sadek et al. 2005).

**- Kharita Formation**

This is a unit of fine to coarse grained sandstone with subordinate shale and carbonate interbeds. The carbonate interbeds increase in frequency and thickness toward the northwest. It underlies the widely-spread Bahariya Formation at the easily recognizable

contact provided by the limestone bed, which is persistently present at the base of the Bahariya Formation (Sadek et al. 2005).

- Bahariya Formation

The Bahariya Formation is from the late Cenomanian Age and according to Dominik (1985) it was deposited first under fluvial conditions (Gebel Ghorabi Member) and finally under lagoonal conditions (EI-Heiz Member). The Gebel Ghorabi Member is made up of cross-bedded, coarse grained, well-bedded, ferruginous clastics carrying a large number of fossils including vertebrates in the lower levels and an assortment of oysters and other fossils in the middle and upper levels. The EI-Heiz Member is made up of dolomites, sandy dolomites and calcareous grits rich in fossils.

- Abu Roash Formation

This is mainly a limestone sequence with interbeds of shale and sandstone. It is a classic Abu Roash structure located to the north of the Pyramids of Giza. The unit is divided by Aadland and Hassan (1972) into seven informal members designated from bottom to top: G, F, E, D, C, B and A. Member G (Cenomanian) is composed of reddish brown sandstone, sandy argillaceous limestone, gypsiferous green shale and glauconitic sandstone. Member F (Cenomanian) is composed of thick bedded, white limestone, highly argillaceous, with foraminifera in the lower part, and cherty limestone in the upper part. Member E (Turonian) consists of reddish, brown sandstone, yellowish green argillaceous limestone, yellowish brown shale and white limestone, becoming sandy and gypsiferous at the base. Member D (Turonian) is composed of white, dolomitic, cherty limestones, with thin sandstone and shale beds. Member C (Turonian) is composed of shale, white, sandy, and high fossiliferous, bryozoan limestone, and sandstone. Member B (Upper Turonian) consists of white, chalky limestone, and Member A (Coniacian-Santonian) is composed of white, partly dolomitized, chalky limestone (Tawadros 2001).

The lowermost member is probably coeval with the EI-Heiz Member of the Bahariya Formation. Members F,E,D,C and B are probably the lateral equivalents of the exposed units in the Abu Roash structure described under the following names: Rudistae series, limestone series, Acteonella series, Flint series and Plicatula series, respectively (Said, 1962). Member A is not recognized on the surface in the Abu Roash structure and was probably eroded (Sadek et al. 2005). The Abu Roash Formation overlies conformably the Bahariya Formation. In the northern part of the area, where most of the formation is made up of limestone, the contact is sharp and easily recognized. In the south, where the lower unit G (EI-Heiz) is made up of interbedded carbonates and clastics, the boundary is taken at the top of the thick sand interval of the Bahariya Formation. The Abu Roash Formation underlies the Khoman Formation where the contact is determined, in the absence of fossils,

by the change of lithology from the crystalline limestones of the Abu Roash to the chalky limestones of the Khoman. The formation was deposited in an open shallow marine shelf during several sedimentary cycles, which developed in response to oscillations of sea level (Sadek et al. 2005).

#### - Khoman Formation

The Khoman Formation is a distinctive unit of snow-white chalk and chalky limestone with patches of very hard siliceous limestone (Cherif et al. 2006). The formation overlies unconformably different units of the Abu Roash or the Bahariya. The formation underlies unconformably the Apollonia or Dabaa Formations (Early Cenozoic). The contact between the Khoman and the overlying formations is easily recognized due to the lithological contrast between the chalky nature of the Apollonia and the chalky nature of the Khoman.

#### (C) Eocene

The Eocene in the Wadi El-Natron area is divided into three units. The lower unit is made up primarily of argillaceous limestone grading upwards to a purer limestone. This unit is overlain by the Hamra formation, which consists of a yellowish-white limestone with sandy claystone and grit intercalations near the top. The whole succession is highly fossiliferous. The upper unit of the Eocene is the Qasr El-Sagha formation which is subdivided from top to base into five smaller units (sandy limestone, loose sandstone, claystone, purple claystone and gypsiferous sandy claystone). The average thickness of the upper Eocene layer is about 160 m (Beadnell 1905).

#### (D) Oligocene

The Oligocene deposits in Wadi El-Natron are represented in Qatrani formation, which is made up of brightly variegated rocks, including red, purple, yellow, gray and brown sandy mudstone and shales, white, red, green and gray sandstones and brown limestone, with occasional gravelly sandstone intercalations (Sadek et al. 2005). The rock unit includes a huge quantity of silicified wood (Said 1962). It overlies unconformably the late Eocene Qasr El-Sagha formation. It underlies, also unconformably, the Widan Al-Faras Basalt, which separates the Qatrani formation from the Miocene Khashab formation.

#### (E) Miocene

The Miocene deposits in Wadi El-Natron have an average thickness of about 250 m divided into two formations from the base to the top as follows:

#### -Gabal Khashab Formation

This formation is made up of vividly colored unfossiliferous sand and gravel (Said 1961). It overlies the basalt layer and underlies the Mikheimin Formation.

#### -Mikheimin Formation

This formation is built up of gray to yellowish gray, moderately hard to hard conglomeratic sandstone and conglomerate (Said 1990 and Cherif et al. 2006). It underlies unconformably the Gar El-Meluk formation and overlies the Gabal Khashab formation. This rock unit forms a high topographical area as in the peripheries of denuded high structures at Wadi El-Natrun.

### (F) Pliocene

The Pliocene sediments in the Wadi El-Natrun are distinguished into two formations (Gar El-Meluk and Hagif formation)

#### -Gar El-Meluk Formation

The formation of Gar El-Meluk forms most of the rocky hills protruding from the floor of the Wadi El-Natrun Depression. The complete succession of this formation attains about 100m in thickness at the central part of Wadi El-Natrun. The rock unit consists mainly of thick, gray, laminated to massive claystone intercalated with fine and well sorted sandstone. Few yellowish-white limestone bands are recorded in the upper part of the succession. The rock unit, however, exhibits a remarkable lateral facies change. The sequence yielding limestone bands at Gar El-Meluk changes laterally to soft chalk with chalcedony lenses at the Deir El-Baramos. Moreover, to the North, the rock unit tends to become gypsiferous, i.e., it changes to a lagoonal facies (Cherif et al. 2006).

#### -Hagif Formation

The Hagif Formation appears in the Northwest of Wadi El-Natrun. It has a thickness varying from 30 to 40 m and can be divided vertically into three parts:

- The first part begins at the base with loose quartzitic, medium grained, well sorted and cross-bedded sandstone with claystone streaks. The sand is topped by a fossiliferous limestone sequence, which is hard and massive at the base.
- The middle part of the succession consists of gray sticky and massive claystone followed by grayish-white, fine-grained argillaceous sandstone.
- The upper part of the succession is made up of a white, massive, moderately hard, fossiliferous limestone bed, followed by a 7 m thick bed of a crystalline gypsum sequence displaying a glassy luster (Omara and Sanad 1975).

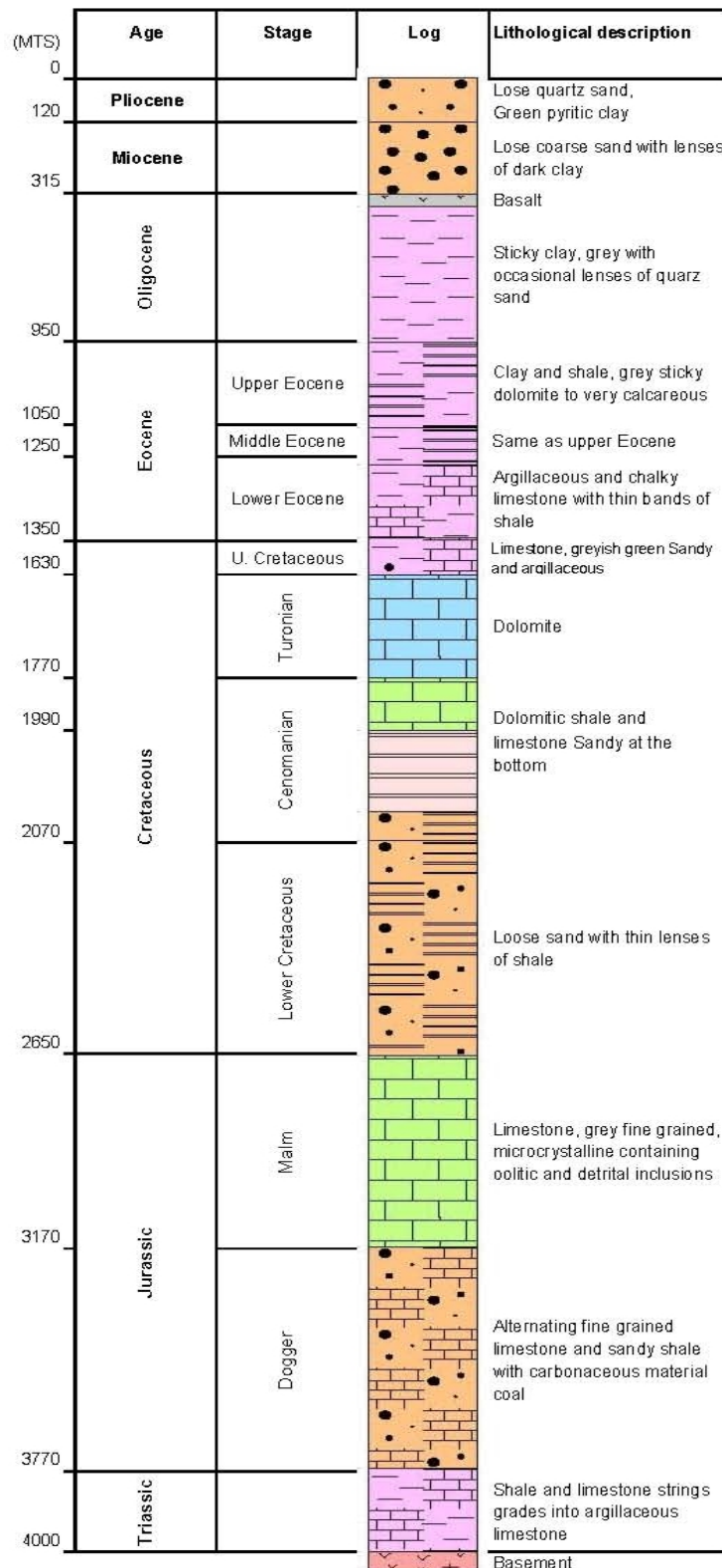


Fig. 7.5: Wadi El-Natrun testing well. Compiled from Shata and El-Fayoumi (1967).

## 7.5 Hydrogeological background

There are two layers of water bearings in the Wadi El-Natrun. The upper layer, “Gar El-Meluk and Hagif Formation” is associated with alluvium deposits by old streams. It consists of an alternation of sandstone and claystone from the Pliocene with an average thickness of the saturated section of about 45 m. The Pliocene layer is underlain by a lower layer that consists of Miocene sand and sandstone of the Gabal Khashab Formation with an average thickness of 250 m, which is characterized by a higher water capacity than in the Pliocene layer. The majority of the Pliocene layer is separated from the Miocene layer by a 10-30 m clay layer from the lower Pliocene and the upper Miocene.

A number of lakes exist approximately along the longitudinal axis of Wadi El-Natrun (Fig. 7.4) such as Gaar Lake (about 2.4 km<sup>2</sup>), Bida Lake (about 2.3 km<sup>2</sup>), Zagm Lake (about 1.6 km<sup>2</sup>), Hamra Lake (about 1.1 km<sup>2</sup>), Roznia Lake (about 0.87 km<sup>2</sup>), Om-Reisha Lake (about 2.45 km<sup>2</sup>) and Fasda Lake (about 0.72 km<sup>2</sup>). The lacustrine deposits of these lakes are differentiated into three groups (El Fayoumi 1967). The first group is fresh water marshes in the northern part of the lakes formed when the water table intersects the ground surface of the depression. This group consists of a complex of dark clayey material from the weathering of the gypseous clays and Aeolian sand. The second group is created by salt deposits underneath the shallow water of salt lakes. The third group consists of wet salt marshes that occupy the eastern areas, which are affected by seasonal fluctuations in water level (Taher 1999). The relative depth to the water table in the Wadi El-Natrun depression varies according to the topography and the wide ranges of elevations of the surface. The depth to groundwater table ranges from 0 to 10 m at the fringes of the lakes and from 15 to 30 m in the other parts.

Many authors have discussed the origin of the groundwater in the Wadi El-Natrun such as Pavlov (1962), El-Fayoumi (1964), Shata and El Fayoumi (1967), and Attia et al. (1970). According to Pavlov (1962), the groundwater flow toward Wadi El-Natrun comes from all directions as a radial flow. Shata and El Fayoumi (1967) pointed out that the groundwater in the depression comes from the seepage of the Rosetta branch and surface water canals. Atia et al. (1970) explained that the flow of the infiltrating water from the Nile through sand and gravel constitutes the main strata separating the Wadi El-Natrun from the river. The lakes in the Wadi El-Natrun act as a natural drainage system for the excess irrigation water from reclaimed lands, where it is lost by the high evaporation rate of about 70 million m<sup>3</sup>/a (Dawoud et al. 2005 and RIGW 2006). The hydrogeologic condition of the high-elevated features such as the shore-parallel rocky carbonate ridges, act as a natural defense system against seawater intrusion towards the Wadi El-Natrun depression (Frihy 2003). The salinity of groundwater in Wadi El-Natrun ranges from 1000 to 2000 ppm in the East changing to be from 2000 to 5000 in the West.

### 7.6 Model input and structure

The regional groundwater flow model for the whole study area was developed and calibrated to serve as a base model and to provide more reliable boundary conditions for local-scale models at selected sites within the study area. Therefore, the input data in the regional model are also valid and used further for the local modeling, with some additional refinement and adjustments for the Wadi El-Natron area according to the locations of the pumping wells. This refinement allowed a precise representation of the wells and consequently, a precise drawdown in the Wadi El-Natron during the simulation from 1990 to 2060.

In the year 2006 there were about 189 private shallow wells extracting groundwater from the Pliocene aquifer and about 473 deep wells extracting about 63 million m<sup>3</sup>/a from the Pliocene (upper) and the Miocene (lower) aquifers. The grid of the model was refined so that it could carry one extraction well in each node. If a certain well was tapping both the shallow and the deep aquifer, then it was divided into two numerical wells at the same node. The wells were imported into the model based on their locations and their functions of the extraction rates with time. The actual extraction rates were applied to the model for all scenarios (refer to Section 6.3.4) and the extraction rates from the other scenarios were divided out on additional wells proportionally. The distribution of the extraction wells within the Wadi El-Natron is illustrated in Figure 7.6.

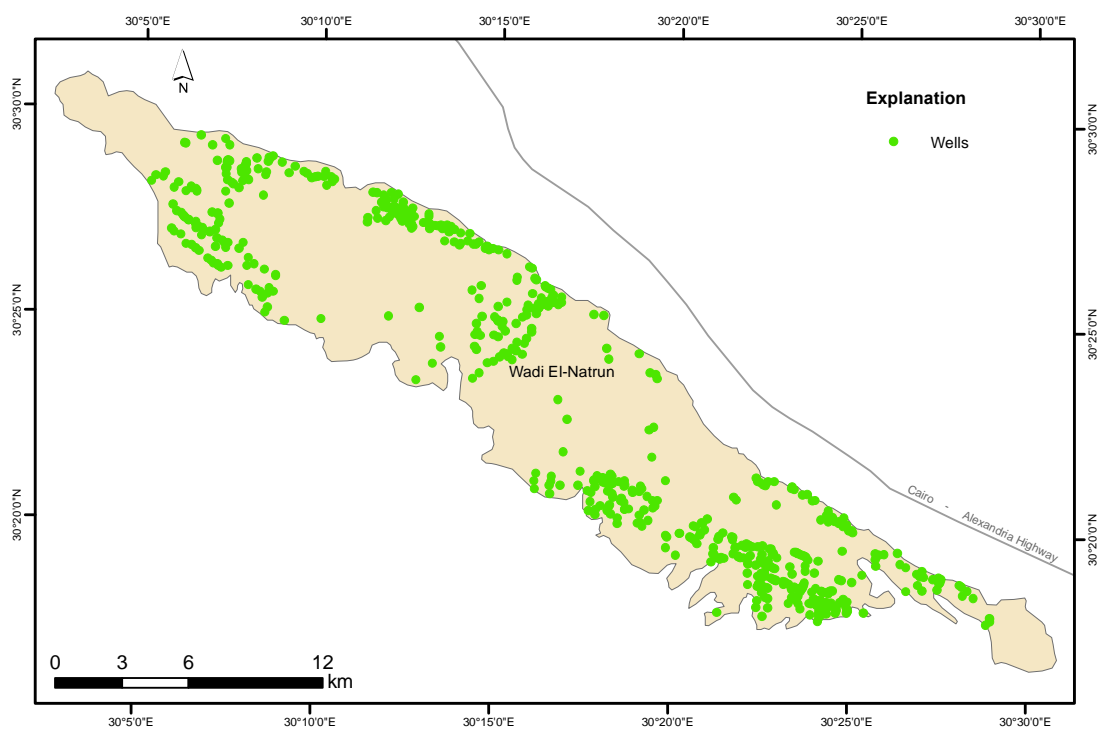


Fig. 7.6: Location map of the Wadi El-Natron showing the distribution of pumping wells.

## 7.7 Model output

The available scenarios were applied in the model to obtain a scientific prognosis of the future behavior of the Miocene aquifer systems in Wadi El-Natrun and to evaluate the feasibility of each scenario taking into consideration the sustainability of the aquifer under each extraction scheme as presented in Table 6.1. The prediction period extended up to the year 2060.

### 7.7.1 Scenario 1

In this scenario the actual extraction rates of  $60.8 \times 10^6$  m<sup>3</sup>/a for the Wadi El-Natrun are considered constant during the prediction simulation. The groundwater flow direction was generally from the different directions toward the Wadi El-Natrun. This general trend is maintained roughly by the year 2010 as can be seen from the hydraulic heads (Fig. 7.7). However, the cone of depression exists in the middle of the Wadi El-Natrun. The hydraulic head pattern will be further developed from 2010 to 2060, as the hydraulic gradient changed from  $15 \times 10^{-4}$  by 2010 to  $20.2 \times 10^{-4}$  by 2060, which induces the cone of depression to become deeper with time (Fig. 7.11). The centre of the cone lies near the north boundary of Wadi El-Natrun.

In the year 2010 the drawdown is less than 5 m at 20% of the Wadi El-Natrun area towards Ras Al-Solimania. The drawdown ranges from 10 to 15 m at about 33% of the area at the Wadi El-Natrun city, Gabal Molouk, Deir Anba Beshoy and the Deir El-Syrian (Fig. 7.8). Nevertheless the drawdown in the year 2035 will range from less than 5 m up to 18 m and by further simulation, the decline of potentiometric heads will increase to reach about 10 m at Ras Al-Solimania, and up to 21.8 m at the Wadi El-Natrun city by the year 2060 (Fig. 7.11). The maximum decline at the potentiometric surface in this scenario (21.8 m) has not overtaken the allowable drawdown (35 m). In the year 2010, about 60% of the Wadi El-Natrun area has a depth to groundwater of less than 20 m (Fig. 7.9), while in the year 2060, about 80% of the area will have a depth to groundwater ranging from 20 to 40 m (Fig. 7.12).



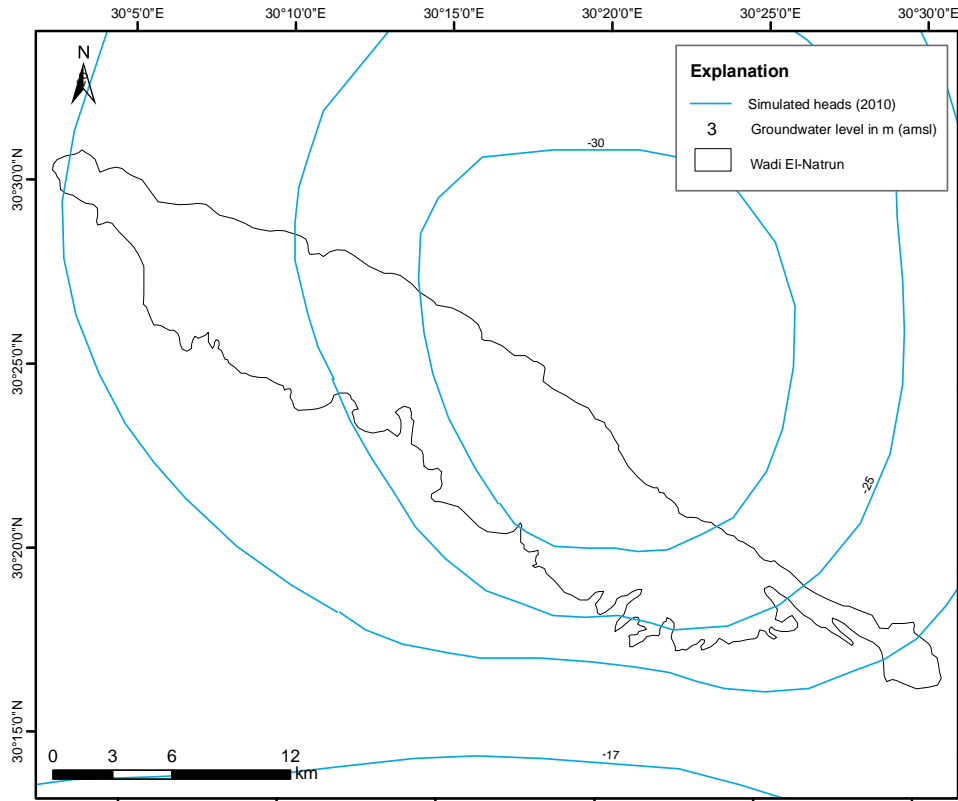


Fig. 7.7: Distribution of the simulated hydraulic heads at the Wadi El-Natron in the year 2010.

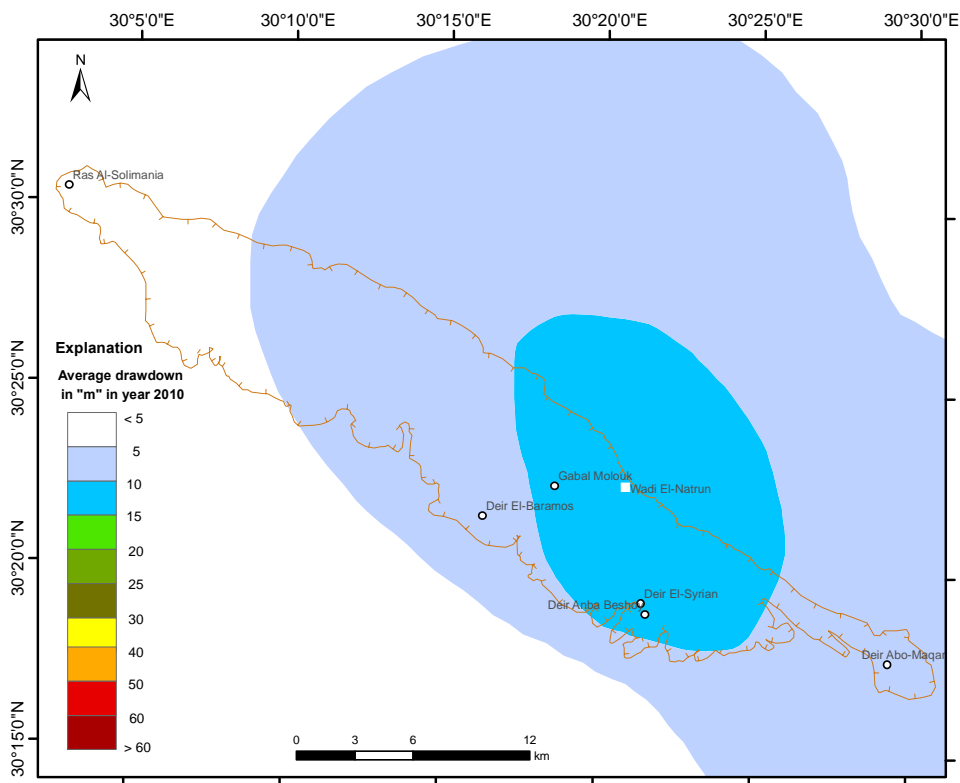


Fig. 7.8: Simulated decline in Wadi El-Natron by 2010.

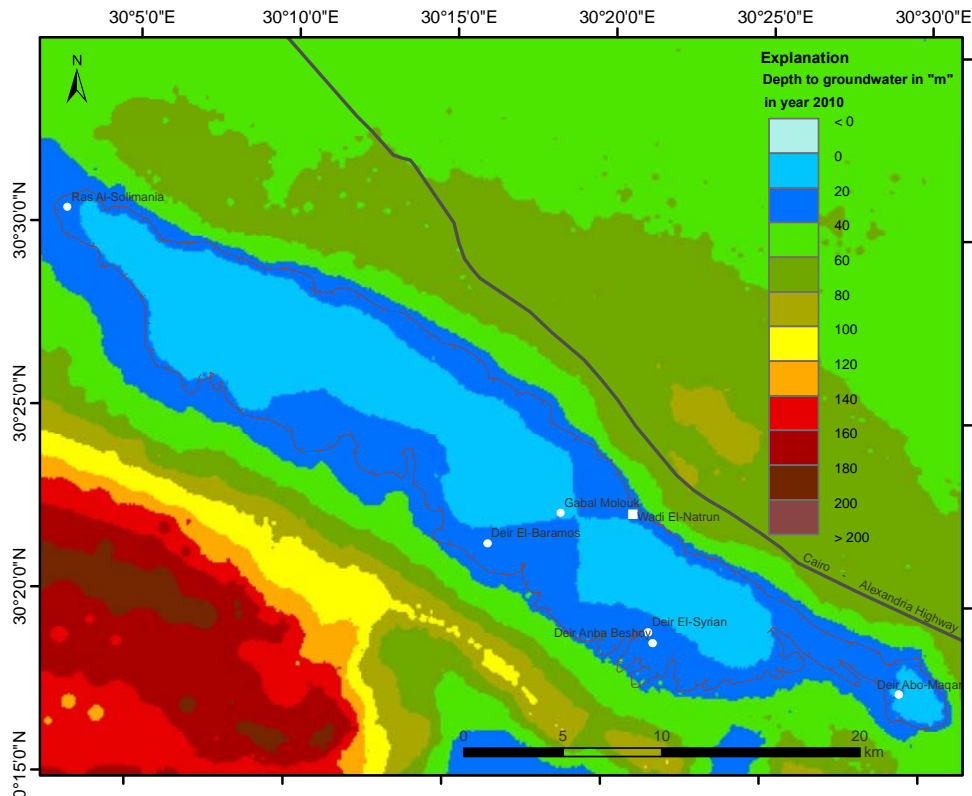


Fig. 7.9: Depth to groundwater in Wadi El-Natron in the year 2010

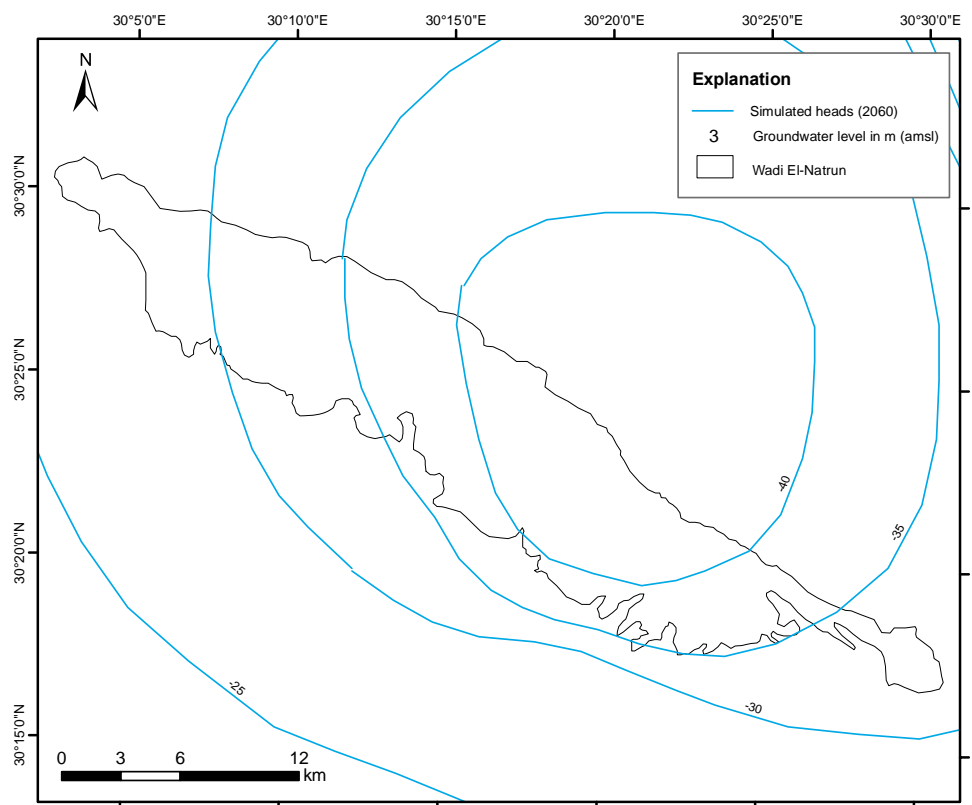


Fig. 7.10: Distribution of the simulated hydraulic heads at the Wadi El-Natron in the year 2060 according to the extraction rates of Scenario 1.

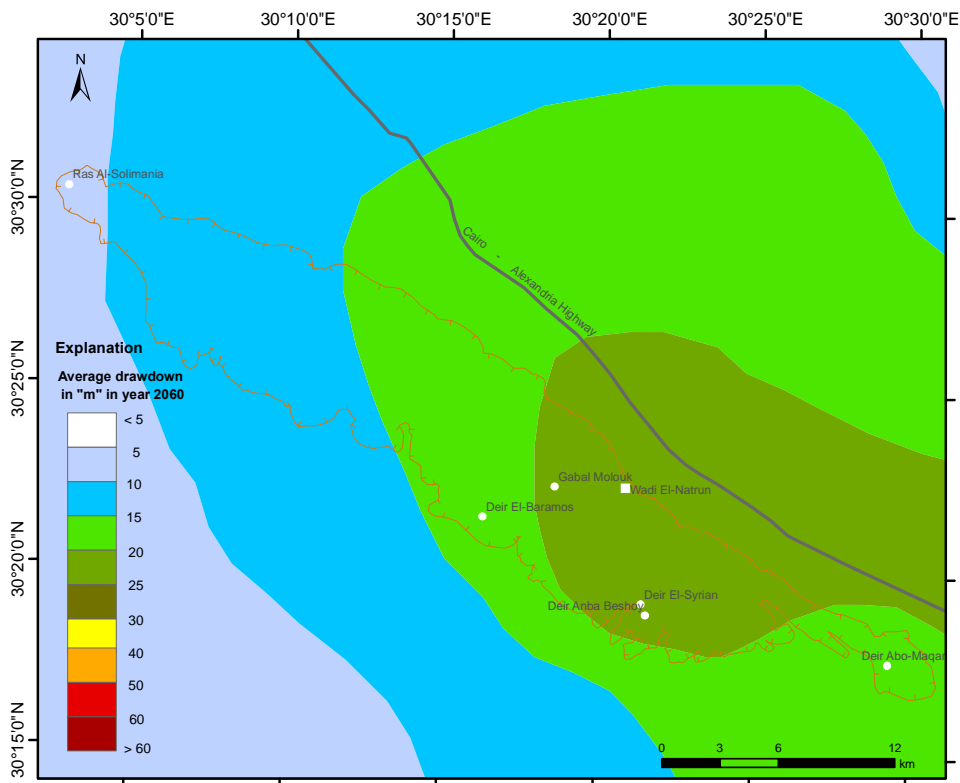


Fig. 7.11: Simulated decline in Wadi El-Natron by 2060 for Scenario 1.

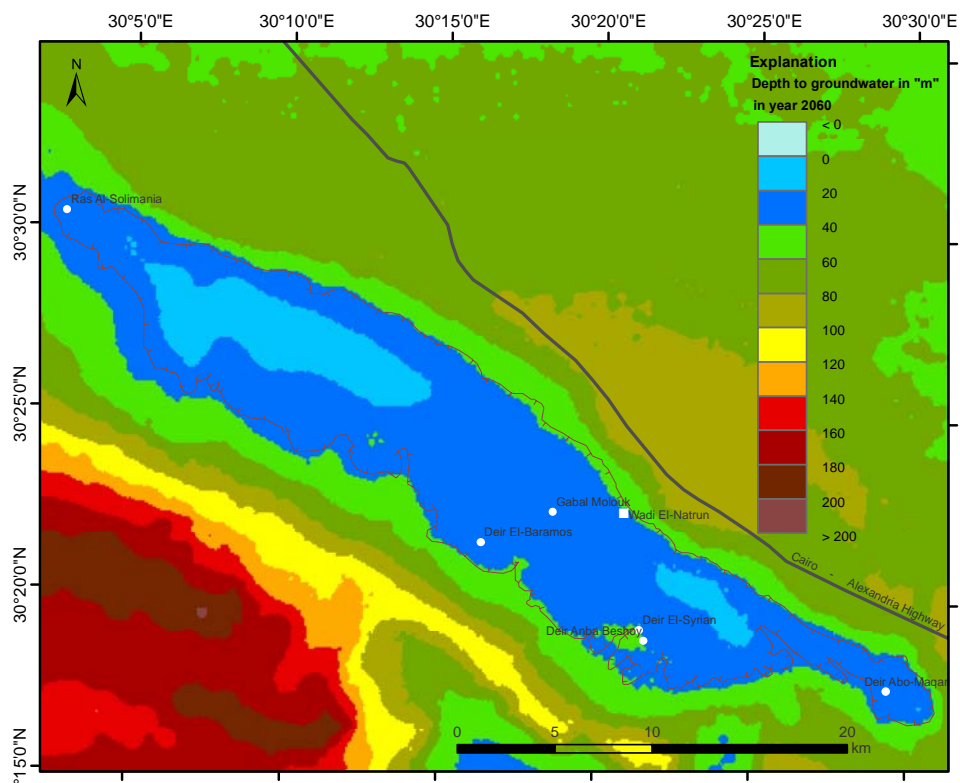
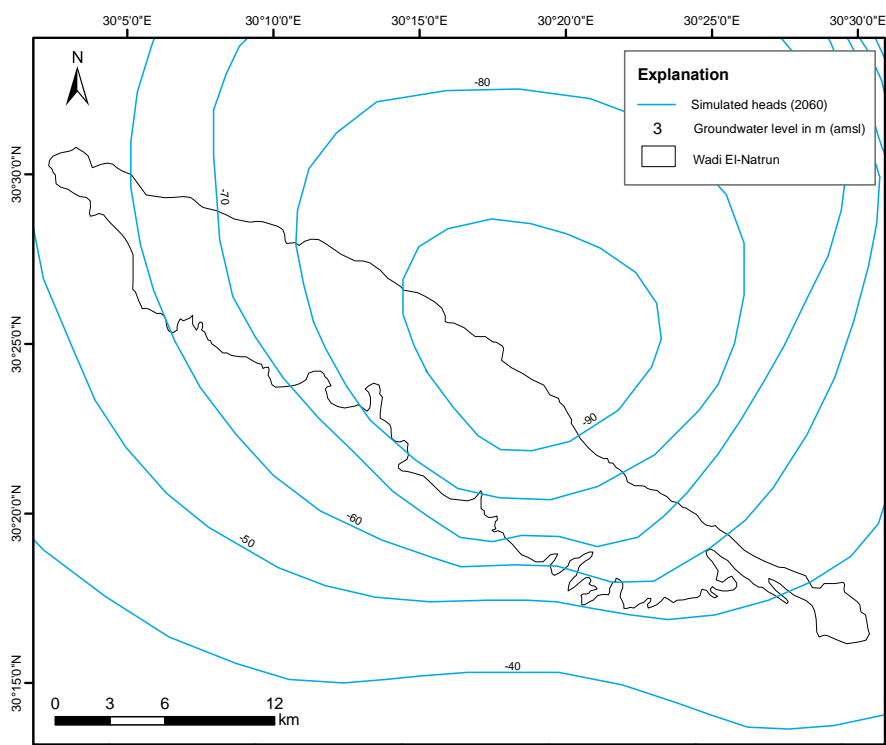


Fig. 7.12: Depth to groundwater in Wadi El-Natron in year 2060 according to the extraction rates of Scenario 1

### 7.7.2 Scenario 2

In the second scenario, the total extraction rate in the Wadi El-Natron is about 311 million  $m^3/a$ , full capacity extraction rate, in order to cultivate an area of about 260  $km^2$  with a rate of 1.2 million  $m^3/a/km^2$  (RIGW and RIGWA 1992). In this scenario it is assumed that the current extraction rate in the Wadi El-Natron ( $60.8 \times 10^6 m^3/a$ ) will increase gradually with a rate of about  $35 \times 10^6 m^3/a$  until reaching the full extraction rate and remaining constant after that for the rest of the prediction time. The attempt to simulate this scenario will help not only to investigate the environmental effects under the maximum extraction rate but also to compare the resultant drawdown from this scenario with the resultant drawdown from Scenario 1 in order to establish a feasible scenario.

In this scenario the hydraulic gradient will be doubled in the next 50 years from  $15 \times 10^{-4}$  in 2010 to  $33.7 \times 10^{-4}$  in 2060. Approximately 95% of the Wadi El-Natron area will have a drawdown of more than 25 m by the year 2035, whereas about 94% of the Wadi El-Natron area will already overtake the allowable drawdown by the year 2060; this includes about 46% that has a drawdown of more than 60 m with an average drawdown of more than 0.9 m/a (Fig. 7.14). Due to this scheme of abstraction, about half of the area of the Wadi El-Natron area will have an average depth to groundwater of about 70 m, whereas 36% of the area will have an average depth to groundwater of about 50 m and the rest will have a depth to groundwater of more than 80 m (Fig. 7.15).



**Fig. 7.13:** Distribution of the simulated hydraulic heads at the Wadi El-Natron in year 2060 according to the extraction rates of Scenario 2.

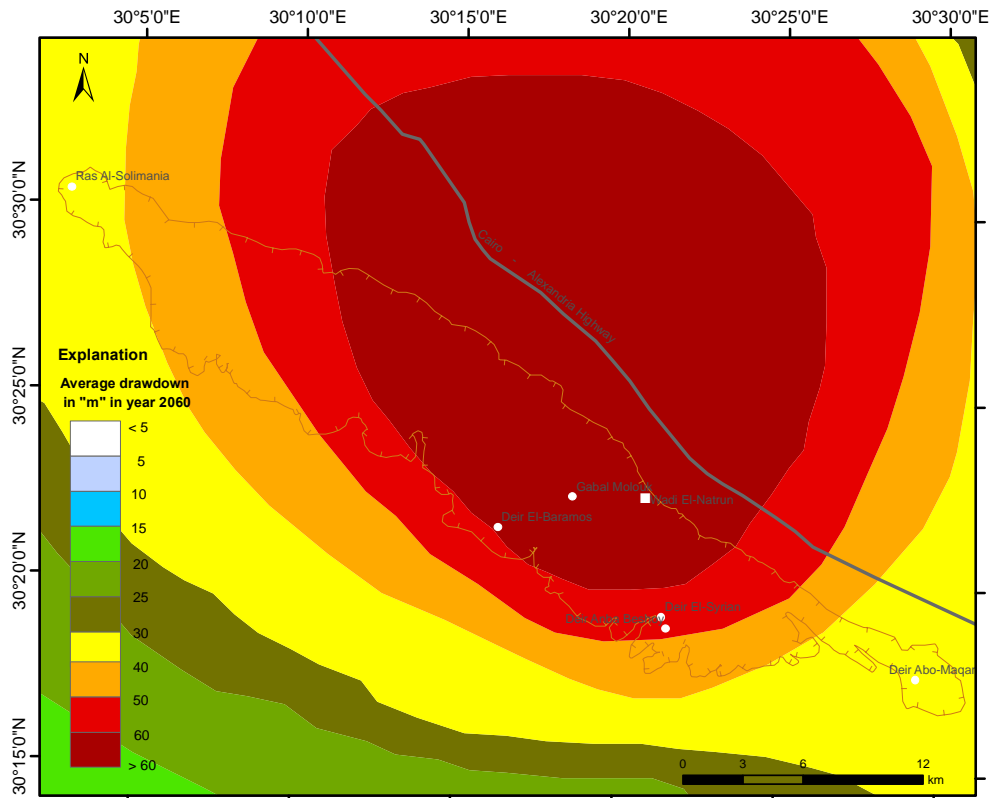


Fig. 7.14: Simulated decline in Wadi El-Natron by 2060 for Scenario 2.

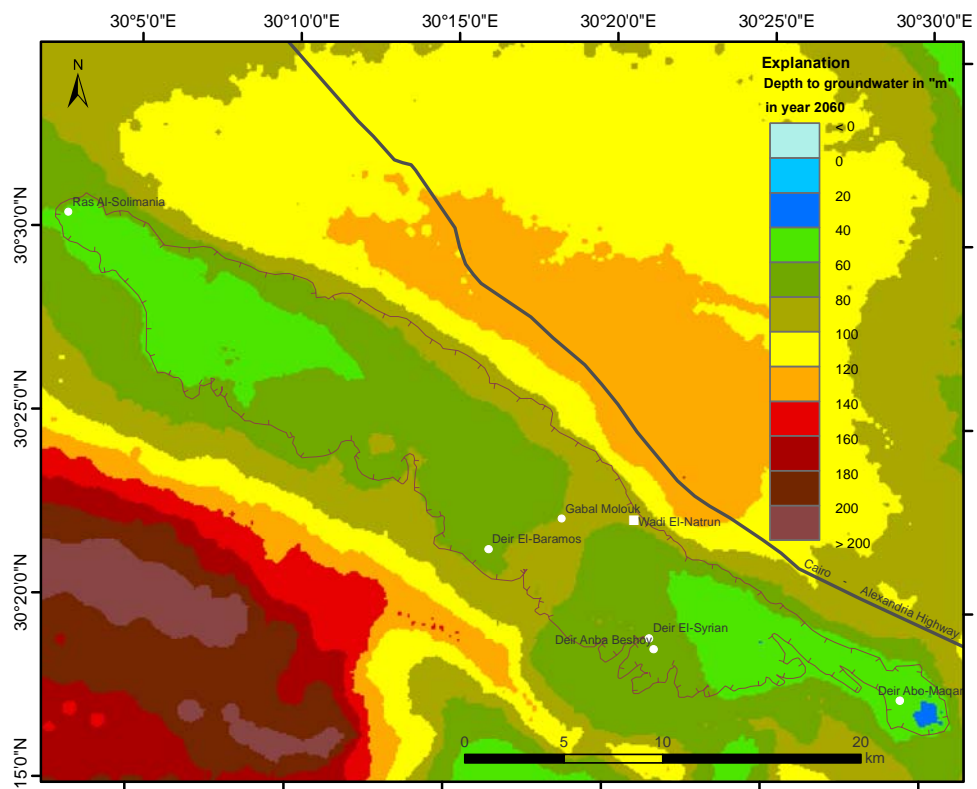
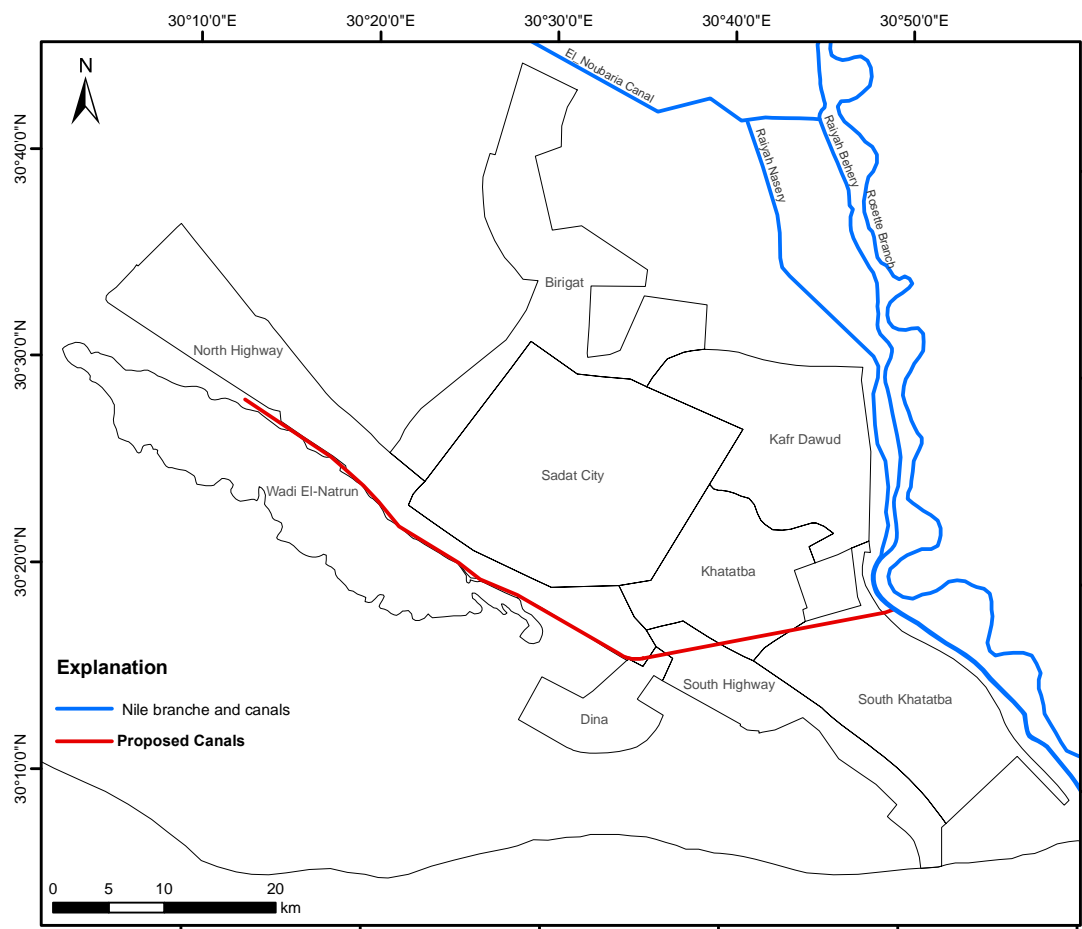


Fig. 7.15: Depth to groundwater in Wadi El-Natron in the year 2060 according to the extraction rates of Scenario 2

### 7.7.3 The conjunctive use between surface water and groundwater

After applying the extraction rates of Scenario 1 and 2, it can be concluded that on one hand, the drawdown in the first scenario is under the permissible drawdown limit, and, on the other hand, the drawdown in the second scenario exceeds the permissible drawdown limit. Therefore, there is a need for another scenario to feed the Wadi El-Natrun area with the required water for irrigation and without overtaking the permissible drawdown.

The available means of solving the problem of excess groundwater exploitation and fostering continued agricultural growth, employment and investment in the area is to think about the conjunctive use between both groundwater and surface water. A solution is proposed to implement a surface water conveyance system (pipeline to avoid losses due to evaporation and to avoid lifting surface water due to the topography) extracting water from the adjacent canals of the Nile River such as the Rayah Nasery to the Wadi El-Natrun depression (Fig.7.16). In order to discover the optimal ratio between annual volume of groundwater and surface water to cultivate an area of about 260 km<sup>2</sup>, two additional scenarios are examined.



**Fig. 7.16:** Proposed canal to Wadi El-Natrun for the conjunctive use between groundwater and surface water.

### 7.7.4 Scenario 3

This scenario was considered to predict the consequences of the future development when the current artificial discharge is increased by two-thirds of the difference between the full capacity and the current rate, where the groundwater extraction rate in the Wadi El-Natrun will be about  $227.5 \times 10^6 \text{ m}^3/\text{a}$  and the integrated annual volume of surface water is about  $83.5 \times 10^6 \text{ m}^3/\text{a}$ .

The simulated hydraulic gradient will be  $28 \times 10^{-4}$  by the year 2060. The drawdown in the Wadi El-Natrun depression will exceed the permissible drawdown in about 68 % of the area by the year 2060 including about 28% of the area will have a drawdown of more than 50 m with an average drawdown of about 0.78 m/a (Fig. 7.18) which exceeds the permissible drawdown by about 56%. Due to this scheme, about 60% of the Wadi El-Natrun area will have an average depth to groundwater of about 50 m, whereas 6% of the area will have an average depth to groundwater of about 30 m and the rest of the area (34%) will have an average depth to groundwater of about 70 m (Fig. 7.19).

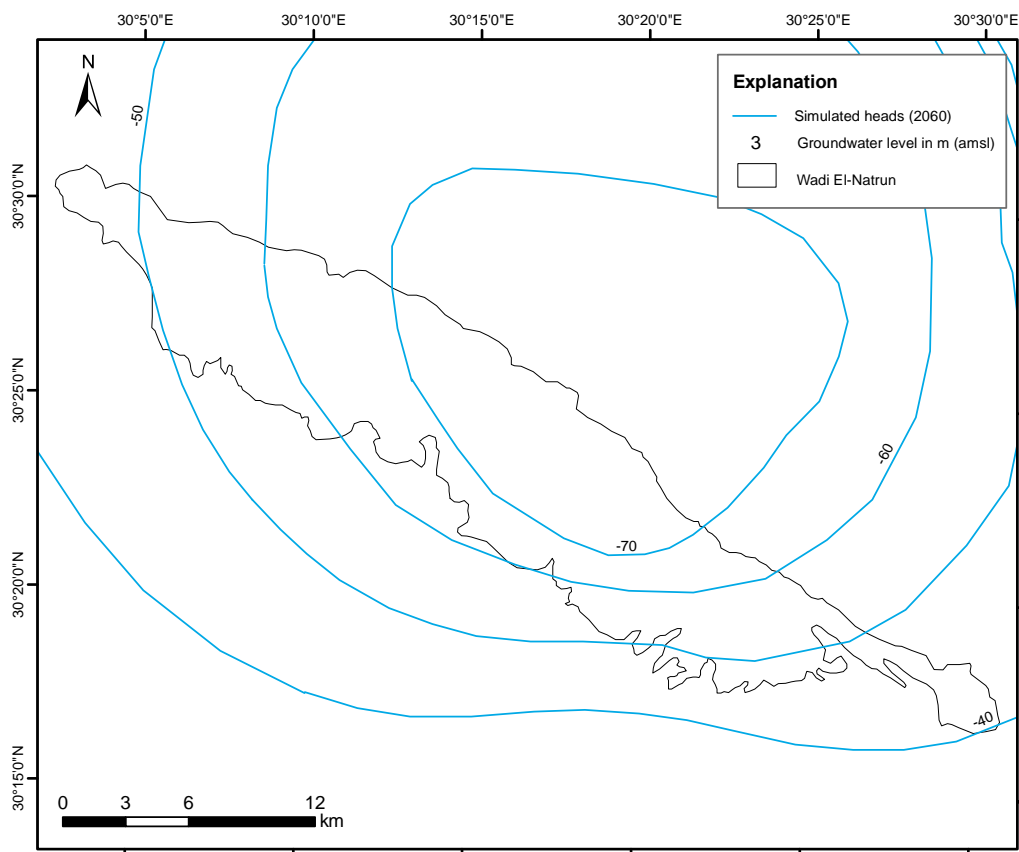


**Fig. 7.17:** Distribution of the simulated hydraulic heads at the Wadi El-Natrun in the year 2060 according to the extraction rates of Scenario 3.



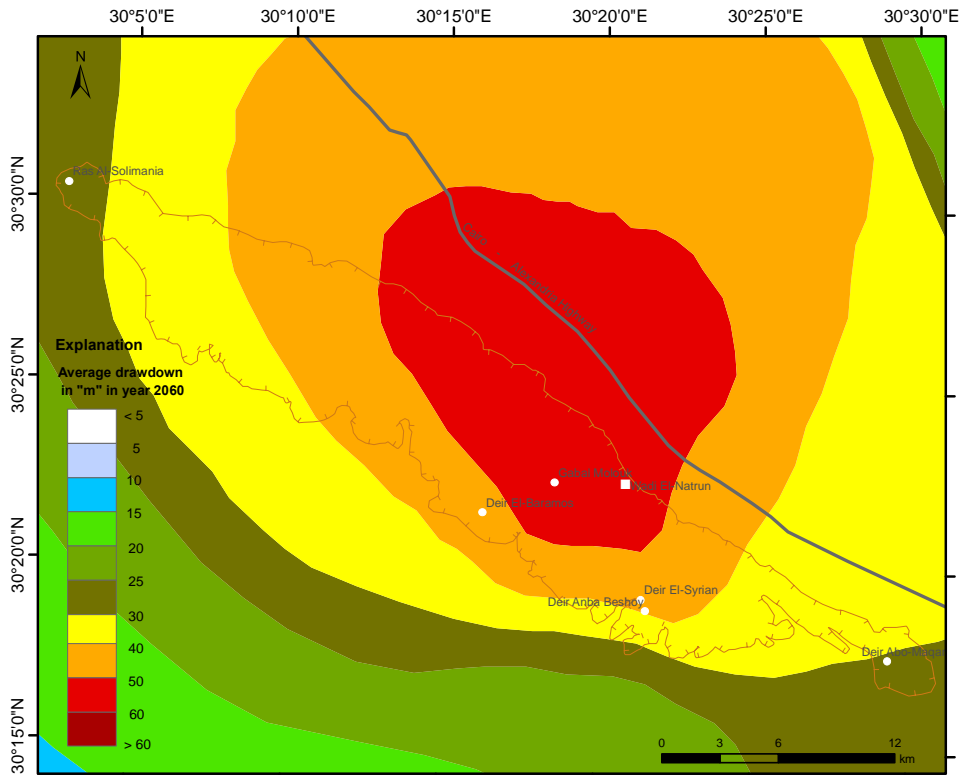


Fig. 7.18: Simulated decline in Wadi El-Natron by 2060 for Scenario 3.

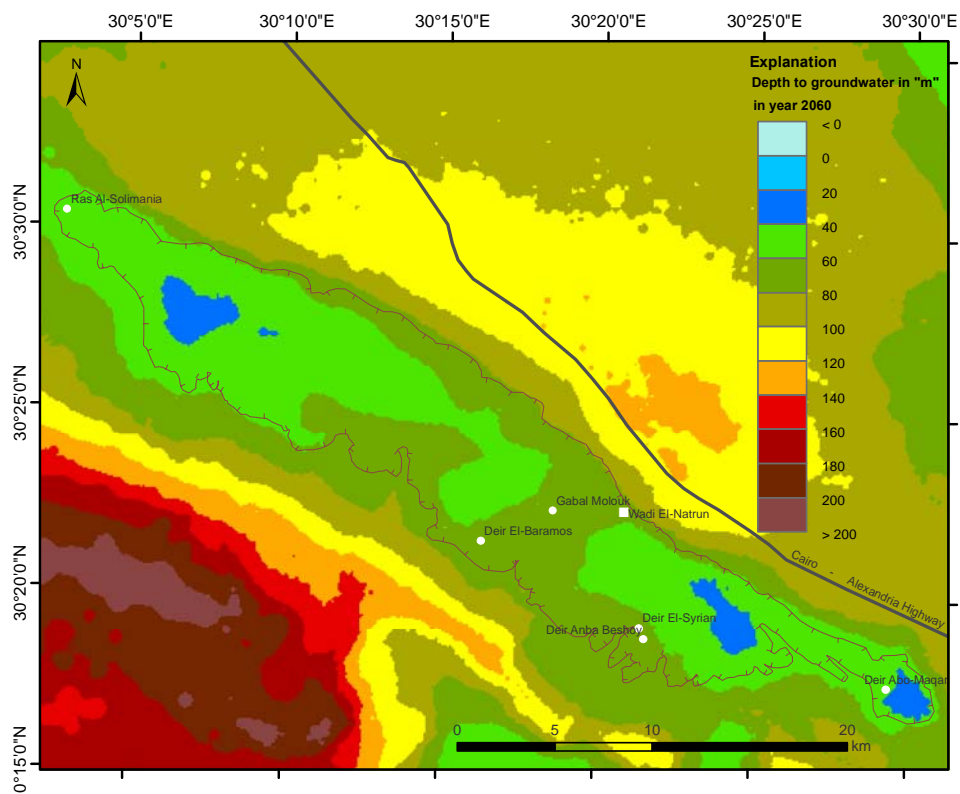


Fig. 7.19: Depth to groundwater in Wadi El-Natron in the year 2060 according to the extraction rates of Scenario 3



### 7.7.5 Scenario 4

This scenario was considered to predict the consequences of future development when the current artificial discharge is increased by one-third of the difference between the full capacity and the current rate, where the groundwater extraction rate in the Wadi El-Natrun will be about  $144 \times 10^6 \text{ m}^3/\text{a}$  and the integrated annual volume of surface water is about  $167 \times 10^6 \text{ m}^3/\text{a}$ .

Successive changes will happen in the simulated hydraulic gradient to be  $21 \times 10^{-4}$  by the year 2060. About 58% of the Wadi El-Natrun area will have an average drawdown of about 35 m and the drawdown in the rest of the area will range from 20 to 30 m, i.e. the drawdown will be within the permissible limit by the year 2060 (Fig. 7.21). Due to this scheme of abstraction, about 59% of the Wadi El-Natrun area will have an average depth to groundwater of about 50 m, whereas 41% of the area will have an average depth to groundwater of about 30 m (Fig. 7.22).

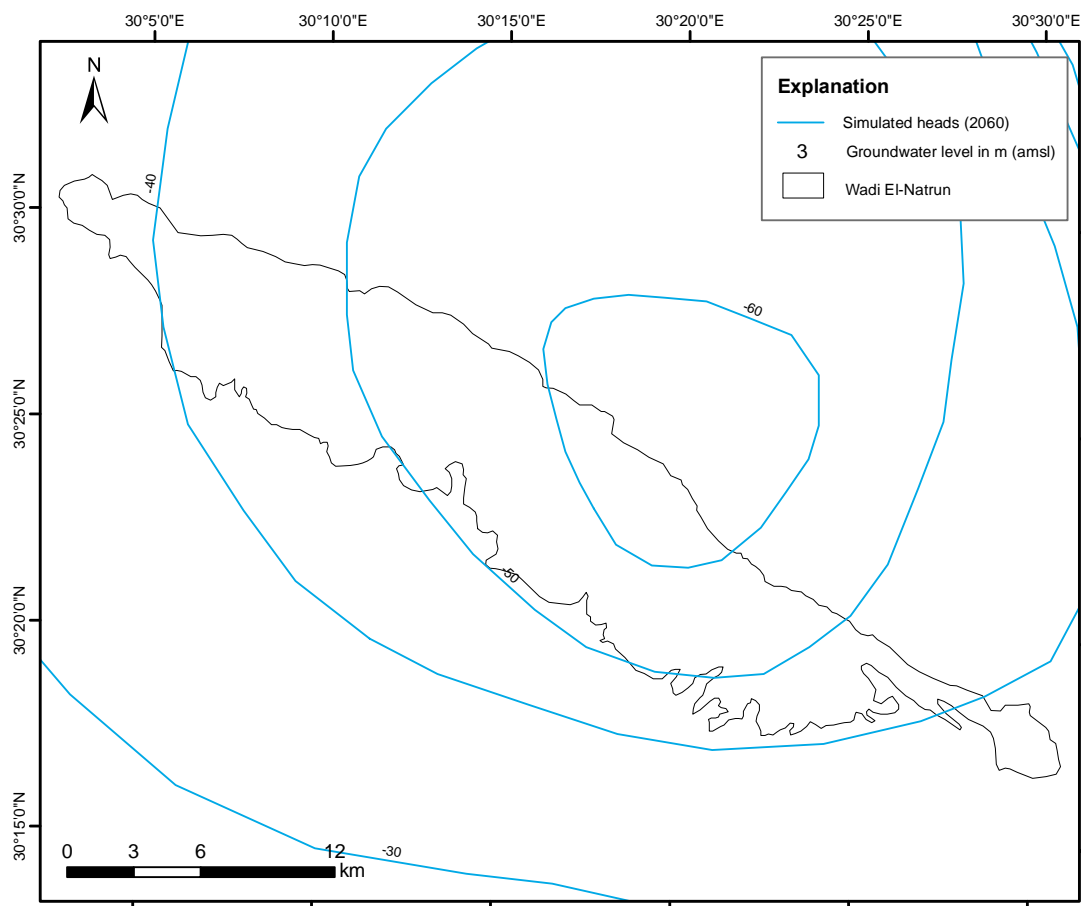


**Fig. 7.20:** Distribution of the simulated hydraulic heads at the Wadi El-Natrun in the year 2060 according to the extraction rates of Scenario 4.

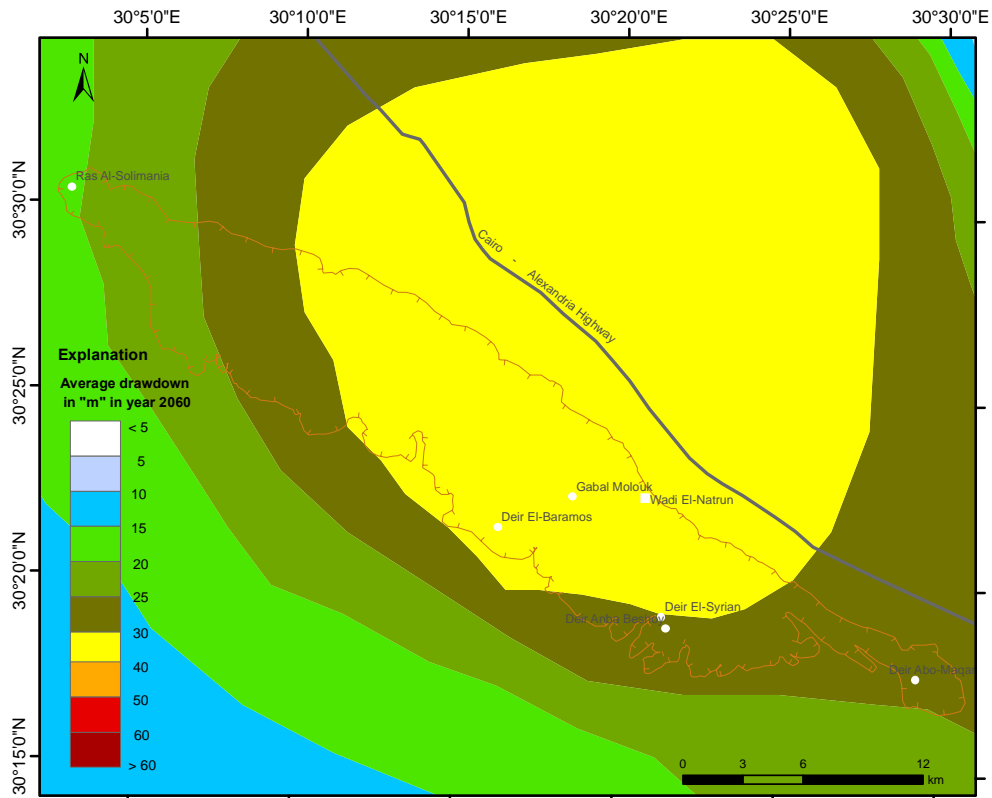


Fig. 7.21: Simulated decline in Wadi El-Natron by 2060 for Scenario 4.

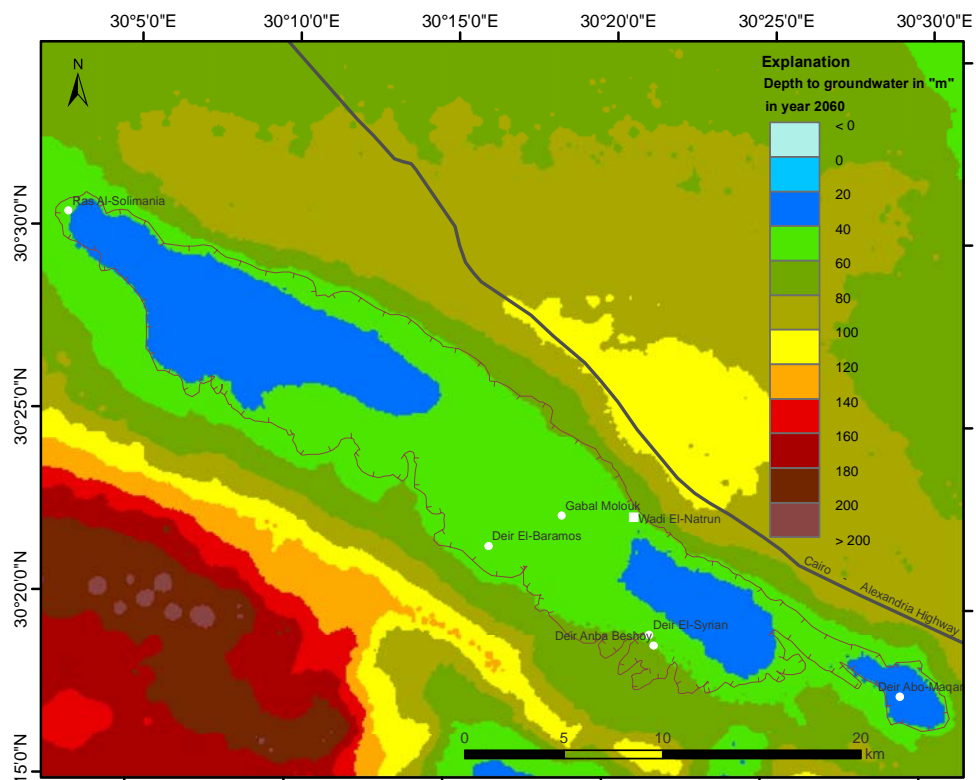


Fig. 7.22: Depth to groundwater in Wadi El-Natron in the year 2060 according to the extraction rates of Scenario 4

## 7.8 Sustainability and feasible scenario

Sustainability and inter-related risk of source degradation are the critical considerations when developing plans for the use of groundwater. Sustainability of a water resource requires a reconciliation of environmental, social and economic demands. These three pillars of sustainability are not mutually exclusive, but mutually reinforced. For many environmentalists the idea of sustainable development is an oxymoron as development seems to entail environmental degradation. It should be a balance between the water resource sustainability and the human sustainability in a certain place and time, which depends on a sustainable agriculture not only in the present but also as a goal for the future. It is concluded from the water balance in Section (6.6.4) that every additional extraction rate added to the current extraction rate will increase the groundwater mining. Therefore, in this study the term “sustainability” tends toward the social context and thus sustainability is not meant to imply preserving the groundwater resource for generations to come, but rather reconciling the use of the limited resource of the study area with the sustainability of human life.

As mentioned previously and according to the standards of the water policy in western Delta, Egypt, the annual yield drawdown should not exceed 0.5 m, i.e. should not exceed in total 35 m from 1990 to 2060. Based on this consideration and the results discussed in Section 7.7, it is concluded that the best option for groundwater management in the Wadi El-Natrun in terms of groundwater extraction is the implementation of an extraction rate of  $144 \times 10^6$  m<sup>3</sup>/a as introduced by Scenario 4 (Section 7.7.5). The results of this scenario emphasize not only that the permissible limit of groundwater drawdown could be retained during the simulation period, but also that the depth to groundwater level will not exceed 50 m, which could be economically feasible in meeting the proposed development plans. The implementation of Scenarios 2 and 3 will be responsible for creating a relatively huge cone of depression that extends far away beyond the Wadi El-Natrun borders, and the depth to groundwater will exceed 70 m (bgl). Furthermore, the potentiometric head will drop below the bottom of the first (Pliocene) aquifer. This, in turn will lead the wells extracting the first aquifer to dry out.

## 7.9 Up-coning effect

The Miocene aquifer in the Wadi El-Natron area is underlain by a disconnected thin layer of basalt that separates the aquifer from Oligocene deposits. The Oligocene deposits are made up of sandy mudstone and shale, sandstone and limestone, with occasional gravelly sandstone intercalations (Sadek et al. 2005). These Oligocene deposits are characterized by relatively high water salinity because of the dissolving salts of the Oligocene fluviomarine deposits during the circulation of the water (Abdel Baky 1983). Due to the disconnection in the basalt layer, the hydraulic contact between the Miocene aquifer and the Oligocene layer may lead, with every increase in the groundwater extraction from the Miocene aquifer, to the increase of salinity in the Miocene aquifer (Abdel Baky 1983) in what is called the up-coning effect. This can happen when fresh water is pumped from an aquifer overlying a body of salt water; where the drawdown of the fresh water table around the well causes a reduction in the pressure on the interface between the aquifer and the salt water body. This in turn causes the interface to rise below the well (Fig. 7.23). If the salt water cone reaches the well, it will discharge a mixture of salt and fresh water.

To study the effect of saline water up-coning from the Oligocene layer on the groundwater quality of the Miocene aquifer in the Wadi El-Natron area due to the extraction rates of Scenario 4, a transport 3 D model is used and a high salinity concentration (15000 to 20000 mg/l) is applied in the underlying layer of the Miocene aquifer. The value of the input salinity in the underlying layer is roughly estimated, as there are no available measured values of salinity distribution in this layer.

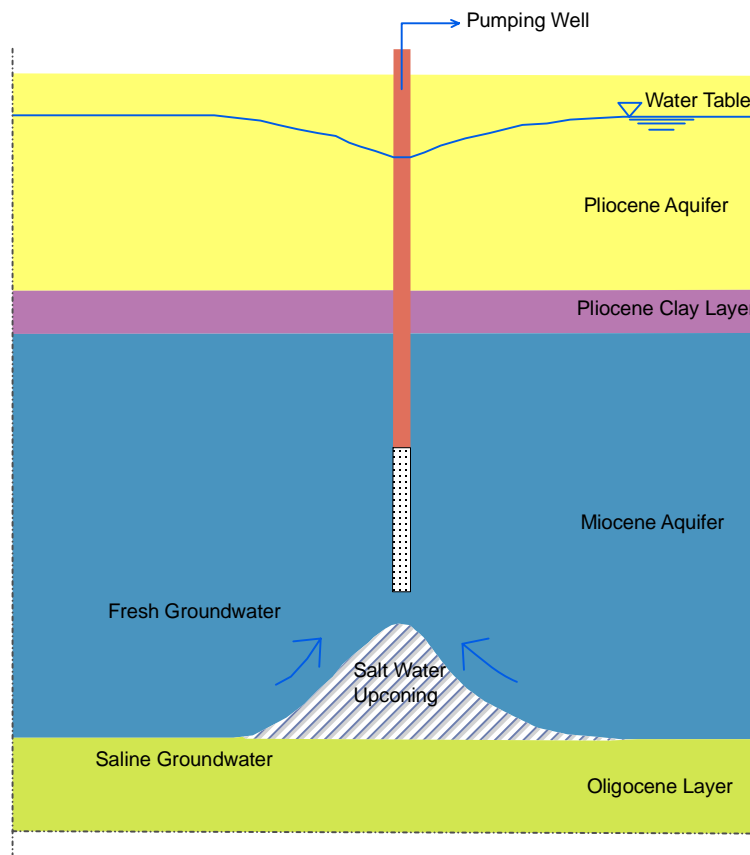


**Fig. 7.23:** Sketch showing the saltwater up-coning beneath a pumping well

After a simulation period through the year 2060, an increase in the salinity of groundwater in the Miocene aquifer in the Wadi El-Natron area is evident. The increase in the degree of salinity ranges from 2000 - 2500 mg/l in 10% of the area, from 2500 - 3000 mg/l in 32% of the area and from 3000 - 3500 mg/l in 58% of the Wadi El-Natron area (Fig. 7.24). Specifically, the ratio of salinity increase in the Miocene aquifer in the Wadi El-Natron area will be about 20% of the degree of salinity in the underlying layer in the next 50 years. Therefore, development of new plant varieties with higher degrees of tolerance to salinity will be appropriate for the future.

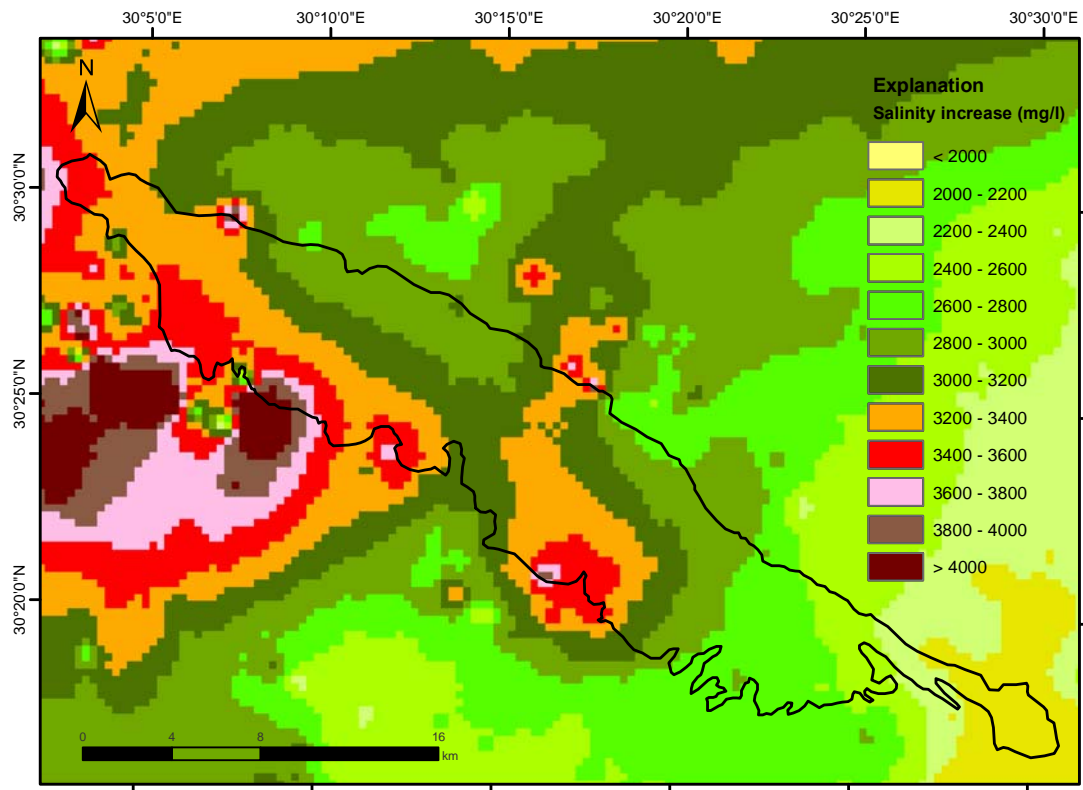


**Fig. 7.24:** Rough estimation for the increase in groundwater salinity in the Wadi El-Natron area in the year 2060 due to the up-coning effect in the Miocene aquifer according to Scenario 4.

# 8 Summary and Conclusions

## Outlines

The area of study lies West to the Rosetta branche between longitudes  $29^{\circ} 30'$  and  $31^{\circ} 00'$  E and latitudes  $30^{\circ} 00'$  and  $31^{\circ} 30'$  N. It covers an area of about 15000 km<sup>2</sup>. The ground surface of the study area reveals a general slope from South to North and ranges roughly from about 200 m (amsl) to the zero level at the border of the Mediterranean Sea except in the depression of Wadi El-Natron, where the ground level reaches about -20 m (amsl). The study area comprises three geomorphological units: 1) The alluvial plains (young and old alluvial plains) with an elevation that varies from 0 to 21 m (amsl) for the young alluvial plains and varies from 20 to 40 m (amsl) for the old alluvial plain. 2) The structural plains (depressions, folded ridges and structural plateaus) such as the Wadi El-Natron and Wadi El-Farigh depressions with a minimum level of about -23 m and -4 m (amsl) respectively; the folded ridges such as Gebel Khashab and Abu Roash with an elevation that ranges from 25 m to 200 m (amsl); and the structural plateaus such as El-Hadid plateau and El-Washika plateau with an elevation of about 180 m and 190 m (amsl). 3) The tablelands such as Maryut tableland and its extension, “the marginal tableland,” south of Wadi El-Natron. The geological layers of the modeled area range in epochs from the early Tertiary (Paleocene) to the Quaternary (Holocene). The aquifer system in the study area consists mainly of three structural basins: 1) The Nile Delta basin (Pleistocene), which consists of graded sand and gravel intercalated by clay lenses, 2) the Wadi El-Natron basin (Pliocene), which is made up of alternating sand and clay with lime stone at top and 3) the Moghra basin (Miocene), which consists of coarse sand and gravel with intercalation of sandstone and clay. The accessibility and the mild climate conditions of the area lead to the continuous establishment of many agricultural, industrial, and recreational projects. The exploitation of the aquifer resources is increasing and forming a cone of depression around the groundwater extracting fields.

## Objectives

- Construct a GIS-database for the study area.
- Construct and calibrate a regional 3D numerical groundwater flow model for the study area by using the data from the Geographic Information System.

- Study the effect of the current extraction rates and the full extraction rates in the development areas on the decline of groundwater levels in the next 50 years by using the calibrated 3D numerical flow model.
- Establish a 3D transport model from the 3D flow model and study the effect of the current extraction rates and the full extraction rates in the development areas on seawater intrusion in the next 50 years.
- Study the feasible scenario for the conjunctive use of groundwater and surface water in the Wadi El-Natron depression in order to pursue development without exceeding the permissible decline in groundwater levels in the year 2060.

### **Establishing the numerical model**

The present study is based on the integration of data that were interpreted from maps (topographical, geological, hydrogeological, hydrochemical), satellite images, cross sections, profiles, and the recorded data of well locations and extraction rates during the period from 1990 to 2006.

An integrated GIS-supported approach (ESRI ® ArcMap™ 9.2 / ArcMap™ 9.3) was used to create and process the different layers of the geological as well as the hydrogeological characteristics. A finite element subsurface flow and transport simulation system (FEFLOW® 5.2 - FEFLOW® 5.4 WASY 2007, 2008) was used to develop a steady state as well as a transient three-dimensional groundwater flow model for the study area by using the database from the GIS. The regional model was calibrated under steady state and transient conditions using the trial and error method in the period from 1990 to 2006 based on the availability and temporal distribution of the data in order to develop a reliable conceptual model for the study area to imitate the real area as closely as possible. Two different scenarios were defined to simulate the environmental effect on the aquifer system for the next 50 years. The first under current extraction rates and the second under full extraction rates for the irrigation of the whole development areas. The simulation process indicated that the direction of the groundwater flow within the regional model area is kept by the original trend of the initial head postulated by RIGW (1990). However, the values of these contours showed some changes in the development areas such as in the North Highway, South Highway, Sadat city, and Dina area where new contour lines with lower values appeared. The regional model was used afterward for the development and integration of a locally refined model for the Wadi El-Natron area.

### **Current situation**

The extraction rates in the study area increased from about 460 million m<sup>3</sup>/a in year 1990 to about 1650 million m<sup>3</sup>/a in year 2006. Under these extraction rates through the year



2010, the simulation indicated that the average hydraulic head decline in the development areas ranged from 5 m to 15 m. The average depth to groundwater was 62 m, 73 m and 101 m (bgl) in the North Highway, Khatatba, and South Highway area, respectively. While in the Kafr Dawud, Birigat and Sadat City, the average depth to groundwater was 25 m, 40 m, and 57 m (bgl). On the other hand, in the Wadi El-Natrun depression, the depth to groundwater ranges from 0 m to 40 m (bgl) with an average depth of 18 m (bgl), which means that the extraction wells are still within the economic range according to their depth to groundwater. The calibrated model was used for further prediction simulations to investigate the response of the aquifer to the different management options during the next 50 years. The scenarios of these prognostic calculations were elaborated on, disregarding the ongoing theoretical discussions about the admissibility of prognostic calculations. The parameters of the calibrated model were kept constant for all scenarios.

### **Scenarios and results of regional model in the next 50 years**

In an attempt to investigate the most feasible groundwater management in terms of the maximum allowable drawdown, two main extraction scenarios were outlined in the study area based on the actual and full capacity extraction rates. The simulation of the actual extraction rates of the first scenario ( $1.1 \times 10^6$  m<sup>3</sup>/a for the development areas) indicated that by the year 2060, the maximum drawdown will occur in the South Highway area with an average value of about 22 m and the drawdown in the Khataba and Dina area will be about 18 m and 20 m respectively. In the North Highway area, Wadi El-Natrun and Sadat City the average drawdown will be about 17.5 m. At the end of the simulation the average depth to groundwater will exceed 100 m (bgl) in the Dina (110 m bgl) and in the South Highway area (114 m bgl). By 2060 the cumulative decrease in groundwater storage in the study area according to Scenario “1” will be about 84 km<sup>3</sup> and the actual extraction rates will keep the drawdown by year 2060 under the permissible decline in hydraulic heads.

The numerical model simulation, when applying the full capacity extraction rates of the second scenario ( $2.5 \times 10^6$  m<sup>3</sup>/a for the development areas), led to severe drawdown within about 35% of the development areas during the simulation period in which the resulted average decline in hydraulic head will exceed the permissible drawdown in the Wadi El-Natrun, North Highway area and the Sadat City. The average depth to groundwater will increase accordingly during the simulation and by 2060 it will overtake 100 m (bgl) in the North Highway area (109 m bgl), South Highway area (123 m bgl) and Dina area (121 m bgl). Although the groundwater volume extracted from the aquifer storage through 2060 is about 156 km<sup>3</sup>, which is about 2.6% from the total groundwater volume of the study area, the consequences are considered objectionable since the decline in potentiometric surface and the depth to groundwater will increase accordingly and the groundwater withdrawal will not be economic. The extraction rates in the development areas under schemes of

Scenario 1 and Scenario 2 have a limited effect on seawater intrusion due to the limited drawdown along the coast and because groundwater levels in the adjacent area of the coast are still higher than sea level up to the end of the simulation.

Since the natural annual recharge of the study area is low compared to the actual discharge, the plan for groundwater development in any development area within the study area should be based on the aquifer depletion concept, which means that every additional extracted rates from the study area are groundwater mining.

### **Local model - Wadi El-Natrun depression**

The Wadi El-Natrun is an elongated depression in the NW-SE direction located about 90 km northwest of Cairo. The first scenario was implemented assuming the actual extraction rate ( $61 \times 10^6$  m<sup>3</sup>/a) is constant until the end of the simulation period in 2060. By 2010, the original groundwater flow direction was generally toward the Wadi El-Natrun from different directions. As a response to successive groundwater extractions in the last 20 years, a maximum drawdown of 12 m was reached at the southeast of Wadi-El-Natrun. Through the continuous rate of extraction through year 2060 (Scenario 1), the cone of depression will expand outside the boundaries of the depression with a maximum value of drawdown of 22 m at the east of the depression. However, the depth to groundwater at all the cultivatable areas within the depression will be less than 40 m (bgl). The average annual change in hydraulic head of the entire simulation period would be 0.4 m per year. Based on these results, it is concluded that the implementation of Scenario 1 is affordable for groundwater management in the Wadi-El-Natrun depression. However, this scenario is still under the permissible potentiality (35 m).

### **Optimal scenario for Wadi El-Natrun depression**

The simulation of Scenario 4 ( $144 \times 10^6$  m<sup>3</sup>/a) led to an average decline in the hydraulic heads of about 33 m in the Wadi-El-Natrun depression by the year 2060. However, the drawdown did not exceed 25 m at the end of the simulation on the eastern and the western side of the depression. The depth to groundwater in the depression will range from about 30 m at the east and the west sides of the depression and will go deeper toward the middle of the depression to reach a value of about 61 m (bgl) by 2060. Based on the groundwater potentiality and development ambitions in the Wadi-El-Natrun depression, this scenario was suggested to be the best development option for domestic, agricultural and industrial activities for the next 50 years, with an increase of about 136% of the current extraction rates. To feed the Wadi El-Natrun area with the total required water for irrigation ( $311 \times 10^6$  m<sup>3</sup>/a) and without overtaking the permissible drawdown, there is a proposal to substitute the difference ( $167 \times 10^6$  m<sup>3</sup>/a) via a conveyance system that extracts water from the Nile River. The ratio in this case between groundwater and surface water will be 46%:54 %.

The implementation of Scenarios 2 and 3 will be responsible for creating a bigger cone of depression that will extend beyond the depression's borders and the depth to groundwater will exceed 70 m (bgl). Additionally, the potentiometric head will drop below the bottom of the first aquifer. This, in turn, will affect the phreatic water levels and accordingly, the wells extracting the first aquifer will dry out.

### **Outlook and prospects**

- The existence of the Mediterranean Sea at the northern boundary of the study area creates a certain complexity to the situation. On one hand, it is considered that the ground water level in the north boundary is about zero (amsl), and, on the other hand, the interface between fresh water and saline water has been proved that it is slightly affected by the extraction rates and can be almost considered as constant. But these facts are relative rather than absolute because any increase in the sea level, for instance due to the global warming, will lead to move the interface between sea water and fresh groundwater into the aquifer system deteriorating groundwater quality. This can be researched further in following studies with help of the numerical model.
- At the end of simulations in the regional model, the groundwater level decreased intensively in the Wadi El-Natrun and its vicinities, which means that there is a possibility that the interface between freshwater in the Miocene aquifer and low quality water in the underlying Oligocene layer deforms causing withdraw of low quality water (the upconing effect). Therefore, there is a need to accurately measure the degree of salinity in the groundwater of the underlying layers of the Miocene aquifer to define it in the numerical model in order to study the changes in salinity in the Miocene aquifer over time.
- Groundwater mining will certainly affect the hydrochemistry of the groundwater. Hence, hydrochemical investigations still are needed, especially in the stressed areas within the study area.
- Due to the huge modeled volume of the study area, large data gaps remain to be filled to improve the consistency and reliability of the modeled aquifer geometry and parameters. Continuous periodic monitoring of groundwater quality and levels is notably required to connect the predicted plan with the real situation. Since the current groundwater flow model for the study area is GIS-supported, it can be updated to match new situations or to be improved when new data are obtained, and it can be easily used for any further simulation purposes.
- Increasing irregularities of constructing wells due to the high rates of abuse on the new land along the Cairo-Alexandria Desert Highway will lead to a rapid deterioration of the aquifer in the region. Therefore, there is a need for preparing a new regulation for permitting groundwater wells whether governmental or private sector, and preventing

the drilling of wells without official permission from the Ministry of Water Resources and Irrigation, according to the technical specifications prescribed by the Ministry.

- It is necessary to rely on modern systems for irrigation and avoid expanding the cultivation of crops demanding high water consumption as well as the development of new plant varieties with short life spans and higher degrees of tolerance to drought and salinity.
- It should be considered imposing fees for the use of groundwater in resorts in the different regions along the Cairo-Alexandria Desert Highway and using the revenue to carry out water projects in the study area.
- A strategic plan to reduce the population growth and develop a follow-up for implementation and measurement of rates should be executed. This can be done by linking the success in this plan to the incentives and the services provided by the government to these provinces according to the different deliverables, and declaring the figures and statistics on the community, which will create competition between the different provinces.
- In the long run, finding another source of water that can be a major share of the current fresh water supply is urgently needed. Therefore, specific attention should be directed towards the researches of seawater desalination by using the solar energy to become affordable for irrigation.

## Bibliography

- Aadland, A.J. and Hassan, A.A. (1972). Hydrocarbon potential of the Abu Gharadig basin in the Western Desert. 8<sup>th</sup> Arab Petrol. Congress, Algiers, 81(B3).
- Abdel Baki, A.M.A. (1983). Hydrogeological and Hydrogeochemical studies in the area west of Rosetta branch and south El Nasr canal. Ph.D. thesis, Faculty of Science. Cairo, 156 pp.
- Abu-Zied, M. (1991). Water resources assessment for Egypt. Proceeding of round table meeting on planning for groundwater development in arid and semi-arid region, Cairo, Egypt, pp. 15-34.
- Ahmed, S.A. (1999). Hydrogeological and isotope assessment of groundwater in Wadi el Natrun and Sadat city, Egypt. Ph.D. thesis, Faculty of Science, Cairo, 237 pp.
- Al Far, D.M. (1966). Geology and coal deposits of Gebel El Maghara, northern Sinai. Geol. Surv. Min. Res. Dept., Egypt, Paper No. 37, 59 pp.
- Allam, A., Saaf, E. and Dawoud, M. (2002). Desalination of brackish groundwater in Egypt. Desalination, Elsevier, Amsterdam Vol. 152: pp. 19-26.
- Anderson, M.P. and Woessner, W.W. (1992). Applied Groundwater Modeling, Simulation of flow and advective transport. Academic Press Inc., San Diego, 381 pp.
- Armstrong, M. (1998). Basic linear geostatistics. Springer, Berlin, 153 pp.
- ASCE. (1996). Hydrology Handbook. American society of civil engineers, Reston, 784 pp.
- Atlas (1996). Climate Atlas of Egypt, Egyptian meteorological authority, Cairo, 95 pp.
- Attia, A.k., Hilmy M.E. and Hagab, O.A. (1970). Mineralogy of the sediments of Wadi El-Natrun Terraces. Desert Institute Bulletin, Cairo, Egypt, V. 20, No.2, pp. 327-357.

- Attia, F.A. (1985). Management of water systems in Upper Egypt. Ph.D. thesis, Cairo University, Egypt.
- Attia, F.A. (1998). Mediterranean Document on Groundwater. Groundwater resources management in Egypt, in the concept of IWRM. In: Proceedings of 7th Nile conference 15-17 March, Cairo, 11:1-16.
- Awad, M.A., Nada, A.A., Aly, A.I.M. and Farid, M.S. (1993). Tritium content of groundwater aquifer in western Nile Delta. *Isotopes in environmental and health studies*, Gordon and Breach science publishers, USA, Vol. 28: pp. 167-173.
- Bahr, B. (1995). Nile Delta aquifer with emphasis on saltwater intrusion in the northern area. M.Sc thesis, Technical University of Berlin, Institute for Applied Geoscience, Berlin, 185 pp.
- Barnes, R (1991). The Variogram Sill and the Sample Variance. *Mathematical Geology*, 23(4): 673-678.
- Beadnell, H.J.L. (1905). The Topography and geology of Fayium Province of Egypt. Surv. Dept. Cairo, 101 pp.
- Bear, J. (1972). Dynamics of fluids in porous media. 1st ed. American Elsevier Inc., New York, 764 pp.
- Beim, U. (1983). Planung, Durchführung und Auswertung von Gütepumpversuchen. *Zeitschrift für angewandte Geologie*, E. Schweizerbart, Stuttgart, 29 (10), pp. 484-492.
- Bohling, G. (2005). Kriging. Open-file report, Kansas Geological Survey, USA, 20 pp <http://people.ku.edu/~gbohling/cpe940/Kriging.pdf>
- Cherif, O.H, Kelani, A.H. and Mostafa, A.R. (2006). Stratigraphic lexicon and explanatory notes to the geological map of the north western desert, Egypt. UNESCO, Cairo, 148 pp.
- Chiles, J. and Delfiner, P. (1999). Geostatistics: modeling Spatial Uncertainty. Willy, New York, 695 pp.

- Conoco (1987). Geological map of Egypt. Egyptian General Authority for Petroleum (UNESCO joint map project), 20 sheets, Scale 1: 500,000. Cairo, Egypt.
- Dagan, G. (1997). Stochastic modeling of Flow and transport: the broad perspective. In Dagan and Neuman, 1997(eds.). Subsurface flow and transport: a stochastic approach. International Hydrology Series, UNESCO, Cambridge University press, 255 pp.
- Dawoud, M., Darwish, M. and El-Kady, M. (2005). GIS-based groundwater management model for western Nile Delta. Journal of Water Resources Management, Nietherland, Vol. 19, pp. 585-604.
- Delleur, J.W (1999). The Handbook of Groundwater Engineering. 1st ed. CRC Press and Springer, Boca Raton and Heidelberg, 949 pp.
- Diab, M., Mahammed, M.A. and Rizk, Z.S. (1995). The role of geology, hydrogeology and human activities in the contamination of shallow water resources northwest of the Rosetta Nile Branch, Egypt. Journal of faculty of Science. Unite Arab Emirates Univ. 8(2): 260-291.
- Diab, M.Sh., Abdel Latif, A.T. and Abdel Baki, A.A. (1980). Groundwater occurrences in the southern sector of Cairo-Alexandria Desert Road. Annals of Geological survey of Egypt, Vol. X, pp. 797-805.
- Diersch, H.-J. G. (1998). FEFLOW, Finite element subsurface flow and transport simulation system. USGS, User's manual for version 5.2. WASY, Berlin, 190 pp
- DMA-TR 8350.2 (1997). World Geodetic System 1984: Its Definition and Relationship with Local Geodetic Systems. Defense Mapping Agency, Technical Report, Third Edition, 54 pp.
- Domenico, P.A. and Schwartz, W. (1998). Physical and Chemical Hydrogeology. 2nd ed. Wiley, New York, 506 pp.
- Dominik, W. (1985). Stratigraphie und sedimentologie (Geochemie, Schwermineral-analyse) der Oberkreide von Bahariya und ihre correlation zum Dakhla-Becken (Western Desert, Ägypten). 2nd ed. Berliner geowiss. Abh. (A) 62, 173 pp.

- EGSMA (1950). Topographic map for the Wadi El-Natron, Scale 1: 100,000. Egyptian Geological Survey and Mining Authority, Cairo, Egypt.
- EGSMA (1951). Topographic map for the Abo El-Matameir and the west of Tanta, Scale 1: 100,000. Egyptian Geological Survey and Mining Authority, Cairo, Egypt.
- EGSMA (1990). Topographic map for the Monuf, Scale 1: 100,000. Egyptian Geological Survey and Mining Authority, Cairo, Egypt.
- El-Banna, M.M. (2007). Vulnerability and fate of a coastal sand dune complex, Rosetta-Idku, northwestern Nile Delta, Egypt. *Journal of Environmental geology*, Springer Berlin, 54: 1291-1299.
- El-Etr, H.A. and El-Baz, F. (1979). Utilization of ASTP photographs in Abo Rawash and Wadi El-Natron, Egypt. Apollo-Soyuz test project summary science report, NASA SP-412, Vol. II, pp. 219-236.
- El-Fayoumy, I.F. (1964). Geology of groundwater supplies in Wadi El-Natron area. M.Sc. thesis, Faculty of Science, Cairo University, Egypt, 109 pp.
- El-Fishawi, N.M., (1993). Sea level changes and their consequences for hydrology and water management. Proc. Int. Workshop, Noordwijkerhout, Session 4.
- El-Ghazawi, M. and Atwa, S. (1994). Contributions of some structural elements to the groundwater conditions in the southwestern portion of the Nile Delta. *Geological society of Egypt, Cairo*, 38(2), pp. 649-667.
- El Shazly, E., Abdel Hady, M., El-Gawaby, H., El-Kassas, K., Khawasik, S.M., El-Shazly, M.M. and Sanad, S. (1975). Geologic interpretation of Landsat satellite images for west Nile Delta area. Remote Sensing Center & Academy of Scientific Research and Technology. Cairo, 38 pp.
- El Sheikh (2000). Hydrogeology of the area north and west of Wadi El-Natron. M.Sc. Thesis, Faculty of Science, Elminufiya University, Egypt, 151pp.
- Farid, M.S. (1980). Nile Delta groundwater study. M.Sc. Thesis, Faculty of Science, Cairo University, Egypt, 93 pp.



- Fanos, A.M. (1992). Coastal process and protection works along the Mediterranean Egyptian coast. Workshop on impact of the Nile Delta coastal road and its effectiveness as defensive measure against the expected sea level rise, 5-8 May 1992, Cairo.
- Fanos, A.M. (1996). Wave climate along the Mediterranean Egyptian coast. Technical progress report No W1, Coastal research institute, Cairo.
- Farid, M.S. (1984). Management of groundwater system in the Nile Delta, Ph.D. Thesis, Faculty of Engineering. Cairo University, Egypt, 250pp.
- Fekry, A.M. (1993). Hydrogeological studies of the southern regions west of the Nile Delta, Ph. D. Thesis, Faculty of Science, Ain Shams University, Cairo, 121 pp.
- Fetter, C.W. (1994). Applied Hydrogeology. 3rd ed. Prentice Hall, New Jersey, 691 pp.
- Focazio, M.J, Plummer L.N, Bohlke, J.K, Busenberg, E, Bachman L.J, Powars, D.S (1998). Preliminary estimates of residence times and apparent ages of ground water in the Chesapeake Bay watershed and water quality data from a survey of springs. USGS, Water-Resources Investigations, Report 97-4225, 75 pp.
- Franke, O., Reilly, T. and Bennett, G. (1987). Definition of boundary and initial conditions in the analysis of saturated groundwater flow systems; in an introduction, techniques of water resource investigations of the USGS, Book 3, Ch. B5.
- Freeze, R.A. and Witherspoon, P.A. (1967). Theoretical analysis of regional groundwater flow: 2. effect of water table configuration and subsurface permeability variation. Water Resources Research. 3: 623-624.
- Freeze, R.A. and Cherry, J.A. (1979). Groundwater. Prentice-Hall, Englewood Cliffs, 604 pp.
- Frihy, O.E. (2003). The Nile Delta-Alexandria coast: Vulnerability to sea-level rise, consequences and adaptation, Mitigation and adaptation strategies for global change, Kluwer academic publishers, Netherlands, 8: 115-138.
- Galati, S. (2006). Geographic information system demystified. Artech house inc., Michigan, 302 pp.

- Gaame, O.M. (2005). Evaluation of well design west of the Nile Delta region with emphasis on Wadi El-Natrun and Wadi El-Farigh areas. GERMENA, Vol. 1, pp. 333-348.
- Gomma, A.M. (1995). Comparative hydrogeological and hydrogeochemical study on some aquifers, West of Nile Delta, Egypt. Ph. D. Thesis, Faculty of Science. Cairo University, Egypt, 236 pp.
- GPC (1987). The groundwater resources of Wadi El-Natrun area, Western Desert, Egypt. Interior report by the General Petrol Corporation, Cairo, 82 pp.
- Hall, W.A. and Dracup, J.A. (1970). Conjunctive use of groundwater and surface water systems. In water resources system engineering, Chapter 8, McGraw-Hill, New York, 372 pp.
- Hantar, G. (1990). North Western Desert. In Said, R (Ed). The geology of Egypt. Balkema Rotterdam, pp. 293-319.
- Hassan, A. (2003). Validation of numerical groundwater models used to guide decision making. Journal of the association of ground water scientists and engineers, Cleveland, Vol. 42, pp. 277-290.
- Hassaneen, A. Gh., El-Shayeb, H.M. and Khalil, M.A. (1997). New result on the waterless area, Wadi el Natrun depression. Scientific Journal of faculty of Science. Elminufiya, Egypt, Vol. XI, pp. 135-161.
- Hefny, K. and Shata, A. (2006). The groundwater in Egypt. Ministry of water resources and irrigation, Cairo, 277 pp.
- Hermina, M., Klitsch E. and List F.K. (1989). Stratigraphic lexicon and explanatory notes to the geologic map of Egypt 1:500 000, Conoco Inc., Cairo, Egypt, 264 pp.
- Herzberg, A. (1901). Die Wasserversorgung einiger Nordseebäder. Zeitschrift für Gasbeleuchtung und Wasserversorgung, R. Oldenbourg, München, Vol. 44, pp. 815-819 and pp. 824-844.
- Hill, M. and Tiedeman, C. (2007). Effective groundwater model calibration. Wiley, Hoboken, NJ, 455 pp.

- Houlding, S. (2000). Practical geostatistics: modeling and spatial analysis. Springer, Berlin, 159 pp.
- Ibrahim, S.M. (2000). Groundwater hydrology of El-Khatatba area and its vicinities, West Nile Delta, Egypt. M.Sc. thesis, Faculty of Engineering, Ain Shams University, Cairo, 124 pp.
- Ibrahim, S.M. (2005). Groundwater resources management in Wadi El-Farigh and its Vicinities for sustainable agricultural development, Egypt. Ph.D. thesis, Faculty of Engineering, Ain Shams University, Cairo, 152 pp.
- Idris, H. (1970). Groundwater investigation in Wadi el Natrun. Symposium of IAEA, Beirut, 26 pp.
- Isaaks, E. and Srivastava, R. (1989). Applied Geostatistics, Oxford University Press, New York, 561 pp.
- Jagelke, J. and Barthel, R. (2005) Conceptualization and implementation of a regional groundwater model for the Neckar catchment in the framework of an integrated regional model. Journal of advances in geosciences, European geosciences union, Vol. 5, pp.105-111.
- Johnson, L.E. (2009). Geographic information systems in water resources engineering, Taylor & Francis group, Boca Raton, USA, 288 pp.
- Kashef, A. (1983). Salt water intrusion in the Nile Delta. Journal of Ground Water, Ohio, vol. 21, Is. 2, pp.160-167.
- Kinzelbach, W. (1992). Numerische Methoden zur Modellierung des Transports von Schadstoffen in Grundwasser. R. Oldenbourg Verlag, München, 343 pp.
- Klitzsch, E. and Wycisk, P. (1999). Beckenentwicklung und Sedimentationsprozesse in Kratonalen Bereichen Nordost-Afrikas im Phanerozoikum. In Klitzsch, E, Thorweihe, U (eds). Nordost-Afrika: Strukturen und Ressourcen, John Wiley & Sons-VCH, Weinheim, pp 61-108.
- Kresic, N. (2006). Quantitative solutions in hydrogeology and groundwater modeling. CRC Press, Florida, 828 pp.

- La Moreaux, P.E. (1962). Reconnaissance report and recommendations for groundwater investigations, Wadi El-Natrun, Western Desert of Egypt. Report prepared for the General Desert Development Organization, Cairo, Egypt, 56 pp.
- Laeven, M.T (1991). Hydrogeological study of the Nile Delta and adjacent desert areas in Egypt with emphasis on hydrochemistry and isotope hydrology. M.Sc. thesis, Free University, Amsterdam.
- Langguth, H.R. and Voigt, R. (1980). Hydrogeologische Methoden. 1st ed. Springer Verlag, Berlin, 486 pp.
- Lee, T.C. (1999). Applied Mathematics in Hydrogeology. CRC Press, New York, 382 pp.
- Lege, T., Kolditz, O., and Zielke, W. (1996). Strömungs- und Transport- modellierung. Bundesanstalt für Geowissenschaften und Rohstoffe, Springer-Verlag, Berlin, 418 pp.
- Matsukawa, J., Finney, B. and Willis, R. (1992). Conjunctive use planning in Mad River Basin, California, USA. Journal of water resources planning and management, Vol.118, pp. 115-132.
- McDonald, M.G. and Harbaugh, A.W. (1988). MODFLOW, A modular three dimensional finite difference groundwater flow model. USGS, Open file report 83-875, Chapter A1, 586 pp.
- Mohamed, M.A. (2002). Study of groundwater development in the western Delta by using the remote sensing and GIS, Egypt. M.Sc. thesis, Faculty of Engineering. Shoubra – Zagazig University, Cairo, 116 pp
- Mostafa, N.E. (1993). Hydrogeological and Hydrochemical studies on Wadi el Farigh area, Western Desert, Egypt. M.Sc. Thesis, Faculty of Science, El-Minoufiya University, Egypt, 132 pp.
- MWRI (1992; 2006; 2007). Observed Data of surface water in canals western Nile Delta. Ministry of water resources and irrigation, Cairo, Egypt.
- NASA (2005). Shuttle Radar Topography Mission data sets. National Aeronautics and Space Administration, <http://www.jpl.nasa.gov/srtm>, last accessed, April 2007.

- Neuman, S.P. (1973). Calibration of distributed parameter groundwater flow models viewed as a multiple-objective decision process under uncertainty. *Water resources research*, 9(4):1006-1021.
- Neuman, S.P. (1992). Validation of safety assessment models as a process of scientific and public confidence building. In proceedings of HLWM conference, Las Vegas, Vol. 2.
- Nonner, J.C. (2006). Introduction to hydrogeology. Taylor & Francis group, London, UK, 251 pp.
- Norton, P. (1967). Rock stratigraphic nomenclature of the Western Desert, Egypt. Gupco, internal report, 18 pp.
- Omara, S.M. and Sanad, S. (1975). Rock stratigraphy and structural features of the area between Wadi El Natrun and the Moghra Depression, Western Desert, Egypt. *Geol. Jahrbuch.*, Schweizerbart'sche Verlagsbuchhandlung, Stuttgart, Reihe B; 16, pp 45-73.
- Pavlov, M. (1962). Geology, hydrogeology and groundwater hydrology of Wadi el Natrun and the adjacent areas. In preliminary report part 2 (Ed). Hydrogeology. Desert institute and the general development organization. Cairo, 63 pp.
- Pilz, J. (2009). Interfacing geostatistics and GIS. Springer, Berlin, 282 pp.
- REGWA (1993). The groundwater in a study area southern of Wadi El Farigh. The general company for research and groundwater, Interior report, Cairo, 74 pp.
- Retchey, J. and Rumbaugh, J. (1997). Subsurface fluid-flow (groundwater and vadose zone) modeling. ASTM, UK, 423 pp.
- Rhoades, J.D., Kandiah, A., and Marshali, A.M. (1992). The use of saline water for crop production. *FAO Irrigation and drainage Paper 48*, Food and Agriculture Organization of the United Nations, Rome.
- RIGW (1980). The groundwater in the Nile Delta. Research Institute for Ground Water, Interior report, Cairo, Vol. 1, 193 pp.

- RIGW (1988). Hydrogeological Map of Egypt, Scale 1:2,000,000. Research Institute for Ground Water, Cairo, Egypt.
- RIGW (1992). Hydrogeological map for the Nile Delta area, Scale 1: 500000. Research Institute for Ground Water, Cairo, Egypt.
- RIGW (1993). The Hydrogeological Map of Egypt. Scale 1:2,000,000. Research Institute for Ground Water, Cairo, Egypt.
- RIGW (2006). Study of groundwater availability in western Delta. Research Institute for Ground Water, Interior report, Cairo, 92 pp.
- RIGW/IWACO (1998). Environmental management of groundwater resources (EMGR): Identification, priority setting and selection of area for monitoring groundwater quality, Technical Report TN/70.00067/WQM/97/20, Research Institute for Ground Water (RIGW), Egypt.
- RIGW and REGWA (1992). The main and fundamental rules of numerical models for western Delta. In groundwater model for the development area of REGWA (2006), Vol. 2, General company for Research and Groundwater, Cairo, pp 1-12.
- Royal Haskoning (1992). TRIWACO, Groundwater modeling system. User's manual for version 6.0. IWACO, Rotterdam, Netherlands.
- Rushton, K. (2003). Groundwater Hydrology. Wiley, West Sussex, England, 430 pp.
- Saad, KF. (1962). Geology, hydrogeology and groundwater hydrology of Wadi el Natrun and the adjacent areas. Part 3, Groundwater hydrology. Desert Institute and the general development organization. Cairo, 61 pp.
- Sadek, A., Pigott, J., Barakat, M., Abu El-Atta A. and Sadek, S. (2005). Hydrocarbon evaluation of Natrun basin, West Nile Delta, Egypt. GRMENA, Cairo, Vol. 1, pp. 3-31.
- Said, R. (1962). The Geology of Egypt. Elsevier, Amsterdam, Netherlands, 377 pp.
- Saleh, M.F. (1980). Some hydrogeological and hydrochemical studies on the Nile Delta. M.Sc. thesis, Faculty of Science, Ain Shams University, Cairo, 139 pp.

- Sayed, A.M. (2006). Hydrogeological and environmental impacts assessment of Damietta branch on groundwater system, Nile Delta, Egypt. M.Sc. thesis, Faculty of Science, Fayoum University, Egypt, 141 pp.
- Schafmeister, M.Th. (1999). Geostatistik für die hydrogeologische Praxis. Springer-Verlag, Berlin Heidelberg, 172 pp.
- Schrödter, H. (1985). Verdunstung: Anwendungsorientierte Meßverfahren und Bestimmungsmethoden. Springer-Verlag, Berlin, 186 pp.
- Seaber, P. (1982). Definition of hydrostratigraphic Units. 2nd annual syposium on Florida hydrogeology, Northwest Florida water management district. Public information bulletin 82-3, 25-26.
- Seaber, P. (1986). Evolution of classification and nomenclature of hydrogeologic units. EOS 67, No. 16: 281.
- Seaber, P. (1988). Hydrostratigraphic Units. In Hydrogeology. The geology of north America, Back, W., Rosenshein, J., Seaber, P. (eds). Geological Society of America Vol. O-2: 9-14.
- Sefelnasr, A. (2007). Development of groundwater flow model for water resources management in the development areas of the western desert, Egypt. Diss. thesis, Martin Luther University, Halle-Wittenberg, 171 pp.
- Shahin, M. (1985). Hydrology of the Nile basin. in Development in Water Science 21, Elsevier, Amsterdam, Netherlands, B.V. 575 pp.
- Shata, A.A. (1962). Geology, hydrogeology and groundwater hydrology of Wadi El-Natron and the adjacent areas. Internal report, Desert Institute, Cairo, PT.1
- Shata, A.A. (1970). Remarks on the hydrogeology of the Nile Delta. Symposium on Hydrology of Delta, UNISCO, Vol. 2, pp. 385-396.
- Shata, A.A. and El-Fayoumy, I.F. (1967). Geomorphological and morphopedological aspects of the region west of the Nile Delta with special reference of Wadi El-Natron area. Desert Institute Bulletin, Cairo, V. XVI, No.1, pp. 1-28.

- Soliman, M., Darwish, M. and Abd El Monem, M. (2005). Integration of geographic information system and remote sensing technology for studying the land reclamation expansion at west Nile Delta region. *GERMENA*, Vol. 1, pp. 255-266
- Spitz, K. and Moreno, J. (1996). A practical guide to groundwater and solute transport modelling. Wiley, New York, 461 pp.
- Sun, N-Z. (1994). Inverse problems in groundwater modeling. Kluwer Academic publishers, Boston, 337 pp.
- Surfer® 8 User's Guide (2002). Countouring and 3D surface mapping for scientists and engineers. Golden Software Inc., Colorado, pp 640.
- Swailam, F.M., Hamza, M.S., Abdel-Monem, A.A., El-Manharawy, M.S. and Nada A.A. (1980). Groundwater hydrology of Wadi el Natrun II Tritium dating. *Isotopes and Rad. Res.*, Vol. 12, No.1: pp.17-23.
- Taher, A.G. (1999). Inland saline lakes of Wadi El Natrun depression. *International journal of salt lake research*, Netherlands, 8: 149-169.
- Tawadros, E. (2001). *Geology of Egypt and Libya*. Belkema, Rotterdam, 480 pp.
- Thomas, E. (2001). System and boundary conceptualization in groundwater flow simulation; in *Techniques of water-resources investigations of the U.S. geological survey*. USGS, Reston, Virginia, Book 3, application of hydraulics, Chapter 8, pp 1-38.
- Townley, L.R and Wilson, J.L (1980). Description of and user's manual for a finite-element aquifer flow model AQUIFEM-1. Cambridge Massachusetts. Ralph M. Parson Laboratory Technology Adaption Program, Technical Report No. 252: 294 pp.
- USGS (2004). SRTM data, USGS Seamless Data Distribution System-Enhanced. United States Geological Survey, <http://srtm.usgs.gov>, last accessed: March 2007.
- Wang, H.F and Anderson, M.P (1995). *Introduction to groundwater modeling: Finite difference and finite element methods*. Academic press, San Diego, 237 pp.

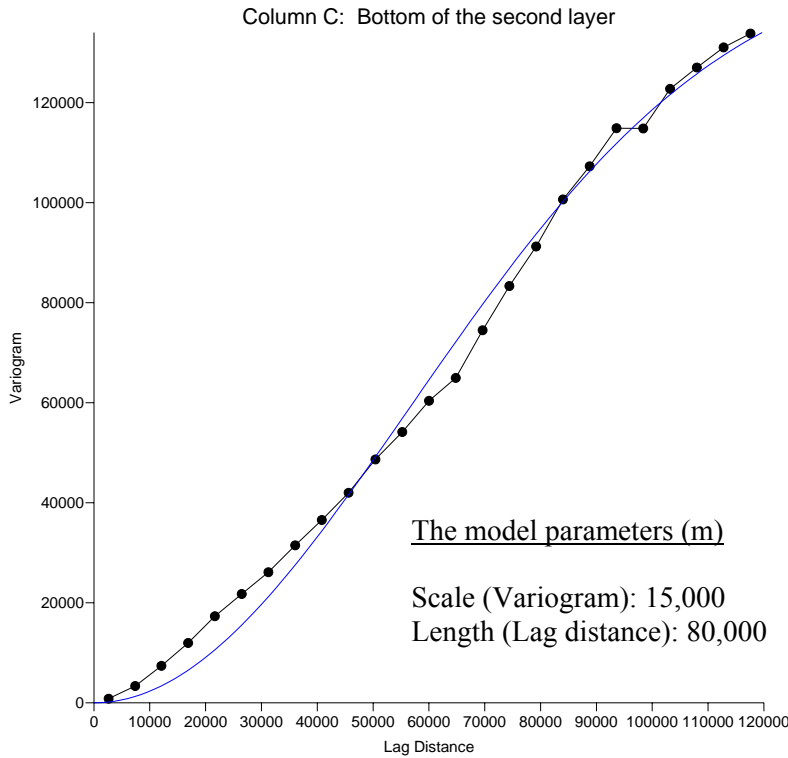


- Wassef, R., Gossel, W. and Wycisk, P. (2008). GIS-basierte Grundwasserströmungsmodellierung im Moghra-Aquifersystem, Westliches Delta, Ägypten.- In: Sauter, M., & Ptak, T., & Kaufmann-Knocke, R., & Lodemann, M., van den Kerckhoff, A. (Ed.): Grundwasserressourcen, Schriftenreihe der Deutschen Gesellschaft für Geowissenschaften, Göttingen, 57, 197.
- Wassef, R., Gossel, W. and Wycisk, P. (2010). Konzeptionell Grundwasserströmungsmodell für das entwicklungsgebiet, Westliches Delta, Ägypten.- In: Levin, C., & Grathwohl, & P., Kappler, A., & Kaufmann-Knocke, R., & Rügner, H., (Hg.): Grundwasser für die Zukunft, Schriftenreihe der Deutschen Gesellschaft für Geowissenschaften, Tübingen, 67, 193.
- Webster, R. (2007). Geostatistics for environmental scientists. Wiley, Chichester, 315 pp
- Wycisk, P. (1993). Outline of the geology and mineral resources of the southern Dakhla Basin, southwest Egypt. In Meissner, B, Wycisk, P (eds). Geopotential and Ecology: Analysis of a desert region, Catena Supplement, 26: 67-89.
- Wycisk, P. (1994). Correlation of the major late Jurassic- Early Tertiary low- and high stand cycles of SW Egypt and NW Sudan. Geol. Rsch. 83: 759-772.
- Verruijt, A. (1982). Theory of Groundwater Flow. 2nd ed. Palgrave Macmillan Press LTD, Hong Kong, 152 pp.
- Yarus, J. and Chambers, L. (1994). Stochastic modeling and geostatistics: principles, methods, and case studies. American association of petroleum geologists. Tulsa, Okla, 379 pp.
- Yeh, W.W. (1986). Review of parameter identification procedures in groundwater hydrology: The inverse problem. Water Resources Research, 22 (2): 95-108.
- Youssef, A. (2000). Impact of the subsurface structures on the groundwater occurrences in the south eastern part of Wadi El Farigh, West of the Nile Delta, Egypt. Desert Institute Bull. Cairo, Vol. 50, No.1, pp. 19-40.
- Youssef, A., Mosry, A., Mossallam, H. and Abd Al-Latif, A. (2009). Vegetation analysis along Alamain – Wadi El-Natron desert road. Australian journal of basic and applied sciences. Australia, 3(1): 167-176, 2009.

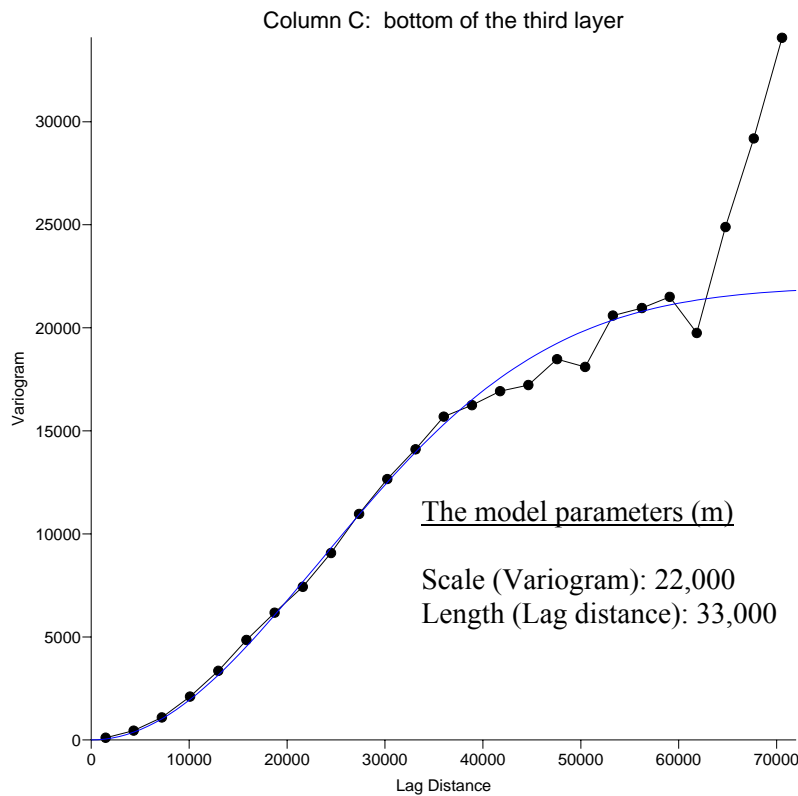
Zeiler, M. (1999). Modeling our world – The ESRI guide to geodatabase design. ESRI press, Redlands, 197 pp.

Zhang, D. (2001). Stochastic methods for flow in porous media. Harcourt Incorporation, Florida, 336 pp.

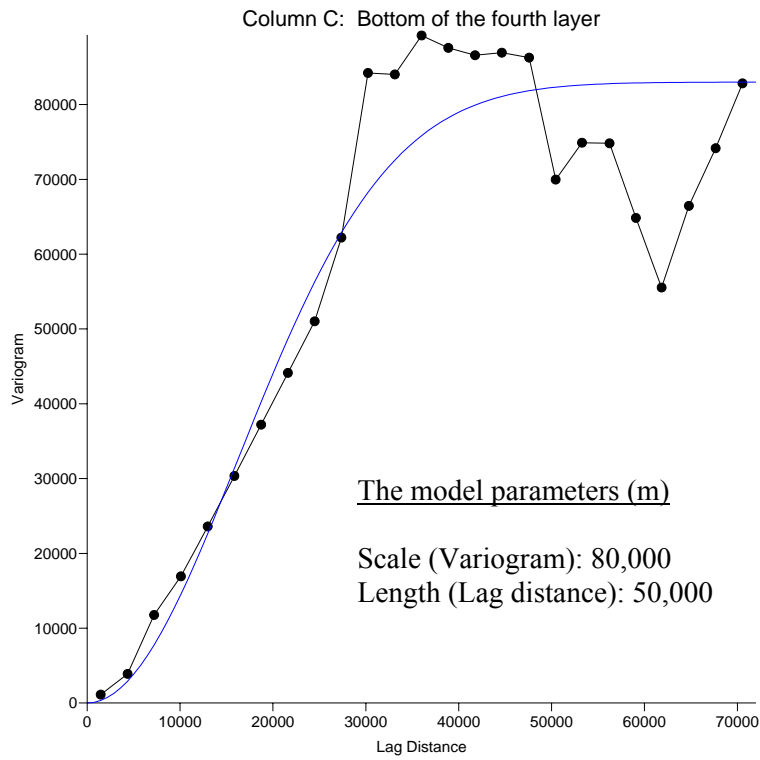
# Appendices



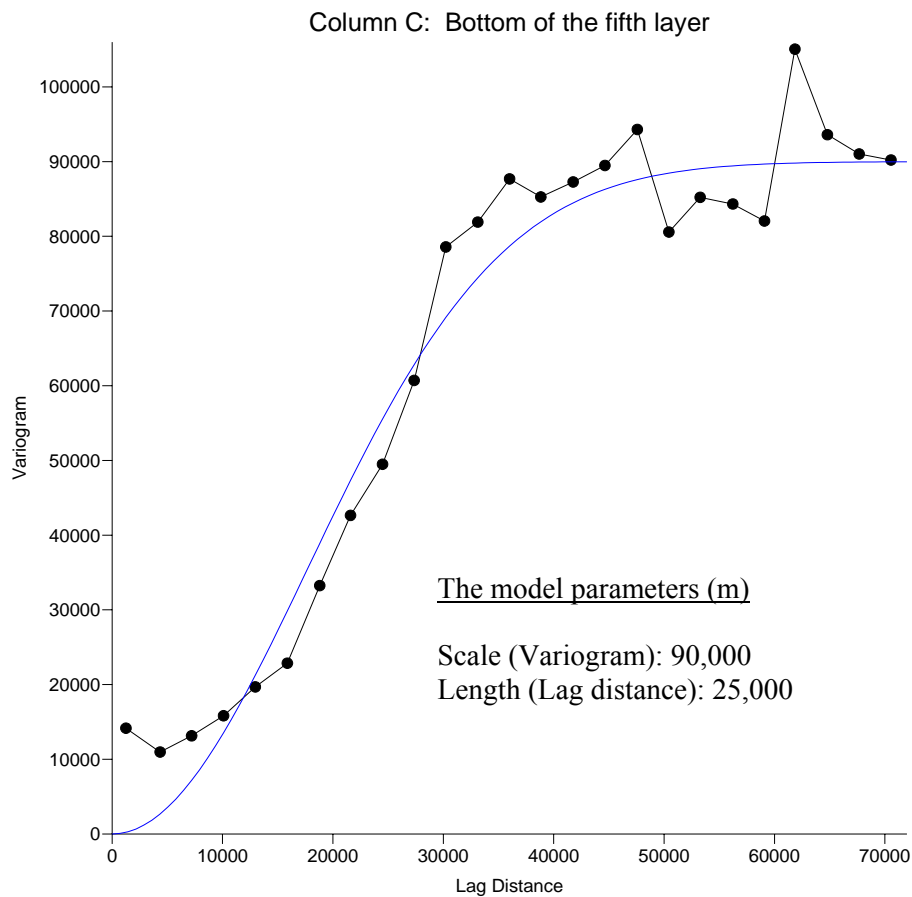
**Appendix 1:** A Gaussian variogram for the bottom of the second layer.



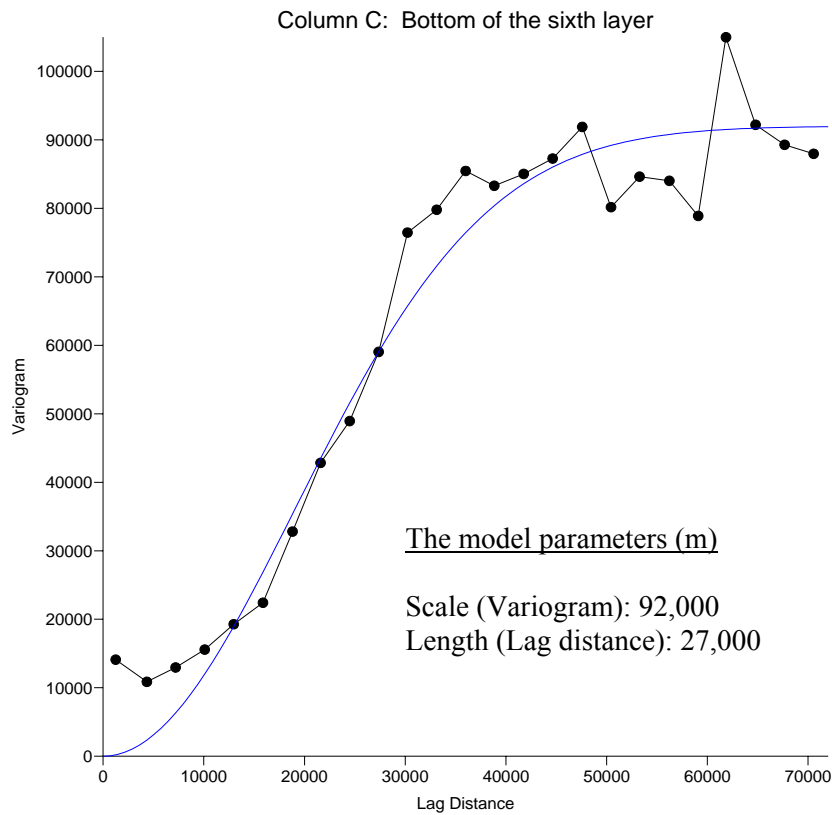
**Appendix 2:** A Gaussian variogram for the bottom of the third layer.



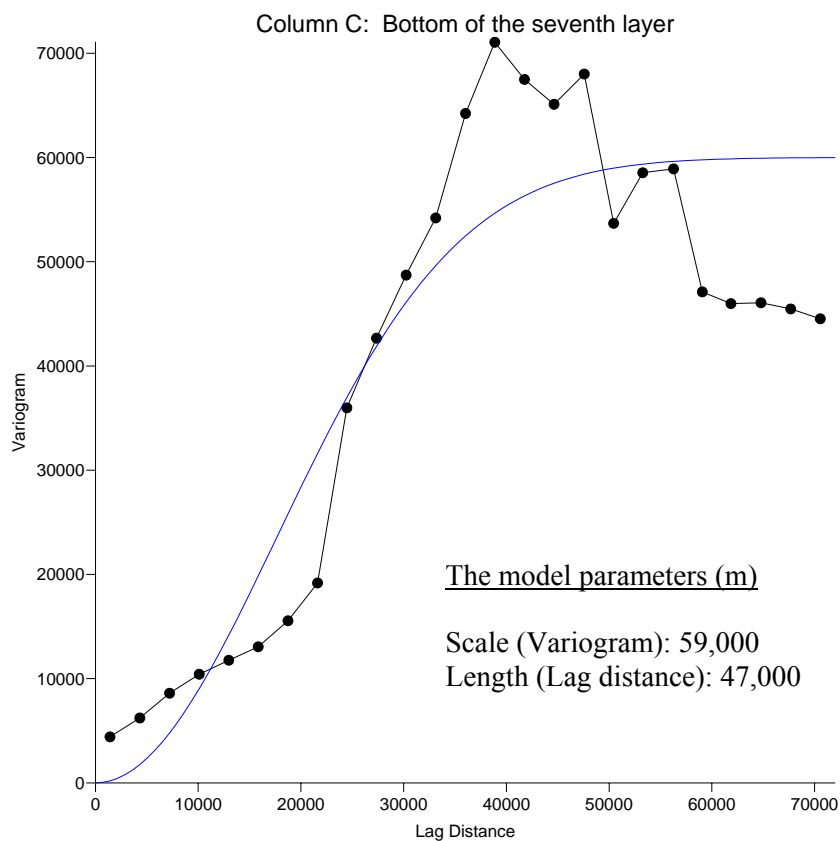
**Appendix 3:** A Gaussian variogram for the bottom of the fourth layer.



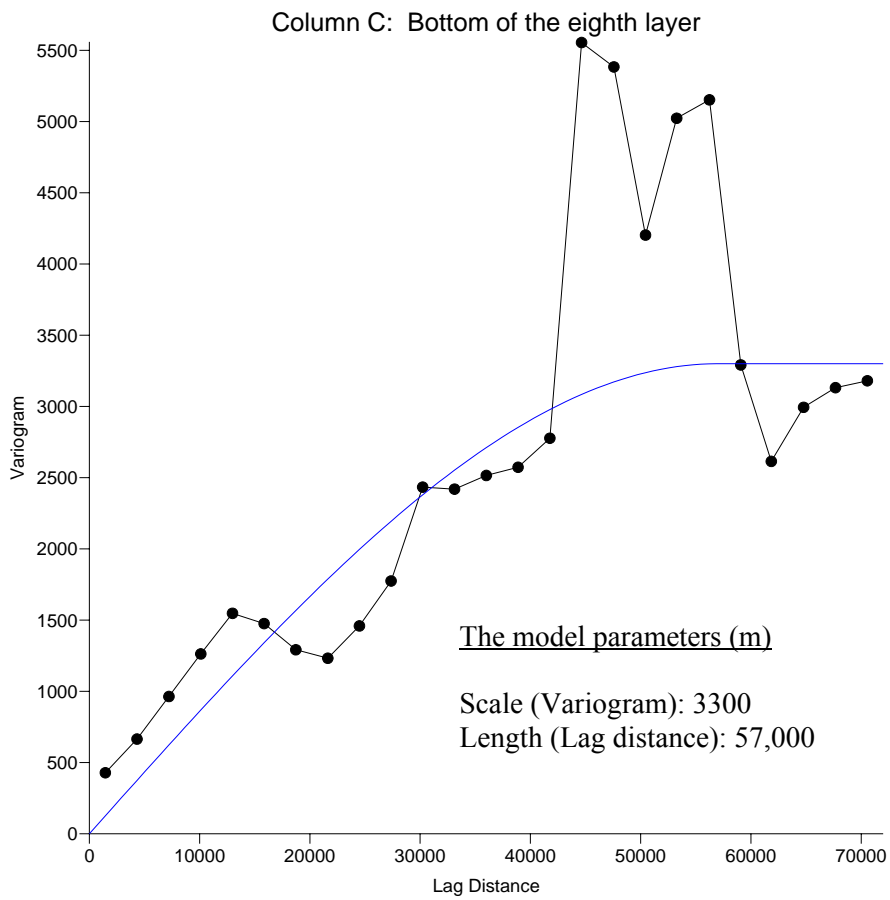
**Appendix 4:** A Gaussian variogram for the bottom of the fifth layer.



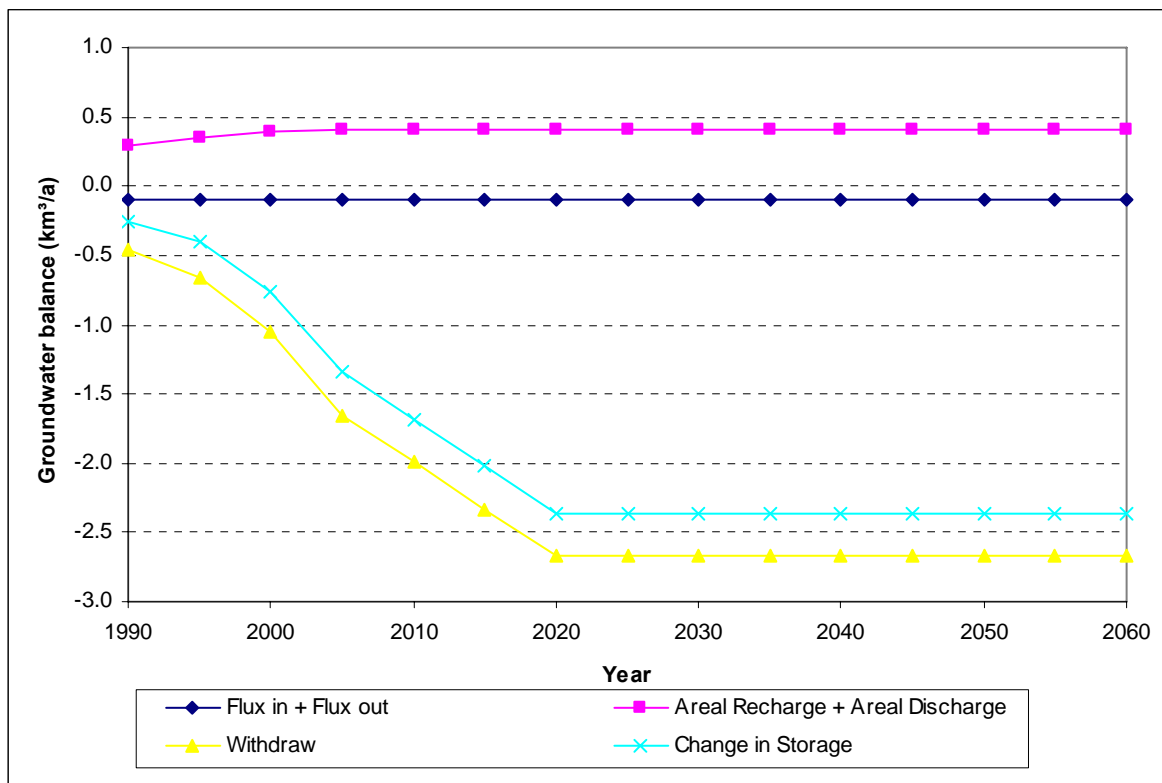
**Appendix 5:** A Gaussian variogram for the bottom of the sixth layer.



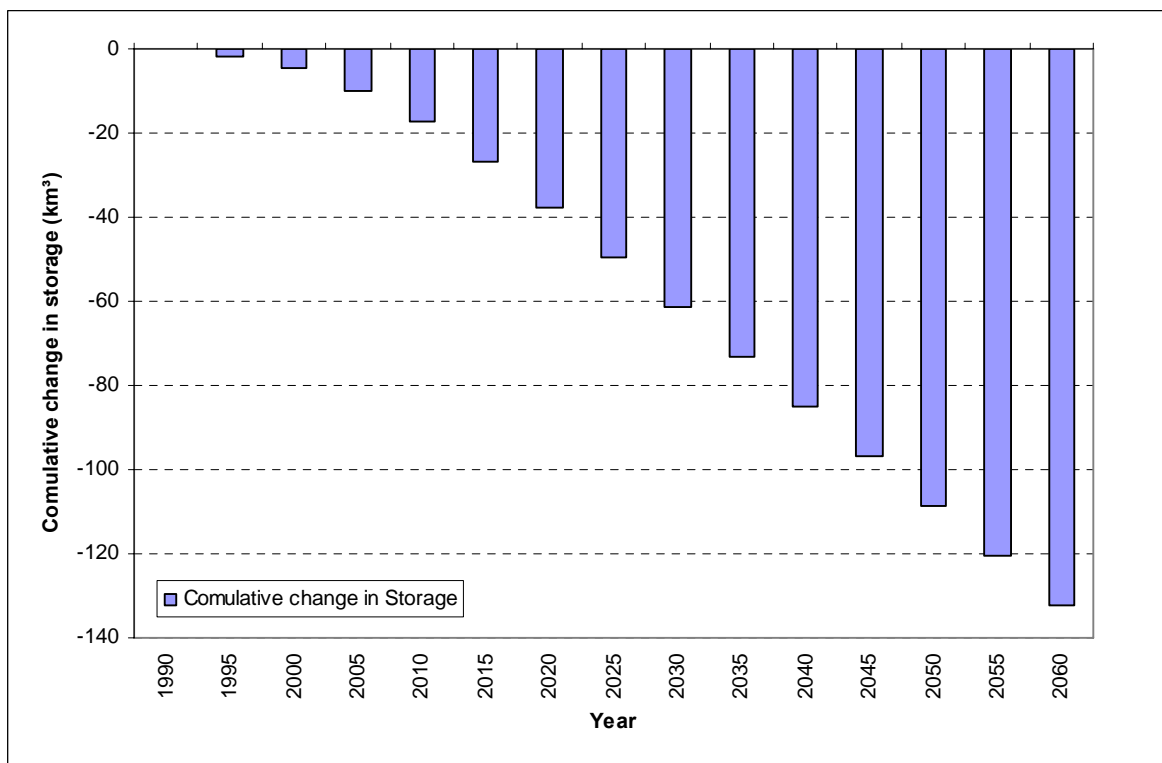
**Appendix 6:** A Gaussian variogram for the bottom of the seventh layer.



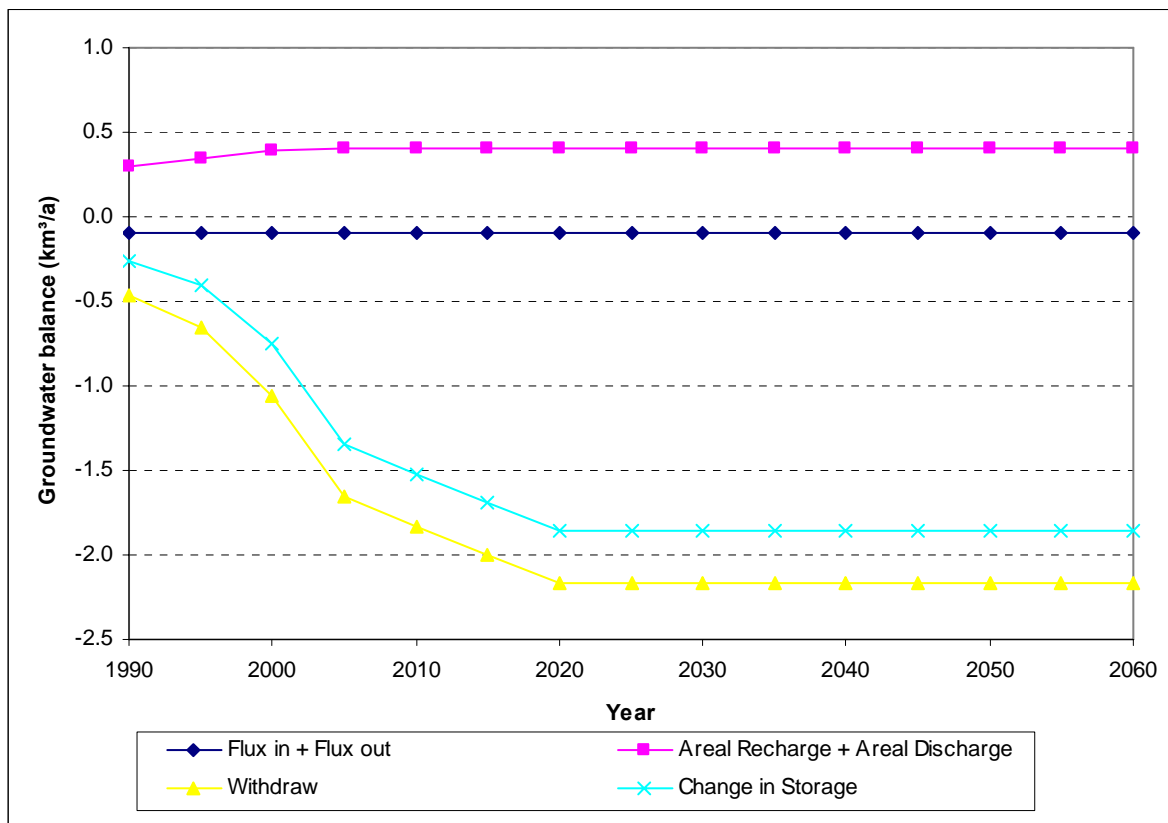
**Appendix 7:** A Spherical variogram for the bottom of the eighth layer.



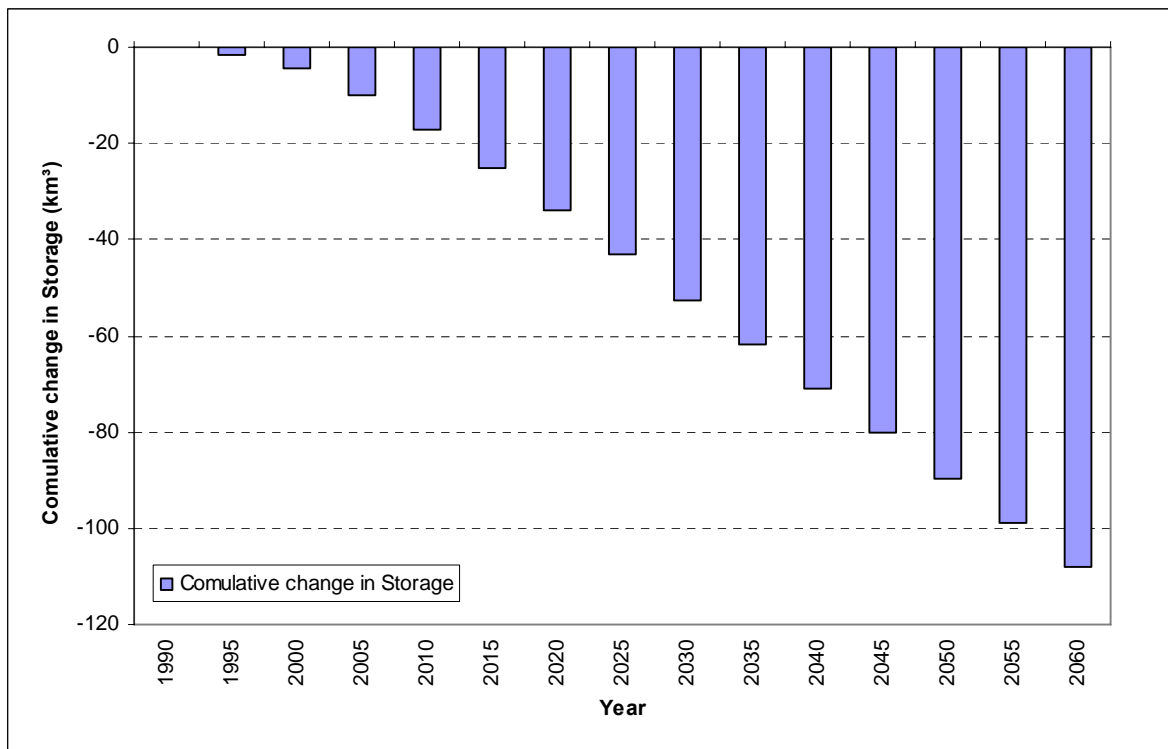
**Appendix 8:** Groundwater balance for Scenario 3 at the study area for the period from 1990 to 2060



**Appendix 9:** Cumulative decrease in groundwater storage of the study area for Scenario 3 at the period from 1990 to 2060.

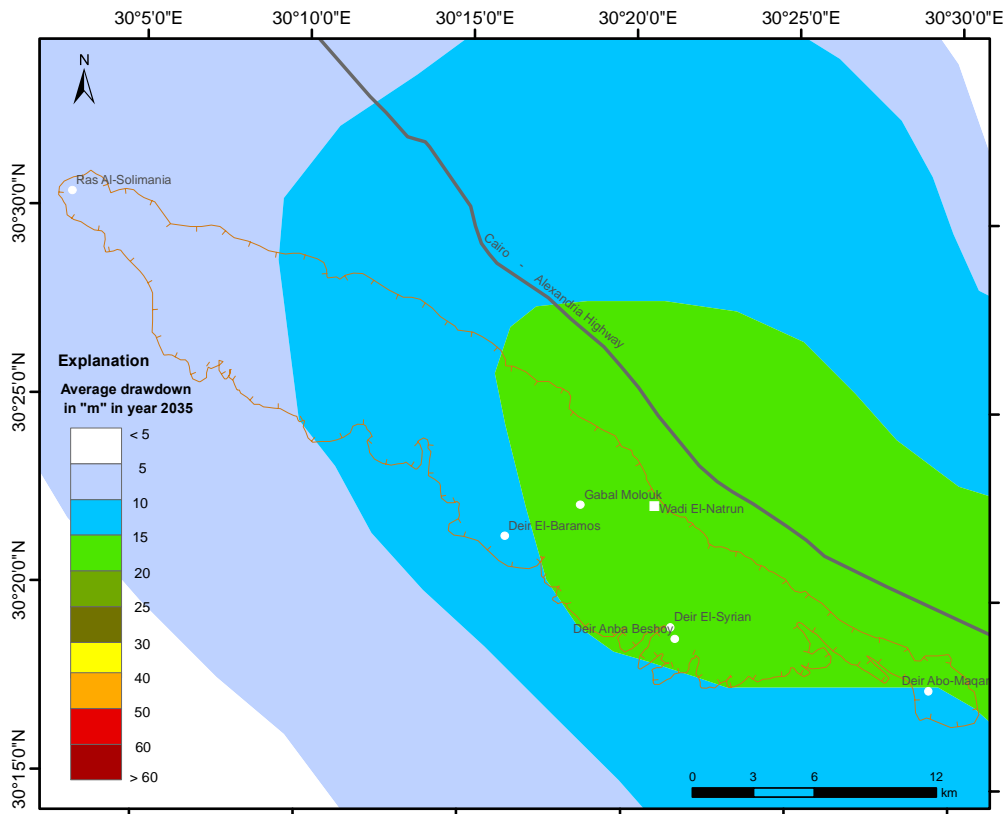


**Appendix 10:** Groundwater balance for Scenario 4 at the study area for the period from 1990 to 2060

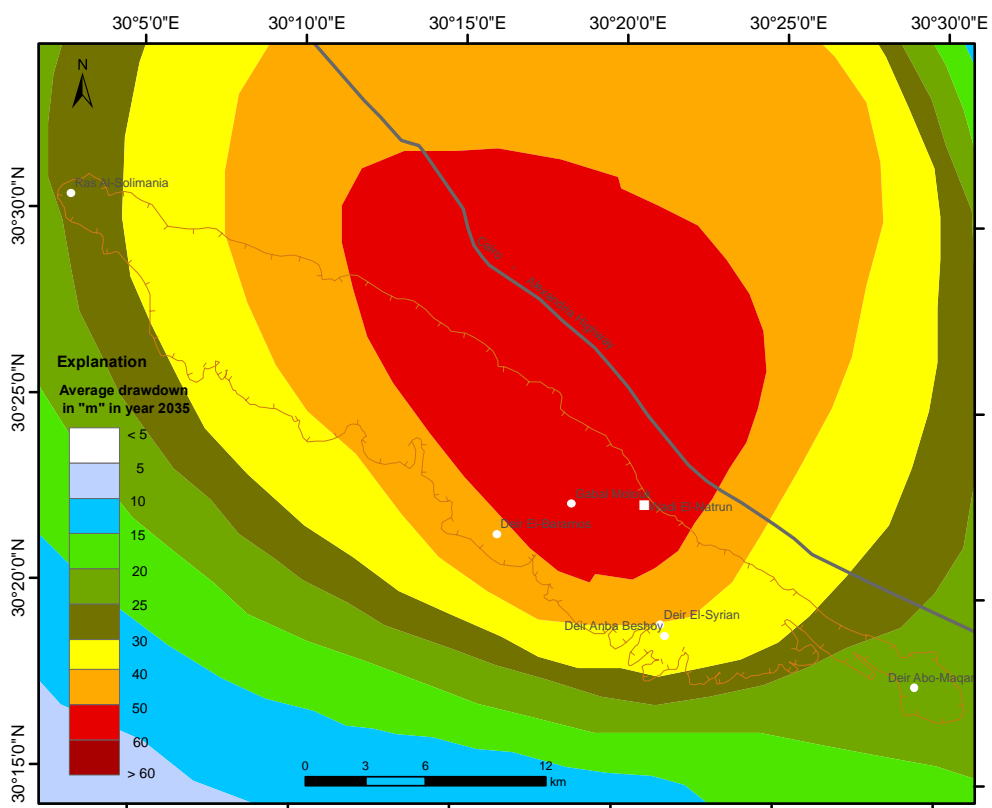


**Appendix 11:** Cumulative decrease in groundwater storage of the study area for Scenario 4 at the period from 1990 to 2060.

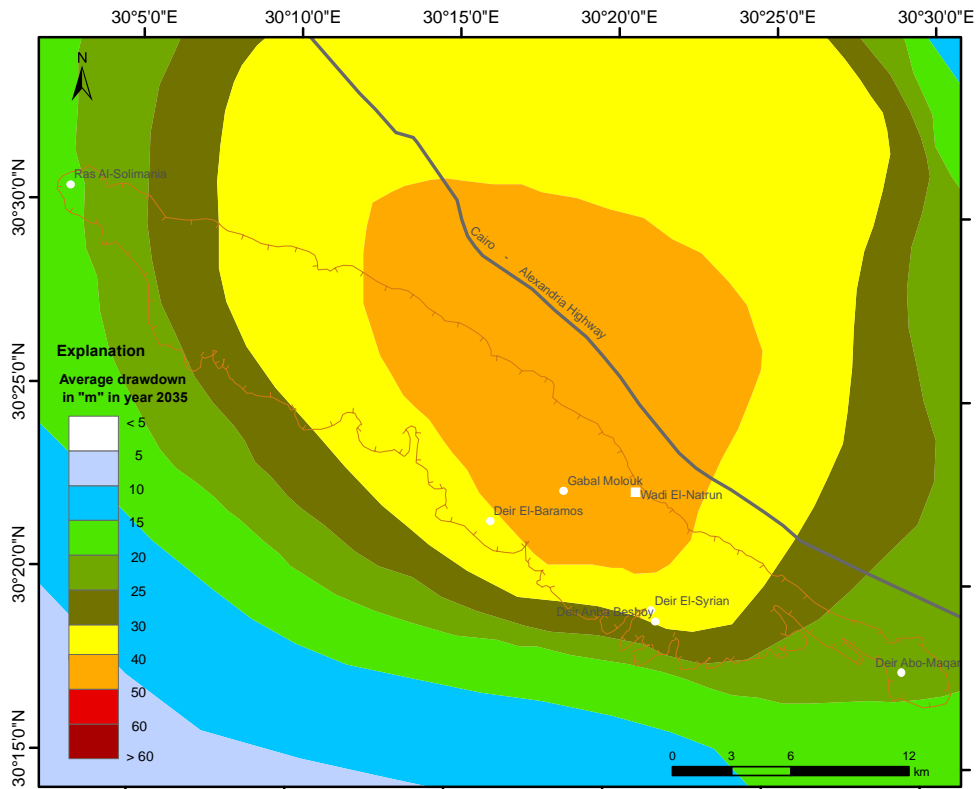




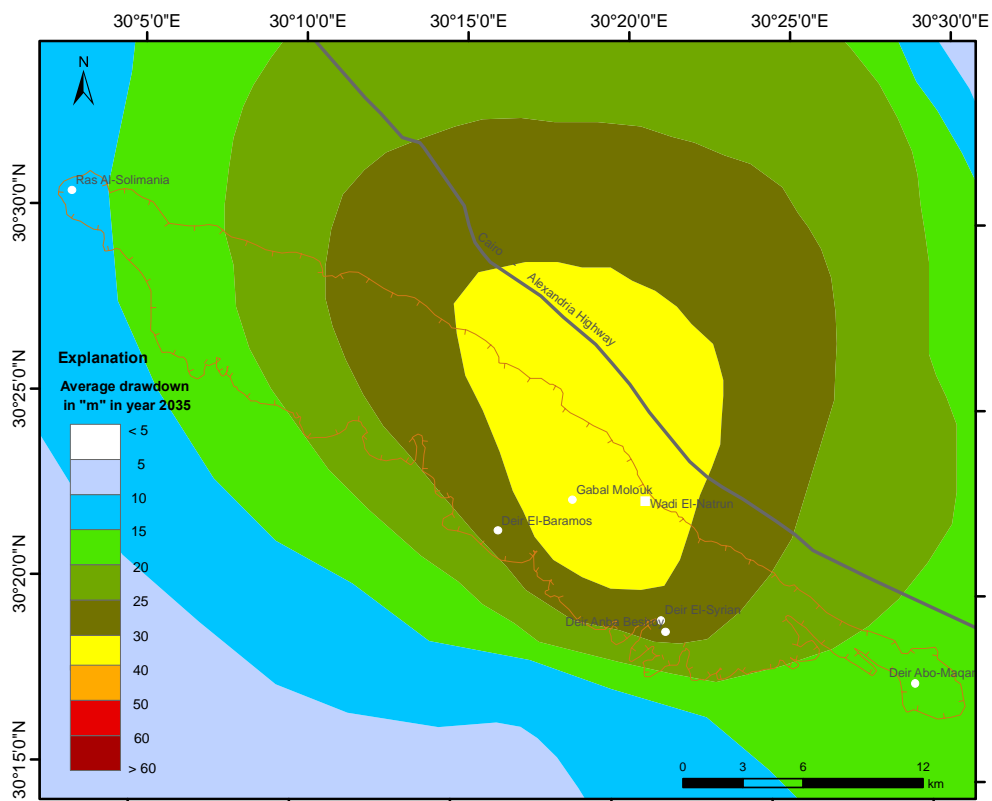
Appendix 12: Simulated decline in Wadi El-Natrun by 2035 for Scenario 1.



Appendix 13: Simulated decline in Wadi El-Natrun by 2035 for Scenario 2.



**Appendix 14:** Simulated decline in Wadi El-Natron by 2035 for Scenario 3.



**Appendix 15:** Simulated decline in Wadi El-Natron by 2035 for Scenario 4.

## **Statement of Original Authorship**

Herewith I affirm that this Dissertation is my own work and it was written independently according to my knowledge and belief, I used no other than the cited references and facilities.

I also affirm that I have never applied or submitted any work for Doctor Degree or such at any other university or institution.

Signature:

Raafat Samuel Wassef

Date:

## **Curriculum Vitae**

### **Personal data:**

Name: Raafat Samuel  
Family name: Wassef  
Gender: Male  
Date of birth: 28. October 1967  
Place of birth: Cairo - Egypt  
Nationality: Egyptian  
Address: Richard-Paulick 13 (App. 307),  
D - 06124 - Halle (Saale)  
Tel. +49(0)1633348795  
E-Mail: raafat.wassef@geo.uni-halle.de  
rswassef@yahoo.com

### **Education:**

02/2007 - 10/2010 Doctoral student at the Institute of Geosciences (Department of Hydro- and Environmental geology), Martin-Luther University, Halle-Wittenberg, Germany.  
10/2002 - 10/2004 M.Sc. in Geotechnique and Infrastructures, University of Hannover, Germany.  
10/1991 - 06/1993 Diploma in Civil Engineering, Cairo University, Giza, Egypt.  
10/1985 - 06/1990 B.Sc. in Civil Engineering, Ain Shams University, Cairo, Egypt.  
10/1982 - 06/1985 Secondary School at El-Qoba Secondary School, Cairo, Egypt.  
10/1979 - 06/1982 Preparatory School at El-Tahrir Preparatory School, Cairo, Egypt.  
10/1973 - 06/1979 Primary School at Saint Marcus Primary School, Cairo, Egypt.

### **Professional activities:**

04/1992 – 11/1993 Civil Engineer at the Engineering Consultant Office (EETC), Giza, Egypt.  
12/1993 – 10/2004 Civil Engineer at the Central Directorate of Groundwater - Ministry of Water Resources and Irrigation, Giza, Egypt.  
11/2004 – 11/2006 Assistant of Works Manager at the Central Directorate of Groundwater for Nile Valley and Delta - Ministry of Water Resources and Irrigation, Giza, Egypt.  
12/2006 Works Manager at the Central Directorate of Groundwater for Nile Valley and Delta - Ministry of Water Resources and Irrigation, Giza, Egypt.

**Awards:**

Certificate of Appreciation from the Minister of Water Resources and Irrigation in 1998 for the qualification in applying the development plan of the Ministry.

**Fellowship awards:**

02/2007 – 10/2010

Scholarship awarded by the Catholic Academic Exchange Service (KAAD) for PhD study.

04/2002 – 10/2004

Scholarship awarded by the German Academic Exchange Service (DAAD) for MSc study.

**Publications:**

Wassef, R., Gossel, W. and Wycisk, P. (2008). GIS-basierte Grundwasserströmungs-modellierung im Moghra-Aquifersystem, Westliches Delta, Ägypten.- In: Sauter, M., & Ptak, T., & Kaufmann-Knocke, R., & Lodemann, M., van den Kerckhoff, A. (Ed.): Grundwasserressourcen, Schriftenreihe der Deutschen Gesellschaft für Geowissenschaften, Göttingen, 57, 197.

Wassef, R., Gossel, W. and Wycisk, P. (2010). Konzeptionell Grundwasserströmungs-model für das entwicklungen Gebiet, Westliches Delta, Ägypten.- In: Levin, C., & Grathwohl, & P., Kappler, A., & Kaufmann-Knocke, R., & Rügner, H., (Ed.): Grundwasser für die Zukunft, Schriftenreihe der Deutschen Gesellschaft für Geowissenschaften, Tübingen, 67, 193.

Halle (Saale),